DE BRUXELLES, UNIVERSITÉ D'EUROPE

Faculté des Sciences

Département des Science de la Terre et de l'Environnement

Service de Biogéochimie et Modélisation du Système Terre (BGéoSys)

Geochemical and isotopic study of urban and rural Watersheds: Assessment of water resources and soil pollution in Lebanon

Thèse présentée par :

Rawaa AMMAR

En vue de l'obtention du grade de Docteur en Sciences

Promoteur:

Prof. Lei CHOU

Co-promoteur:

Prof. Zeinab SAAD

Prof. Véronique Kazpard

adémique 2013-2014

Université Libanaise
École Doctorale
Sciences et Technologies

ULB
Université Liber
de Bruxelles

Doctorat Université Libanaise

THESE EN COTUTELLE

Pour obtenir le grade de Docteur délivré par

L'Universite Libre de Bruxelles

et

L'Ecole Doctorale des Sciences et Technologie

(Université Libanaise)

Spécialité :

Présentée et soutenue publiquement par

Rawaa AMMAR

19 June 2014

Geochemical and isotopic study of urban and rural Watersheds: Assessment of water resources and soil pollution in Lebanon.

Directeur de thèse : **Zeinab Saad**

Co-encadrement de la thèse : **Lei Chou**

Membre du Jury

M.Alain Préat, Professeur, Université Liber de Bruxelles	Président du jury
M.Pierre Regnier, Professeur ,Université Liber de Bruxelles	Secrétaire du jury
M. Hussein Hamad, Professeur, Université Libanaise	Examinateur
M.Vincent Hallet, Professeur, Université de Namur	Expert externe
M.Mahmoud Wazne, Professeur, Lebanese American University	Expert externe
Mme.Lei Chou, Professeur, Université Liber de Bruxelles	Directeur
Mme.Zeinab Saad, Professeur, Université Libanaise	Directeur
Mme.Véronique Kazpard, Professeur, Université Libanaise	Co- Directeur

"The test of our progress is not whether we add more to the abundance of those who have much; it is whether we provide enough for those who have little."

Franklin Delano Roosevelt

Acknowledgment

I would like to acknowledge the support of Azm and Saadé Association, and PCSI programs of AUF for the financial aid. Additional funding was provided by the Bureau of International Relations (BRIC) and the gratitude to Xénophilia Funders of the Université Libre de Bruxelles (ULB) Mr. and Mrs. Lepage.

In addition to my personal efforts in this thesis, the success of this achieved project was by the exerted efforts of many others, and I will take the opportunity to express my deep gratitude to all who contributed in the accomplishment of this work. I would like to show my greatest appreciation to my supervisor Prof. Veronique Kazpard for her constant guidance, continuous encouragement, and patience along the thesis preparation. I am grateful to the trust she gave me, and the moral support she provided. I highly appreciate her confidence in my ambitious goals, and her enormous efforts to provide me with all the required facilities on field, laboratory, and abroad in the collaborating institutes. She has been a tremendous mentor and allowed me to grow as a research scientist. I am so thankful for her priceless advices that will pave the road for my future career. Prof. Kazpard was the driving force of the successful completion of this thesis; she kept the faith and sense of humor during the hard times when I had lost mine. I won't be able to complete this journey without the support and guidance of my supervisor Prof. Lei Chou whom I am so grateful for welcoming me in her laboratory and for the facilities she had provided for the experimental work hosted at ULB. I highly acknowledge the massive assistance of Prof. Chou academically, and administratively. Her directions, patience, and attention to tiny details taught me to strive towards my goal with steady steps. Thanks to her I was able to perform analytical measurements on high level in collaborating laboratories that raises the standards of this work. I greatly appreciate the personal support she dedicated to me during my stay in Brussels which is rare between supervisor-student relationships. I would also like to express my gratitude to my supervisor Prof. Zeinab Saad for her support and encouragement since the beginning of this thesis thanks to all the efforts that she invested in the better production of this doctoral thesis. I am indebted to Prof. Antoine El Samrani for the continuous scientific assistance, fruitful discussions and the academic advices he always provided. My special appreciation and deep gratitude are expressed to Prof. Bruno Lartiges, his valuable contribution aids in the success of this thesis, I am so thankful for giving me the opportunity to perform my analysis in his laboratory, and for all the encouragement and leadership he provided for my research. I would express my specific appreciation to Prof. Mathieu Benoit for his generous help and assistance which guide me through laborious experimental analysis.

I would also like to thank my committee members, Prof. Alain Préat, Prof. Pierre Regnier, and Prof. Vincent Hallet whom never delayed in providing support, advices, and suggestions that adjusted my work and were vital for putting this thesis on the right track. I am thankful to Prof. Hallet for the precious time he spent to provide me with the required knowledge. Allow

me also to express my great gratitude to Prof. Regnier, who motivated me to consider modeling and gave me the opportunity to follow his course and work with his research team. I am so pleased with the experience I gained working with Dr. Goulven Laruelle on the model that crowned this work, I am thankful for all the time and effort and hardworking he put to achieve the modeling part in this thesis. In addition, I want to express my indebted to Prof. Mahmoud Wazne for his discussions, valuable assistance and attentive care to achieve the desired goals in the best way. I would like to acknowledge Prof. Hussein Hamad for accepting to be a member in my jury and I want to thank all the jury members for the time and effort they employed to read and evaluate my thesis manuscript. Words cannot express my gratitude and appreciation for Litani River Authority, especially for Dr. Nabil Amacha for all the support, data, knowledge, and help to achieve the field work. The field work that was the bases for this thesis would never been achieved without the help and assistance of LRA staff represented by Mr. Ali Tarrif whom make the fieldwork a joyful and approachable task.

Special thanks and appreciation are expressed to Dr. Hussein Kazan, for his good will and administrative support. He was always supportive during my stay in Brussels even before he knew me in person.

I would like also to express my gratitude for laboratory staff for their help in need, and assistance to overwhelm the encountered obstacles, in UL (Sarah Haddad, Sahar Rihan, Manal Houhou, and Mohamad Hajj), UPS (Jonathan Prunier and Manuel Henry), and ULB. Mainly to Mme. Nathalie Roevros whom showed a great will of assistance, support and encouragement. Her generosity, love and care compensated the feelings of loneliness, foreignness, and weakness I have experienced during hard moments away from home. My doctoral life span would never be better without the immense help of my colleagues who voluntarily provide their help during field campaigns even during hardship. I can't thank enough Mr. Elias Maatouk, Mr. Hussein Kanbar, Ms. Eliane Hayek, Ms. Nathalie Sleiman, and Ms. Fatima Yassine for their generous help in field work and the follow up of my experimental work at my home university when I am abroad.

At the end, I would like to express my profound gratitude and high appreciation to my family and friends for their precious support, and their continuous encouragement and prays, for all the sacrifices that they have made on my behalf. They have literally contributed in the success of this work by conducting the field campaigns with me side by side and provide me with all the facilities that made my PhD a manageable experience.

Praising my mighty God whom has blessed my life and enlightened my way...

Table of Contents

List of Figures vii

List of Tables xii

List of abbreviations xiv

Abstract 1

1. Chapter 1: Introduction 4

1.1 Rationale and objectives 4

1.2 Previous international geochemical studies 5

1.2.1 Chemical species used to trace pollutants in water bodies under the impact of industrial and agricultural activities 5

1.2.2 Chemical species used to trace pollutants in soils and sediments 8

1.2.3 The inter-mechanism of the partition between the dissolved and particulate phases of contaminants during precipitation and remobilization. 10

1.3 National studies 12

1.3.1 Similar geochemical studies conducted in Lebanon on point and diffuse sources of pollutants 12

1.3.2 Final outcome and scope of studies on the hydraulic resources and pollution in Lebanon. 18

1.4 Data Deficiency 24

1.5 Thesis outline 25

2. Chapter 2: Materials and Methods 27

2.1 Study sites 27

2.1.1 Environmental and socio-economical context 27

2.1.2 Industrial watershed 30

2.1.3 Agricultural watershed 30

2.2 Sampling Schedule 32

2.2.1 Preliminary sampling 32

2.2.2 Sampling program over two years 33

2.2.3 Sampling and sample storage 34

2.3 Sample characterization 35

2.3.1 Water samples 35
2.3.2 Sediments and soils 36
2.3.2.1 Grain Size 36
2.3.2.2 Functional groups 37
2.3.2.3 Total and organic carbon 37
2.3.2.4 Mineralogy 37
2.3.2.5 Determination of metals in the particulate phase 37
2.3.2.6 Pb isotopes 38
2.3.2.7 ^{210}Pb and ^{137}Cs chronology 38
2.3.3 Characterization of algae 38
2.3.4 Data source 39

2.4 Packed soil columns experiment 39

2.4.1 Soil preparation 39
2.4.2 Physicochemical characteristics of soil in packed columns 39
2.4.3 Soil column leaching experiment 42
2.4.4 Leachate analysis 43
2.4.5 Characterization of soil in packed columns 43

2.5 Characterization of Phosphogypsum (PG) 44

2.5.1 Physicochemical characterization of PG 44
2.5.2 Effect of pH on PG suspension behavior 44
2.5.3 Effect of PG suspension load and organic ligands on the suspension behavior 45

2.6 Metal Speciation using Chemical titration 45

3. Chapter 3: Applying physicochemical approaches to control Phosphogypsum heavy metal releases in aquatic environment **46**

3.1 Introduction 47

3.2 Materials and methods 49

3.2.1 PG samples 49
3.2.2 Physicochemical characterization of PG 49
3.2.3 Effect of pH on PG suspension behavior 50
3.2.4 Effect of PG suspension load and organic ligands on the suspension behavior 50

3.3 Results and discussion 51

3.3.1 Influence of PG suspension load on its behavior 51
3.3.2 Effect of citrate ligand on PG dissolution at various pHs 54

3.4 Conclusion 64

4. Chapter 4: Geochemical Investigation of Two contrasted Mediterranean watersheds: Tracing the origin and pathways of contaminants using Pb isotopes .66

4.1 Introduction 67

4.2 Study sites 68

4.2.1 Environmental and socio-economical context 68
4.2.2 Industrial watershed 69
4.2.3 Agricultural watershed 69

4.3 Materials and methods 70

4.4 Results and discussion 71

4.4.1 Evolution of Pb pollution in an industrial soil 71

4.4.2 Evolution of Pb pollution in an agricultural area 77

4.4.3 Comparison of the two contrasting watersheds 80

4.4.3.1 Excess Pb isotopic ratio 80

4.4.3.2 Binary model 81

4.4.3.3 Three-isotope plot 84

4.5 Conclusion 86

5. Chapter 5: Metal behavior in intact cores and packed columns: Comparison between industrial and agricultural watersheds in eastern Mediterranean 88

5.1 Introduction 89

5.2 Materials and methods 90

5.2.1 Study area 90

5.2.2 Intact soil cores 92

5.2.3 Leaching soil columns 92

5.2.4 Analytical methods 93

5.3 Results and discussion 95

5.3.1 Reservoir impact on watershed 95
5.3.2 Comparative analysis between agricultural and industrial watersheds 104
5.3.3 Factors that control metal behavior in soil 110
5.3.3.1 Soil characterization 110
5.3.3.2 Leaching columns experiment 112

5.4 Conclusion 120

6. **Chapter 6: Reservoir sediments: A sink or source of chemicals at the surface water-groundwater interface** **122**

6.1 Introduction 123

6.2 Materials and Methods 124

6.2.1 Study area and sampling 124
6.2.2 Characterization of water samples 125
6.2.3 Characterization of sediments and algae 126

6.3 Results and discussion 127

6.3.1 Characterization of reservoir sediments 127

6.3.2 Reservoir hydrodynamics 130

6.3.2.1 Fill hydrological mode 131

6.3.2.1.1 Physicochemical characteristics and transport direction of chemica 131

6.3.2.1.2 Sediments act as a sink for chemicals 134

6.3.2.2 Spill hydrological mode 136

6.3.2.2.1 Physicochemical characteristics and transport direction of chemic 136

6.3.2.2.2 Sediments act as a source for chemicals 138

6.3.3 Reservoir eutrophication and biological processes 139

6.3.4 Hydrological and chemical connectivities of the system 142

6.3.4.1 Hydrological connectivity 142

6.3.4.2 Chemical connectivity 143

6.3.5 Reservoir vulnerability and capacity to retain and liberate chemicals ... 145

6.4 Conclusions 148

7. **Chapter 7: Hydrodynamics influence on reservoir sustainability in semi-arid climate: physicochemical analysis coupled to an environmental isotopic study** **150**

7.1 Introduction 151

7.2 Background 153

7.2.1 Geographical location, Geology and Topography 153

7.2.2 Climate and Hydrology 154

7.3 Materials and Methods 155

7.3.1 Data Source 155

7.3.2 Sampling program 155

7.4 Results and discussion 156

7.4.1 Closed system (no groundwater inflow: Ri zone) 156

7.4.2 Open system (no groundwater inflow: Cz and Dz zone) 162

7.4.3 Isotopic response of the reservoir to climatic and land-use changes 167

7.4.4 Hydrological units and mixing depths 169

7.5 Conclusions 172

8. Chapter Eight: Hydrodynamics Quantification of groundwater fluxes using hydrological box model: Balancing the water budget of a semi-arid reservoir 174

8.1 Introduction 175

8.2 Methodology 177

8.2.1 Study site 177

8.2.2 Model description 179

8.2.3 Forcings and isotopic values 181

8.2.4 Model set-up 183

8.3 Results and discussion 183

8.3.1 Hydrological regime of the reservoir 183

8.3.2 Identification and qualification of the source using isotopes 188

8.3.3 Environmental implications and method limitations 194

8.4 Conclusions 196

9. Chapter Nine: Conclusions **197**

10. References **202**

11. Annexes **220**

Annexes 1 Al Jouz basin 220

Annexes 2 Sediments 221

Annexes 3 Soil cores 222

Annexes 4 Litani basin-Mid of the rainy season 224

Annexes 5 Litani basin-transition season 227

Annexes 6 Litani basin- End of the dry season 228

Annexes 7 Litani basin- First flush 230

Annexes 8 Litani basin- Piezometers 233

Annexes 9 Litani basin- Environnemental isotopes (δ18O ; δ2H) 234

Annexes 10 Publications 239

List of Figures

Figure 1.1 Map of Lebanon showing various land-use activities, which indicates the industrial-urban coast and the agricultural inland valley. Source: Lebanon Post–Conflict Environmental Assessment UNEP, 2007. 13

Figure 1.2 (a) Point and diffuse sources of pollution in the Upper Litani Basin, and (b) land-use cover surrounding the reservoir 16-17

Figure 1.3 Lebanese rivers watersheds, where the wastewater outfalls are denoted by red triangles. 19

Figure 2.1 Topographical map of Lebanon, and the geomorphological cross-section that shows different compartments. 28

Figure 2.2 Geological map of Lebanon... 28

Figure 2.3 The distribution of climatic different types (a) and the precipitation map of Lebanon (b).... 28

Figure 2.4 Land-use distribution of majorly economical activities (a), and agricultural practices (b) in Lebanon 29

Figure 2.5 Hydrographic basins in Lebanon, where the Litani basin is an agricultural used watershed (green), and Levantine basin is an industrial used watershed (red)..... 29

Figure 2.6 Superficial soil samples (S1-S4) in the industrial watershed (a), and the three different sampling zones river inlet (Ri), central zone (Cz) and dam zone (Dz) in the reservoir in agricultural watershed 33

Figure 2.7 Soil texture triangle (USDA) 40

Figure 2.8 Leaching columns system. 42

Figure 3.1 Proposed chemical structure of PG in the suspensions 52

Figure 3.2 Evolution of conductivity (a), and released sulfate (b), as a function of both citrate concentrations and pH. 55

Figure 3.3 Evolution of size distribution of PG suspensions and mean diameter of populations in 0.025 M citrate (a) and 0.05 M citrate (b), and potential zeta as a function of both citrate concentrations and pH (c) 59

Figure 3.4 Evolution of released metals for Pb (a), Zn (b), Cu (c), Cr (d) and Cd (e) as a function of both citrate concentrations and pH. 61

Figure 3.5 Evolution of infrared spectra regarding different intensity ratios I1/I0 and I2/I0 of PG suspensions as a function of citrate concentrations and of pH. 63

Figure 4.1 Sampling locations of soils and sediments in both agricultural and industrial watersheds. 70

Figure 4.2 Plots of (a) $^{208}Pb/^{206}Pb$ vs. $^{206}Pb/^{207}Pb$, and of (b) the inverse of Pb content vs. $^{206}Pb/^{207}Pb$ in the surface soils of the industrial area. 74

Figure 4.3 Vertical distributions of (a) Pb contents and (b) enrichment factors in an industrial soil core. 75

Figure 4.4 Vertical distributions of $^{206}Pb/^{207}Pb$ in (a) an industrial soil core and (b) a marine sediment core. 76

Figure 4.5 Plots of (a) $^{206}Pb/^{207}Pb$ vs.1/Pb content, and (b) $^{208}Pb/^{206}Pb$ vs. $^{206}Pb/^{207}Pb$ showing the mixing trend. All data refer to the industrial soil core 77

Figure 4.6 Seasonal distributions of (a) $^{208}Pb/^{206}Pb$ and (b) $^{206}Pb/^{207}Pb$ in lacustrine sediments of the agricultural watershed: Ri (river inlet), Cz (central zone) and Dz (dam zone). 79

Figure 4.7 (a) Correlation of Ca content with $^{206}Pb/^{204}Pb$ ratio for the agricultural lacustrine sediments and (b) plot of $^{206}Pb/^{204}Pb$ against $^{207}Pb/^{204}Pb$ showing the binary mixing of two endmembers.. 80

Figure 4.8 Plot of $^{208}Pb/^{206}Pb$ against $^{206}Pb/^{207}Pb$ showing the mixing trends for industrial and agricultural soils and sediments 82

Figure 4.9 Plot of $^{206}Pb/^{207}Pb$ vs. $^{208}Pb/^{207}Pb$ for samples from the agricultural and industrial watersheds, in comparison with values found in major Pb ores and leaded fuels (A, B, C) and regional aerosols 85

Figure 5.1 Study areas, where the industrial soil core (Ic) and agricultural soil core (Ac) and the bank core (Bc) localities are shown in the studied watersheds. 91

Figure 5.2 Plot of Fe/Al ratio and the plot of Fe vs. Al in agricultural soil (Ac) core (a and b) and core Bc retrieved from the reservoir bank (c and d respectively). 96

Figure 5.3 The comparison of (a) total organic carbon, (b) Cu, (c) Pb, (d) Cd content in the profiles of cores retrieved from soil (Ac) and reservoir banks (Bc) in the agricultural area.. . 98

Figure 5.4 Chronology of old core Ac (a) and modern core Bc (b) in the agricultural area, and core Ic (c) retrieved from the industrial area 101

Figure 5.5 Metal fluxes in the core Ac (a), core Bc (b) collected from the agricultural watershed and in core Ic (c) collected from the industrial watershed 103

Figure 5.6 Evolution of anthropogenic sources contribution percentages in industrial (Ic) and agricultural (Bc) cores (a), and the 206Pb/207Pb distribution in regard to anthropogenic and natural sources 106

Figure 5.7 Enrichment factor profiles for metals in soil cores retrieved from industrial (Ic) and agricultural (Ac) watersheds. 109

Figure 5.8 Physicochemical characteristics of soils from agricultural and industrial areas, grain size (a), functional groups (b) and mineralogy (c) 112

Figure 5.9 Cations and anions concentration in the leachates of soil packed columns of industrial soil (Ip). 115

Figure 5.10 Cations and anions concentration in the leachates of soil packed columns of agricultural soil (Ap). 116

Figure 5.11 Cd concentration in the leachates and the residual content in the top 10 cm of the packed soil columns of industrial soil (a, b,c) and agricultural packed columns (c,d,e); and the Pb behavior in the packed soil columns in industrial soil (g) and agricultural soil (h). 118

Figure 6.1 Characterization of reservoir lacustrine sediments, (a) grain size, (b) mineralogy, (c) elemental analysis, and (d) functional groups at the dam zone (Dz) during spill hydrological mode (September 2011) 128

Figure 6.2 Geochemical characterization and spatial variation in lacustrine sediments at Ri, Cz, and Dz during spill hydrological mode (November 2011). 130

Figure 6.3 Physicochmical characteristics of the water column during fill mode (April 2013), showing chmical stratification and the bottom water enriched by chemicals at the level of oxic hypolimnion at Dz. 133

Figure 6.4 Sediment characterization in fill (March 2012) and spill (November 2011) hydrological modes at dam zone (Dz). 135

Figure 6.5 Physicochmical characteristics of the water column during spill mode (October 2012), showing the presence of an anoxic hypolimnion and a flux of nutrients from resuspended sediments upward the water column at Dz. 137

Figure 6.6 Anthropogenic influence on the nutriens concentration in the reservoir during fill mode (March 2012) and their assimilation by primary productivity during spill mode (September 2012) at Dz. Epi denotes epilimnion (top 5 m), mix is mixilmnion (5-15 m), and Hypo is hypolimnion (the bottom water). 140

Figure 6.7 Vertical distributions of (a) temperature, (b) electrical conductivity, (c) chlorophyll-a, (d) dD, showing respectively thermal, chemical, biological and isotopic stratification, (e) reservoir eutrophication leading to biogenic preciptaion and alternation in the biogeochmical setings of the dam 141

Figure 6.8 Strong hydrological connectivity between reservoir (diamonds) and piezometers (triangles) during both fill (open symbols) and spill (filled symbols) and their rapid response to changes in the upper watershed (2011-2013). Data on piezometers (□) and reservoir water (●) during transition season in June 2012 are also shown. 143

Figure 6.9 Environmental isotopic ratios indicating the water infiltration from the reservoir (♦) to the adjacent piezometers (Δ) where Pb is remobilized from the sediment and migrates with reservoir water to groundwater in spill mode (October 2012) in Dz. 145

Figure 6.10 Reservoir vulnerability at the watershed scale and its capacity to retain and liberate chemicals, showing that endogenic process dominates over the watershed impact. Data were provided by the Litani River authority... 146

Figure 7.1 Sampling locations of the water columns collected in the river inlet (Ri), central zone (Cz) and dam zone (Dz) in the Qaraaoun reservoir, Upper Litani Basin 154

Figure 7.2 (a) Seasonal river inflow and water outflow from the reservoir during the study period (2011-2013), (b) Seasonal precipitation during the study period (2011-2013) 157

Figure 7.3 Historical annual records of electrical conductivity (Ec) and total dissolved solids (TDS) of surface water in the reservoir showing mineralization during the wet season. 158

Figure 7.4 Temporal variation of electrical conductivity and water isotopic signature of surface water, showing anti-correlation in between water mineralization and □18O and □2H during dry and wet seasons 160

Figure 7.5 Seasonal and spatial variation of Ec and hydrogen isotopic signature in the reservoir during second annual cycle 2012-2013 161

Figure 7.6 Evolution of environmental isotopes in the calm zone of the reservoir (Dz) over 2 annual cycles. The numbers indicate the profiles of various sampling campaigns (see text). 166

Figure 7.7 Isotopic response of the reservoir to changes in precipitation (histogram) and hydrodynamics, same characters represent the samples for each annual campaign, where closed and open characters resample samples in dry and wet seasons respectively 168

Figure 7.8 schematic diagram showing different hydrological zones and layers, and mixing depths in the reservoir. 171

Figure 8.1 Topography of the surroundings of Qaraaoun reservoir (a) and bathymetry of the reservoir under spill (b, 836 m a.s.l) and fill conditions (c, 858 m a.s.l) 178

Figure 8.2 Conceptual scheme of the Qaraaoun reservoir box model. All fluxes are reported with their corresponding symbol and that of their isotopic signature 180

Figure 8.3 Hydrological water budget of the reservoir, ignoring all interaction between the lake and groundwater. Input are represented by river flow (Fr) and precipitation (Fp) while outflow comprises the water withdraw (Fo) ,potential evaporation (Fevp), and evacuated excess water (Fevc) 184

Figure 8.4 The extension of water volume in the reservoir and in both epilimnion and hypolimnion (a), and the surface expansion of reservoir surface area (b) upon water level increase in the dam 185

Figure 8.5 The imbalanced water budget represented by the difference in actual water volume in the reservoir and the expected volume 185

Figure 8.6 The fluxes difference (in-out) and the accumulated volume change in the reservoir (a), source flux (b), and the response of water dynamics to source volume and water level in the dam (c). 187

Figure 8.7 The model simulations of water level (a), and the resulted output from increasing the intensities of mixed volumes (*GWm*) of the source (b), and the water residence time in the reservoir (c) 190

Figure 8.8 The isotopic response of the reservoir to the source flux intensities resulting from compatible isotopic signature with the surrounding piezometers (a), and the water residence time in the reservoir (b)..... 192

Figure 8.9 The model output that best fits the observation (a) and the water residence time in the reservoir (b)..... 193

List of Tables

Table 2.1 List of different industries in the agricultural watershed and their rejected contaminants 32

Table 2.2 Samples collected in the industrial and the agricultural watersheds. 34

Table 2.3 The geographical location and nature of samples in the agricultural watershed sampled over biannual years. 35

Table 3.1 Physicochemical parameters and the amount of metals released as a function of PG suspension load 53

Table 3.2 Chemical and physical characterization and the amount of metals released from PG suspensions in the presence of different citrate concentrations 56

Table 3.3 Physicochemical parameters and the amount of metals released of PG suspension with 0.1 and 0.2M citrate as a function of pH 57

Table 4.1 Characteristics, Pb contents, Pb isotopic ratios and excess 206Pb/207Pb of samples collected in the industrial and the agricultural watersheds 72

Table 4.2 Compilation of $^{206}Pb/^{207}Pb$ and $^{208}Pb/^{206}Pb$ isotopic ratios of anthropogenic and natural sources 83

Table 5.1 Pearson correlation coefficient between metals for soil core in agricultural watershed (Ac) 98

Table 5.2 Pearson correlation coefficient between metals for sediment core in agricultural watershed (Bc) 99

Table 5.3 Pearson correlation coefficient between metals for soil core in industrial watershed (Ic). 107

Table 5.4 Coordinates of the retrieved cores and the reference value (at 70 cm depth) used for normalization for each metal 108

Table 5.5 Physicochemical parameters for soil used in the Leaching columns experiment from both watersheds. 111

Table 6.1 Spatial variation of metal contents in the reservoir sediments during dry season 130

Table 6.2 Physicochemical characteristics of the water column at Dz during fill mode, showing the electrical conductivity and the concentration of certain dissolved elements ... 131

Table 6.3 Physicochemical parameters and mean concentration of dissolved elements in the epilimnion and hypolimnion, and the calculated execs % in Dz for both fill and spill mode135

Table 6.4 Physicochemical characteristics of the water column at Dz during spill mode, showing the electrical conductivity and the concentration of certain dissolved elements. .. 139

Table 6.5 Limnology of hypolimnion at Dz and the surrounding piezometers during spill hydrological mode. 144

Table 6.6 Physico-chemical parameters and dissolved metal concentrations in the incoming water and outgoing water of the reservoir during both fill and spill hydrological modes..... 147

Table 7.1 Physicochemical parameters and environmental isotopes ratios at Ri during dry and wet season 158

Table 7.2 Physicochemical parameters and environmental isotopes ratios at lateral slides of the reservoir during dry and wet seasons 162

Table 7.3 Physicochemical parameters and environmental isotopes of Cz and Dz at the end of Summer (Oct 2012) 164

Table 7.4 Physicochemical parameters and environmental isotopes of Cz and Dz during Winter (April 2013) 164

Table 8.1 Environmental isotopic notion of water entering the reservoir by the river, precipitation, evaporation, in the moisture and the estimated delta 18O of Qaraaoun reservoir 188

Table 8.2 Estimated delta 18O of the source depending on the intensity of the two-ways mixing between the groundwater and surface waters. 189

Table 8.3 Estimated flux intensity and delta 18O of the source for the best fit in 1st scenario, and the 2nd scenario relying on piezometers isotopic signature. 191

List of abbreviations

BOD: biological dissolved oxygen

COD: chemical dissolved oxygen

Cz: central zone

Dz: Dam zone

Ec: Electric conductivity

GMWL: Global meteoric water line

IAEA: International atomic energy agency

LCC: Lebanese chemical company

LLB: Lower Litani basin

LMWL: Local meteoric water line

LRA: Litani river authority

m a.s.l: Meters above sea level

m.a.s.l: Meters above sea level

MCM: Million cubic meters

MoE: Ministry of Environment

NIST: National institute of standards and technology

NPK 20 20 20: Fertilizer type constituted of nitrogen, phosphorous and potassium nutrients.

OCP: Organochlorine pesticides

PAHs: Polycyclic aromatic hydrocarbon

PCB: polychlorinated biphenyls

PDAC: Present day average crust

PET: Potential evapotranspiration

PG: Phosphogypsum (hemi-hydrated gypsum)

POPs: Persistent organic pollutants

PR: Phosphate rock

Ri: River inlet

TDS: Total dissolved solids

TOC: Total organic carbon

ULB: Upper Litani basin

V-SMOW: Vienna Standard Mean Ocean Water

δa: Delta notion of atmospheric nature

δevp: Delta notion of evaporation

δL: Delta notion of the top layer of the reservoir

δp: Delta notion of precipitation

δQ: mean delta notion of Qaraaoun reservoir

δr: Delta notion of the river inlet

δs: Delta notion of the source

Abstract

Lebanon is situated in a Mediterranean semi-arid region rich in hydraulic resources but strongly under the impact of anthropogenic pressure, mainly after the industrial boost in the last 50 years. In this thesis our research is devoted to the study of water resources and the assessment of soil pollution in two contrasting watersheds that may resemble similar regions in the world. Rivers act as a collective funnel of contaminants derived from rock weathering, industrial, agricultural and urban practices. Thus we focus our study on the two main contrasting watersheds in Lebanon: an industrially dominated watershed located northwest of the country on the Mediterranean coast (Al Jouz basin), and a rural historically agricultural watershed that lies in the continental valley between the two mountainous chains (Litani basin). Geochemical analysis coupled to multi-isotopic applications was used as tools to investigate the collective influence of land-use cover, geomorphological processes, topography, soil type, geology, geography, orography, climate, and hydrological variability on drainage basin evolution. A two-year sampling strategy was followed (2011-2013) to collect not only water samples at various depths in the reservoir and in the piezometers, but also sediments (lacustrine, riverine and coastal) and soils (surficial and cores) to cover seasonal variations (rainy, first flush and dry seasons) in both studied areas. The results highlight the entire mechanism of characterization, origin, and partitioning between the dissolved and particulate phases of pollutants. Furthermore, the environmental implication of the Qaraaoun reservoir was assessed by emphasizing water hydrodynamics and its interaction with the watershed. Characterizing industrial and agricultural pollution allows the understanding of metal behavior and the prediction of its fate, in association with the environmental receiving media in semi-arid and Mediterranean areas. This work was the first to trace pollution sources and to reconstruct the metal fluxes in two of the most environmentally significant watersheds in the country. Stable and radioactive Pb isotopes were used in addition to ^{137}Cs to study the geomorphological influence and the chronology of the environmental stress exerted by the factory and the dam on basin ecology. Moreover, the nature of the Qaraaoun reservoir and the internal hydrological dynamics were explored using stable hydrogen and oxygen isotopes to delineate the reservoir water layers and its fast response to meteorological and hydrodynamic changes in the watersheds, and to demonstrate its strong hydrological connectivity with groundwater. Reservoir water balance was made, indicating groundwater influx into the reservoir which was reported for the first time. The water hydrodynamics was also assessed using a box model, which in its role can be used to evaluate the reservoir water balance and hydro-project functionality and to establish the basis for water sustainability in the long term. This work has yielded a better understanding of biogeochemical processes under different environmental conditions. The treated issues in this thesis will provide a foundation for future hydropower projects and allow one to draw a road-map for national management plans, and to raise the alert for remediation processes and management methods to preserve the environment and resource sustainability, and ultimately the wellbeing of the local population.

Résumé

Le Liban est situé dans une région méditerranéenne semi-aride riche en ressources hydrauliques mais fortement sous l'influence de la pression anthropique, principalement après la révolution industrielle de ces 50 dernières années. Dans cette thèse, notre recherche est consacrée à l'étude des ressources en eau et l'évaluation de la pollution des sols dans deux bassins versants contrastés qui peuvent ressembler à des régions similaires dans le monde. Les rivières agissent comme un entonnoir de collecte des contaminants provenant de l'érosion des roches, des pratiques industrielles, agricoles et urbaines. Ainsi, nous concentrons notre étude sur les deux principaux bassins versants contrastés au Liban: un bassin versant industriel situé au Nord-Ouest du pays, sur la côte méditerranéenne (bassin Al Jouz), et un bassin ayant un passé historique agricole et rural qui se trouve dans la vallée continentale entre deux chaînes montagneuses (bassin du Litani). L'analyse géochimique couplée à des applications multi-isotopiques a été utilisée comme outil pour étudier l'influence combinée de la couverture du territoire, des processus géomorphologiques, de la topographie, du type de sol, de la géologie, de la géographie, de l'orographie, du climat et de la variabilité hydrologique sur l'évolution du drainage du bassin. Une stratégie d'échantillonnage de deux ans a été suivie (2011-2013) pour recueillir non seulement des échantillons d'eau à différentes profondeurs dans le réservoir et dans les piézomètres, mais aussi les sédiments (lacustre, fluvial et côtier) et des sols (surface et carottages) pour couvrir les variations saisonnières (saison des pluies, première chasse d'eau et saisons sèches) dans les deux zones étudiées. Les résultats mettent en évidence l'ensemble des mécanismes influençant la caractérisation, l'origine et la répartition entre les phases dissoutes et particulaires des polluants. En outre, l'implication de l'environnement du réservoir Qaraaoun a été évaluée en soulignant l'hydrodynamique de l'eau et son interaction avec le bassin. La caractérisation de la pollution industrielle et agricole permet de comprendre le comportement des métaux et de prédire leur devenir, en association avec le support de réception de l'environnement dans les zones semi-arides et Méditerranéens. Ce travail a été le premier à retracer les sources de pollution et à reconstituer les flux de métaux dans deux des bassins versants les plus importants du pays. Les isotopes stables et radioactifs du Pb ont été utilisés, ainsi que le ^{137}Cs, pour étudier l'influence géomorphologique et la chronologie de la contrainte exercée par l'environnement de l'usine et le barrage sur l'écologie du bassin. En outre, la nature du réservoir du Qaraaoun et la dynamique hydrologique interne ont été examinées à l'aide des isotopes stables d'hydrogène et d'oxygène pour délimiter les couches d'eau du réservoir et sa réponse rapide aux changements météorologiques et hydrodynamiques dans les bassins versants, et pour démontrer sa forte connectivité hydrologique avec les eaux souterraines. Le bilan des eaux du réservoir a été établi, mettant en évidence pour la première fois un flux d'eaux souterraines vers le réservoir. L'hydrodynamique de l'eau a également été étudiée en utilisant un modèle de boîte (box model), qui, peut être utilisé pour évaluer le bilan des eaux du réservoir et la fonctionnalité hydro-projet

et peut constituer une base de gestion durable de l'eau à long terme. Ce travail a permis de mieux comprendre les processus biogéochimiques dans différentes conditions environnementales. Les problèmes traités dans cette thèse fourniront une base pour de futurs projets hydroélectriques et permettront d'établir une feuille de route pour les plans de gestion nationaux, et à donner l'alerte pour les processus d'assainissement et des méthodes de gestion pour préserver l'environnement et la durabilité des ressources, et, finalement, pour le bien-être de la population locale .

CHAPTER 1
INTRODUCTION

1.1. Rationale and objectives

Lebanon is situated in a Mediterranean semiarid region rich in hydraulic resources but strongly under the impact of anthropogenic pressure, mainly after the industrial boost in the last 50 years. In this thesis our research is devoted to the study of water resources and the assessment of soil pollution in two contrasting watersheds that may resemble similar regions in the world. Rivers act as a collective funnel of contaminants derived from rock weathering and industrial, agricultural, and urban practices. Thus we focus our study on the two main contrasting watersheds in Lebanon: an industrially dominated watershed located northwest of the country on the Mediterranean coast (Al Jouz basin), and a rural historically agricultural watershed that lies in the continental valley between the two mountainous chains (Litani basin).

The Levantine basin (Al Jouz basin) is an industrial area where the inorganic fertilizer factory was established in 1956 on the Lebanese Mediterranean coast, and acts as an active passage to link the North with the capital Beirut. The factory produces for each ton of phosphate fertilizers 5 tons of phosphogypsum (PG, hemi-hydrated gypsum) waste products, rich in heavy metals and radioactive materials. The industrial wastes are either discharged to the sea via the liquid industrial effluents or stored next to the production site on the seashore without any pretreatment. The Litani basin is the largest agricultural watershed in Lebanon, where the 170-km River terminates at a dam constructed in 1955 as part of the national water management plan to irrigate more than 22000 hectares of cultivated land and to produce hydropower. The river main course, tributaries, and the reservoir, are under direct and indirect environmental stress of socio-economical activities in the upper basin.

The main interest of this study was to investigate the collective influence on drainage basin evolution of land-use cover, geomorphological processes, topography, soil type, geology, geography, orography, climate and hydrological variability. These processes control the behavior of contaminants in a particular receiving environment, and in turn the water and soil quality. In addition, we have explored the significant impact of discrete factors such as soil type, and pollution type and level, on the fate of contaminants in the two hydrographic basins studied. Furthermore, the matching date of the factory establishment and the dam construction can be of great interest, since this coincidence will allow the pollution flux chronology to be referred to the same period and to examine the contaminant behavior in different environmental contexts.

Our main objective is to investigate the impact of land-use on the watershed (agricultural vs. industrial) by applying a multi-isotopic approach coupled with geochemical analyses as a tool to trace the sources and the pathways of pollutants and to predict their behavior and fate in a particular basin. This research will focus on the pollutant characterization, origin, and partitioning between the dissolved and particulate phases. This will improve our understanding of biogeochemical processes taking place under different environmental conditions. Moreover, the environmental implication of the reservoir is assessed by highlighting the water hydrodynamics and its interaction with the watershed. The particularity of this work lies in characterizing the pollution and understanding the associated environmental context in semi-arid and Mediterranean areas that has a deficiency in this field of research. Such areas are subjected to severe climate changes and desertification and are in great need to preserve present-day hydraulic resources and implement future hydro-projects. The treated issues in this thesis will provide a foundation for future hydropower plans. It will allow the authorities to draw a road-map for national management strategies and to raise the alert for remediation and management methods to preserve the environment and resource sustainability, and ultimately the wellbeing of the local population.

1.2 Previous international geochemical studies

1.2.1 Chemical species used to trace pollutants in water bodies under the impact of industrial and agricultural activities

Numerous studies were conducted to investigate both natural and anthropogenic impacts on water quality worldwide. Surface water-groundwater interaction was also observed in global basins (Yin et al., 2011; Petelet-Giraud et al., 2007; Singh et al., 2010; Cartwright et al., 2012; Diaw et al., 2012). So far, scientists have been interested to evaluate the impact of diverse land-use activities (agriculture, urbanism, industry and forestry) mainly on open water systems such as rivers, lagoons, and lakes (Delfino, 1976; Rhodes et al., 2001; Lavilla et al., 2006; Fitzpatrick et al., 2007; Mouri et al., 2011). Land-use plays an important role in identifying the ID of contaminants distributed in watersheds (Yuan et al., 2011). As a consequence, a list of organic and inorganic elements associated to natural and anthropogenic practices were established to be used as tracers for pollution in hydrographic basins.

Nutrients like nitrogen and phosphorous are used to trace anthropogenic pollution and to evaluate contamination levels (Yuan et al., 2011, Mouri et al., 2011). Nitrogen species including nitrate, nitrites and ammonia are mainly investigated to address agrochemical contamination exerted on watersheds (Ocampo et al., 2006). Agricultural practices and agrochemical applications act as a main player in polluting arid areas which will lead to surface water eutrophication and groundwater contamination. Nitrogen isotopes were used as a tool to trace and document agricultural contamination as well (Vitoria et al., 2004). Chloride and bromide levels in surface water and groundwater aquifers were primarily associated with urbanism and agricultural practices, where higher concentrations were

detected during wet season and in aquifers with shallow water table (Mullaney et al., 2009). Likewise, sodium and chloride fluxes to water bodies increased with population density and land-use cover, derived mainly from septic tanks, re-infiltration of water used for irrigation, industrial practices and leaching from cement infrastructure (Steel and Aitkenhead-peterson, 2011). Contaminants from household effluents, agrochemicals, and coal combustion were traced by S, C and Sr isotopes coupled with nutrients such as Cl^-, NO_3^-, SO_4^{2-} and Na^+. It has been shown that rivers and groundwater are highly contaminated by anthropogenic activities derived from both agricultural and industrial practices (Li et al., 2010).

In contrast, organic contaminants are strictly associated with anthropogenic activities and human lifestyle, and they reach water bodies by storm runoff, and industrial and household effluents. Emerging organic compounds including estrogen, pharmaceuticals, drugs, and pesticides have been measured and monitored in both surface water and groundwater (Jurado et al., 2012; Lapworth et al., 2012; Meffe and De Bustamante, 2014) that reflect recent and historical anthropogenic activities over the watersheds. Persistent organic pollutants or the so called POPs have received a great deal of attention due to its hazard and toxicity in the environment; this family of man-made organic compounds comprises 12 different organochlorine composites. Three main compounds are wildly used as tracers for anthropogenic contamination in water bodies: organochlorine pesticides (OCP), polychlorinated biphenyls (PCB), and polycyclic aromatic hydrocarbon (PAHs) (Fu et al., 2003, Wang et al., 2009). Furthermore, in addition to PCBs, dichlorodiphenyltrichloroethane (DDT) and sterol biomarkers were used as unconventional tracers to investigate hydrological route and contamination transport to rivers and seas (Kannan et al., 2012). Molecular tracers were found to be effective chemicals to trace the origin of contamination sources at the level of the watershed, such as consumer product fragrance materials (galaxolide and tonalid used in detergents), petroleum derivatives and combustion byproducts (Standley et al., 2000).

Reactive compounds such as ammonium, strontium, and atratone in addition to non-reactive tracers like uranine, bromide, and naphthionate were used to trace urban roof runoff. Non-reactive tracers showed a week sorption abilities and fast infiltration to aquifers highly hydraulic connected with surface water (Ammann et al., 2003). Certain chemicals like organic wastewater contaminants (chelating agents, surfactants, steroids, pharmaceuticals, and hormones), pesticides, and endocrines in addition to inorganics such as boron, gadolinium and lithium are considered as efficient tracers to identify pollutants derived from anthropogenic activities (Barber et al., 2006). A particular study was conducted to distinguish between fecal coliforms of human and animal origin in water from storm sewer outflows to a coastal lake, relying on several chemical tracers such as anionic surfactants, fluorescence whitening agent, fluoride and caffeine. Caffeine and fluoride were found to be reliable tracers for human implication in the aquatic environment (Sankararamakrishnan and Guo, 2005).

Metals are extensively used as tracers in environmental problems due to their amplified hazard on ecosystem in minor concentrations, and their ability to distinguish the natural from the anthropogenic pollution sources (Benoit and Rozan, 2001; Clark et al., 2014).

Researchers believed that metal fluxes should be documented to better understand micropollutants dynamics in watersheds, and recently stable isotopes became a tool to assess the contamination of micropollutants in water systems. Thus in order to improve our understanding of the dynamics and origin of the sources and to explore the fate of contaminants, chemical analyses together with isotopic fractionation studies are applied to investigate environmental problems in watersheds. Industrial practices discharge an important load of metals, and their permanent flux into aquatic basins will cause enrichment of trace metals in water and sediment (Gupta et al., 2011). As a consequence, metals are being monitored in river basins to investigate the impact of industrial and agricultural practices on watersheds. Seasonally dependent metal flux is related to human life style and diverse land-use activities that reflect different pollution sources (Duman et al., 2007). In addition, spatial and seasonal metal fluxes are accompanied by different environmental conditions that may increase metal hazard such as their toxicity during dry season (Stein and Tiefenthaler, 2005). Furthermore, tracing atmospheric deposition is accomplished by measuring metal concentration in pristine lakes (Lavilla et al., 2006).

Contamination of metals such as Cd, Cu, As, Cr, Hg and Fe transported by a network of tributaries to the main river course and lake reflect land-use activities (Poulton, 1992; Tuna et al., 2007). Metals such as Fe, Pb, Zn and Mn in surface waters can be attributed to industrial activities, while other metals such as Cu and Cd are strongly associated with agrochemical applications (Aprile et al., 2010; Ebrahimpour and Mushrifah, 2008). Analysis of metals can be coupled to that of stable isotopes (δ^2H, $\delta^{18}O$, $\delta^{15}N$, $\delta^{13}C$) and hydrochemical indicators in water systems such as major ions (Na^+, K^+, Mg^{2+}, Ca^{2+}, Cl^-, SO_4^{2-}, HCO_3^-) to precisely trace the origin of pollution sources in hydrographic systems (Asante et al., 2008; Carey et al., 2013; Li et al., 2014). Chromium isotopes were used as a tool to quantify anthropogenic Cr reduction in natural waters, and certain studies used Sr as a conservative tracer that could constrain metal and isotopic measurements (Vitoria et al., 2004; Ebrahimpour and Mushrifah, 2008).

Lakes and reservoirs are a key player in hydrological water cycle; these water bodies reveal the interaction between surface water and groundwater and could act as a sink of natural and anthropogenic fluxes that will interfere with the total nutrient budget in basins (Froehlich et al., 2005). As a consequence, scientists established the foundations of environmental isotope applications in the last 60 years in order to understand the hydrogeochemical cycles and regulate enactments for both water and waste management (Masson and Meilliez, 2008; Wei et al., 2009; Hoefs, 2009; Meredith et al., 2009; Akin et al., 2010). Water stable isotopes ($\delta^{18}O$ and δ^2H) became a strong tool to investigate hydrological processes such as addressing water sources, tracing water flow dynamics, and defining mixing patterns resulting from seasonal and spatial variations. Water isotopic signature is the outcome of evaporation and mixing of rain water with the existing water body (Petelet-Giraud et al., 2007). Small lakes and reservoirs are much more sensitive to climate and anthropogenic changes, where water stable isotopes are used to fill hydrogeological gaps, to trace water sources and its pathways over a specific watershed (Butler, 2007; Kumar et al., 2008; Singh et al., 2010). Furthermore,

it is a promising approach in studying lakes and groundwater recharge due to its conservative capabilities and resistance to rock-water interactions (Grünberger et al., 2004; Froehlich et al., 2005; Petelet-Giraud et al., 2007; Gibson and Reid, 2010; Wassenaar et al., 2011; Al-Charideh, 2012). Multi-isotopic approaches of measuring $\delta^{18}O/\delta^{2}H$, $^{3}H/^{3}He$, ^{85}Kr, coupled to chloroflurocarbons (CFCs) and hydrochemicals were performed to determine recharge areas and hydrological routes of contaminants derived from agricultural and urban practices at the watershed scale (Kaown et al., 2009; Kralik et al., 2014). Furthermore, coupling water isotopes (oxygen and deuterium) to CFCs indicated the significance of local human influences on groundwater quality (Qin et al., 2011).

1.2.2 Chemical species used to trace pollutants in soils and sediments

In the past decades, additional land areas were engaged to meet the demands of increasing population, and the needs for water, food, and residence. Thus, population growth and industrial revolution exert an environmental stress on watersheds worldwide, and many socio-economical challenges arise. Diverse land-use activities such as urbanism, agricultural practices, industries and mining consume natural resources and reject the contaminants to different receiving media. Dissolved metals in the aquatic system do not usually exist for long periods of time, it's either associated with colloids or fixed by the organic matter and mineral fractions in the sediments (Ebrahimpour and Mushrifah, 2008). Soils and sediments contain environmental archives by which pollution stress history and pollutant behavior as reflected by both seasonal and annual fluxes are well recorded, and can be revealed by coupling geochemical analysis to isotopic approaches (Kober et al., 1999; Fagel et al., 2010; Izquierdo et al., 2012).

Previous studies used soil and sediment metal contents (Ni, V, Zn, Cu, Cr, Co, As, Mo and Pb) to evaluate the influence of land-use activities on watersheds (Alaoui et al., 2010; Shakeri and Moore, 2010; Gupta et al., 2011). In urban and industrial watersheds, Sb and As were attributed to industrial smelters, sewage outfalls and agrochemical usage (Filella et al., 2002; Baeza et al., 2010). Pb and Zn were also related to population density and anthropogenic activities which document street runoff and industrial practices such as manufacturing of plastics, ceramics, paper, tires and metalloids (Callender and Rice, 2000). Moreover, Cu, Mn, Zn, Pb and Hg indicate the atmospheric deposition and anthropogenic sources of contamination in surface soils (Blais and Kalff, 1993; Bookman et al., 2010; Herndon et al., 2011). Mikac et al., (2011) demonstrated that multi-elemental analysis could be an effective tool to investigate anthropogenic effect and discriminate it from lithogenic sources, and they coupled metal analysis to organic tracers such as PAHs. PAHs are significant anthropogenic contaminants used as tracers to characterize land-use impact on soil pollution. It was found that PAHs are mainly derived from pyrogenic practices and fossil fuel combustion associated with industrial and urban zones (Banger et al., 2010).

Geochemical indicators coupled with isotopic applications are used to trace the origin of pollutants in soils and sediments (Chappaz et al., 2008). Unconventional metal stable isotopes were recently applied to environmental studies for Cu, Zn, Fe, Se, Mo, Cr, Hg. Mercury is

considered as a promising tracer for natural and anthropogenic sources of Hg pollution and fractionation cycle in different environmental context (Yin et al., 2010). Stable isotopes of Zn and Cr were used to document metal sources in nature (Thapalia et al., 2010). Additionally stable Pb isotopes and radioactive ^{210}Pb with ^{210}Po were used in parallel with inorganic carbon, organic carbon and nitrogen as geochemical tracers to investigate agro-industrial pollutions (Bookman et al., 2010; Fagel et al., 2010)

In order to address the origin of metal contamination and to investigate its magnitude, most researchers rely on Pb isotopic signatures in soils and sediments. Pb has a high stability and affinity to accumulate in top soils (Stille et al., 2011). Most studies show that Pb is enriched in the upper layer of the soil column and is associated with organic matter due to its continuous loading, whose concentration then decreases with depth. Mostly Pb is linked to mineral phases such as iron oxides followed by carbonates, and finally a small fraction is trapped in the residual fraction (Stone and Droppo, 1996; Harlavan et al., 2010; Wong and Li, 2004). Pb isotopic ratios depend on the uranium/thorium concentration and the age of the original material, since Pb is the decaying daughter atoms of uranium and thorium (Komárek et al., 2008; Harlavan et al., 2010; Bird et al., 2010). Pb isotopes are considered as a robust tool, frequently used by researchers due to its high precision and resistance to biodegradation and physicochemical fractionation (Hu et al., 2011). It is thus an ideal approach to trace the contamination source and its pathway (Komárek et al., 2008; Zhu et al., 2010).

Environmental scientists unlike geologists rely on ^{206}Pb/^{207}Pb ratios due to their abundance, and the precise distinction between natural and anthropogenic sources, which is not affected by the mineral composition of the sample (Roussiez et al., 2005; Komárek et al., 2008). Pb isotopes have been determined to trace the contamination source and evolution in different environmental context: coastal and marine sediments (Roussiez et al., 2005, Abi Ghanem et al., 2009, Harlavan et al., 2010), superficial soils (Hansmann and Köppel, 2000; Erel and Torrent, 2010; Schucknecht et al., 2011; Izquierdo et al., 2012), soil and sediment cores (Farmer et al., 1997; Chillrud et al., 2003, Fagel et al., 2010, Frostick et al., 2011), riverine sediments (Bird et al., 2010) and lacustrine sediments (Kober et al., 1999; Östland and Sternbeck, 2001, Hu et al., 2011; Escobar et al., 2013), peat bogs (Kylander et al., 2005), tree rings and plants (Othman et al, 1997; Bindler et al, 2004) and even ice cores (Hong et al., 2011).

Environmental scientists agreed that the ^{206}Pb/^{207}Pb isotopic ratio of the natural crust or so called PDAC (Present Day Average Crust) is 1.20 and values below this ratio down to 0.96 are considered as anthropogenic (Harlavan et al., 2010; Frostick et al., 2011). Many scientists agreed that leaded gasoline was the major source of Pb contamination (Kober et al., 1999, Hansmann and Köppel, 2000; Bollhöfer and Rosman, 2002; Harlavan et al, 2010), exhibiting the least radiogenic signature among anthropogenic sources (Hansmann and Köppel, 2000), followed by smelting, mining, industrial activities and agricultural practices (Izquierdo et al., 2012). After the industrial revolution and the increased usage of organo-Pb in tetra ethyl fossil fuel as an additive for gasoline at the beginning of the 1920s (Östlund and Sternbeck

2001), along with vast industrial applications, the eastern Mediterranean acts as a second point source of Pb contamination for the Atlantic ocean (Harlavan et al., 2010).

^{210}Pb chronology is a very common method used to study the anthropogenic signature on a sediment or soil profile. Radioactive ^{210} Pb dating is able to reconstruct pollution history, and ^{137}Cs dating is used in parallel to constrain sediment accumulation rates in soil and sediment cores (Appleby and Oldfield, 1983; Benoit and Rozan, 2001; Dabous, 2002; Ruiz-Fernández et al., 2007; Liang et al., 2014). ^{210} Pb is a naturally occurring radionuclide decayed from ^{238}U with a half-life of 22.3 years. There are two types of ^{210}Pb, the supported and unsupported Pb. The supported type is naturally found in soils from decayed ^{222}Rn and ^{226}Ra. While the unsupported type or so called excess is derived from atmospheric deposition. Following the decaying law, unsupported ^{210}Pb declines with age in sediment layers of a core, thus it allows the estimation of sediment accumulation rate (Appleby and Oldfield, 1983).

The occurrence of anthropogenic fallout of ^{137}Cs with a half-life of 30.14 years is associated with nuclear weapon testing (1950s) and is measured together with ^{210}Pb since they report two different measurements for sediment burial in the same soil or sediment core (Ruiz-Fernández et al., 2007). Metal fluxes and ^{210}Pb chronologies were investigated by Clark et al., (2014) in two contrasting man-made lakes in the USA, one situated in forest and the other in a watershed with modern high residential and industrial areas. The authors showed that the geomorphological context of the watersheds played an important role in sediment accumulation rate even in the pristine watershed, and their results indicated the influence of the recent urbanized areas, and industrial activities in addition to atmospheric deposition.

1.2.3 The inter-mechanism of the partition between the dissolved and particulate phases of contaminants during precipitation and remobilization

Heavy metals in water systems could partition between the water and the solid phases in the form of suspended mater and sediments. Speciation of heavy metals may occur upon their association with different organic and inorganic ligands and precipitate, which may aid in water self-purification since sediments will entrap hazardous metals (Korfali and Davies, 2005; Gupta et al., 2011). The fate of chemicals in aquatic systems is dependent on their transport mechanism, solute mixing and redox potential (Peretyazhko et al., 2005). Blais and Kalff (1993) classified the reactions that are able to remove elements from aquatic systems into two categories; adsorption reactions by cation exchange or ligand exchange, and precipitation reaction with oxides and carbonates (Blais and Kalff, 1993). In addition, biological process plays an important role in controlling the fate of metals in both water and sediments (Sigg et al., 1995; Audry et al., 2010).

In order to trace contaminants and their fate in aquatic environments, scientists rely on sediments as a tool to document chemical behavior in different aquatic conditions (Duman et al., 2007; Alaoui et al., 2010; Yuan et al., 2011). Sediments represent a potential reservoir for contaminants brought in by rivers, surface runoff and atmospheric deposition (Callender and Rice, 2000; Roussiez et al., 2006; Yuan et al., 2007). Thus, river, lake, and sea bottom-

sediments may act as a sink for contaminants derived from the upper watershed in the form of suspended matter (Skoulikidis et al., 2008; Hiller et al., 2010; Akin et al., 2010). Nutrients and metal adsorption onto particulate phases are controlled by multivariante factors such as pH, temperature, electric conductivity, redox state, sediment texture, cation exchange capacity (CEC), contamination magnitude and organic matter content (Mortimer and Raeà, 2000; Morford et al., 2001; Miao et al., 2006; Audry et al., 2010; Hiller et al., 2010; Gupta et al., 2011). Metals have a high affinity to be adsorbed to sediments where redox conditions controls metal speciation (Gupta et al., 2011). Any changes in these factors could liberate the sorbed chemicals to the water system (Hiller et al., 2010). Metals that are associated with the residual or refractory fraction are more stable in the sediment matrix (Gupta et al., 2011).

Under anoxic conditions, natural (humic acid) or anthropogenic organic substances (EDTA) and minerals are able to scavenge metals from the water column and embed it on its lattice (Jiann et al., 2005; Chappaz et al., 2008). Each metal has its distinctive behavior and its interaction with ligands and colloids in aquatic systems (Jiann et al., 2005). For example, Cu forms a strong complex with organic matter while Zn is mostly present in the aqueous phase (Sigg et al., 1995). However, the mobility of most metals (Cu, Zn, Cr, Pb and Ni) increases in oxic conditions and reduced in anoxic alkaline conditions except for As which becomes more labile under anaerobic conditions (Hartley and Dickinson, 2010). The adsorption and co-precipitation of As, Cr, Hg, and Ni are associated with Fe oxyhydroxides unlike Co that is controlled by Mn oxyhydroxides (Rigaud et al., 2013). The adsorption of metal to organic matter or minerals such as iron or manganese oxides is limited by the presence of ligands in the system (Sigg et al., 1995). Under oxic conditions Fe/Mn hydroxides and/or Fe/Zn sulfides are the major players to scavenge trace metals from the water column and co-precipitate them in the sediment matrix (Audrey et al., 2010; Rigaud et al., 2013). During early diagenesis influenced the organic matter input, redox-sensitive metals such as Fe and Mn maybe altered causing their re-precipitation with other mineral fractions (Mortimer and Raeà, 2000).

The physiochemical properties of the water column and sediments in addition to the metrological and hydrodynamic particularities of the watershed may cause the sediment to resuspended and act as a source of contaminants thus impacting the overlying water quality (Miao et al., 2006; Atkinson et al., 2007; Yuan et al., 2007; Chon et al., 2012). In other words, the geochemical interaction at the sediment-water interface may trap the chemicals in the sediments, or it could release them upward to the overlying water column or downward to the groundwater ultimately (Wildi, 2010; Kraus et al., 2011; Banks et al., 2012). Any changes in physicochemical parameters such as pH and redox gradient would alter the flux of chemicals across the water-sediment interface (Hiller et al., 2010).

Metals such as Mn, V, Mo, U, and Cd are more sensitive than other metals to oxic-anoxic alternations at the sediment-water interface, by which sediments rich in organic matter in oxic conditions will lead to their mobility and remobilization (Morford et al., 2001). Dissolved Pb is more influenced by changes in dissolved oxygen, salinity, conductivity and redox state in the water column, thus it maybe adsorbed faster to finer grained particles and transferred to

the sediments (Ekpo and Ibok, 1998). Mo in the iron hydroxide fraction was found to be mobilized when it is subjected to reduction during which Mo is partially released to the water (Chappaz et al., 2008). The acidic pH in sediment matrix as a result of redox reactions will lead to the release of dissolved metals such as Pb, Ca, Mg, Al, and Zn to the aquatic systems (Miao et al., 2006). Moreover, organic matter was found to enhance the remobilization of Cu and Pb while acid volatile sulfides showed efficient immobilization of Zn, thus it is crucial to investigate sediment intrinsic properties to understand the metal behavior (Durán et al., 2012). Similarly, Fe, Mn and As are highly associated with acid volatile sulfides and resuspended from the anoxic sediments to the oxic overlying water column (Saulnier and Mucci, 2000). This study further highlighted the importance of mechanical resuspension of fine sediments due to dredging activities and waves in the behavior of metals (Saulnier and Mucci, 2000). In addition to hydrodynamics, redox shifts, and sediment characteristics, metals associated with suspended particles play an important role in metal lability at the sediment-water interface. The anthropogenically derived metals (Pb, Zn, Cd, and Cu) were found to be associated with more labile phases such as sulfides and easily mobilized to the water column compared to those derived from lithogenic origins which are associated with the refractory phases (Argese et al., 1997).

1.3 National studies

1.3.1 Similar geochemical studies conducted in Lebanon on point and diffuse sources of pollutants

Nonpoint or diffuse sources of pollution in Lebanon are represented by the domestic waste discharge, leakage of septic tanks, untreated solid and liquid waste disposal, surface runoff, atmospheric deposition, vehicles emission, farms and agricultural practices (Khair et al., 1994; Korfali and Davies, 2000; Jurdi et al., 2002; Korfali and Davies, 2004; Waked and Afif, 2012; Shaban, 2014). Direct discharges of industrial effluents and wastewater from treatment plants into water bodies act as a point source of pollution in the country (Greenpeace, 1998; Korfali and Davies, 2000; El Fadel et al., 2003; Moussa et al., 2006; Aoun et al., 2010; Bou Kheir et al., 2010; Geara et al., 2010).

An estimation of 3800 ton/day of solid waste is disposed in Lebanon, including normal domestic wastes, batteries, and hazardous hospital and industrial wastes. Industrial solid wastes alone are estimated to be 326000 ton/year mostly generated in Mount Lebanon and the capital Beirut. However, liquid industrial wastes in some industrial factories on the coast and inland discard their untreated effluents directly to the Mediterranean Sea and adjacent river streams respectively. Moreover, some industrial units permit their waste effluents to indwell in inland boreholes thus contaminating the groundwater as well as surface water bodies and thus threatening the water quality. Toxic trace metals and chemicals were documented in leachates of industrial effluents and dumpsites in the North and in Beirut; in addition both groundwater and marine water close to coastal industrial factories in the North were

contaminated by industrial effluents (Greenpeace, 1998). The industrial firms are mainly located on the Lebanese coastal shore (80%) from Tripoli in the North passing by Beirut and reaching Saida in the South (Greenpeace, 1998) as shown in Figure 1.1.

Figure 1.1: Map of Lebanon showing various land-use activities, which indicates the industrial-urban coast and the agricultural inland valley. Source: Lebanon Post–Conflict Environmental Assessment UNEP, 2007.

Pollution point sources on the coast such as the Lebanese Chemical Company (LCC), a phosphate fertilizer factory situated in the Levantine basin on the Northern Lebanese coast, classified in 1997 by Ecodit-Iaurif as one of the top ten effective industrial factories in the country. Coastal marine sediments collected in summer 2003 were found to be under the direct effluent of the plant outlet. Inorganic phosphate enrichment in marine sediments ranges between 8068 and 64256 µg PO4/g at the direct reaches of the outlet (NW), while at the eastern sides it ranges between 597 and 2279 µg PO4/g where industrial effluents hydrodynamics overage natural ones (Fakhri et al., 2008-2009). The impact of PG stockpiles on the surrounding area near the phosphate fertilizer industry was investigated in 2006-2007 by Aoun et al., (2010). Leaching, atmospheric depositions and wind dynamics were found to be the main factors controlling the transfer and mobilization of trace elements from PG to sediments and soils. Metals were enriched in the fine size fraction of the soil, were Cr enrichment was reported to be 100 times, and followed by Cu (32), Pb (15), and Zn (10). Moreover, measured radioactive ^{210}Po activity was 100 Bq/kg in most samples with an enrichment factor of 56 times. However, the authors did not take into account the variability of the soils, sediment properties, and the particularity of the receiving area.

In 2006, marine sediments from three coastal areas of different land-use activities were explored. The first core was taken from Akkar which was assumed to be a remote area not affected by anthropogenic contamination since Pb content in sediments is within the shale background values (6-16 ppm); however, Pb isotopes indicated an anthropogenic signature. The second core was retrieved from a very active area with high population density in the Dora bay where high anthropogenic contamination was reflected on Pb isotopes signatures (^{206}Pb/^{207}Pb: 1.16-1.17). The third sampling location was in front the fertilizer factory in Selaata where sediment profiles indicated a high variability with depth (30 cm) and represented a high isotopic ratio (^{206}Pb/^{207}Pb: 1.25-1.6). Furthermore, elemental analyses indicated the presence of PG and fluorite in the sediments related to the effluents discharged from the factory (Abi Ghanem et al., 2009). Phosphate fertilizer factory emissions were found to possess a potential hazard for the flora and groundwater quality in the watershed (Kassir et al., 2012a).

The Levantine Basin was further chosen by Bou Kheir et al., (2010) to apply a regression-tree model to predict spatial distribution of Zn concentration in soils in a basin bearing various soil types, vegetation cover, and multiple land-use practices. The basin extends from Mount Lebanon highlands in the East to the coastal plains in the west, thus expressing different geomorphological units (Bou Kheir et al., 2010). The major soil type in the watershed (71%) is comprised of discontinuous red mountainous soils mixed with marl limestone and sandy soils. pH was found to be the dominant factor influencing Zn mobility in the soil, followed by the proximity to waste disposal areas, roads and urban zones. Spatial distribution of Zn in soils is also linked to land-use cover and drainage areas, in addition to the influence of soil texture, organic matter content and soil depth (Bou Kheir et al., 2010). Similarly, the Fe source in riverine sediments (collected in dry season in north of Lebanon) was reported to be derived mainly from weathering of basaltic outcrop and industrial activities, namely the iron

and steel manufactory. However, the authors reported that metals in sediments could be derived from the disposal of domestic wastes and garbage incineration. Zinc was originated from zinc coating and Cu could be derived from manufacturing of furniture and electroplating, while high Pb concentration was associated with combustion of leaded fuel (Korfali and Davies, 2000). Previous studies based on metal speciation experiments concluded that rivers underlain by limestones and characterized by alkaline water pH are aiding in the sorption of metals such as Pb, Zn, Fe and Cu and coprecipitation with it in the sediment bed; as a result carbonate species are participating in self-purification of the river system in Lebanon (Korfali and Davies, 2000; 2004).

In the southern reaches of the Lebanese coast, marine sediment cores were collected in 2007, in which metal content and PAHs deposition increased in 1950, suggesting coal as the contamination source. Regardless the fact that there was a reduction in coal usage worldwide, trace metal concentration, mainly Pb and Hg, continued to increase in the sediment core by 3-5 folds. The same trend as Pb and Hg was observed for PAHs levels that increased by 4-7 folds compared to pre-industrial background levels. This study suggested that contamination from Europe could reach the Mediterranean coasts by atmospheric deposition (Azoury et al., 2013). In the same context, El Samad et al., (2013) determined natural (^{238}U, ^{232}Th, and ^{40}K) and anthropogenic (^{137}Cs) radioactivity in the Northern Lebanon terrain. They reported that natural radionuclides were similar to the world average value, and the anthropogenic ^{137}Cs decreases exponentially with depth with activity in surface sediments ranging from 0.1 to 5 KBq/m^2. The radioactivity of ^{137}Cs was documented in northern soils varying between 2 and 113 Bq/kg which was associated with atmospheric deposition after nuclear weapon testing in the 1960s succeeded by the Chernobyl nuclear accident in 1986 (El Samad et al., 2013). Lebanese topography and variant soil type and precipitation can influence the atmospheric deposition of ^{137}Cs from the radioactive cloud (Chernobyl nuclear accident in 1986). Soils in the Northern Lebanese coast and Western Mountains contain more ^{137}Cs compared to the Southern terrain and the Bekaa valley. The mean concentration of ^{137}Cs in the top 3 cm of the Lebanese soil was estimated to be 59.7 Bq/kg (El Samad et al., 2007).

The inland industrial point sources are located in the central Bekaa industrial area that comprises manufacturing factories of plastics, rubber, metalloids, paper production, food processing, mining and quarries that discharges its effluents directly into the water basin without any pretreatment (El Fadel et al., 2003; BAMAS, 2005). It was reported that the major pollutants in the upper Litani basin were derived from domestic wastewater, where the percentage of inhabitants connected to the sewer system was estimated to be 50%. Thirteen million cubic meter (MCM) of sewages are discharged to the river basin yearly (39899 m^3/day), in addition to leachates from landfills and waste disposals. Zahle city alone discharges to the Litani River 64.4% of the total household and liquid industrial wastes, which represents the major industrial area in the basin (Greenpeace, 1998; El Fadel et al., 2003; BAMAS, 2005). The diffuse sources of pollution in the Bekaa plain are nutrients and chemicals derived from fertilizer and pesticide applications to the cultivated valley and

reflow of irrigated water, in addition to effluents from urbanism and road runoff (Figure 1.2) (BAMAS, 2005; Kouzayha et al., 2013).

The metal content in the sediments collected from the Litani river basin during the period extending from 1993-2004 ranges between 2-21.51 ppm for Cr, 2-18 ppm for Cu, 1.8-127.3 ppm for Ni, 0.7-7.9 ppm for Pb, and < 0.1-7.7 for Cd (BAMAS, 2005). A previous study conducted on lacustrine sediments of Qaraaoun reservoir during the dry season in 1997 reported that the sediments at the river inlet has the highest total metal content, and near the dam, sediments exhibits reducing conditions (Korfali et al., 2006).

(a)

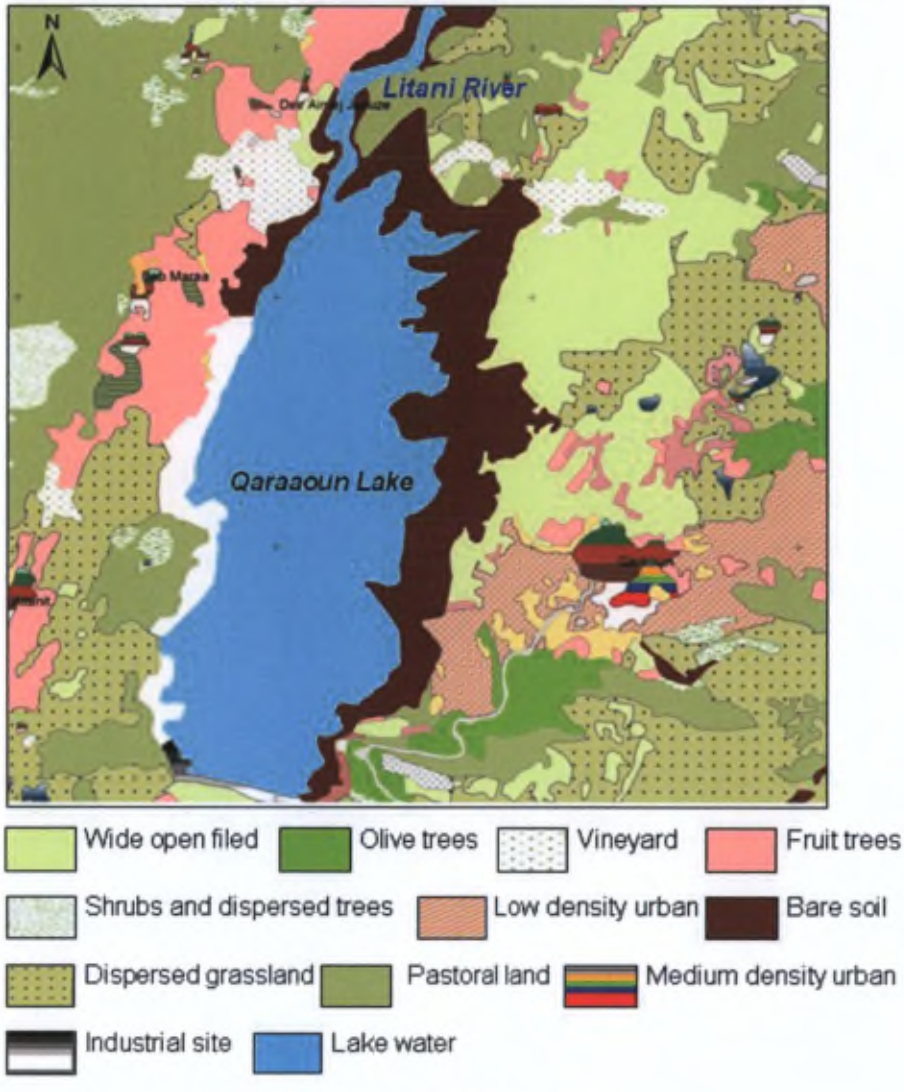

Source: Shaban and Nassif (2007)

(b)

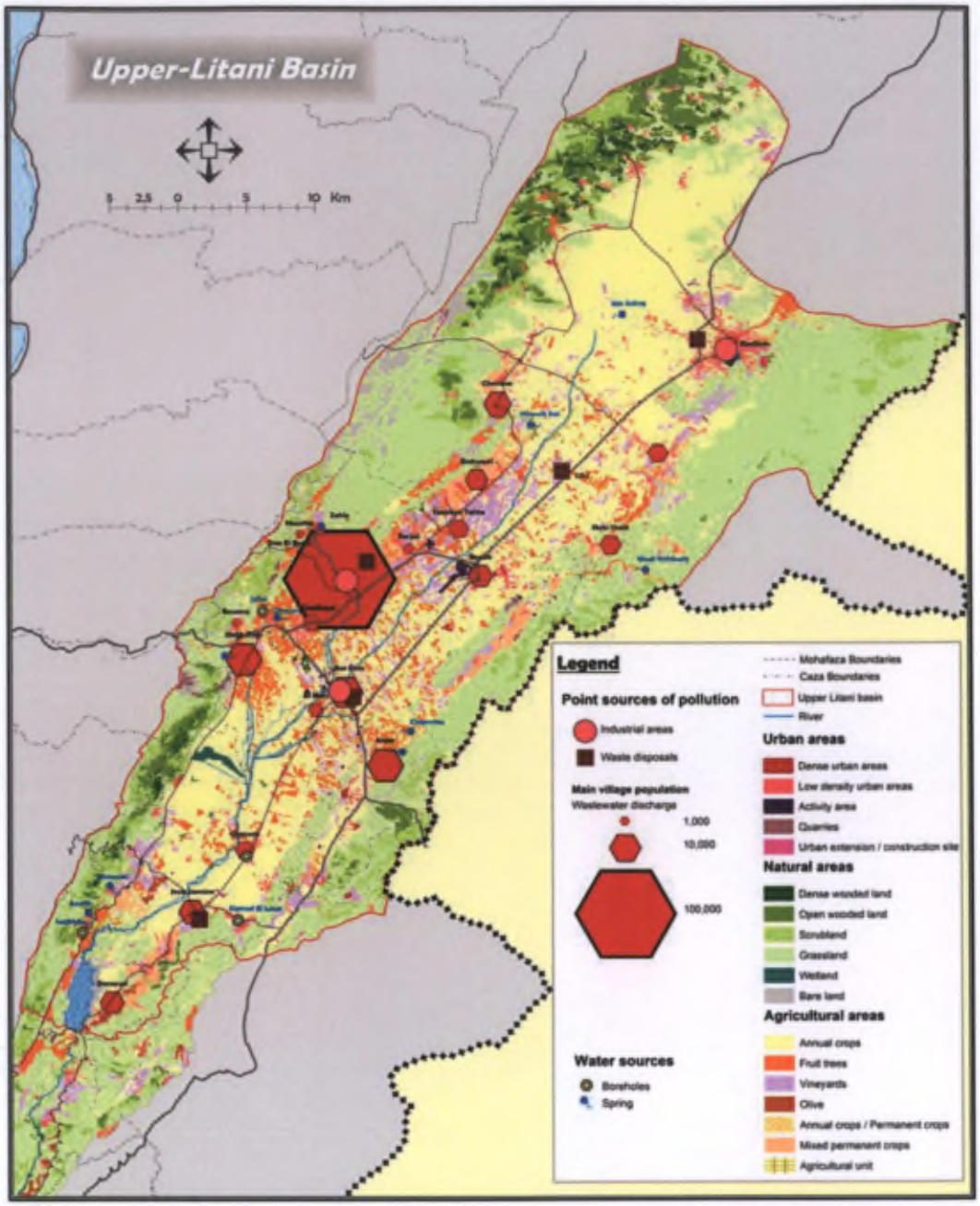

Source: Rapid review report BAMAS (2005)

Figure 1.2: (a) Point and diffuse sources of pollution in the Upper Litani Basin, and (b) land-use cover surrounding the reservoir.

A further study was conducted to determine the metal speciation in the Qaraaoun reservoir during the dry season in 2008 (Korfali and Jurdi, 2011a). The authors assumed that Fe, Cr, and Ni were mainly found in the residual phase while Cu and Pb were associated with the organic fraction in addition to carbonates that represented the metal bearing phase for Pb and Cd. Comparatively, another experimental study was conducted to investigate metal bioavailability in the Mediterranean red soil collected from Mount Lebanon area in 2009, and massively amended with phosphate fertilizers and PG (Kassir et al., 2012b, c). The highest

concentration of trace metals was observed 4 months after phosphate fertilizer application, where trace metal (Cu, Zn, and Pb) bearing phases were altered from residual to exchangeable with the fastest mobility observed for Zn. As a result, increasing metal mobility will lead to their penetration into deeper soil layers (Kassir et al., 2012c). Upon PG application to the studied soil, trace metal content increased in the soil column where Cu, Zn, Cd and Pb were mainly present in the exchangeable fraction while Cd showed a high bioavailability and capability to bioaccumulate in the food chain thus threatening the groundwater quality (Kassir et al., 2012b). Precipitation, soil pH, total organic carbon, and cation exchange capacity were found to be the major factors that influence trace metal behavior in the studied soil (Kassir et al., 2012b, c).

Mechanical transport of soils and sediments is the main transferring mechanism of pollutants from their source to open water bodies. The erosion potential of Lebanese soil was estimated by conducting soil erosion risk mapping on representative study area (9% of the total country area), extending from the coast in the west, passing by Mount Lebanon and ending in the Bekaa valley in the east. The study area is comprised of 32 soil units which exhibit variant runoff potential, landscape sensitivity related to vegetation cover and land slope, and erodibility. The model results indicated that more than half of the study area was susceptible to erosion mainly due to high runoff potential thus inducing erosion risk with high erodibility associated with sandy soil, and moderate erodibility detected for Bekaa valley (Bou Kherir et al., 2006).

1.3.2 Final outcome and scope of studies on the hydraulic resources and pollution in Lebanon

The hydraulic abundance in water resources renders Lebanon the water tower of the Middle East, in comparison to the neighboring arid countries in the Eastern Mediterranean (Shaban, 2014). Geomorphological features give Lebanon the privilege to harvest high precipitation rates up to 1500 mm/year and an extending snow cover (2500 km^2) for several months (El Fadel et al., 2001; Shaban, 2014). National hydraulic resources are represented by 12-17 permanent rivers and more than 25 seasonal rivers. Coastal rivers drain from Mount Lebanon highlands to the Mediterranean coast, in addition to 3 inland rivers as presented in Figure 1.3. Additionally, there are more than 2000 principal water springs distributed throughout the country (El Fadel et al., 2001; Shaban, 2014). However, physical and anthropogenic challenges such as population burst, industrial development, expanding irrigated agricultural areas, and extensive groundwater exploitation induce water shortage, reaching unsustainable water supply at the national scale (El Fadel et al., 2001; Shaban, 2014).

Due to the harsh socio-economical circumstances and the absence of national management plans during the period of security unrest extending from 1960 till 1980, a high withdrawal of the groundwater and the installation of private wells were realized to meet the increasing population needs in Lebanon. Furthermore, the civil war that extended from 1975 till the early 1990s induced a great damage to the national infrastructure of both municipal water

network and sewage system (Khair et al., 1994; Geara et al., 2010). This was further accompanied with irresponsible activities of citizens, resulting in severe water deterioration due to uncontrolled waste discharge and industrial waste disposal into river basins (Figure 1.3). The overexploitation of coastal wells led to seawater intrusion and increased aquifer salinity; moreover most of aquifers in Lebanon are karstic that are well known by their high leachability, thus causing a decrease in groundwater table and deterioration of water quality (Khair et al., 1994).

Figure 1.3: Lebanese rivers watersheds, where the wastewater outfalls are denoted by red triangles.

In the North, Nahr-Ibrahim river water chemistry was investigated during the dry season of 1996 and 1997; the river was mainly composed of carbonic water due to the karstic nature of the catchment (Korfali and Davies, 2000). The land-use impact on the water quality of the Abou Ali River (Northern Lebanon) was examined through two years of sampling (2002-2004) during both dry and wet seasons. Researchers found that urbanization and high population densities were the major sources of contaminants in the river basin, followed by agricultural practices and livestock slaughtering. Reported contaminants (nutrients, chloride, and coliform) indicated seasonal and spatial variations along the river and tributaries regarding water courses in the proximity to point and nonpoint sources of pollution (Massoud et al., 2006). Sewages were found to be the major polluting contributor for 8 coastal rivers (Kabir, Bared, Abu Ali, Ibrahim, Antelias, Damour, Awali, and Kassmieh River) studied during the dry season in 2004. The Abu Ali and Antelias rivers were the highest polluted rivers by coliforms, while the Awali River discharged the highest contaminated fluxes to the Mediterranean Sea (Houri and El Jeblawi, 2007). A simulating model was conducted to evaluate seawater quality in the Abu Ali estuary North of Lebanon. The simulation outcome indicated that the coastal water was affected by pollution plumes resulting from raw sewages, and industrial wastes (mainly the seasonal olive oil industry, where the olive mill debris was discarded in the river course and transported to the Mediterranean Sea) that are mainly controlled by local hydrodynamics and wind activities (Awad and Darwich, 2009). An investigation of natural and anthropogenic activities on water quality in two coastal rivers (EL-Kalb and Ibrahim rivers) was carried out seasonally during 2007-2008. Both physicochemical and microbiological parameters were explored to monitor river water quality at different stations using multivariate analysis. A higher anthropogenic contamination was detected at the lower reaches of the El Kalib River, while a mineralogical enrichment was found in the Ibrahim River related to land-use activities (Daou et al., 2013).

Similarly, a multi land-use watershed was investigated in the Southern reaches of the Lebanese coast (Damour basin). The river water quality was primarily affected by urban effluents followed by agricultural practices and the river estuary entering the Mediterranean Sea was reported to have the poorest water quality in the basin (Massoud, 2012). In addition, the Awali river water exhibits contamination by sewages and solid wastes as reflected by the detected coliform levels, in addition to Cd derived from extensive pesticide applications in the upper watershed (Korfali and Jurdi, 2011b). However, in the lower Litani basin (LLB) extending from the Qaraaoun dam and draining southwest into the Mediterranean Sea, researchers found seasonal variations in metal concentration, where anthropogenic activities and land-use practices control the spatial distribution of metals along the river course (Nehme et al., 2014).

While in the continental valley, a previous study was conducted on the Qaraaoun reservoir in order to evaluate its water quality in 1995, where it was found that the water quality in Qaraaoun reservoir met the WHO norms and could be used for multipurpose activities such as drinking, domestic usage, irrigation, fisheries and aquatic sports (Jurdi et al., 2002). This investigation suggested that the water quality at the central zone of the reservoir was the

finest only due to its capability of bio-chemical purification. The authors also recommended establishing a database for the water quality in order to secure the water sustainability of the dam. The carbonate fraction was the major predicted metal bearing phase in the Qaraaoun reservoir water, where the toxicity of Pb and Zn depended only on pH while that of Cd and Zn was affected by both bicarbonates and water pH (Korfali and Jurdi, 2011a). However, due to the population growth and the environmental stress exerted on the Litani basin, water quality was deteriorated and influenced by eutrophication, which prohibited its usage for domestic purposes and fisheries and even posed a risk for crop irrigation (El Fadel et al., 2003). The dramatic decline in reservoir water levels was due to evaporation, water withdrawal for irrigation purposes, and dam maintenance that increased both biological and chemical oxygen demand, bacterial growth, and metal content (As, Cd, Cr, Cu, Fe, Hg, Ni, Pb, and Zn) (El Fadel et al., 2003).

A water quality survey for the Litani basin was conducted by the Litani basin management advisory services (BAMAS), covering surface water, groundwater and wastewater in the basin during the period from 1993 to 2004. It showed that the Qaraaoun reservoir, the Litani main river course, and major tributaries delivering water to the main stream from all directions of the basin (Berdaouni (NS), Qabb Elias (WS), and Ghozayel (ES)) are under the great influence of untreated domestic wastewater. As a consequence, the organic matter content, ammonium (5.35 mg/L in the reservoir and 2375 mg/L in the river) and bacteria levels (Fecal Coliform 300 CFU/ 100 ml in the reservoir and 10000 CFU/100 ml in the river) in the water were high, thus rendering the water usage for domestic practices unsuitable. The groundwater in the studied basin was found to be contaminated with organic matter, and metals (Fe, Zn, and Hg) coming from the wastewater and leaching from the dumpsites and wastewater. In addition to receiving water reflow used for irrigation in the karstic basin that has high rock infiltration capacity (BAMAS, 2005). This survey was followed up by monitoring the surface water and groundwater quality in Litani basin during the period from 2005 to 2010 (Saadeh et al., 2012). The Qaraaoun reservoir alkaline water (pH= 8-8.5) is mainly affected by the surrounding C4 limestone outcrop. The upper Litani watershed was subjected to salinization and eutrophication, and the Berdaouni tributary that passes by Zahle city was the most contaminated river. It was reported that the groundwater table in the Litani basin dropped by 100 meters compared to 1970; even more the groundwater was subjected to contamination by sewage leading to phosphate and nitrate enrichment. Lucy wells (located in the eastern Bekaa valley) were the most contaminated by sewage water referring to its high nitrate levels (30-70 mg/L) (Saadeh et al., 2012).

In order to evaluate the contamination level in the Qaraaoun reservoir and to address the sources and locations of contaminants, Shaban and Nassif (2007) conducted a study during the dry season in 2004 on reservoir surface water. They expected an insignificant variation in the physicochemical parameters during different periods of the dry season. Physicochemical characteristics of the surface water indicated that 75% of the reservoir water was polluted by total and fecal coliform in addition to major nutrients (nitrates and phosphates). They found that the river and the eastern side of the reservoir were the most contaminated parts and were

under the influence of environmental stress exerted by anthropogenic activity in the region (Shaban and Nassif, 2007). Furthermore, vegetation cover influenced nitrate and chloride mobility in Bekaa agricultural soils; the study conducted during 2007-2009 indicated contamination of shallow groundwater in the Litani basin with nitrate derived from agricultural practices and sewage input (Darwish et al., 2011). Likewise, a GIS-based decision support system simulation indicated the growing hazard of the untreated wastewaters discharged into the Litani upper basin mainly during dry periods, leading to surface water deterioration, which rendered inappropriate its usage for multipurpose and influenced the aquatic biota (Assaf and Saadeh, 2008).

Correspondingly, extensive agrochemical applications, mainly pesticides, contaminated the Lebanese drinking water. Sixty-seven different types of pesticides were investigated in surface water, rain water, drinking water and groundwater samples that were collected in 2010-2011 from major Lebanese cities. In drinking water and groundwater, insecticides and fungicides were detected mainly belonging to the organochlorine and organophosphate families, and regardless of the prohibition of POPs in 1992 they are still measurable in the Lebanese waters. Among the detected surface waters, the Litani river and Qaraaoun reservoir exhibit the highest concentration of pesticides (n=28), mainly insecticides, and herbicides. Kouzayha et al., (2013) showed seasonal variations in pesticide concentrations in water, mainly associated to their application and runoff by which it was mainly found in spring and summer with the highest concentration detected in May and June. The authors showed also that the pesticides could be mobilized by air currents and transported to distant areas far from their application zones and fall out with precipitation.

An Environmental setback was documented in air, soil, and water in Lebanon after the conflict of summer 2006 with Israel. The bombardment of Jiyeh thermal power plant and oil tanks in Beirut international airport contaminated the soil, groundwater, and 150 kilometers of the Lebanese coast with 10000 – 15000 tons of heavy fuel oil spill. The baseline data collected by UNEP on the environmental situation following this conflict, reported a sharp increase in hazardous wastes due to bombing of urban zones and many industrial factories, yielding considerable amounts of rubbles which were of potential hazards in dumping sites. In addition to the great destruction that occurred for the infrastructure (water and sewer networks) that threatens soil and groundwater quality (UNEP, 2007).

Researchers relied on environmental stable isotopic approaches to fill the hydrological gaps in characterizing basins. Hydrogen and oxygen isotopes were recently used to get better insights about water cycle and hydrological routes in national studies. Litani watershed received particular attention, where isotopic applications were conducted to understand the dam functioning in the past years. The Mediterranean Sea is the source of precipitation in Lebanon (Awad, 2011). The Mediterranean rain is subjected to evaporation and thus has high d-excess values of around 22‰ compared to the Global Meteoric Water Line GMWL: $\delta D = 8\delta^{18}O + 10$ (Siebert et al., 2009; Develle, 2010). However, the Lebanese local meteoric water line is delineated as $\delta D = 7.13\delta^{18}O + 15.98$ (Saad et al., 2005), where evaporation enrichment

of rainfall is taking place in November. In addition, the isotopic fractionation of rain water is influenced by altitude effect, where rain is isotopically depleted in ^{18}O in the inland semi-arid areas compared to the coast (Saad and Kazpard, 2007). Previous studies on the Litani River focused on water quality evaluation in the river, reservoir and adjacent piezometers. Saad et al., (2006) stated that Qaraaoun reservoir was a warm Monomictic lake isotopically enriched compared to the river by 3 ‰ in $\delta^{18}O$ and 10 ‰ in $\delta^{2}H$, which is well mixed in winter and stratified only in summer with no spatial variation observed. Artificial infiltration from the reservoir to groundwater was observed and estimated to be 28.5 % at the reservoir entrance compared to 20.7 % at the dam (Saad et al., 2006). Additionally, altitude thermal gradient influenced highly the isotopic fractionation in the Bekaa (Develle, 2010). As δD and $\delta^{18}O$ composition of aquifers in the area are altitude dependent, more negative values were observed in the Cenomanian aquifers compared to Jurassic and Eocene (Awad, 2011, 2013). A recent study on temperature and precipitation trends in the upper Litani basin reported that the basin was subjected to a drying trend by which the annual local precipitation decreased by 1.1 mm/decade mainly observed in spring. December represented the driest season where precipitation decreased by 6.3 mm/decade. In contrast, temperature did not show any changes in its trend except for November where it decreased by 0.1 °C/decade (Ramadan et al., 2013).

Water loss via evaporation (50%), groundwater seepage (12%), and surface flow to neighboring countries and the Mediterranean Sea was estimated to be more than half of the total annual precipitation (8600 Mm^3) in Lebanon. This would leave only 2600 Mm^3 as available surface water and groundwater of which 2000 Mm^3 were exploited. Water demand for irrigation was the highest (675 Mm^3), followed by domestic usage (250 Mm^3) and industrial practices (60 Mm^3). A recent estimation indicated that the national groundwater deficiency reached 14 % due to lower replenishment from precipitation (Masciopinto, 2013). Surface and subsurface water flow from the Lebanese coastal rivers to the Mediterranean Sea represented an important loss of available water resources, related to metrological (climate change), hydrological (fractures and karstic rock type drains aquifers into the sea or unreachable aquifers) and geomorphological setting (steep sloping surface) of the watersheds (Shaban et al., 2009; Shaban, 2014). Moreover, a long-term variation of the Litani river flow was extracted from monthly stream flow data at 7 major stations along the river course. The analysis indicated a common behavior where the stream flows showed a continuous decrease; however, flow peak anomalies were detected and correlated to higher rainfall and snow cover that were directly reflected on the flow. Regional climatic factors, geological context and anthropogenic interference affect the national water budget (Shaban et al., 2014). In order to manage national water hydrological resources, the Ministry of Environment implemented a strategy to satisfy the future water demand in Lebanon by establishing a water plan 2008-2018 comprised of constructing 41 dams over the different Lebanese provenances for potable water and irrigation (UNDP/MoE, 2010).

Lebanon is well known by the climatic oscillation which is assumed to witness an increase in temperature and thus reduction in precipitation (Shaban, 2014). The Litani basin will respond to the hydroclimatological alternation in the area by decreasing its runoff in the long term

(Ramadan et al., 2013). Lebanon is facing major water challenges, including geomorphological, hydrological and climatic aspects. Shaban (2014) summarized the previous models conducted on Lebanon to investigate hydrological and climatic changes, and highlighted the deficiency of these models and their output unreliability due to lack of sufficient data. Correlation of precipitation-flow data and water balance are currently not available for Lebanon to provide projections of water regimes in the long term.

1.4 Data Deficiency

There exists no accurate estimation for the Lebanese water budget. The evaluation of hydrological situation and water quality during the civil war period (1975-1992) was null, leaving an important gap in the knowledge of national environmental resources (Khair et al., 1994; Korfali and Daives, 2000; Jurdi et al., 2002). Moreover, the severity of environmental problems due to socio-economical stress and chaotic land-use practices was amplified in the absence of governmental control; the Ministry of Environment (MoE) was only founded in 1993 (El Fadel et al., 2000). Similar environmental issues suffering from knowledge shortage relied on water stable isotopes to fill hydrological gaps and to trace the origin of water sources by tracking its pathway over a specific watershed (Butler, 2007; Kumar et al. 2008; Singh et al., 2010). Few studies investigated the isotopic response of both natural and anthropogenic changes in the semi-arid artificial lake either temporally (seasonal short and/or annual long terms) or spatially. Studying the hydrogeochemical cycles in dammed reservoirs is crucial for the determination of water recharge areas and for the assessment of potential contamination sources and fate in order to establish efficient management plans to preserve the groundwater sustainability and dam functioning in the basin.

Previous national studies have investigated only the surface water quality in the investigated rivers and Qaraaoun reservoir, and mainly in the dry season during a particular sampling year, and they have ignored the sensitivity of the studied area to altering hydrological and meteorological conditions spatially and seasonally. The physiochemical characteristics of the water column above the sediment bed have not been investigated, which are crucial to understand the metal behavior at the water-sediment interface. In addition, groundwater characterization and evaluation require more attention in order to estimate the recharging zone and the extent of hydrological connectivity with the upper basin and to assess the potential threats to the shallow water table.

Surface mapping of the watershed was used to identify the source and type of contaminants, without taking into consideration the reachable part and form of the contaminants to the reservoir; the accurate source of pollution was not explored either. Furthermore, there is lack of sedimentary data not only in Lebanon but also in the Mediterranean regions (Azoury et al., 2013). Previous works mostly studied riverine and lacustrine sediments during the dry season, and they did not investigate the sediments behavior during the wet season. Few studies relied on multivariate analysis or coupling of variant applications to study metal

behavior in soils and sediments, such as combining metal evaluation, elemental characterization and isotopic applications to better understand the implication of different factors in controlling the fate of metals in the environment. For the Qaraaoun dammed lake, the reservoir hydrodynamics and seasonal pollutant loads were not considered in biogeochemical studies and the chemical partitioning between the dissolved and particulate phases in the water column and at the sediment-water interface were never explored. The particularity of the environmental receiving media and the intrinsic characteristics of soils and sediments were insufficiently studied in previous works which might result in ambiguous conclusions.

There is an inadequate understanding of the impacts of land-use cover on national hydraulic and soil quality which leads to poor environmental assessment. Historical evolution of the watersheds upon increasing population densities, geomorphological land change, and industrial revolution received humble scientific efforts in Lebanon. A few researchers attempted to investigate the complex topographic and geological influence of Lebanese land morphology on pollution distribution and fate in watersheds. However, there is a severe deficiency in national studies, including collective influences of land-use, geomorphology, topography, demography, climate, pedology, and land morphology on metal behavior in both aquatic and sediment/soil compartments of the watersheds. Knowledge about pollution magnitude, extent, age, flux, and behavior in the Lebanese watersheds is humble, and data acquisition is of utmost necessity to provide reliable results for risk assessment and national management plans.

Little information is available on the hydrodynamics and biogeochemical cycle of the Qaraaoun reservoir whose response to hydroclimatological and geomorphological changes has not been examined. To our knowledge, the reservoir hydrodynamics and water budget were not previously estimated neither related to watershed runoff. Insufficient knowledge, unexciting hydrological records and the lack of reliable environmental information are great obstacles to define environmental management strategies and water policies, since they require accurate and sufficient data that characterize water resources in order to clarify the challenges to decision makers (El Fadel et al., 2001; Shaban, 2014). Simulating models are a pioneer tool to help developing management plans and predicting the future consequences of environmental problems on the long term for decision makers and stakeholders to take the proper measures (Awad and Darwish, 2009). Poor knowledge of hydrological routes and meteorological implications on water budget can be solved by applying isotopic tracing methods and reliable scenarios for hydrological water models to achieve efficient water management plans (El Fadel et al., 2001; Shaban, 2014).

1.5 Thesis outline

Chapter 2 presents first the contrasting characteristics of the two studied watersheds from the geological, geographical, geomorphological, hydrological and land-use perspectives. A two-year sampling strategy is detailed and followed (2011-2013) to collect not only water samples at various depths in the reservoir and in the piezometers, but also sediments

(lacustrine, riverine and coastal) and soils (surficial and cores), covering seasonal variations (rainy, first flush and dry seasons) in both investigated areas. The materials and methods used in this thesis are explained, in addition to a detailed description of the leaching column experiments conducted in the laboratory in parallel to the field investigation.

Our study starts with the characterization of contaminated material mainly present in the industrial watershed as a byproduct (Phosphogypsum), which can be used however as agricultural amendment material (**Chapter 3**). The nature of contaminants in the studied watersheds varies due to land-use changes. Therefore, the origin and fate of contaminants are investigated by coupling Pb isotopes to geochemical analysis in soils and sediments to address the industrial and agricultural pollution. This approach allows the understanding of metal behavior and the prediction of its fate, in relation to the environmental receiving media in semi-arid and Mediterranean areas. These results are presented in **Chapter 4**. The entire mechanism of characterization, origin, and partitioning between the dissolved and particulate phases of pollutants is highlighted in **Chapter 5** in order to understand the biogeochemical cycle of possible contaminants and to predict their potential hazard for both surface water and groundwater qualities. Furthermore, the environmental implication of the Qaraaoun reservoir is assessed by emphasizing the water hydrodynamics and its interaction with the watershed.

In **Chapter 6**, factors that may influence the metal behavior are examined, including land-use, and soil type and age, to trace pollution sources and to reconstruct the metal fluxes in two of the most environmentally significant watersheds in the country. Stable and radioactive Pb isotopes are used in addition to ^{137}Cs to study the geomorphological influence and the geochronology of the environmental stress exerted by the factory and the dam on basin ecology. In addition, the influence of contamination type and magnitude on metal behavior is examined for each soil type in the corresponding study areas. Moreover, in **Chapter 7**, the nature of the Qaraaoun reservoir and the internal hydrological dynamics are explored using stable hydrogen and oxygen isotopes to delineate the reservoir water structure and its fast response to meteorological and hydrodynamic changes in the watersheds, and to demonstrate its strong hydrological connectivity with groundwater. The reservoir hydrodynamics is also assessed using a hydrological box model, which in its role can be used to evaluate the reservoir water balance and hydro-project functionality. The groundwater influx to the reservoir and the water seeping from the reservoir are assessed so that the basis for water sustainability can be established in the long term (**Chapter 8**). Finally, the findings of this dissertation research are synthesized and recommendations are given in **Chapter 9**. They help to improve our knowledge of the case studied and provide a foundation for future hydropower projects, allowing the authorities to establish a road-map for national management plans and to raise the alert for mitigation and management methods to preserve the environment and resource sustainability.

Chapter 2

Materials and Methods

The study area is divided into two contrasting watersheds that are different at several levels, thus their environmental significance and socio-economical context must be acknowledged. In addition, geomorphological features, geographical location, climatic aspects and hydrological settings of each watershed should be considered, to better understand contaminants behavior. A two-year sampling strategy that was followed (2011-2013) to collect not only water samples at various depths in the reservoir and in the piezometers, but also sediments (lacustrine, riverine and coastal) and soils (surficial and cores). In order to cover contaminants origin, behavior and to predict their fate, samples were subjected to classical measurements and elemental characterization (using XRD, SEM, FTIR, Granolumetry, and zeta potential), chemical evaluation (utilizing IC, CNS analyzer, AAS, ICP-AES, and ICP-MS), and isotopic analysis (by IRMS, TIMS, γ-spectrometry). In parallel to the field work, an experimental leaching column test was conducted in the laboratory to examine the impact of soil type, contamination nature, and dose on contaminant behavior and fate in order to mimic natural environment.

2.1. Study sites

2.1.1 Environmental and socio-economical context

Lebanon is a representative example that includes a variety of regions with multivariate topography and different microclimate that characterize the eastern Mediterranean. The orographic formations separate the coastal plain from the inland valley (Figure 2.1), thus inducing the presence of different environmental phenomena controlled by geological formations (Figure 2.2), microclimate properties, demographic distribution and land-use activity (Ministry of Agriculture 2003; El-Fadel et al., 2003). Lebanon is affected by Mediterranean to semi-arid climate (Figure 2.3), where the rainy season occurs between November and February (80% of annual precipitation) and the dry season extends from May to October (Edgell, 1997). Nonetheless, the meteorological and climatic properties differ with geographical locations within the country. Urbanism and industrial factories are dispersed in the capital Beirut and along the coast, while the Bekaa district represents the agricultural fertile plain (Figure 2.4) and house 20% of the Lebanese population (El-Fadel et al., 2003). The country witnesses a flourish in both agricultural and industrial sectors in the past 30 years. The urbanization level has amplified from 79.4% of total population living in urban areas in 1985 to 89.7% in 2000 and is expected to reach 93.5% by 2025 (ministry of agriculture 2003).

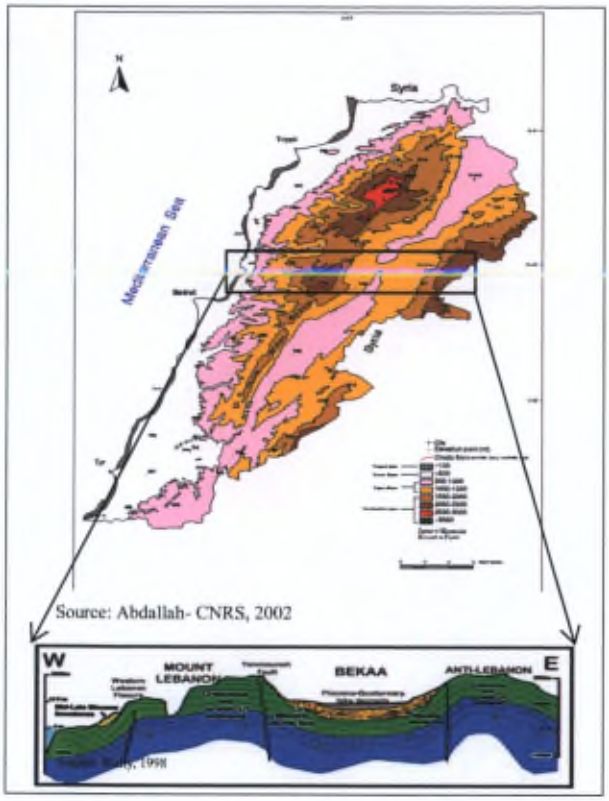

Figure2. 1: Topographical map of Lebanon, and the geomorphological cross-section that shows different compartments.

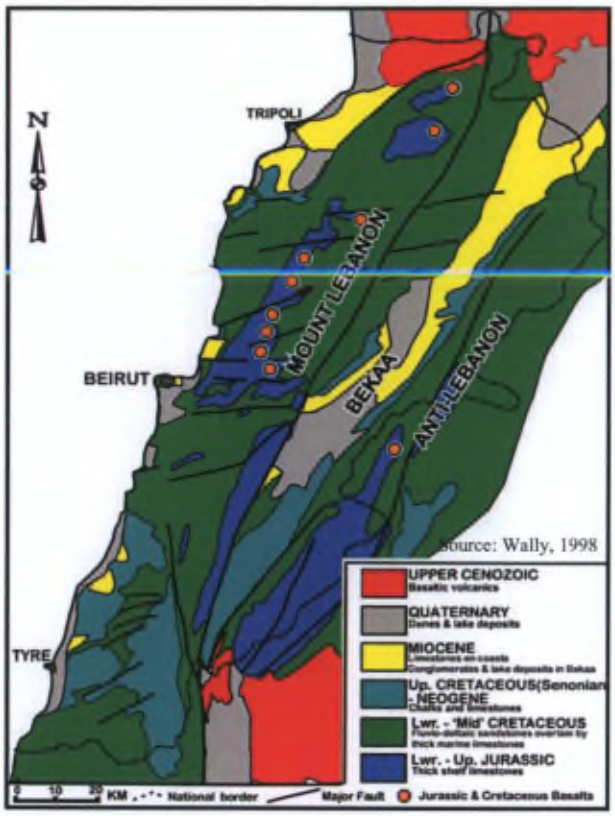

Figure 2.2: Geological map of Lebanon.

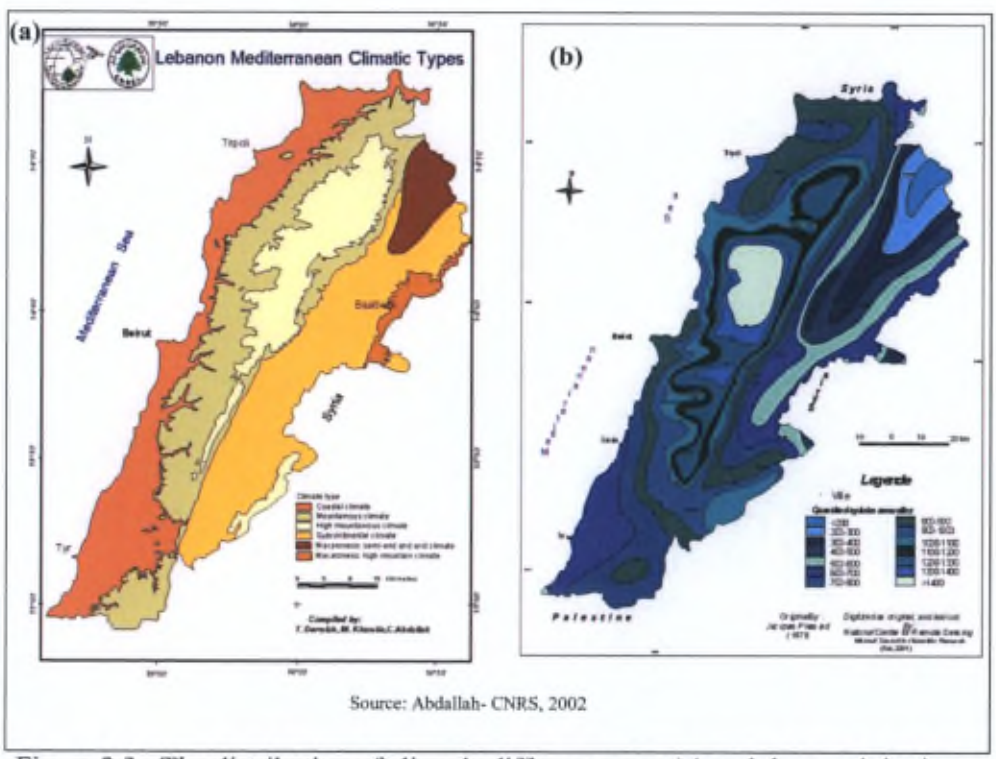

Source: Abdallah- CNRS, 2002

Figure 2.3: The distribution of climatic different types (a) and the precipitation map of Lebanon (b).

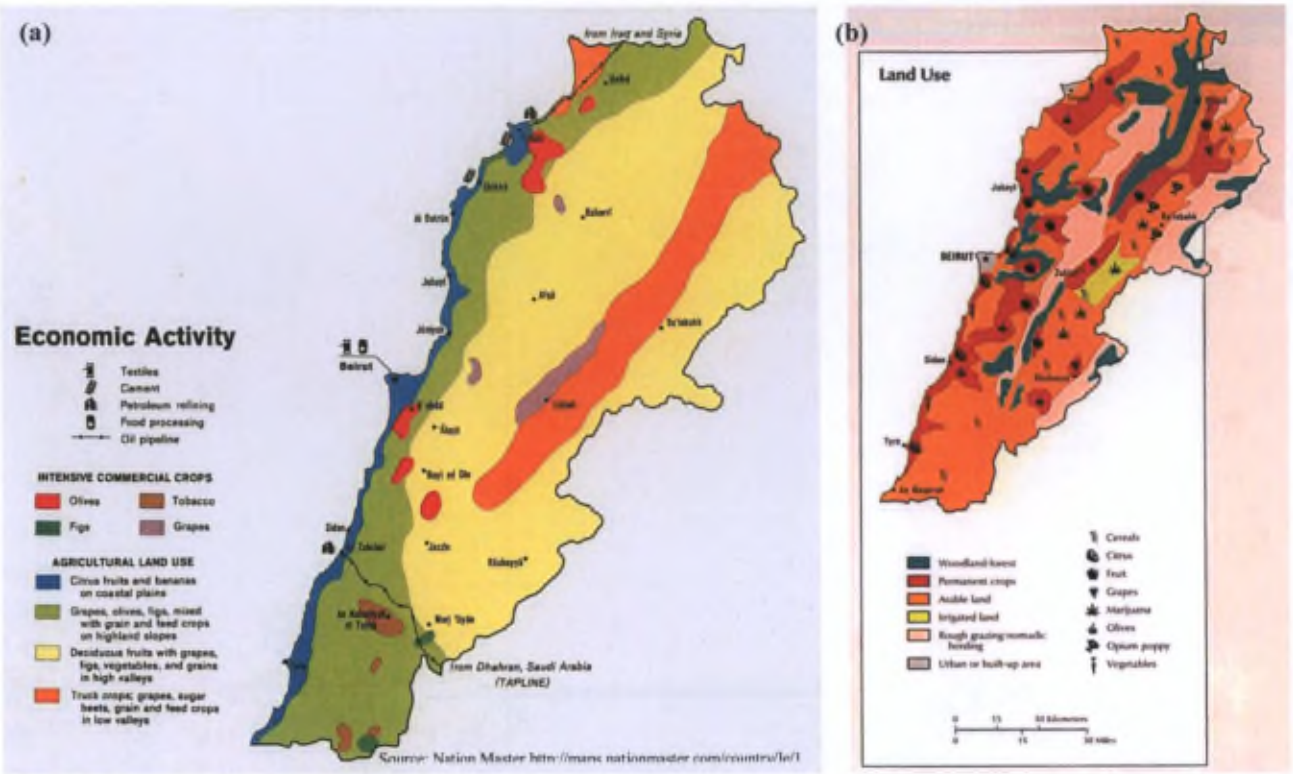

Figure 2.4: Land-use distribution of majorly economical activities (a), and agricultural practices (b) in Lebanon.

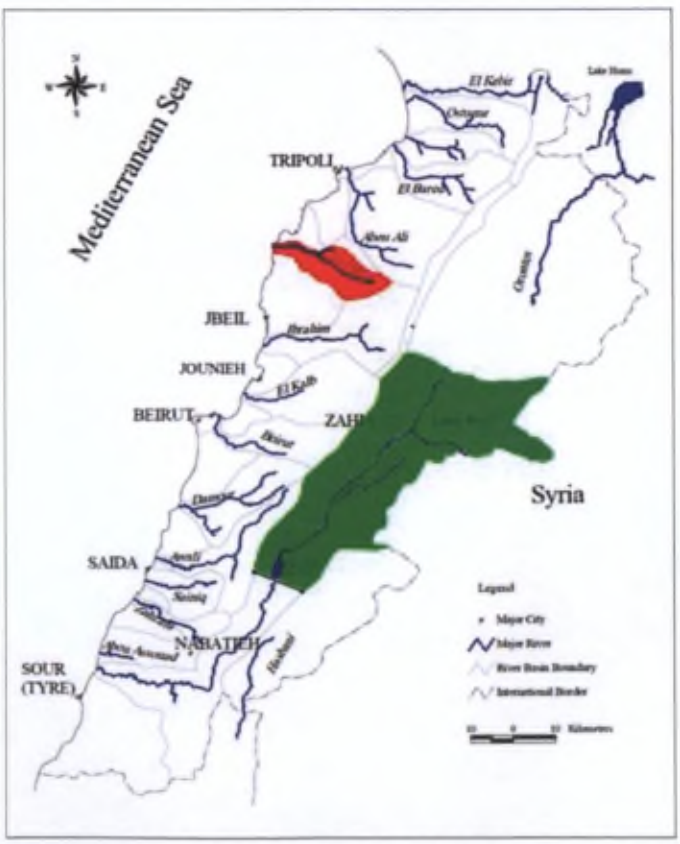

Figure 2.5: Hydrographic basins in Lebanon, where the Litani basin is an agricultural used watershed (green), and Levantine basin is an industrial used watershed (red).

Additionally, there has been an increased usage of motor vehicles as reflected by the rising in car numbers from 250000 to 1.6 million vehicles in the past 40 years (Choueiri et al., 2010). Thus, the transportation sector is the prime sector of energy consumption in Lebanon and the main cause of air pollution, where Pb concentration in the aerosols is found to be 14 $\mu g/m^3$ (Chaaban et al., 2001). Correspondingly, World Bank data estimated the CO_2 gas emission from fossil fuel combustion to be about 4.9 $MTCO_2$/cap in 2009. Many obstacles faced phasing out of leaded gasoline in Lebanon and tetra ethyl fuel usage was only banned in 2002 (Kaysi et al., 2000). Environmental dilemma in Lebanon is represented by major pollution point sources, a predominant industrial land-use area and an intensive agricultural watershed (Figure 2.5).

2.1.2 Industrial watershed

The Levantine basin, a typical karstic basin, is a relatively small funnel shape watershed where the Jouz River (38 km) runs from Mount Lebanon chain (NE) highlands and drains into the Mediterranean Sea (Figure 2.5). The river has a mean annual discharge of 67 Mm^3/y (Ministry of Agriculture, 2003). The mean annual precipitation in the watershed ranges between 1000 and 1100 mm (Figure 2.3b) and the mean annual temperature is 20℃ (UNDP/MoE2010). The geology of the watershed (Figure 2.2) is mainly composed of middle Cretaceous and Eocene strata layered by Neogene marine strata, also a sandy-marly limestone in addition to partially marly rocks interbred with basalt, which could range in thickness from 100 to 400 m on the coast (Edgell, 1997; Walley, 1997).

This watershed is a well-known industrial area since the phosphate fertilizer factory establishment downstream to the river in 1956, as well as a significant traffic conjunction linking the North to the capital Beirut. The fertilizer plant is considered not only as one of the top 10 industries in Lebanon but also as one of the most polluting industries in the Mediterranean (Bridgen et al., 2002). The factory imports phosphate rocks from Syria, produces phosphate fertilizers and phosphoric acid and eliminates phosphogypsum (PG) as a byproduct (Othman and Al-Masri, 2007; Aoun et al., 2010; Yammine et al., 2010). PG is an acidic material, soluble, radiogenic and rich in heavy metals (Rutherford et al., 1994; Al-Masri et al., 2004; Aoun et al., 2010; Ammar et al., 2013 [detailed in Chapter 3]). Apatite rock and PG wastes are found at the sea bottom facing the industry, in the atmospheric depositions dispersed by the factory's smelter and in the stockpiles on the shore (Fakhri et al., 2008; Abi Ghanem et al., 2009; Yammine et al., 2010; Ammar et al., 2013).

2.1.3 Agricultural watershed

The Litani Basin is the largest hydrographic basin in Lebanon (Figure 2.5), where the Litani River (170 km) flows through it longitudinally from the NE to SW and drains into the Mediterranean Sea with a mean annual discharge of 793-830 Mm^3/y (Ministry of Agriculture, 2003). The Mediterranean Sea is the origin of precipitation in the studied area, by which the basin receives between 700 and 1000 mm/y as mean annual precipitation (Figure 2.3b) (Develle et al., 2010; Awad, 2011). The inland Litani basin tolerates a continental semi-arid climate affected by the Mediterranean. The collective impacts of the Bekaa diverse

topography, its proximity to Mediterranean influence from west, in addition to Syrian Desert in the north-eastern reaches, create specific microclimates with drastic varying temperatures, humidity values and precipitation distribution in the region (Figure 2.3) (FAO, 2008; Ramadan et al., 2013). The rainy season extends from November till May by which 90 % of the precipitation falls in winter, followed by a severely dry season from May till September. The temperature ranges mainly from 5℃ to 26℃ in winter and summer respectively with an average annual temperature of 16℃. However the mean annual evaporation in the Bekaa plain is 1200 mm/y with maximal recorded values in July (FAO, 2008, Ramadan et al., 2013). Humidity is high at the coast and decreases toward the Bekaa plain ranging thus between 35 and 75 %. Orography plays an important role in micro-climate changes, where snow falls 30 days/y on the mountains flanking the basin (El Fadel et al., 2003; Develle et al., 2010). The Litani basin lies in the Bekaa valley between the two mountainous chains with a mean altitude of 800 m above sea level, and a surface area of 2.17 km^2. The basin is fringed by rain shadow flanks of Lebanon Mountainous chain from the west (highest summit 3087 m) and Anti-Lebanon chain from the east (highest summit 2800 m) as shown in Figure 2.1 (El Fadel et al., 2003; FAO, 2008; Develle et al., 2010; Awad, 2011). The orographic structure of high steep slopes induces crustal erosion from soil superficial strata. The geological age of Litani watershed dates back to Mid Eocene, where the plain is overlaid by a Quaternary alluvium limestone with a chalk and marly chalk outcrop that ranges in thickness from 150 to 900 m (Figure 2.2). Also, alluvial soils are covering the central and western reaches of the basin (Edgell, 1997; Walley, 1997; FAO, 2008). The zone of the watershed extending from the natural source to the dam is called upper Litani basin (ULB) representing 70% of the total watershed area (Ramadan et al., 2013) (Figure 2.5), where 67 dumpsites are found in the basin with a total surface area that equals 429150 m^2. Dumping leakage reaches the river banks and the lake boundaries.

Both surface and groundwater serves to fulfill the needs of 160 communities composed of 350000 habitants, almost 20 % of the total Lebanese population (BAMAS, 2005; Saad et al., 2009). Bekaa Valley serves 40 % of the total national cultivated area (FAO, 2008). According to a statistical study conducted by ministry of agriculture (1998), the Litani basin is the major producer in the country regarding industrial agricultural yields (62 %), cereals and legumes (57 %), vegetables (57 %), fruit and olive trees (37 %). However, this basin is subjected to enormous environmental stress, since it is historically known as a major agricultural area but now witnesses multi industrial practices expansion after the dam construction. This induced a rise of diverse industrial factories for food and dairy products, plastics, paper mills and carton, furniture and textiles, chemicals, paints, metalloids and batteries in addition to considerable rock cutting activities related to quarries and manufacturing of building materials (Table 2.1). The 288 different industrial units discharge their untreated effluents into the river main course, the tributaries and the reservoir. This surge of contaminants, enriched in heavy metals (Cr, Ni, Zn, Co, Fe, Cd, Cu) mainly Pb, arrives in the reservoir which is loaded with organic matter, minerals, solvents and suspended solids (Callender and Rice, 2000; Östlund and Sternbeck, 2001; El Fadel et al., 2003; Legret et al., 2005; Gondal and Hussain, 2006; Manzoor et al., 2006; Battaglia et al., 2007)

The Litani River has an annual average discharge of 9.34 m^3/s and a volume of 750 million cubic meters (MCM). As part of the national water management plan, the Qaraaoun Dam was constructed in 1956 to terminate Litani river flow in a 2.2 km^2 reservoir, for hydropower production and irrigation. The dam in Qaraaoun village is 110 m long and 61 m wide and stores water delivered by the Litani main river, nine tributaries, surface runoff, and groundwater discharges from the upper drainage area which is estimated to be 2180 km^2. The reservoir has a minimum allowed volume of 40 MCM, though 70 % of the total water volume (220 MCM) is used to produce electric power via al Zahrani electric power plant during full capacity (El-Fadel et al., 2003; Saad et al., 2006; Assaf and Saadeh, 2008; FAO, 2008; Saad et al., 2009). Furthermore, the Qaraaoun reservoir is aiming to supply more than 22000 hectares of cultivated land with irrigating water (30 MCM/y) via Canal 900.

Table2.1: List of different industries in the agricultural watershed and their rejected contaminants.

Industry Type	Number	Details	Contaminants
Plastic industries	30	Plastic bags, pipes, PVC PET	Pigments, solvents, acids, toxic metals ***Pb*** (Ostlund and Sternbeck 2001)
Food industry	77	Bakery, vinery , chicken and meta slaughters, canned food and wheat grinders	Organic matter, suspended solids, preservatives, grease and oils, blood, bone and feathers.
Wooden industries	20	Furniture, boards	Paints, latexes, glues, solvents ***Pb*** (El Fadel et al.,2003)
Dairy products	45	Some has farms	Sewages, organic matter and suspended solids. ***Pb***
Building materials	56	Concrete, rock cutting, tails, ceramics, granites and marbles	Minerals, heavy metals (Cr, Ni, Cu, Ca, Sb, Zn & ***Pb***)and suspended solids (Callender and Rice 2000, El Fadel et al.,2003)
Cosmetics	4	Cosmetics, shampoo	Solvents
Sponge industries	5	sponges	
Agrochemicals	1	Fertilizers	Organic and inorganic materials, and metals (***Pb***) (Callender and Rice 2000)
Chemicals	2	Detergents	Solvents, suspended solids
Fodder	3		
Paper mills	11	Papers, cartoon recycled boards, sanitary napkins and diapers	Organic and inorganic materials, suspended solids, chemical solvents, heavy metals mainly Hg, Pb, Zn and Cu (Callender and Rice 2000, Battagliaet al., 2007)
Metal industries	24	Metals, alloys, batteries machines and vehicles	Al, Fe, ***Pb***, other metals oil (Ostlund and Sternbeck 2001, El Fadel et al., 2003, Wijaya et al., 2010)
Fabrics and textiles	2	Tissues and leather	Suspended solids, metals such as Cr, ***Pb***, Ni, Co, Fe, Ca, Na, K and Zn, solvents pigments and dyes (Manzoor etal.,2006)
Paints	3	Paints and dies	Pigments, solvents, organic and inorganic materials and heavy metals(Ca, Mg, Ba, Al, Fe, ***Pb***, Cu, Cr, and Ni) (Gondal and Hussain 2006)
Asphalt	4		Polycyclic aromatic hydrocarbons , Zn, ***Pb***, Cd, Cr , Cu and Ni) (Legret et al.,2005)
Piggery	1		Sewages
Total	**288**		

2.2 Sampling Schedule

2.2.1 Preliminary sampling

During 2011, a preliminary sampling campaign was conducted during which water, soil and sediments from the two studied areas were collected in order to examine the levels of contaminants and address the objectives of the research.

2.2.2 Sampling program over two years

- Industrial area

In the industrial area, two sampling campaigns were accomplished, the first in summer and the second in winter. Coastal and riverine sediments were collected along with surficial soils (15 cm × 15 cm) at various. distances from the factory (1-4 km) (Figure 2.6) and soil cores were also retrieved (Table 2. 2). In addition costal water from both sides of the factory was collected as well.

Figure 2.6: Superficial soil samples (S1-S4) in the industrial watershed (a), and the three different sampling zones river inlet (Ri), central zone (Cz) and dam zone (Dz) in the reservoir in agricultural watershed.

- Agricultural area

Sampling schedule was chosen to cover both temporal and spatial variations in order to distinguish potential sources that could contribute to the isotopic fractionation in the reservoir. Therefore, field surveys were conducted over two annual cycles (2011 – 2013) during which 4 sampling campaigns were carried out each year: at the end of the dry season (September), first flush (October/November), mid of the rainy season (February/April), and at transient season (May-June). In order to trace the water source and to follow the recharge pathway in the lake water column, and adjacent piezometers, water samples were taken from the Qaraoun reservoir (33.5° N and 35.6° E), from three sampling locations that passes latitudinally across the middle of the lake (N-S) using the LRA Zodiac boat. Additionally, two minor locations at the central transversal cross-section of the reservoir on both eastern and western sides were sampled to identify the possible lateral runoff. The first sampling point Dz is located near the dam zone, sampling point Cz is in the center of the reservoir and point Ri is in the river inlet zone which is the entrance of the reservoir as shown in Figure 2.6. A total of 181 water samples were collected in the reservoir at the surface and at various depths, in addition to 19 samples from piezometers and 5 samples from the river and tributaries (Table 2.3). Along with water samples, 19 samples of lacustrine sediments and

alluvial soils were sampled from the 3 different zones under the collected water columns (Figure 2.6) crossing the center of the reservoir longitudinally. In addition to soil core that was collected from the eastern side of the reservoir, additional core was retrieved from the reservoir eastern bank to investigate the reservoir hydrodynamics impact on soil (Table 2.3).

Table 2.2: Samples collected in the industrial and the agricultural watersheds.

Sampling site	Sample type	Coordinates	Depth
Industrial watershed	Riverine sediments	34.267611°N 35.659651°E	Top 2cm
		34.267843°N 35.658190°E	
	Coastal marine sediments	34.278796°N 35.654909°E	1-5cm
	Surficial soils	< 1 km 5 m a.s.l 34.269181°N 35.657136°E	Top 2cm
		1-2 km 15 m a.s.l 34.278058°N 35.659441°E	
		2-3 km 120 m a.s.l 34.283004°N 35.667837°S	
		<4 km 220 m a.s.l 34.277568°N 35.687982°E	
	Soil core	34.280264°N 35.659654°E	70cm
Agricultural watershed	Lacustrine sediments	Ri 33.586996°N 35.699037°E	
		Cz 33.571739°N 35.695442°E	
		Dz 33.555250°N 35.690590°E	
	Alluvial soils	33.560410°N 35.703654°E	Top 2cm
		33.547915°N 35.695761°E	
	Soil core	33.331601°N 35.421696°E	70 cm
	Sediment core	33.325236°N 35.414405°E	85 cm

2.2.3 Sampling and sample storage

- Water samples

Water samples were collected from the reservoir using a depth dependent sampler along the water column at successive distances of 5 meters each, with a higher sampling frequency at the top 5 meters to investigate the biological activity at the level of epilimnion. Water level increased up to 16 meters during the winter of 2012 compared to summer, where full capacity of the dam was reached. Water samples from the piezometers were extracted by pumping the water from the adjacent wells for a period of time before filling the 50 ml polyethylene tubes.

Water pH, temperature, electric conductivity, total dissolved solids (TDS), and dissolved oxygen were measured simultaneously on board using a pH meter (HANNA pH211 microprocessor pH meter), conductivity-meter (WTW cond i), and a portable LaMotte pocket multi Tracer-1766, and oxymetre (JLO30 Jeulin) respectively. In addition alkalinity and ammonia were measured using colorimeter (smart3 Lamotte) on field. Water samples were filtered directly onboard over 0.45 µm ministart filters stored in two divided batches of polyethylene 50 ml tubes. First group of samples were filled to the brim to avoid any water evaporation prior analysis for environmental isotopic analysis, and the other were acidified by HNO_3 to reach pH 1 for metal analysis, all collected samples were conditioned at 4 degrees to be analyzed.

Table 2.3: The geographical location and nature of samples in the agricultural watershed sampled over biannual years.

Sample nature	Sample ID	Coordinates		Depth	Altitude (m.a.s.l)
Lacustrine sediments	Ri	33.586996°N	35.699037°E	na	815
	Cz	33.571739°N	35.695442°E	na	815
	Dz	33.555250°N	35.690590°E	na	815
Water column	Ri	33.586996°N	35.699037°E	15	815
	Cz	33.571739°N	35.695442°E	25	815
	Dz	33.555250°N	35.690590°E	25	815
Piezometers	S1	33.5517°N	25.6824°E	1.81	856.88
	S5	33.5484°N	35.6852°E	6.06	861.07
	S6	33.5481°N	35.6976°E	3.78	859.03
	KCO309	33.5502°N	35.6828°E	21.93	871.8
	KCO209	33.5527°N	35.6841°E	20.91	874.39
	RM Bis 17	33.5470°N	35.6904°E	9.88 m	807.55

- Suspended matter, sediments and soils

Lacustrine sediments were obtained with a stainless steel sediment grabber (Fieldmaster Mighty Grab II Dredge). The core was collected via a motorized core drill (COBRA TT, Carottage à Percussion- SDEC) with an inox coated core of 7 cm inner diameter. The sample cores were partitioned into layers of increasing thickness with respect to the surface (5 x 3 cm, 7 x 5 cm and 2 x 10cm layers). Samples were stored in polyethylene bags in a fridge then freeze-dried using an Alpha 1-4 LD plus freeze drier. The filters used for sample filtration of the water column were conditioned as water samples and recovered to be later analyzed.

2.3 Sample characterization

2.3.1 Water samples

The acidified samples were subjected to heavy metals measurements (Ca, Mg, Cd and Cu) using Atomic Absorption Spectrometry (Rayleigh WFX-210 AA Spectrophotometry with

flame and graphite furnace mode) and ICP-MS (Thermo Scientific) for trace metals measurement (Ni, Co, Cr, Pb). Major ions Cl^-, NO_2, NO_3, PO_4^{3-}, Br^-, F^-, and SO_4^{2-} were measured using Ion Chromatography (Shimatzu - shim pack IC-A3) accompanied with a conductivity detector CDD-10AVP, and flame photometry (model 420 from Sherwood). Oxygen and hydrogen stable isotopes in water samples were measured using a Liquid Water Isotope Analyzer (LWIA-24d) with a precision of <0.1 ‰ for $\delta^{18}O$ and <0.3‰ for $\delta^{2}H$. Isotopic ratio was expressed as delta notion ($\delta^{18}O$ - $\delta^{2}H$) and six measurements are performed according to a standard calibration curve using V-SMOW certified standards in consistency with IAEA norms. Two additional water samples at 0 m and 3 m depth below the water surface were also collected and directly frozen for dual isotopic approach ($\delta^{15}N$ and $\delta^{18}O$) in order to delineate the nitrate source in the reservoir (Liang et al., 2013). Denitrifier method was used to measure the isotopic signature of nitrogen and oxygen at the Vrije University of Brussels (VUB) according to Sigman et al., (2001) and Casciotti et al., (2002). Briefly, nitrate is biologically converted to N_2O gas by *P. aureofasciens* bacterial strain, which is later purified by gas chromatography and measured by isotopic ratio mass spectrometer (V IRMS-ThermoScientific) coupled with open split interface. The method of bacterial culture, and nitrate conversion to nitrous oxides, purification and measurement is detailed in Mangion (2011).

For chlorophyll–a, water samples (100 mL) were filtered on glass fiber filters and then extracted with acetone according to the method described by Arnon (1949). The extracted chlorophyll was measured using a photometer (SP 2000 UV Spectrophotometer VWR) over two wavelengths, λ= 645 and 663 nm. The total chlorophyll was calculated according to equation 2.1:

$$\text{Chlorophll (total)} = 20.2\,(A645) + 8.02\,(A663) \quad (2.1)$$

Where A645 and A663 is the absorption value detected at λ= 645 and λ= 663 nm respectively.

2.3.2 Sediments and soils

2.3.2.1 Grain size

Grain size distribution was examined in order to investigate grain size effect on metal distribution. The grain size population of soils and sediments from both studied areas were measured via laser scattering particle size distribution analyzer (Patrica LA-950V2 Horiba) equipped with a laser diodes of 1.6 mW with λ= 405nm - 650nm. Sample dry weight ranging from 10 mg to 5 g per 100-160ml MQ water volume was used for analysis. The method relies on the Mie scattering theory with measuring size ranging from 0.01 µm to 3000 µm and an ultrasonic probe was used to break aggregates at 20 kHz frequency.

2.3.2.2 Functional groups

Chemical functional groups were determined by FT-IR-6300 (Fourier Transform Infrared Spectrometer) from JASCO. A mixture of the powdered samples with potassium bromide (1% wt/wt) was prepared and compressed into a pellet of 0.7 cm diameter for measurement.

2.3.2.3 Total and organic carbon

In order to analyze total and organic carbon in dry soil or sediment samples we use the CNS analyzer (Interscience Fisons instrument NA 1500 series 2). All the materials and tools were decontaminated with HPLC graded acetone. For total carbon analysis, Pre-cleaned tin cups were used to weight between 5 and 10 mg in duplicates for each sample, and with the aid of pincer and cup holder we have firmly sealed the cup and fold it in a proper way, by which no particles are percolating. However, for organic carbon analysis a pre-cleaned Ag cups were used to weight about 2 mg of the sample which is treated by HCl acid 5 N. HCl was added equally to the cups, that will react with the particles and left to dry totally under the infrared light. The samples are introduced to the automatic sampler disc on the device, where the method stars by sample contact with pure oxygen under 1000°C (tungsten oxide). Therefore the sample would be readily combusted, and the output will be mainly in the form of CO_2, N_2 and H_2O. At the end of the column the gases are in a mixture form, where H_2O is eliminated by water trap, and the remaining gazes continue their way to the chromatographic column which is a packed column constituting of porapack Qs50-80 mesh. Then after C, N and S are detected via thermal conductivity detector (cathetometer). Analytical values were calculated according to calibrated reference material stream sediments reference material (STSD-2 with 1.6% of carbon content).

2.3.2.4 Mineralogy

Mineralogical phases in the samples were determined using a D8 Bruker X-ray diffractometer (copper anticathode of wavelength $\lambda K\alpha = 0.154060$ nm). A 2θ window ranging from 10° to 60° was chosen with each leap at 0.02° and 1 sec designed for measurement. Collected diffractograms were analyzed using the software EVA and the powder diffraction files provided by the International Centre for Diffraction Data (ICDD). Sediments were also examined by scanning electron microscope SEM (JEOL JSM 6360LV), accompanied by a silicon drift detector (SDS), PGT Sahara. Samples were placed on a suitable support and covered by the carbon for ionization purpose to be prepared for analysis.

2.3.2.5 Determination of metals in the particulate phase

Collected samples were homogenized using pestle and mortar, sieved over 63 µm acid-cleaned nylon mesh, and extracted for particulate metals using a microwave acid digestion

method. An amount of 50 mg of 63 µm sieved samples was digested in Teflon bombs along with suprapur acids: 1 ml of 10 N HCl, 2 ml of concentrated HNO_3 and 250 µl of 40% Hydrofluoric acid (HF). The filters used for sample filtration of the water column were stored and digested using the same method as sediments. Samples were analyzed by Graphite Furnace Atomic Absorption Spectroscopy (GFAAS) with Zeeman-effect background correction (Varian AA-400) and Inductively Coupled Plasma Atomic Emission Spectroscopy (ICP-AES) (Varian Liberty series II). Certified standard materials (UN 3264 from MERCK) along with blanks were measured with sample batches, and the limit of detection was respected.

2.3.2.6 Pb isotopes

For Pb isotope analysis, 100 - 200 mg of the < 63 µm fraction samples were digested in an acid mixture (9 ml of concentrated HNO_3, 3 ml of HF and 2 ml of 10 N HCl) using a microwave digestion MARS 5 system CEM, followed by chromatographic separation in a clean lab (GET-Université Paul Sabatier). Pb in the digested samples was purified using 2 layered resins in pre-cleaned polyethylene columns. Two-thirds of the columns were packed with CG-71C and topped with the Sr resin. After resin cleaning and conditioning, the sample aliquots (4-5 ml) were loaded and the matrix was eluted by 3 ml of 3 N HNO_3 followed by 2 ml of 0.05N HNO_3; pure Pb was subsequently leached by 4 ml of 6 N HCl (Makishima et al., 2007). All the acids used were bi-distillated ultrapure acids. NIST certified materials (2711a Montana II soil and LKSD-3 sediments) were also digested as for soil and sediments samples. Pb isotopic ratios were determined on Thermal Ionization Mass Spectrometer TIMS (TIMS "MAT 261", Finnigan) and values for samples were normalized with respect to that found in the NIST SRM 981 Pb standard material.

2.3.2.7 ^{210}Pb and ^{137}Cs chronology

Lyophilized solid samples of the intact cores were ground by agate mortar and sieved over 63 µm acid clean nylon mesh, and aliquots of 5 g fine solid fractions were used to measure ^{210}Pb, ^{226}Ra and ^{137}Cs by gamma spectrometry, using a low-background, high-efficiency, well-type germanium detector (Canberra, Ge volume 280 cm^3). The radioactivity for ^{210}Pb, ^{226} Ra and its decay product were determined by 46.5 keV, 295 keV and 352 keV respectively. Standard materials were used for calibration of g-detector in accordance with IAEA reference materials (RGU-1, RGTh-1). Unsupported ^{210}Pb or ^{210}Pbxs was calculated from the total Pb after the subtraction of ^{226}Ra activity. Furthermore, counting errors of ^{210}Pbxs were computed by propagation from ^{210}Pb total and ^{226}Ra (Ruiz-Fernández et al., 2007; Schmidt et al., 2009; Azoury et al., 2013).

2.3.3 Characterization of algae

Algae material collected from the eutrophicated reservoir water was examined by SEM. The algae samples were prepared for SEM analysis in a similar way to the preparation of the

sediment samples as described in §2.3. In addition, the morphology of algae samples and the presence of chlorophyll was examined by Epifluorescence microscopy (Leica - DMRXA) equipped with a brightfield and darkfield inspection and coupled with motorized sextuple type nosepiece and HC PL Fluotar BD objectives: 5x/10x/20x/50x/100x. The tilting trinocular viewing head with 10x/25 eyepieces is associated with a 12V/100W lamp and automatic Koehler illumination. Finally, a DAPI staining analysis was performed with chlorophyll filter as described by Sherr et al., (1993) to investigate the nature of the material.

2.3.4 Data source

Historical data for the past 10 years were collected for dam hydrology, including the Litani River inflow, water level in the reservoir, and water outflow to Markhaba electric power station, piezometer level, as well as water quality of the lake and tributaries. That were monitored and provided by the Litani River Authority (LRA). Air temperature, relative humidity, and precipitation were measured at the nearest station to the reservoir in Kherbit Kanafar on a daily basis during the study period.

2.4 Packed soil columns experiment

2.4.1 Soil preparation

In order to understand metal behavior in the intact cores, and to study the soil type impact and the influence of contaminant type and its concentration; packed soil leaching column experiments were prepared in the laboratory in parallel to the field study. Soil designated for the packed columns were collected from the A-horizon from both watersheds right next to where the intact cores were collected. Soil for the agricultural packed columns experiments was comprised of a mixture of soils collected from lateral sides of the reservoir in order to have a better representative soil sample. The densities of the soils in the PVC columns were calculated by referring to the masses and calculated volumes of the studied soils in the columns. Volumetric and gravimetric water holding capacities (Θv and Θg) were determined by demonstrating how much water can be held in terms of volume and mass, respectively, by each set of soil.

2.4.2 Physicochemical characteristics of soil in packed columns

A dried Soil sample (oven dried at 105°C) was prepared for pH and conductivity determination. For pH, soil was mixed with distilled water at a 1:5 ratio (w/v) for an hour, it was left to settle, then the pH of the supernatant was measured using ADWA pH bench meter AD1000 coupled with a temperature electrode (NF ISO 10390). The same experiment was repeated, but 1N KCl was used instead of distilled water to determine pH-KCl in order to conclude the salt effect by subtracting the latter from the former. The salt effect represents the pH difference that is due to salts present in xenobiotic. For electric conductivity, a 1:5 ratio of soil:water (w/v) was agitated vigorously for 5 minutes, left for two hours to settle, then the

electrode was inserted in the clear supernatant and measured by Conductivity meter (Cond 330i) coupled with a tetraCon 325 electrode (from Weilhein). Electric conductivity was determined without vacuum; as a result, the true saturation extract EC is the product of EC (1:5) ratio multiplied by 6.4. The pH and TDS were measured according NF ISO 10390 and NF ISO 11265 respectively

The bulk density was calculated according to equation 2.2 by taking a mass of dry soil and dividing it over the volume it occupies. Particle density was calculated according to equation 2.3; however, the volume of soil solids can be determined by adding a specific volume of water to a volume of soil. The difference between the total volumes (water and soil) and water volume is the actual volume of the solid part of the soil. The percentages of solid space and porosity were calculated according to equation 2.4 and 2.5 respectively (Thien and Graveel, 2003).

$$\text{Bulk Density} = \frac{\textit{Oven Dry soil mass (g)}}{\textit{Volume of soil (with pores)(ml)}} \quad (2.2)$$

$$\text{Particle Density} = \frac{\textit{Oven Dry soil mass (g)}}{\textit{Volume of soil solids (ml)}} \quad (2.3)$$

$$\text{Solid space \%} = \frac{\textit{Bulk density}}{\textit{Particle density}} \times 100 \quad (2.4)$$

$$\text{Porosity \%} = 100 - \frac{\textit{Particle density}}{\textit{Bulk density}} \times 100 \quad (2.5)$$

Soil texture was determined by the Bouyoucos hydrometer method using an ASTM-E-100 Soil solution hydrometer (range 5 to 60 g/L) (Thien and Graveel, 2003). Forty grams of oven-dried soil was treated with H_2O_2, then dispersing solution (composed of 35.7 g of Sodium hexametaphosphate and 7.9 g of Sodium Carbonate in one liter deionized water), transferred to 1000 mL volumetric cylinder and filled with distilled water till mark line. Then readings were made at 40 seconds and 2 hours, where sand, and sand and silt had settled respectively. Corrected reading at 40 sec and 2 hours were calculated according equations 2.6 and 2.7 respectively.

$$R_{40sec} = h_{40sec} + 0.25\,(T_{40sec} + 18) \quad (2.6)$$

$$R_{2h} = h_{2h} + 0.25\,(T_{2h} + 19) \quad (2.7)$$

Where R_{40sec} and R_{2h} is the corrected reading at 40 seconds and 2 hours, h_{40sec} and h_{2h} are the hydrometer readings and T_{40sec} and T_{2h} are the measured temperatures at 40 seconds and 2 hours respectively.

Figure2.7: Soil texture triangle (USDA)

Where mass of sand = the total soil mass - R_{40sec}. While mass of clay is R_{2h}, and the mass of silt is the total soil mass – (R_{40sec}+ R_{2h}). The percentages of sand, clay and silt equals to their masses divided by 2 and multiplied by 100. Then after the soil type can be known by referring to the United State Department of Agriculture (USDA) texture triangle according to NF X31_107 (Figure 2.7).

The organic content percentage of the soil was estimated by the dry combustion method using wise therm furnace/oven calcinatory (ASTM D 2974). A certain mass of dry soil was heat-treated in a calcinator at 550°C for 24 hours, the mass loss of the soil represent the organic fraction. Therefore, the organic fraction percentage can be calculated by dividing the mass loss of soil by its initial mass. From that value, the content of organic carbon can be estimated by dividing the OM by 1.724 (Golueke and McGathey, 1971).

The total content of calcium carbonate ($CaCO_3$) in the soil can be divided into active and inactive calcareous. The active form of $CaCO_3$ is the clayey and silty fraction that is easily soluble in the water phase. Active calcareous of the soils was determined by titration method with potassium permanganate ($KMnO_4$) according to NF X-31-106 norm, and calculated according to equation 2.8:

$$\%CaCO3 = \frac{(V1-V2)}{10} \times 50 \times \frac{N}{0.02} \times \frac{V3}{V4} \times \frac{M}{m} \qquad (2.8)$$

Where V_1 and V_2 are the volumes of $KMnO_4$ used to develop color in the blank and the sample respectively. N is the normality of ammonium oxalate and V_3 is the total volume (ml) of the prepared ammonium oxalate, and V_4 is the volume (ml) of the sample used in the titration reaction. M is the MW (g/mol) of $CaCO_3$ while m is the mass (mg) of soil sample.

The total calcareous content was determined by Calcimeter Bernard method (NF ISO 10693) using 4 N HCl according to equation 2.9:

$$Total\ \%CaCO_3 = \frac{(m1 \times V2)}{(V1 \times m2)} \times 100 \qquad (2.9)$$

Where V_1 and V_2 are the volumes displaced by CO_2 released from $CaCO_3$ and from the soil sample, and m_1 and m_2 are the masses of $CaCO_3$ and soil sample respectively.

The available fractions of Potassium (K^+) and Sodium (Na^+) in the soils were determined by Protocol P05-001A. K^+ and Na^+ were extracted from the soil by a 0.5 M extracting solution of ammonium acetate and glacial acetic acid, and the dissolved portions of K^+ and Na^+ were measured using the Flame photometer model 420 from Sherwood. Cation Exchange Capacity (CEC) of a soil sample represents the capacity of cations a soil can handle per mass of soil. CEC is usually a measure of fertility of the soil, however in this study, CEC is important to estimate the rate of cations leaching through the columns by knowing how much cations that mass of soil can hold. CEC was determined by filling all the negative sites of the soil by Copper acetate according to equation 2.10; and then leaching of those adsorbed copper by

ammonium acetate. The content of copper was certified by SP 2000 UV Spectrophotometer VWR (Thien and Graveel, 2003).

$$CEC\ (meq) = \frac{C\ (mg) * 1g * 1mol * 100cmol * valence\ \acute{e} * V\ (L)}{1(L) * 1000(mg) * M\ (g) * 1(mol) * 1(cmol) * m\ (Kg)} \qquad (2.10)$$

Where C is the sample concentration, valence e^- is the number of electrons (which is 2 for Cu), V is the added volume of leaching solution (ammonium acetate) and M and m are the molar mass of Cu and mass of soil sample respectively. While grain charge was measured by zeta potential using a Zeta-Meter System 4.0 unit, equipped with an electrophoresis cell (type GT-2) of 10 cm long and 4 mm in diameter with K factor and two platinum electrodes. The Zeta-Meter is also equipped with a direct Video Imaging Assembly with overall magnification of about 160 times.

2.4.3 Soil column leaching experiment

A total of 28 packed columns were divided into two groups, where each group was designated for each watershed. The first set of packed columns contains soil from the Industrial watershed (Ip, n=14) whereas the second set of soils came from agricultural watershed (Ap, n=14). The air dried samples were sieved over 2 mm mesh and were homogenized and used to pack the PVC columns (L= 40 cm; r = 4.75 cm) up to a depth of 36 cm. The columns were placed over a Büchner funnel connected to polyethylene bottle and supported by a wooden rack, and a filter paper was placed on the top layer of each column to guarantee the homogeneous distribution of added/irrigated water (Figure 2.8). The column tests were conducted according to the OECD norms (OECD 312, 2004).

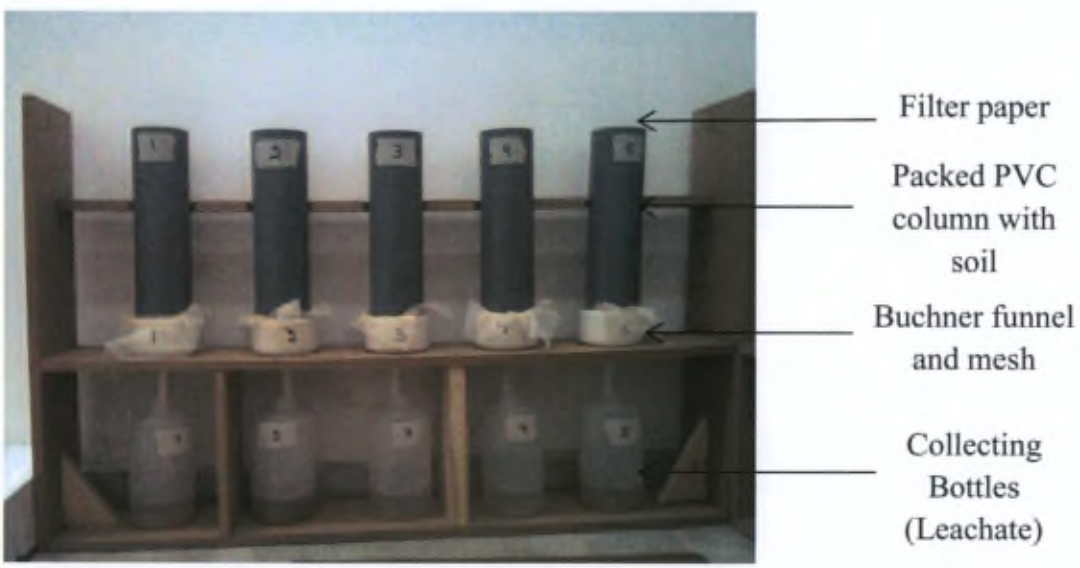

Figure 2.8: Leaching columns system.

After the system has been installed, and the soil has been packed, 70 % of the water capacity was reached in all 28 columns by ultrapure water to mimic natural conditions and allow biological growth. Fertilizers and PG were chosen as potential contaminants to be applied in

the column tests, due to the presence of these contaminants in the agricultural and industrial studied areas respectively. PG was collected from a slurry of the industrial factory, and two concentrations were chosen for the treatment, PG 1X and PG 2X. The two dosages represent the saturation phase (2 g/l) and double saturation phase (4 g/l) in ultrapure water, respectively (Ammar et al., 2013) as detailed in Chapter 3. A local survey was conducted to investigate a very common fertilizer in the agricultural area. The survey suggested the widespread use of NPK 20, 20, 20 which is a mixture of nitrogen, phosphate and potassium nutrients.

In order to resemble fertilizer's application in the field, we have calculated the concentration of applied fertilizer with regard to the surface area of the column. The application rate of NPK 20-20-20 is 10 pounds/acre, thus the required fertilizer concentration for each column was determined at 7944.82 µg (1X) and 15889.65 µg (2X). Each set was further divided into subsets of Blanks (n = 2), columns spiked by NPK 1X (n = 4), columns spiked by NPK 2X (n = 2), columns spiked by PG 1X (n = 4), and columns spiked by PG 2X (n= 2). The soil columns tests were run for 72 days including 50 artificial raining events, where the total applied water volume was similar to the relative volume produced by the average annual precipitation in Lebanon (900 mm) (Shaban, 2014). Thus the annual precipitation volume that would actually precipitate on the specific PVC column surface area would be 6.308 L, by which each raining event resample an irrigated volume to be 126 ml/column. At the end of the experiment the soil profile in each column was partitioned into increasing thicknesses as function of depth (2, 2, 2, 4, 5, 5, 5, 5 and 6cm), stored in polyethylene bags at -80°C, and freeze-dried by Lyophilizator.

2.4.4 Leachate analysis

Leachates were collected on daily basis and were filtered through 0.45 µm filters stored at 4°C for later analysis. Major ions Cl^-, NO_2^-, NO_3^-, PO_4^{3-}, F^-, and SO_4^{2-} were measured using Ion Chromatography (Shimatzu - shim pack IC-A3), where Na^+ and K^+ were measured using flame photometer model 420 from Sherwood. However samples targeted for metal analysis were acidified were acidified using concentrated HNO_3 to reach pH 1 once they were collected, and later subjected to heavy metals measurements (Fe, Mn, Zn, Cr, Cu and Cd) using Atomic Absorption Spectrometry (Rayleigh WFX-210 AA Spectrophotometry equipped with a WF-10A auto-sampler with flame and graphite furnace modes).

2.4.5 Characterization of soil in packed columns

The grain size population of the soils used for packed columns was measured via laser scattering particle size distribution analyzer (Patrica LA-950V2 Horiba). Chemical functional groups were determined by FT-IR-6300 (Fourier Transform Infrared Spectrometer) from JASCO. In addition, mineralogical phases in the samples were determined using a D8 Bruker X-ray diffractometer.

Collected sample layers from packed columns were freeze-dried and homogenized using pestle and mortar, sieved over 63 µm acid-cleaned nylon mesh, and extracted for particulate metals using a microwave acid digestion method as described in § 2.3.2.5.

2.5 Characterization of Phosphogypsum (PG)

Phosphogypsum samples were collected from the Lebanese Chemical Company (LCC) that imports phosphate rock ore from Syria which is of sedimentary origin (Yammine et al., 2010). PG was taken directly from the slurry at a depth of 20 cm, dried in an oven for two days at 70 °C, crashed using a IKA-WERKE model MF 10 basic stainless steel blade grinder, then sieved through a 0.25 mm mesh and stored in air-tight polyethylene bags to avoid rehydration.

2.5.1 Physicochemical characterization of PG

One gram of PG powder was suspended in one liter of milli-Q water (18.2 MΩ) at room temperature and homogenized for 30 min using a magnetic stirrer. Solution pH and electric conductivity were measured simultaneously using a pH meter (HANNA pH211 microprocessor pH meter) and conductivity meter (WTW cond i) respectively. Suspensions are filtered through 0.22 µm filters (Ministart sterile filter) and filtrates were collected for the determination of major ions by ion chromatography (Shimatzu - shim pack IC-A3). In order to understand and discriminate the behavior of PG particle charges and its interaction, the zeta potential was measured using a Zeta-Meter System 4.0 unit. PG grain size distribution was determined using a laser scattering particle size distribution analyzer (Patrica LA-950V2 Horiba). In order to investigate the different chemical groups in the samples, Fourier Transform Infrared spectroscopy (FT-IR, 6300 JASCO) was used. In the same time X Ray diffraction was used to detect the different crystal phases, using a diffractometer D8 Bruker. Heavy metal (Cd, Cr, Cu, and Zn) contents in the suspensions were measured using Atomic Absorption Spectrometry (Rayleigh WFX-210 AA Spectrophotometry) with flame or graphite furnace mode using certified standard materials and respecting limit of detection.

2.5.2 Effect of pH on PG suspension behavior

PG behavior in the suspension was studied in order to predict its behavior under various natural conditions at different pH. Eleven suspensions of PG powders at 1 g/L in ultrapure water were prepared. One is left at its initial pH to be treated as blank while the other 10 suspensions were adjusted to desired pH values (pH 2, 3, 4, 6, 7, 8,10,11,12 and 13). The pH adjustment was made by adding to the suspension while stirring with a magnetic stirrer at 300 rpm, appropriate volume of a 0.1 N HCl solution or a 0.1N NaOH solution. Each of the suspensions was agitated and left to equilibrate on the magnetic stirrer for 5 minutes at 300 rpm before pH measurement and then filtered through a 0.2 µm micro filter. Electric conductivity, potential zeta, particle size distribution, major anions and released metals were measured.

2.5.3 Effect of PG suspension load and organic ligands on the suspension behavior

In order to investigate the influence of the PG concentrations on the behavior of metal and ion release and exchange in the solution, four suspensions of increasing PG concentrations were prepared (1, 2, 3 and 4 g/L of PG) in ultrapure water.

Dihydrated trisodium citrate $Na_3C_6H_5O_7.2H_2O$ is used as an organic ligand in PG suspensions in order to evaluate its influence on PG dissolution in ultrapure water as a function of pH. This ligand is chosen in particular, since the three carboxylic groups enable it to complex with specific cations and heavy metals, which in its role facilitate their extraction from contaminated solid matrix. Also, citrate was categorized by different authors as the strongest polycarboxylic additive described as Gypsum plaster water retarder during hydration process (Escalante-García et al., 2009; Lanzon and Garcia-Ruiz, 2011; Boisvert et al., 2000; Singh and Middendrof, 2007). Four increasing concentrations of citrate were prepared (0.025, 0.05, 0.1, and 0.2M) in 1 g/L of PG suspensions along with a PG sample free of citrate acting as a blank. Each citrate concentration was prepared in a range of solutions from acidic to basic pH values as described in above, except for higher concentrations of 0.1 and 0.2 M of citrate that were studied only at three major pH values (pH 2, 7 and 12). The PG citrate suspensions were filtered using a filter of 0.22 µm and the suspended solids were recovered on a watch glass by scraping them off the filter and then dried in an oven at 60 °C for 20 minutes. The infrared spectrum of the solid phase was first obtained by FTIR characterization in order to investigate if any interactions of the new chemical groups had taken place upon citrate addition. The filtrates were analyzed for dissolved ions and other associated parameters.

2.6 Metal Speciation using Chemical Titration

Acidimetric titration was conducted on particular sediment samples to trace meal speciation and predict metal mobility. This method allows the mass balance calculation of solubilized element in regards to H^+ ions. Four grams of dry weight sample were dissolved in 500 ml of MQ water and placed on shaking board for one hour. 15 well homogenized aliquots of 20 ml were extracted from the mother suspension, and dispatched into pre-weighted 50 ml polyethylene tubes. In parallel HCl solution of 1 N is prepared and different concentrations are added to the tubes in propagating order from 25 to 2000 µl, except for two tubes that will act as blanks. All samples are agitated on a shaking board for 16 hours. Then after, subsample of 10 ml of each sample was filtered and in the same time pH of the remaining unfiltered 10 ml was measured. Prior to analysis the filtered samples should be adjust to pH equal to 1 in order to make the Cl^- ions in all the samples equal. Samples are then measured using ICP AES and atomic absorption (Petit et al., 2009).

Chapter 3

Applying physicochemical approaches to control Phosphogypsum heavy metal releases in aquatic environment.

Abstract[1]

One of the most important sources of solid waste in the Mediterranean Basin ecosystem originated from the phosphate fertilizer industries, which discharge Phosphogypsum (PG) directly into the aquatic environments or stacked on stock pile. The present study investigates metal release from PG under the influence of variable pH, increasing PG mass content and complexing organic matter ligands. Major ions from PG leachates, grain size and charge, main functional groups along with metal leachability (Pb, Cd, Cr, Cu, and Zn) were determined using ion chromatography, laser diffraction, zetameter, FTIR, and atomic absorption spectroscopy respectively. The complete dissolution of PG recorded is at 2 g/L. Saturation and super-saturation with respect to PG may occur at concentrations of 3 g/L and 4 g/L respectively revealing a clustering phenomenon leading to heavy metal encapsulation within the aggregates. Organic ligands such as citrate may trigger the cationic exchange within the PG suspension leading to ion release. As these factors are considered as specific process involving the release of contaminants from PG during storage under natural conditions, this study could set the foundations for PG remediation in aquatic environment. Organic ligands under controlled pH conditions could be utilized in treating fertilizer industrial wastes, by taking in consideration the particularity of the receiving area and thus decreasing metal hazardous impact on natural media.

[1] Adapted from the published article (Ammar R., El Samrani AG., Kazpard V., Bassil J., Lartiges B., Saad Z., Chou L. Applying physicochemical approaches to control phosphogypsum heavy metal releases in aquatic environment, Environmental Science and Pollution Research 20 (2013) 9014- 9025.

3.1 Introduction

Land-based activities and their impacts on different ecosystems in the Mediterranean Basin are related to the direct discharge of municipal wastes either as solid or liquid domestic and industrial effluents. One of the most important sources of waste originated from the phosphate fertilizer industries where multiple hot spots and sensitive aquatic ecosystems have been reported in Tunisia, Morocco, Algeria, Spain, Cyprus, Syria and Lebanon (Tayibi et al., 2009; Rentería-Villalobos et al., 2010; Rez-Loépez et al., 2007; Lysandrou and Pashalidis, 2008; Al-Masri et al., 2004; Othman and Al-Masri, 2007; Bridgen et al., 2002; Fakhri et al., 2008; Fakhri et al., 2009; Aoun et al., 2010). These industries mostly use phosphate ores originated from sedimentary marine deposits of the upper Cretaceous and Eocene of the Mediterranean phosphogenic province (Da Conceição et al., 2006). These ores are known to have a higher content of impurities than those of igneous origin (Kroschwitz and Howe-Grant, 1995; Tranchida et al., 2010). The by-product of most fertilizer industries, Phosphogypsum (PG), is directly discharged to the aquatic media and/or accumulated as stockpiles in large stacks (Aoun et al., 2010; Rez-Loépez et al., 2007; Battistoni et al., 2006; Lysandrou and Pashalidis, 2008). The exposure of PG stock piles to natural weathering process by wind and precipitation enhances the leachability of harmful trace metals released to the surrounding aquatic environments, including both sea and ground water (Carbonell et al., 1999; Lee et al., 2004; Canete et al., 2008; Firsova, 2010). This natural risk is increased due to the fact that most of the coastal regions of the eastern Mediterranean Sea receive a high amount of rainfall, about 600 to 800 mm per year (Bridgen et al., 2002; Rez-Loépez et al., 2007; Al-Masri et al., 2004, and Yammine et al., 2010).

Physical and chemical characterization of PG shows that it is mainly di-hydrate and hemi-hydrate calcium sulfate ($CaSO_4.2H_2O$, and $CaSO_4.1/2H_2O$), with impurities such as residual acids inherited from the wet acid process, fluorides, sulfate ions, trace metals (Cd, Cr, Cu, Zn), organic matter and radionuclides (Ra, U, Th) (Rutherford et al., 1994; Luther et al., 1996; Tayibi et al., 2009). Heavy elements and radionuclides are transferred to PG from the raw phosphate rock (Rentería-Villalobos et al., 2010). Concentrations for Cu and Zn in local PG are 52 ppm and 38 ppm respectively (Al-Masri et al., 2004; Othman and Al-Masri, 2007). Hence, PG waste shows contamination with a higher range of potentially toxic heavy metals compared to other PG composition (phosphate rock) reported in the literature (Renteria-Villalobos et al., 2010). Trace elements are found to be concentrated in fine particles of stockpiled PG, enhancing a serious environmental risk due to the leaching of these elements (Rutherford et al., 1994; Dudas et al., 1995; Al-Masri et al., 2004; Othman and Al-Masri, 2007).

Research studies suggested several ways to reuse the massive amounts of PG by-product. The common similarities of PG with gypsum allow its utilization as gypsum substitute in construction and engineering practices. Also, PG enrichment by nutrients makes it feasible to be used as an agrochemical in soil amendment. PG is able to lime acidic soils due to the

dissolution of Ca ions (Alva and Sumner, 1988), and to decrease the soil phosphate loss via aggregation (Jaakola et al., 2012). Researchers mixed the hydrated gypsum species with organic compounds as organo-mineral fertilizers to improve soil fertility (Mishra et al., 2011, Zhumanova et al., 2012). However, the utilization of PG is dangerous, if PG is neither free of radioactive elements nor of bioavailable metal fractions. Consequently treatments were applied to reduce PG solubility and dust emission, by adding either natural humic acid or synthetic polyelectrolytes (Firsova, 2010). Attallah et al., (2010) designed a physical separation of PG based on grain size, and a chemical treatment with different solutions including deionized water, alkaline solutions and nitric acid leachates, since contaminants are enriched in the fine fraction which is easily weathered (Attallah et al., 2010). Lee et al., (2004) recommended to construct a vertical hydrodynamic barrier systems at the roots of the PG stockpiles to trap the seepage and reduce its ecological hazard (Lee et al., 2004).

The treatment of PG is thus based on its solubility. Marshall and Slusher, (1966) indicated that the ionic strength of gypsum and its hydrates controlled its solubility in suspension, by which the solubility related to different physico-chemical parameters such as temperature, pH, salts, and organic matter concentration. Ersen et al., (2006) studied the retarding effect of carbonic acids such as malic and citric acids on gypsum and PG crystallization, and referred this process to the fact of adsorption of organic ligands on the surface which decrease its dissolution. Citric acid modifies the crystal form of PG from needle-like to sharp pyramids thus deforming its strength and combines with dissociated Ca^{2+} ions (Qu et al., 2011). Previous studies show that pH controls the Al toxicity in PG amendments used on agricultural soils, since the SO_4^{2-} from the hydrated $CaSO_4$ forms ion-pairs with Al and affects the Al toxicity within pH 4.1-4.8 (Alva and Sumner, 1988). At basic pH, Smith and Sweett, (1971) postulated that crystallization decreases as pH increases, and Yaun et al., (2010) observed a constant dissolution of $CaSO_4.2H_2O$ with time during addition of low concentrations of NaOH. Carbonell et al., (1999) studied the leachability of metals at different pH and founded that major elements like Ca, Mg, P, and K were controlled by the pH of PG and not that of the receiving media, while the reverse was true for minor and trace metals. Also, the mobility of metals increased in acidic media and decreased at basic pH.

In a recent study, impact of PG stock piles on the surrounding area near a phosphate fertilizer industry was investigated (Aoun et al., 2010). Leaching, atmospheric deposits, and wind dynamics were found to be the main factors controlling the transfer and mobilization of trace elements from PG to sediments and soils (Aoun et al., 2010). However, the authors pointed out that they did not take into account the variability of soils, sediment properties and the particularity of the receiving area. The physicochemical characteristics of soil controls metal biogeochemical process (Chen et al., 2006). Metals are well known for their high affinity for clay minerals, fine fraction materials, and soil rich in organic matter content (Pathak et al., 2004; Roussiez et al., 2005; Wu et al., 2011). Metals will complex with organic matter in acidic soil and precipitate in basic soil (Das and Narwani et al., 2009). Fe solubility decreases as pH increases (Korfali and Davies, 2004). Zinc and copper show high mobility in acidic sand soils (Chen et al., 2006); however Zn shows the highest mobility. In contrast,

Mediterranean carbonate soils exhibit the highest mobility for Ni and the lowest for Pb (Lafuente et al., 2008). Previous studies have shown that some metals released from PG amended on alluvial sediments complexed with organic matter were fixed on clay minerals (Carbonell et al., 1999). Canete et al., (2008) examined the variation in leachability of radioactive ^{226}Ra in PG through four different soils and found that sandy loam was the least capable to detain the ^{226}Ra from the PG leachate. Mishra et al., (2011) studied the impact of PG amendment on modifying the soil physico-chemical characteristics and improving the soil flora activity. In general, variation of pH in the stockpile itself and the role of natural organic and inorganic ligands in the receiving environment are not considered when studying metal release from PG to the environment under arid or rain-based leaching and erosion conditions.

The environmental safety use of the resulting PG is thus crucial in our case and an extensive study must be conducted to delineate the mobility and availability of trace elements under the specific local conditions. The objective of the present study is to determine the releases and leachability of trace elements in PG under the influence of pH, suspension load and organic ligands as these factors are considered as specific process involving the release of contaminants from PG during storage under natural conditions. Zetameter, laser diffraction, ion chromatography, FTIR, and atomic absorption spectroscopy were used to investigate the behavior of heavy metals in PG in aquatic media.

3.2 Materials and methods

3.2.1 PG samples

Phosphogypsum samples were collected from the Lebanese Chemical Company that imports phosphate rock ore from Syria which is of sedimentary origin (Yammine et al., 2010). PG was taken directly from the slurry at a depth of 20 cm, dried in an oven for two days at 70 °C, crashed using a IKA-WERKE model MF 10 basic stainless steel blade grinder, then sieved through a 0.25 mm mesh and stored in air-tight polyethylene bags to avoid rehydration.

3.2.2 Physicochemical characterization of PG

One gram of PG powder was suspended in one liter of milli-Q water (18.2 MΩ) at room temperature and homogenized for 30 min using a magnetic stirrer. Solution pH and electric conductivity were measured simultaneously using a pH meter (HANNA pH211 microprocessor pH meter) and conductivity meter (WTW cond i) respectively. Suspensions are filtered through 0.22 µm filters (Ministart sterile filter) and filtrates were collected for the determination of major ions by ion chromatography (Shimatzu - shim pack IC-A3) accompanied with a conductivity detector CDD-10AVP. In order to understand and discriminate the behavior of PG particle charges and its interaction, the zeta potential was measured using a Zeta-Meter System 4.0 unit, equipped with a electrophoresis cell (type GT-2) of 10 cm long and 4 mm in diameter with K factor and two platinum electrodes. The Zeta-Meter is also equipped with a direct Video Imaging Assembly with overall magnification of about 160 times. PG grain size distribution was determined using a laser scattering particle

size distribution analyzer (Patrica LA-950V2 Horiba). The measurement method relies on the basis of Mie scattering theory, with measuring range varying between 0.01 to 3000µm using a ultrasonic probe with measuring time of 20 sec at a frequency of 20 kHz. The devise is equipped with an optical system of two light sources, a laser diode of approximately 1.6mW with λ equal to 650 nm and a 405 nm light emitting diode (LED) of approximately 0.3 mW. Samples were well mixed and homogenized in their powder state prior to their analysis.

In order to investigate the different chemical groups in the samples, Fourier Transform Infrared spectroscopy (FT-IR, 6300 JASCO) was used. Powdered samples were mixed with potassium bromide (KBr) in the amount of 1% wt/wt of the sample. The prepared pellet was compressed into a 0.7 cm diameter holder. In the same time X Ray diffraction was used to detect the different crystal phases, by which homogenized powder samples were previously prepared on PVC lenses (diameter 2.5 cm, thickness 2 mm) and measured using a diffractometer D8 Bruker (anticathode cupper that emits X-ray with wave length $\lambda K\alpha$ = 0.154060 nm). Range of 2θ between 10 and 60 degrees were chosen to obtain maximum clarity of crystal phase's diffractogram, with leaps each 0.02 degrees and one second were designed for measurement. Collected diffractograms were analyzed by the software EVA based on powder diffraction files provided by the interactive center for diffraction data ICDD. Heavy metal (Cd, Cr, Cu, and Zn) contents in the suspensions was measured using Atomic Absorption Spectrometry (Rayleigh WFX-210 AA Spectrophotometry) with flame or graphite furnace mode using certified standard materials and respecting limit of detection.

3.2.3 Effect of pH on PG suspension behavior

PG behavior in the suspension was studied in order to predict its behavior under various natural conditions at different pH. Eleven suspensions of PG powders at 1 g/L in ultrapure water were prepared. One is left at its initial pH to be treated as blank while the other 10 suspensions were adjusted to desired pH values (pH 2, 3, 4, 6, 7, 8,10,11,12 and 13). The pH adjustment was made by adding to the suspension while stirring with a magnetic stirrer at 300 rpm, appropriate volume of a 0.1 N HCl solution or a 0.1 N NaOH solution. Each of the suspensions was agitated and left to equilibrate on the magnetic stirrer for 5 minutes at 300 rpm before pH measurement and then filtered through a 0.22 µm micro filter. Electric conductivity, potential zeta, particle size distribution, major anions and released metals were measured.

3.2.4 Effect of PG suspension load and organic ligands on the suspension behavior

In order to investigate the influence of the PG concentrations on the behavior of metal and ion release and exchange in the solution, four suspensions of increasing PG concentrations were prepared (1, 2, 3 and 4 g/L of PG) in ultrapure water.

Dihydrated trisodium citrate $Na_3C_6H_5O_7.2H_2O$ is used as an organic ligand in PG suspensions in order to evaluate its influence on PG dissolution in ultrapure water as a function of pH. This ligand is chosen in particular, since the three carboxylic groups enable it to complex

with specific cations and heavy metals, which in its role facilitate their extraction from contaminated solid matrix. Also, citrate was categorized by different authors as the strongest polycarboxylic additive described as Gypsum plaster water retarder during hydration process (Escalante-García et al., 2009; Lanzon and Garcia-Ruiz, 2011; Boisvert et al., 2000; Singh and Middendrof, 2007). Four increasing concentrations of citrate were prepared (0.025, 0.05, 0.1, and 0.2 M) in 1g/L of PG suspensions along with a PG sample free of citrate acting as a blank. Each citrate concentration was prepared in a range of solutions from acidic to basic pH values as described in §3.2.3, except for higher concentrations of 0.1 and 0.2 M of citrate that were studied only at three major pH values (pH 2, 7 and 12). The PG citrate suspensions were filtered using a filter of 0.22 µm and the suspended solids were recovered on a watch glass by scraping them off the filter and then dried in an oven at 60 °C for 20 minutes. The infrared spectrum of the solid phase was first obtained by FTIR characterization in order to investigate if any interactions of the new chemical groups had taken place upon citrate addition. The filtrates were analyzed for dissolved ions and other associated parameters.

3.3 Results and discussion

3.3.1 Influence of PG suspension load on its behavior

The increased mass content may alter the behavior of ions and metals released in PG suspension. Table 3.1 summarizes the results of physicochemical parameters and the amount of metals released for the various suspension loads. Conductivity of ions released from PG suspension to the medium increased with PG suspension load in a logarithmic manner where R^2 equals to 0.978 and slope 281.2. It increased from 943 to 1630 µS/cm when the PG load was 2 g/L. However, no significant change took place when the suspension load increased further, suggesting that the PG solubility was reached at a concentration close to 2 g/L, in agreement with the observation of Haynes (2011). Our data also show that the insoluble residue is estimated to be about 25%.

Grain size of 63 µm is well known as a threshold to separate fine grains from coarse ones (Zingg et al., 2008). The size of 70 µm was thus chosen to compare the evolution of the fine size fraction as a function of PG suspension load. Table 3.1 indicates the disappearance of the small grains, in favor of the presence of large populations, with increasing suspension load of PG. This could show an aggregation phenomenon which is highlighted by passing from 1 g/L to 4 g/L of PG. This particle size distribution is in coherence with electric conductivity values and solubility. Whereas the 3 and 4 g/L suspensions may lead to super-saturation of the solution, inducing the particles to aggregate and form larger grain sizes. When 3 g and 4 g of PG were added to 1 L to Milli-Q water, the 2 first grams should be solubilized completely in the solution, and the remaining 1 g and 2 g will stay in solid phase respectively. Thus the solid matrix remained in the 3 g/L and 4 g/L suspension may interact with the released Ca^{2+} and SO_4^{2-} from the 2 g of solubilized PG. So we assume that the released ions will coat the undissolved portion of PG, and branching sequences of attracted opposite ionic charges will enhance the growth of the crystal (Figure 3.1). PG has higher solubility than $CaCO_3$ (Carbonell et al., 1999). Marshall and Slusher, (1966) stated that the calcium sulfate in

solution dissociates completely to Ca^{2+} and SO_4^{2-} ions. However, if HPO_4^{2-} ions are present in the main crystal, they will compete with SO_4^{2-}, since both anions share the same radius (4-4.5 angstroms) and high affinity to calcium cations (Strydom et al., 1997). Even more calcium ions are able to bridge with soil particles forming aggregates (Jaakola et al., 2012), so we assume that Ca ions will bridge to undissolved PG in the saturated and super-saturated suspensions. This postulation was attested by the slight increase in the zeta potential from -29 mV to -22 mV, accompanied by the increase in average grain size in suspensions and growth of the frequencies of large populations. Almost 50% of (PG matrix) comprised sulfate ions, and might contain impurities of sulfate from the usage of H_2SO_4 acid in the manufacture process (Lysandrou and Pashalidis, 2008; Tayibi et al., 2009). Thus the released sulfate ions from 1 g/L of PG to the suspension indicates its total dissolution in the solution, by which PG maximum solubility is reached at a concentration of 2 g/L. Although the concentration of sulfate ions in the solution increased with PG concentrations as was the case for conductivity, the amount of sulfate released per gram of PG decreased (Table 3.1).

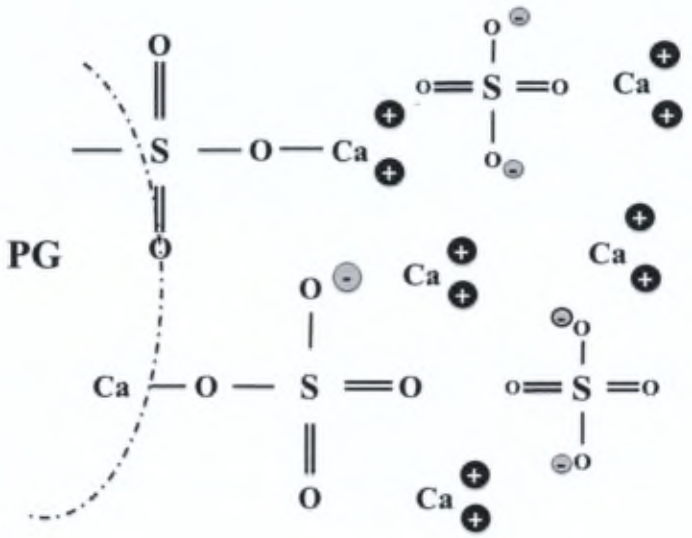

Figure 3.1: Proposed chemical structure of PG in the suspensions.

This suggests that a more stable and thus less soluble phase of phosphogypsum is formed with the increasing PG concentration. The amounts of Pb, Zn, and Cu released per gram of PG show a linear relationship with increased PG concentrations where R^2 equals 0.89, 0.79, and 0.94 respectively. In contrast, the amounts of Cd and Cr released per gram of PG in suspension show a (natural) logarithmic relation with PG concentration, where R^2 equals 0.74 and 0.55 respectively. This is due to the fact that only a minor amount of Cu and Cr were released for the first g of PG/L. The amount of Pb, Zn, and Cu released per gram of PG decreased as the amount increases from 1 to 4 g/L where they all have negative slope values. Hence released Pb decreases from 14 to 10 µg/g when PG concentration increased from 1 to 4 g/L respectively. In the same manner, released Zn and Cu in the suspension decreased to its

half amount from 35 to 18 µg/g and from 1.8 to 0.9 µg/g respectively when the PG concentration increased four times. Regarding the strong linearity in addition to the abundance of Zn over Pb, these two bivalent metals may compete for the adsorption sites of the matrix and the released metals could not be absorbed again (Venäläinen, 2011). The amount of Cd and Cr released in 1 g/L was small, while their maximum release was recorded at 2 g/L suspension of PG (8.5 and 1.05 µg/g respectively). When PG concentration increased from 3 g/L to 4 g/L the amounts of both released metals (Cd and Cr) decreased very slightly, indicating that the concentrations of these metals were approaching gradually a constant value as PG concentrations increased. This observation may be explained by metals reabsorption to the solid matrix or the solubility of another phase containing these metals is being reached. This metal behavior confirms PG behavior when it increases in solution. As a consequence the majority of these metals might be trapped in the large aggregates formed by increasing the concentration of PG. These results highlight the PG solubility interference in heavy metal release. We assume that the reaching of PG solubility is delayed by entrapment of particles. Thus increasing PG concentrations can be considered as a limiting factor to exchange phenomena between Ca and metals. As a result, metals will be trapped in the PG and become less labile in the aqueous medium. Our results indicate that in severely contaminated cases where the concentration of phosphogypsum becomes saturated or even supersaturated in the medium, the mobility of certain metals such as Pb, Zn, and Cu may become increasingly limited, while the establishment of PG solubility is delayed by aggregation. This will increase the environmental hazards of these metals in stockpiles when later reuses or special treatments are planned. Mobilization of other metals such as Cd and Cr seems to decrease with increasing PG concentrations.

Table 3.1: Physicochemical parameters and the amount of metals released as a function of PG suspension load.

Phosphogypsum (g/L)	Conductivity (µS/cm)	% of Grain size (<70 µm)	Zeta Potential (mV)	SO_4^{2-} (mg/g)	Released heavy metals (µg/g)				
					Pb	Zn	Cu	Cd	Cr
1	943	99.4	-29.05	518.7	14.3	35.2	1.8	0.4	0.5
2	1630	50	-28.5	458.8	11.9	22.1	1.3	8.5	1.05
3	1512	50	-27.1	386.5	11.1	20.3	1.1	8.3	1.03
4	1693	70	-22.3	337.5	10.5	18.3	0.9	8.1	0.9
Regression R^2	0.7842 Natural Logarithmic	0.238 Linear	0.829 Linear	0.995 Linear	0.891 Linear	0.787 Linear	0.940 Linear	0.741 Natural Logarithmic	0.551 Natural Logarithmic
Slope	504.73	-8.9	2.17	-61.59	-1.21	-5.25	-0.29	5.66	0.32

3.3.2 Effect of citrate ligand on PG dissolution at various pHs

Trisodium citrate was added to PG suspensions in different concentrations at a PG concentration of 1 g/L and its effect on PG behavior in suspension was studied as function of pH. Electrical conductivity evolution of PG suspension prepared in increasing concentration of citrate is presented in (Fig 3.2a). The electrical conductivity of PG suspension with 0.025 M of citrate addition is 4 times greater than suspension without citrate. It increased 8 times more when we increase the amount of the organic ligand to 0.05 M. This can be seen at any pH value. However data obtained for PG suspensions without the addition of citrate ligand (0 M) as a function of pH, demonstrates that the conductivity at acidic medium (pH 2) is higher than that that in the basic medium. The same trend is followed by the other plots of increasing citrate concentrations. The increase in suspension conductivity with citrate concentration may be attributed to the increase of Na^+ ions surge provided by trisodium citrate. Furthermore its behavior regarding pH changes could be explained by cation extraction from PG material into the suspension by citrate, by which each citrate molecule will interact with two calcium cations leading to its complexation (Li et al., 2011) and the decrease in free Ca^{2+} ions present in the suspension as shown by the decrease in electrical conductivity. This is coherent with a previous review, stating that as the concentration of the ligand increases, its adsorption to the particles surface increases, resulting in a rise in electrical conductivity (Singh and Middendrof, 2007). However, other authors indicated that the affinity of COO^- group to Ca^{2+} in PG could cause the increase in electric conductivity (Lanzon and Garcia-Ruiz, 2011).

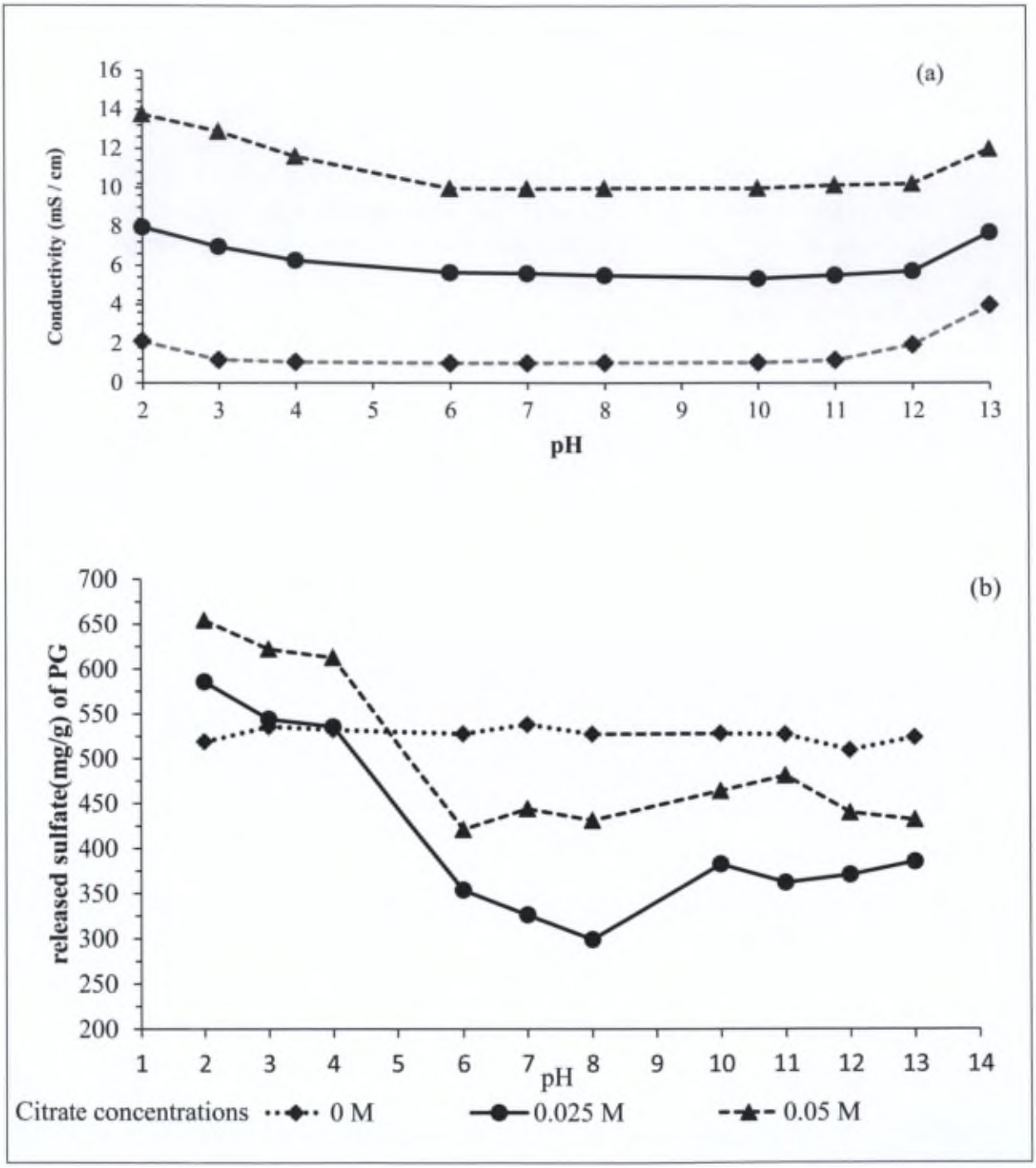

Figure 3.2: Evolution of conductivity (a), and released sulfate (b), as a function of both citrate concentrations and pH.

The amount of sulfate released in PG suspension at 1 g/L as a function of both citrate ligand concentration and pH is in agreement with the conductivity measurements (Figure 3.2b). Comparison of results obtained in the presence and in the absence of citrate indicates that released sulfate increased in the range varying from 357 mg/g to 752 mg/g of PG suspension when citrate concentration was added from 0.025 M to 0.2 M respectively (Tables 3.2 and 3.3). Regardless of the citrate concentration, the amount of sulfate released exhibits maximal values at pH 2 which then decreases as the pH values approaches 7 and fluctuates slightly between pH 6 and 12 (Tables 3.2 and 3.3). Thus it is well shown that increasing citrate ligand concentrations enhance the dissolution of PG grains, which is confirmed by the increase in sulfate released and high conductivity. Furthermore, higher amount of sulfate released was observed in higher concentrations of citrate and at acidic pH, whereas at basic pH the presence of citrate has less influence. Sulfate released per gram of PG increases with citrate concentration from 0.025 M to 0.1 M and then decreases from 0.1 M to 0.2 M, which may be explained by the citrate obstruction after reaching a concentration threshold.

Table 3.2: Chemical and physical characterization and the amount of metals released from PG suspensions in the presence of different citrate concentrations.

Blank *	Conductivity (mS/cm)	Released sulfate (mg/g)	Zeta potential (mV)	Mean Diameter (µm)	Pb (µg/g)	Zn (µg/g)	Cu (µg/g)	Cr (µg/g)	Cd (µg/g)
0M	0.853	519	-29	8-39	13	35	2	0.4	0.5
0.025	5.400	357	-45	2-56	10.6	47	56	31	64.5
0.05	9.880	460	-59.4	2.9	37	72.5	80	121	100

(*) Blank: represents the suspension of PG without pH adjustment.

Table 3.3: Physicochemical parameters and the amount of metals released of PG suspension with 0.1 and 0.2M citrate as a function of pH.

Citrate (M)	0.1	0.2	0.1	0.2	0.1	0.2	0.1	0.2	0.1	0.2	0.1	0.2
Released ions in (mg/g)	SO_4^{2-}		Pb		Zn		Cu		Cr		Cd	
pH = 2	752	721	254	381	268	430	286	439	310	555	286	439
pH = 7	631	533	220	273	120	321	236	395	263	474	236	395
pH=12	629	545	152	254	82	118	259	466	167	359	140	166

Sulfate results are well correlated with those of particle size growth as shown in Figure 3.3 a and b where the grain size distribution of PG is plotted as a function of citrate concentration and pH. The particle size distribution for suspensions of 0.025 M citrate is highly dependent on pH. At pH 2 the fine grains are distributed in a monomodal population with an average size of 5 µm. As pH increases, the monomodal size distribution transforms into a bimodal one, indicating the occurrence of aggregation phenomenon of particles much bigger than those clusters observed for citrate-free PG suspensions. While as pH increases from 4 to 13, the bimodal mean particle size distribution decreases, which may be due to filling of the pore sizes with smaller grains shown as a wide peak summit. Citrate may be adsorbed onto PG particles and form calcium citrate (Escalante-García et al., 2009), where this newly formed compound promotes the nucleation of the crystal and increases its size, which is in agreement with previous studies (Escalante-García et al., 2009).

By increasing the citrate concentration to 0.05 M (Fig. 3.3b) and 1 M, the bimodal population disappears and a monomodal population is observed where the pH influence is limited. The observed average size was approximately 3 µm regardless of pH for the two concentrations studied. The increased citrate concentration may increase the ion substitution in the matrix where a repulsive force will be created leading to aggregates of finer size. As well in the same scope, a recent study noted that citrate concentration at 1 mg/g have a negative impact on PG strength, where microstructural crystallization delayed (Lanzon and Garcia-Ruiz, 2011). However, at 0.2 M citrate addition there size populations sizes appear at pH 7 and 12 (data not shown). It was previously deduced that high citrate concentration has great influence on PG dissolution; furthermore, citrate may possibly contribute indirectly to dissolution of PG particles via cation entrapment.

Mean grain size evolution is further evaluated by following the zeta potential as a function of pH and citrate concentrations. Zeta potential for citrate-free PG suspensions show contradictory trend compared to that of citrate-added suspensions. In the presence of citrate, the zeta potential decreases as pH increases reaching -50 mV at pH 13 for both citrate concentrations (Fig. 3.3c). In acidic media zeta potential values of PG samples accompanied with citrate addition were higher than those of citrate-free PG suspensions until close to pH 5. From that point onward, the zeta potential decreases with increasing pH from -18 mV at pH 4 to -50 mV at pH 13. In contrast, citrate-free PG sample values increase and pass by the isoelectric point to reach positive charge values equal to +20 mV at pH 13. This decrease in zeta potential due to citrate addition can be explained by cation extraction from the PG, which in its role will reduce the charge loads on the surface. Elmotfy and Shokir, (2003) stated that organic molecules are adsorbed to the solid surface of particles by both electrostatic energy and chemical bonds, and their negative charge will contribute to decrease zeta potential values. Thus in the present study a comparable phenomenon could be established owing to the negative charge of the carboxylic groups of citrate ligand. At acidic pH citrate will transform to form citric acid. Thus under these conditions, the sodium citrate solution will aid in the formation of the ionic cloud around PG particles, which will decrease the negativity of zeta potential values at pH less than 5. Li et al., (2011) stated that citric acid could continuously react with hydroxyapatite and dissolve it because there was no charge transfer. This may take place when citric acid is formed at acidic pH leading to the dissolution of PG. In contrast, at basic pH there might be an ion exchange phenomena between free citrate ions, added NaOH and PG that transport negative charges to the matrix preventing further crystal growth.

Metal interaction with organic fractions in the PG/citrate suspensions was studied and Figure 3.4 illustrates the influence of citrate on the release of heavy metals present in the phosphogypsum. It is clearly observed that citrate is able to mobilize metal from PG matrix and that increased citrate concentrations are accompanied by increased metal release. This behavior is attributed to the high affinity of metals to citrate. However, each metal responds in a different way to the increasing amount of citrate, ionic strength and pH which in turn reflects the specificity of metal–citrate interaction in the suspension as a function of pH.

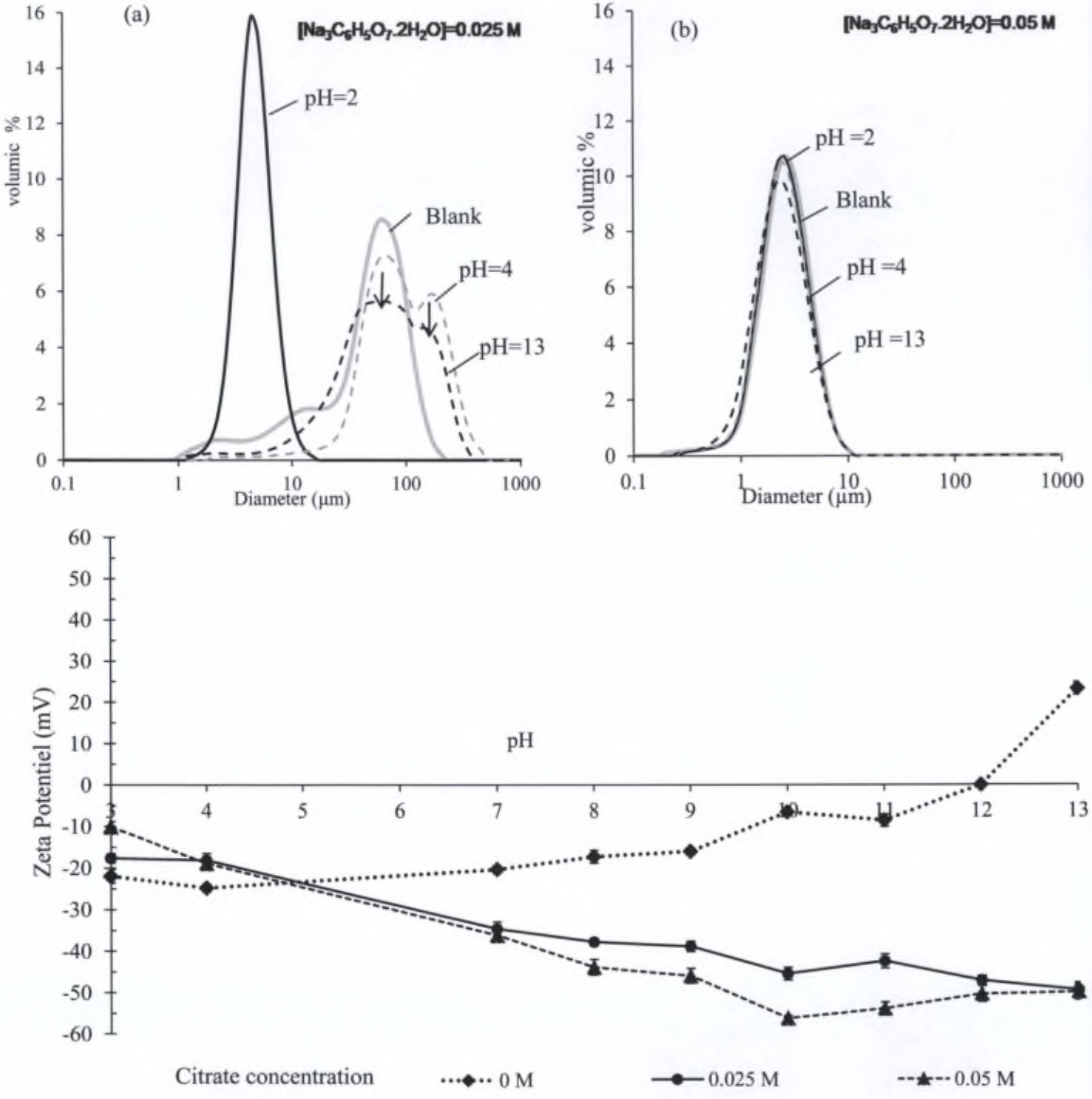

Figure 3.3: Evolution of size distribution of PG suspensions and mean diameter of populations in 0.025 M citrate (a) and 0.05 M citrate (b), and potential zeta as a function of both citrate concentrations and pH (c).

Pb, Zn, and Cr behave in a similar manner in the PG suspension when citrate is added. The maximum metal release was observed at pH 2 and the release decreased as the medium becomes alkaline. Since these divalent metals are easily scavenged from the suspension, they may either co-precipitate with calcite, or compete with other metals and substitute Ca^{2+} at high pH values. Lead will be in the form of $PbOH^{+}$ at basic pH and will compete with Al and Fe (Venäläinen, 2011). Another study found that Pb would be released from mineral dissolution at acidic pH, while at pH >6 Pb will be insoluble (Chrysochoou et al., 2007). However, Cd as shown previously is a refractory metal and shows a weak mobility when low amounts of citrate were added. Nevertheless, when high concentrations of citrate (0.1 M and 0.2 M) were added, maximum Cd release was observed at pH 2 (286 µg/g and 436 µg/g respectively).

Furthermore, Cu shows a similar behavior as a function of pH and in the presence of citrate its behavior can be divided into two stages addressing both acidic and basic pH ranges. Copper release decreased from pH 2 to pH 7 then its release increased again when pH reached 13. This trend is clearly observed when high concentrations of citrate were added as shown in Table 3.3. Readsorption phenomena may take place at neutral pH. Furthermore, calcium in the PG crystal at neutral pH as shown in Figure 4.3a may be exchanged by Cu ions in the suspension. Copper may be more competitive than the other metals found in the medium to substitute the calcium on the crystal lattice. As a consequence, levels of released metal decrease as pH increases, which may be linked to the retarded dissolution of PG at basic pH. Since trisodium citrate increases the ionic strength of PG suspension, thus increasing the aggregation of the double layer, this would make it more difficult to dissolve at basic pH where Cu affinity sites could be exposed to the upper layer rendering them more susceptible to be released.

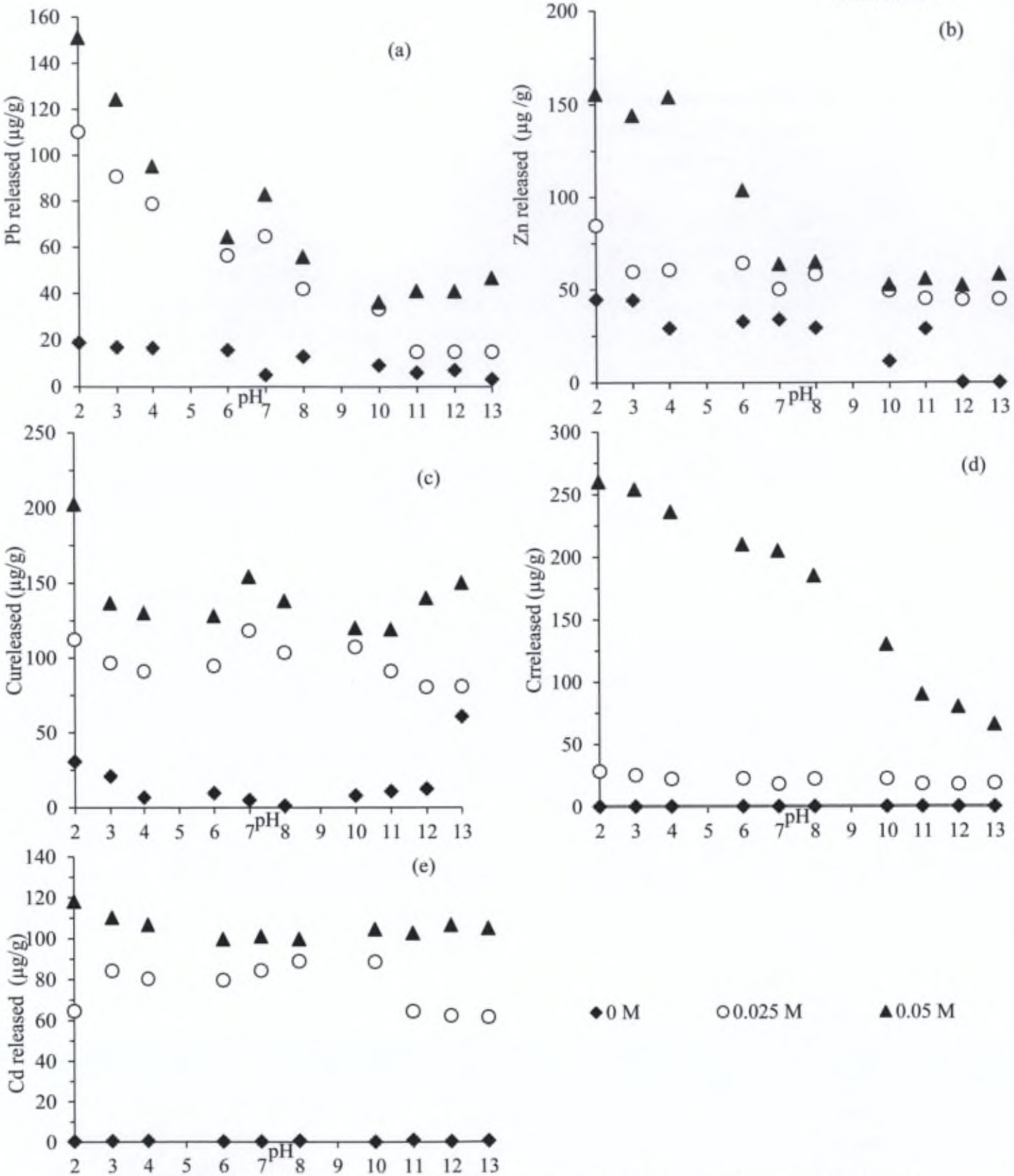

Figure 3.4: Evolution of released metals for Pb (a), Zn (b), Cu (c), Cr (d) and Cd (e) as a function of both citrate concentrations and pH.

Infrared spectra of PG particles in suspension as a function of both citrate concentration and pH were studied. I_0 represents the stretching of v_3SO4, where the two peaks identified were named I_1 (775 cm^{-1}) and I_2 (1650 cm^{-1}) corresponding to the functional groups SO-R and COO^- respectively. Figure 3.5 demonstrates the changing of intensity ratios I_1/I_0 (SO-R/SO4) and I_2/I_0 (COO^-/SO4) as a function of both pH and of trisodium citrate concentration. The sulfate intensity is presented by I_0, while I_1 and I_2 peaks imitate the citrate complexation or grafting on the surface of PG particles. Thus, the abundance of I_1 and I_2 over I_0 shows a grafting of the citrate groups on the surface of PG at any pH and for any citrate concentration. Ratios of I_1/I_0 and I_2/I_0 decrease sharply as citrate concentration increase from 0.025 M to 0.05 M at any pH. After that dose, these ratios decrease slowly as citrate concentration increases to 0.2 M. This decrease of intensities with increasing citrate concentration is accompanied by sulfates and metal release in the aqueous medium. Since the ratios show a decrease in intensities, it reveals the decrease of citrate grafting on PG surfaces. Furthermore, lowest intensity ratios were observed for pH 7 and 12, while highest intensities were obtained at pH 2. Thus disassociation of the functional groups occurs at basic pH and in the presence of carboxylic ligands which was also observed by Li et al., (2011). In addition, PG may react with NaOH forming portlandite, calcium hydroxide, at basic pH (Cardenas-Escudero et al., 2011). However, the ratios of I_2/I_0 at any pH can be clearly correlated with the mean grain size distribution shown in Figure 3.3 (a and b). Subsequently high intensity ratios revealing citrate grafting on PG surface, shows larger grain size distribution when 0.025 M of citrate was added. The presence of 0.05 M and 0.1 M of citrate reveals less grafting and finer grain size distribution, less than 10 μm. Results for 0.2 M citrate shows that the intensity ratio increases slightly and a bimodal size distribution was observed. This may be explained by dissolution of PG enhanced by citrate at low pH and its particles recrystallization at basic pH.

As a consequence, citrate is a very effective organic ligand that affects PG particles dissolution and nucleation which in its role is limited to mass concentration and pH values. It is now clear that organic ligands could be utilized under controlled pH conditions to treat fertilizer disposal waste and PG recycling in order to decrease the hazardous impact of released metals on natural media.

Electric conductivity conjugated to grain size detection, in addition to particles electric charge were able to address PG solubility. The understanding of the behavior of PG in suspension is fundamental to predict the hazardous metal mobility. PG dissolution reaches equilibrium at 2 g/L. Calcium ion bridging will take place when increasing PG concentrations, making stable aggregates. The increased suspension load will reduce the mobility of some metals such as Zn and Cu; however some metals are able to be re-entrapped on the solid matrix. The high electric conductivity observed with increased citrate concentration reveals the dissolution of PG via cation extraction phenomenon mainly at acidic pH, thus increasing released labile metals into the suspension. The synergetic effect of (1) acidic pH, (2) low suspension load and (3) presence of organic ligand will enhance PG dissolution. Hence, the hazardous metals will be expelled out and then the residual PG could be used in construction or agricultural practices. Nevertheless, encapsulation of the hazardous

elements in the PG matrix under alkaline conditions in large amounts of solid free of organic matter is an alternative approach for pre-recycling of the massive amounts of PG stored in stockpiles next to factories in the proximity to natural aquatic media.

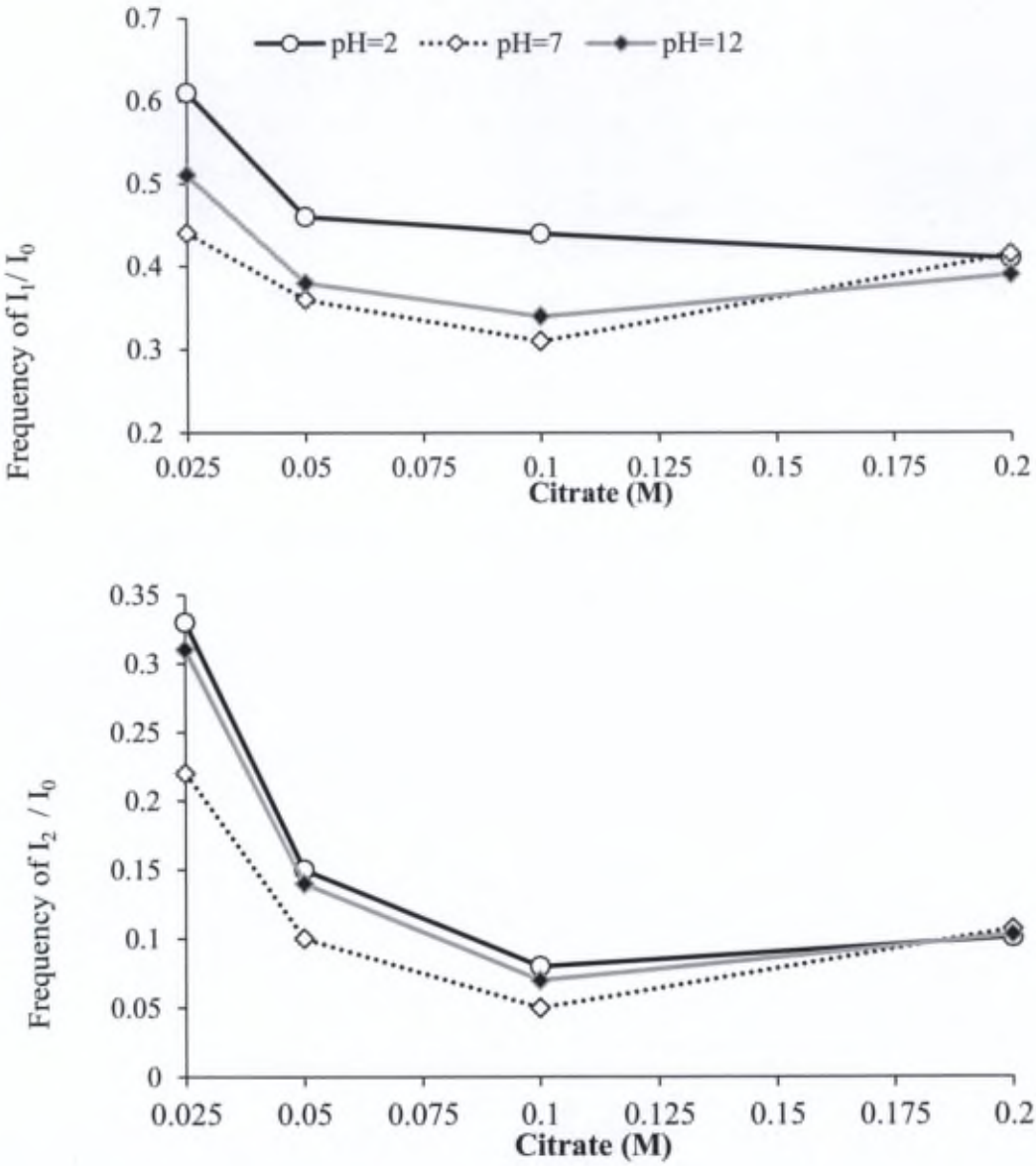

Figure 3.5: Evolution of infrared spectra regarding different intensity ratios I_1/I_0 and I_2/I_0 of PG suspensions as a function of citrate concentrations and of pH.

3.4 Conclusion

PG behavior was investigated in this study under the influence of pH, increasing suspension load and organic complexing ligands such as citrate. Solubility of PG particles shows a decrease as its concentration increases, due to the cumulative ionic strength leading to the formation of stable aggregates. This delay in the establishment of solubility due to saturation becomes a limiting factor for Pb, Zn, and Cu mobility. As a consequence, this will increase the environmental hazards linked to metal release from PG in stockpiles when later recycling actions are taken. However, Cd and Cr are irreversibly mobilized to aquatic environments in spite of PG concentration. Metals showed a high affinity to citrate which is able to increase their mobility from the matrix to the suspension. The presence of citrate increases PG dissolution at acidic pH and recrystallization at basic pH.

This study addresses certain approaches to improve the quality status of aquatic environments exposed to industrial solid wastes. The aim is to remediate PG wastes and enhance their reusability as economically beneficial gypsum substitute. Subjecting PG wastes to alkaline treatment in order to encapsulate the hazardous contaminants within the matrix, or treating these wastes with acid will render them ecofriendly reusable. Controlled stockpiles and organic ligands could be utilized under various pH conditions to treat fertilizer disposal waste and PG recycling with the objective of reducing their hazardous impact of released contaminants on natural biota.

Characterization of PG allows us to identify its nature and expect its behavior since it is a potential contaminant in both watersheds. PG is strictly associated with the industrial activity in Levantine basin as a byproduct of manufacturing process. Furthermore, PG is considered as a major potential contaminant for soil, sediment, and water in the industrial area due to its chaotic discharge on the coast and into the Mediterranean Sea. In addition, PG could be used by itself as a soil amendment for cultivation purposes due to the inherited nutrients it gained during production of phosphate fertilizer. Phosphate fertilizers share many characteristics with PG, and are extensively used in Litani basin in order to enhance the agricultural yields. As a consequence, the two studied watersheds are indirectly under the influence of the same potential contaminant. Thus our interest is focused on the environmental implications of the factory functioning and the agricultural practices on their corresponding watersheds. Pollution magnitude and extent in the receiving media of both watersheds should be explored. Pollution source and dynamics must be precisely originated and documented in order to accurately evaluate the impact of land-use activities on watersheds and explore the diverse contributing factors. Soil (superficial soil and cores), costal marine sediments, and riverine sediments in the industrial watersheds can witness and preserve indications of the environmental stress exerted by the phosphate fertilizer over the watershed. As a result, the coverage area which is influenced by the industrial practices should be estimated and classified. In the other hand, lacustrine sediments may summarize all the anthropogenic effluents derived from the upper Litani watershed, and their study will allow the identification of pollutants in the multiuse lands of Litani basin. Upon dam construction during late 1950s, the agricultural sector flourished in the Bekaa plain, and more lands were engaged in agricultural reclamation due to the increasing irrigation potentials. Industrial activities and tourism services have expanded in the upper Litani basin as well, thus anthropogenic contaminants are no longer only associated to agricultural and farming practices in the Litani watershed. A selective and robust analytical tool such as Pb isotopes should be utilized to permit the distinguishment and identification of pollution sources and magnitude in both watersheds. This in its role will aid in the better understanding of the environmental implications and assess their threats on soil and water quality.

Chapter 4

Geochemical Investigation of Two contrasted Mediterranean Watersheds: Tracing the Origin and Pathways of Contaminants Using Pb Isotopes

Abstract[2]

Diverse land-use activities induced by socio-economical challenges exert an environmental pollution stress on hydrographic basins. In order to originate pollution sources and to trace their pathways in nature, Pb isotopic ratios are determined in sediments and soils collected from the industrial and agricultural watersheds in Eastern Mediterranean. Pollution dynamics has been studied by using Pb isotopic mixing models to compare the impact of industrial and agricultural land-use practices. Topography and geomorphological processes govern the behavior of contaminants in both watersheds, where Pb isotopic compositions of samples suggest a strong mixing of natural bedrock with contaminated fuels and aerosols. Socio-economical impacts are reflected by the deterioration of soil quality, where pollution extends to 3 km away from the factory and Pb penetrates a depth of 15 cm in the industrial watershed soils. Moreover, high $^{206}Pb/^{207}Pb$ ratios in coastal marine sediments (1.62-2.02) due to the decaying of uranium from phosphate rocks and phosphogypsum waste stockpiles that act as a secondary point source of Pb pollution for the Mediterranean Sea. In the agricultural watershed, seasonally dependent human activities reflected by allocthonous sources of Pb induce seasonal and spatial variation of lacustrine contaminants accumulated in the reservoir that threatens ultimate groundwater quality.

[2] Adapted from the submitted article (Ammar R, Kazpard V, El Samrani AG, Benoit M, Lartiges B, Amacha N, Saad Z, Chou L. Geochemical Investigation of Two contrasted Mediterranean Watersheds: Tracing the Origin and Pathways of Contaminants Using Pb Isotopes. Submitted to Journal of hazardous material; HAZMAT-D-14-01124, under review).

4.1 Introduction

Ever since existence, human activities have extensively affected the biogeochemical cycle of nature by adding and concentrating pollutants in urban, industrial, and agricultural areas. Several studies investigated the impact of land-use activities on the distribution of contaminants in the environment. The approach of Pb isotopic analyses has been used to better understand the anthropogenic impact in soils and sediments (Juteau et al., 1986; Kylander et al., 2005; Zhang et al., 2007; Fagel et al., 2010; Grezzi et al., 2011; Stille et al., 2011; Wijaya et al., 2012; Wang et al., 2013). As modern geomorphic agents humans have mobilized metals via mass flows and redistributed them in the nature (Rauch, 2010; Thapalia et al., 2010). Hence, soils and sediments contain environmental archives by which pollution stress history and behavior in both seasonal and annual fluxes are well recorded, and could be revealed by using isotopic approaches (Fagel et al., 2010; Kober et al., 1999; Izquierdo et al., 2012). In order to identify metal contamination origin and to investigate its magnitude, researchers rely on Pb isotopic signatures in soils and sediments. Most studies show that Pb is enriched in the upper layer of soils and is associated with organic matter and minerals, whose concentration then decreases with depth (Stone et al., 1996; Wong and Li, 2004; Harlavan et al., 2010; Stille et al., 2011). Pb isotopic ratios depend on the uranium/thorium composition and the age of the original material, since Pb is the decaying daughter atoms of uranium and thorium (Komárek et al., 2007; Bird et al., 2010; Harlavan et al., 2010). Pb isotopes are considered as a robust tool, frequently used by researchers due to its high precision and resistance to biodegradation and physicochemical fractionation (Hu et al., 2011). It is an ideal approach to trace the contamination source and its pathway (Komárek et al., 2007; Zhu et al., 2010).

Environmental scientists rely on $^{206}Pb/^{207}Pb$ ratios due to their abundance, and the precise distinction between natural and anthropogenic sources, which is not affected by the mineral composition of the sample (Roussiez et al., 2005; Komárek et al., 2007). Pb isotopes have been determined to understand the contamination source and evolution in different environmental context (Farmer et al., 1997; Hansmann and Köppel, 2000; Roussiez et al., 2005; Abi Ghanem et al., 2009; Erel and Torrent, 2010; Schucknecht et al., 2011). Environmental scientists agreed that the $^{206}Pb/^{207}Pb$ isotopic ratio of natural crust or so called PDAC (Present Day Average Crust) is 1.20 and values below this ratio down to 0.96 are considered as anthropogenic (Harlavan et al., 2010; Frostick et al., 2011). Many scientists agreed that leaded gasoline was the major source of Pb contamination (Kober et al., 1999; Hansmann and Köppel, 2000; Erel and Torrent, 2010; Harlavan et al., 2010), exhibiting the least radiogenic signature among anthropogenic sources (Hansmann and Köppel, 2000), followed by smelting, mining, industrial activities and agricultural practices (Izquierdo et al., 2012).

Lebanon was chosen as a typical semi-arid country located on the Eastern Mediterranean coast. Like many emerging countries, multiple land-use activities are being practiced over its area without proper organization and geographical separation by socio-economical activities.

Few studies on the Eastern Mediterranean coast identified pollution sources in coastal soils and sediments (Chaaban et al., 2011; Abi Ghanem et al., 2009; Erel and Torrent, 2010; Harlavan et al., 2010). None of these works investigated the particularity of semi-arid areas and the impact of its various environmental factors on pollutant behavior and distribution. Previous studies did not show the seasonality for Pb isotopic signatures in Mediterranean soils and sediments. Duman et al., (2007) did not observe a seasonal difference for Pb concentration in the lacustrine sediments, while Othman et al., (1997) found a higher concentration of Pb in road side soils in dry season but not its isotopic signature.

The present study will provide a detailed description of seasonally dependent Pb source and its temporal variation mainly in a dammed reservoir. Mixing models with two or three endmembers in addition to calculations of Pb isotopic ratio excess were used to compare the two contrasting watersheds: an industrial land-use basin influenced by Mediterranean climate on the sea coast vs. a continental agricultural basin affected by semi-arid climate. The land-use impact alongside with geographical, climatic, and pedologic diversities will be investigated in this study by applying geological radiogenic analysis of Pb isotopic fingerprints (^{204}Pb, ^{206}Pb, ^{207}Pb and ^{208}Pb) that will precisely identify contamination source, trace its pathway and discriminate natural from anthropogenic sources.

4.2 Study sites

4.2.1 Environmental and socio-economical context

Lebanon is a representative example that includes a variety of regions with multivariate topography and different microclimate that characterize the eastern Mediterranean. The orographic formations separate the coastal plain from the inland valley, thus inducing the presence of different environmental phenomena controlled by geological formations, microclimate properties, demographic distribution and land-use activity (Edgell, 1997; Ministry of Agriculture, 2003; El Fadel et al., 2003). Urbanism and industrial factories are dispersed in the capital Beirut and along the coast, while the Bekaa district represents the agricultural fertile plain and house 20% of the Lebanese population (El Fadel et al., 2003). The country witnesses a flourish in both agricultural and industrial sectors in the past 30 years. The urbanization level has amplified from 79.4% of total population living in urban areas in 1985 to 89.7% in 2000 (Ministry of Agriculture, 2003). Additionally, there has been an increased usage of motor vehicles as reflected by the rising in car numbers from 250000 to 1.6 million vehicles in the past 40 years (Choueiri et al., 2010). Thus, the transportation sector is the prime sector of energy consumption in Lebanon and the main cause of air pollution, where Pb concentration in the aerosols is found to be 14$\mu g/m^3$ (Chaaban et al., 2001). Many obstacles faced phasing out of leaded gasoline in Lebanon and tetra ethyl fuel usage was only banned in 2002 (Kaysi et al., 2000). Environmental dilemma in Lebanon is represented by major pollution point sources, a predominant industrial land-use area and an intensive agricultural watershed.

4.2.2 Industrial watershed

The Levantine basin, a typical karstic basin, is a funnel shape watershed (Ministry of Agriculture, 2003), composed of middle Cretaceous and Eocene strata layered by Neogene marine strata, also a sandy-marly limestone in addition to partially marly rocks interbred with basalt (Edgell, 1997; UNDP/MoE, 2010). It is a well-known industrial area since the phosphate fertilizer factory establishment downstream to the river in 1957, as well as a significant traffic conjunction linking the North to the capital Beirut. The fertilizer plant is considered not only as one of the top 10 industries in Lebanon but also as one of the most polluting industries in the Mediterranean (Bridgen et al., 2002). The factory produces phosphate fertilizers and phosphoric acid and eliminates phosphogypsum (PG) as a byproduct (Rez-Loépez et al., 2007; Aoun et al., 2010; Yammine et al., 2010). PG is an acidic material, soluble, radiogenic and rich in heavy metals (Rutherford et al., 1994; Al-Masri et al., 2004; Aoun et al., 2010; Ammar et al., 2013); as described in chapter 3. Apatite rock and PG wastes are found at the sea bottom facing the industry, in the atmospheric depositions dispersed by the factory's smelter and in the stockpiles on the shore (Fakhri et al., 2008; Abi Ghanem et al., 2009; Yammine et al., 2010; Ammar et al., 2013). Coastal and riverine sediments were collected along with surficial soils at various distances from the factory (1-4 km) and soil cores were also retrieved (Table 4.1).

4.2.3 Agricultural watershed

The Litani Basin is the largest hydrographic basin in Lebanon (Ministry of Agriculture, 2003), a typical continental watershed affected by semi-arid climate (UNDP/MoE, 2010). The Litani watershed has a Mid-Eocene geological age lined by a Quaternary alluvium limestone with a chalk and marly chalk outcrop (Edgell, 1997; Walley, 1997). In 1955, a dam was constructed to block the river flow forming the Qaraaoun reservoir (Figure 4.1), a 2.2 km^2 lake used for hydropower production and irrigation for the historically used watershed (El Fadel et al., 2003; BAMAS, 2005; Saad et al., 2006; Assaf and Saadeh, 2008). This induced a rise of diverse industrial factories for food and metalloids in addition to considerable rock cutting activities. Surge of contaminants, enriched in heavy metals mainly Pb from the 288 different industrial units arrives in the reservoir which is loaded with organic matter, minerals, solvents and suspended solids (El Fadel et al., 2003; Gondal et al., 2006; Manzoor et al., 2006; Battaglia et al., 2007). Lacustrine sediments and alluvial soils were sampled from 3 different zones (Figure 4.1) crossing the center of the reservoir longitudinally (River inlet Ri, Central Zone Cz, and Dam zone Dz) during the mid of the rainy season (February), the end of the dry season (September), and the first flush (November) of 2011.

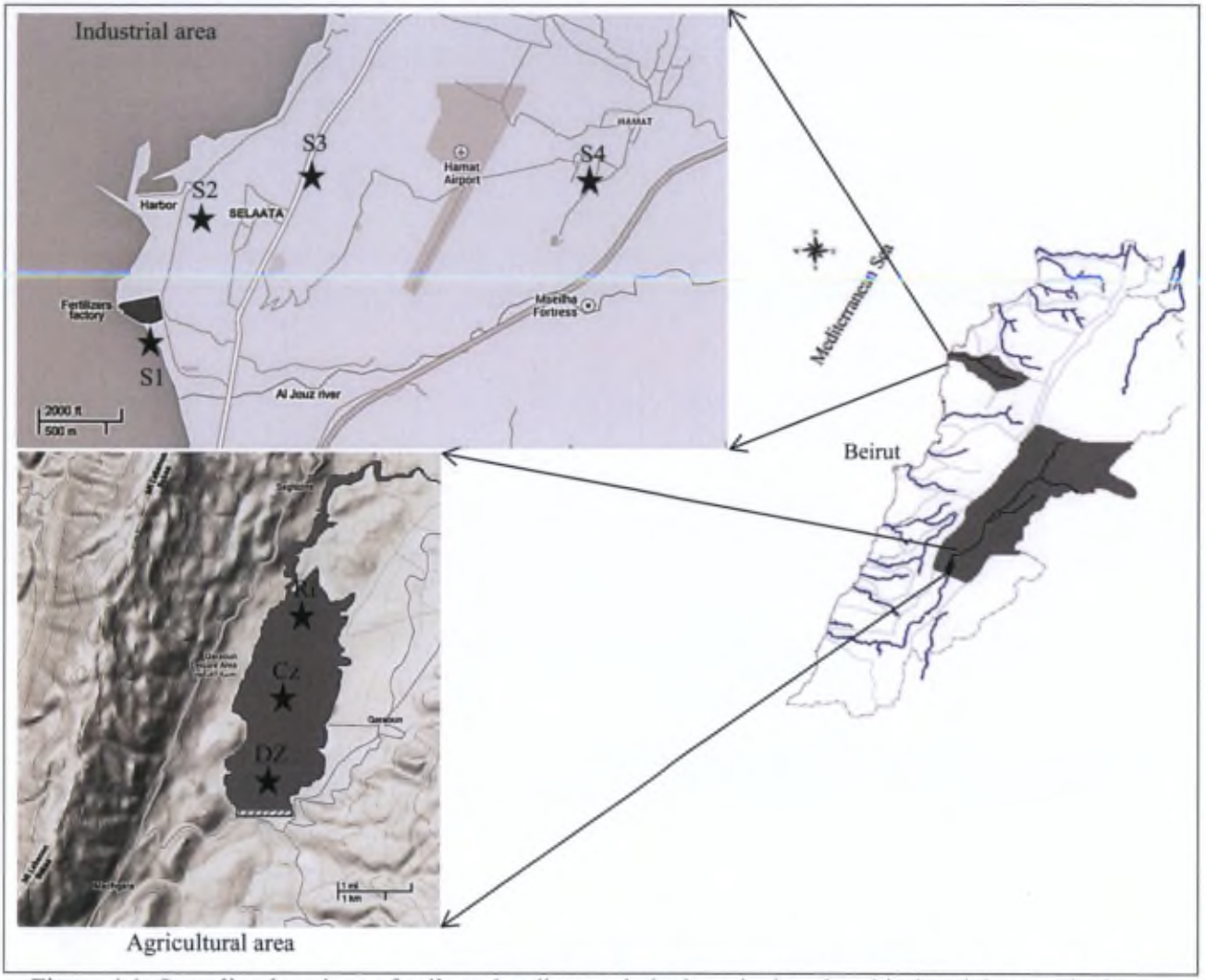

Figure 4.1: Sampling locations of soils and sediments in both agricultural and industrial watersheds.

4.3 Material and Methods

Riverine sediments, coastal marine sediments, and surficial soils were sampled from the surface (15 cm × 15 cm), while lacustrine sediments were obtained with a stainless steel sediment grabber (Fieldmaster Mighty Grab II Dredge). The core was collected via a motorized core drill (COBRA TT, Carottage à Percussion- SDEC) with an inox coated core of 7 cm inner diameter. The sample core of 70 cm length was partitioned into layers of increasing thickness with respect to the surface (5 x 3 cm, 7 x 5 cm and 2 x 10 cm layers). Samples were stored in polyethylene bags in a fridge then freeze-dried using an Alpha 1-4 LD plus freeze drier.

Collected samples were homogenized using pestle and mortar, sieved over 63 µm acid-cleaned nylon mesh to reduce the effect of grain size and sample heterogeneity, and extracted for particulate Pb using a microwave acid. Samples were analyzed by Graphite Furnace Atomic Absorption Spectroscopy (GFAAS) with Zeeman-effect background correction

(Varian AA-400) and Inductively Coupled Plasma Atomic Emission Spectroscopy (ICP-AES) (Varian Liberty series II). For Pb isotope analysis, sieved samples were digested and separated by chromatographic separation procedure in a clean room as described by Makishima et al., (2007). All the acids used were bi-distillated ultrapure acids. NIST certified materials (2711a Montana II soil and LKSD-3 sediments) were also digested as for soil and sediments samples. Pb isotopic ratios were determined on Thermal Ionization Mass Spectrometer TIMS (TIMS "MAT 261", Finnigan) and values for samples were normalized with respect to that found in the NIST SRM 981 Pb standard material.

4.4 Results and Discussion

4.4.1. Evolution of Pb pollution in an industrial soil

The effect of the smelter on the particulate Pb contents in different types of deposits was investigated. The concentration of Pb in surface soils was further examined as a function of the radial distance relative to the industrial source. As shown in Table 4.1, Pb concentration decreased from 52.9 ppm in the vicinity of the smelting factory to 15.1 ppm at a distance of about 4 km away from the source. In soil and sediment profiles, the Pb concentration alone could not reflect the contamination level in the studied samples, since the clay content and rock background could vary and thus interfere with the matrix results. Pb concentration was normalized with respect to aluminum content, and enrichment factor (EF) for Pb was calculated according to equation 4.1 described in (Othman et al., 1997; Kylander et al., 2005; Roussiez et al., 2005; Shakeri et al., 2010; Hu et al., 2011). In this study, particulate Pb and Al contents found in soil core sample at 70 cm depth in the soil core (Table A3.1) or at 4 km away from the factory represent our reference levels (Renberg et al., 2002; Roussiez et al., 2005).

$$EF = \frac{[M/Al]_{sample}}{[M/Al]_{ref}} \qquad (4.1)$$

Table 4.1: Characteristics, Pb contents, Pb isotopic ratios and excess $^{206}Pb/^{207}Pb$ of samples collected in the industrial and the agricultural watersheds.

Sampling site	Sample type	Coordinates	Depth	Pb ppm	$^{206}Pb/^{204}Pb$	$^{207}Pb/^{204}Pb$	$^{208}Pb/^{204}Pb$	$^{206}Pb/^{207}Pb$ excess	Grain size µm (50%)
Industrial watershed	Riverine sediments	34.267611°N 35.659651°E	Top 2cm	4.4	18.484 ± 0.001	15.636 ± 0.001	38.196 ± 0.003	1.207	101.4
		34.267843°N 35.658190°E		11.9	18.373 ± 0.001	15.638 ± 0.001	38.229 ± 0.003	1.273	17.4
	Coastal marine sediments	34.278796°N 35.654909°E	1-5cm	1.5-3.5	26.015 ± 0.002 33.059 ± 0.008	15.988 ± 0.001 16.354 ± 0.003	38.091-38.985 ± 0.003		200
	Surficial soils	< 1km 5m a.s.l 34.269181°N 35.657136°E	Top 2cm	52.9	18.015 ± 0.001	15.595 ± 0.001	37.897 ± 0.002	1.136	67.5
		1-2 km 15 m a.s.l 34.278058°N 35.659441°E		31.4	18.575 ± 0.001	15.649 ± 0.001	38.518 ± 0.002	1.173	na
		2-3km 120m a.s.l 34.283004°N 35.667837°S		37.2	18.332 ± 0.001	15.621±0.001	38.266 ± 0.002	1.153	na
		<4 k m 220m a.s.l 34.277568°N 35.687982°E		15.1	18.620 ± 0.001	15.650 ± 0.001	38.518 ± 0.002	1.355	na
	Soil core	34.280264°N 35.659654°E	70cm	23.2-101.1	18.156 ± 0.001 18.903 ± 0.004	15.616 ± 0.002 15.679 ± 0.005	38.102 ± 0.005 38.967 ± 0.018	1.168-1.218 (1.156 at 9cm depth)	51.4
Agricultural watershed	Lacustrine sediments	Ri 33.586996°N 35.699037°E		14.1-27.10	18.413-18.595 ± 0.001	15.632-15.638 ± 0.001	38.211-38.318 ± 0.003	1.123-1.283	19.9
		Cz 33.571739°N 35.695442°		11.4-15.2	18.420-18.593 ± 0.001	15.634-15.647 ±0.001	38.217-38.323 ± 0.002	1.185-1.617	22.7
		Dz 33.555250°N 35.690590°E		10.64-20.72	18.393-18.595 ±0.001	15.632-15.644 ±0.001	38.200-38.318 ± 0.002	1.097-1.222	19.9
	Alluvial soils	33.560410°N 35.703654°E	Top 2cm	5.8	19.171 ± 0.001	15.647 ± 0.001	38.605 ± 0.002	1.187	29.9
		33.547915°N 35.695761°E		8.8	18.889 ± 0.001	15.664 ± 0.001	38.489 ± 0.002	1.193	39.2

Enrichment factor calculations, attest the severe local contamination of soils adjacent to the factory at around 1 km (EF= 6.4); the EF values decrease to a moderate enrichment of 2.64 and 2.43 with a radial distance of respectively 2 km and 3 km away from the contaminant source. The correlation of Pb isotopic signatures for surficial soil samples collected in the

industrial watershed reflects the mixing occurring in the watershed between the two endmember groups (Frostick et al., 2011) (Figure 4.2a). The higher Pb content, together with the lower $^{206}Pb/^{207}Pb$ ratio, indicates the anthropogenic source of Pb in the vicinity of the factory; as we move away from the pollution source, a significant decrease in the Pb content accompanied by a considerable increase in the $^{206}Pb/^{207}Pb$ isotopic ratio are observed (Figure 4.2b). The strong correlation between 1/Pb and the $^{206}Pb/^{207}Pb$ ratio for the first 3 sampling locations closer to the factory's smelter suggests that the area under the direct impact of the factory extends to less than 3 km away, whereas areas at 4 km away from the pollution source could be referred as remote regions (Figure 4.2b). Pb content measured in the local aerosols (17 ng/m^3) was found to be enriched in the downwind direction compared to upwind (Yammine et al., 2010). Thus, the isotopic signature of Pb in the top soils could reveal the recent industrial pollution and reflect the actual environmental stress exerted by the factory on a certain area. Previous studies showed that Pb contamination associated with the top soils which are more subjected to atmospheric deposition, precipitation and natural weathering (Farmer et al., 1997; Grezzi et al., 2011; Hu e al., 2011; Schucknecht et al., 2011).

The vertical distribution of Pb was also examined in cores of both soils and coastal marine sediments in the industrial watershed, aiming to evaluate the contamination penetration from the direct disposal of liquid wastes and solid stockpiles near shore. The Pb isotopic signatures in soil cores reflect the long-standing pollution and contaminant dynamics in the particular receiving media. Vertical distribution of Pb in the studied soil core sampled near the fertilizers factory shows that the top 15 cm of the soil column is highly enriched in Pb with EF greater than 2 (Figure 4.3a,b). EF values greater than 2 is indicated in the top 10 cm with the highest one observed at a depth of 9 cm (EF=4) (Figure 4.3b), and exhibits lower $^{206}Pb/^{207}Pb$ ratios (Figure 4.4a). The slight shift in both EF and isotopic ratio at 40 cm depth could be attributed to the soil internal enrichment resulting from pedogenic processes taking place in the transition zone of two soil horizons (Hansmann and Köppel, 2000). The strong correlation between $^{208}Pb/^{206}Pb$ and $^{206}Pb/^{207}Pb$ indicates a binary mixing between two endmember sources (Kober et al., 1999, Renberg et al., 2002; Wong and Li, 2004; Bird et al., 2010). When the $^{206}Pb/^{204}Pb$ isotopic ratio is plotted against 1/Pb (Figure 4.5a), distinctive trends are also observed for the top and the lower. The deeper layers of the soil core exhibit isotopic ratios close to the natural bedrock and the top soil samples reveal those approaching the anthropogenic endmember (Figure 4.5b). Association of high Pb contents with low $^{206}Pb/^{204}Pb$ ratios reflects the anthropogenic contamination (Miralles et al., 2006) strictly in the top 15 cm (Figure 4.5a). The penetration of anthropogenic Pb in the top 15 cm of the soil with the maximal Pb content recorded at 9 cm could be associated to the onset of the factory establishment in 1957 and to the leaded gasoline usage which was banned only 11 years ago (Hansmnn and Köppel, 2000; Erel and Torrent, 2010).

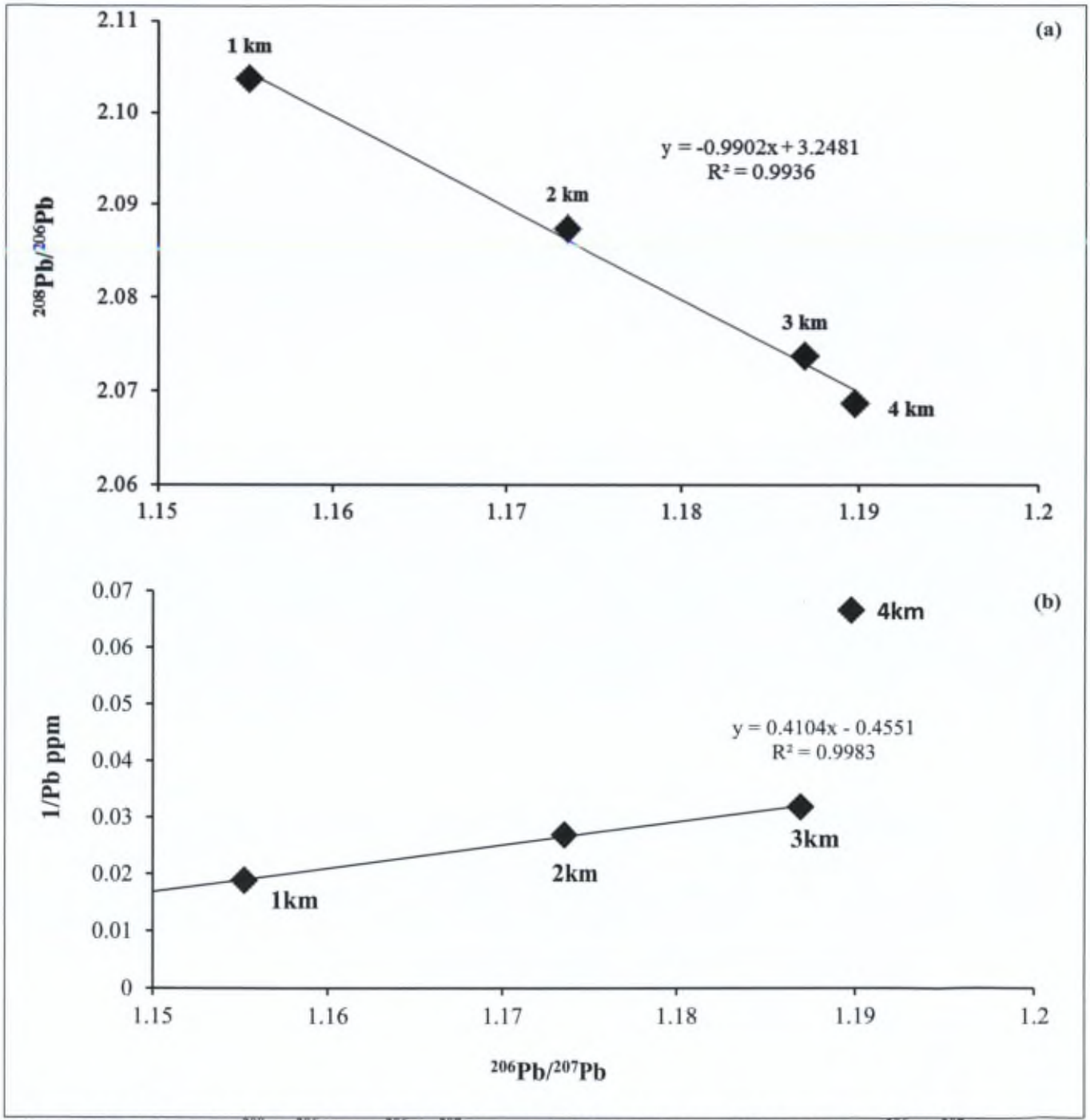

Figure 4.2: Plots of (a) $^{208}Pb/^{206}Pb$ vs. $^{206}Pb/^{207}Pb$, and of (b) the inverse of Pb content vs. $^{206}Pb/^{207}Pb$ in the surface soils of the industrial area.

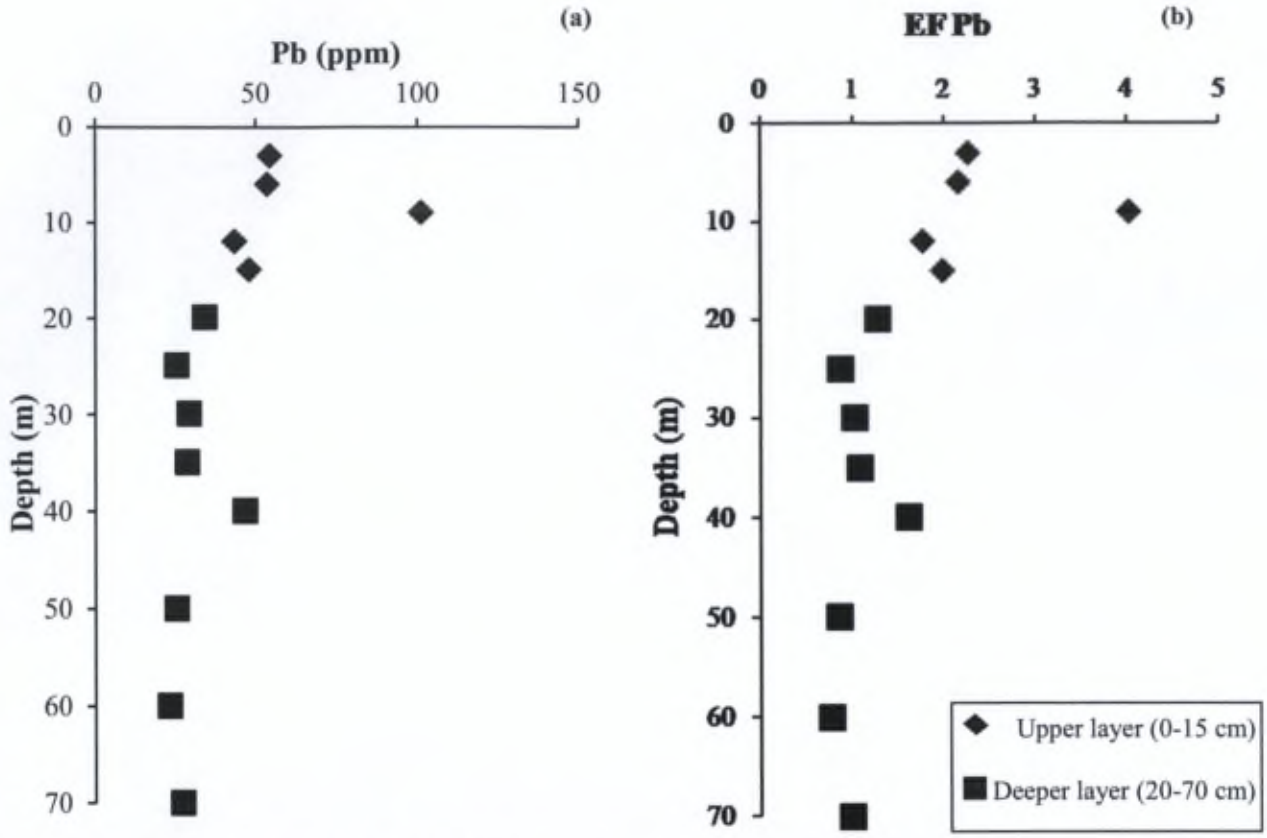

Figure 4.3: Vertical distributions of (a) Pb contents and (b) enrichment factors in an industrial soil core.

A coastal marine core of 5 cm long was also sampled in front the industrial factory NW to the industrial waste outlet and to the southern reaches of the piled apatite rocks and PG stocks. A vertical distribution for Pb was observed whose value increased from 1.6 ppm at 1 cm to 3.5 ppm at 5 cm. The surprisingly high $^{206}Pb/^{207}Pb$ ration (>1.6) found in the coastal marine sediments near the fertilizer factory (Figure 4.4b) could be associated to the excess uranium in the source region. Burnett et al., (1988) showed that phosphate rocks contain uranium and release series of isotopic decay elements including Pb with high radiogenic signature. PG could also contain high radiogenic signatures where 17% of uranium is transformed from the Syrian phosphate rock to PG during the manufacturing process (Othman and Al-Masri, 2007). Moreover, Aoun et al., (2010) indicated that the content of ^{210}Po, the parent isotope of ^{206}Pb, in the local PG is equal to 289.0 Bq/kg. As a result, the Pb isotopic anomaly in the coastal marine sediments can be attributed to the excess uranium in the used source rock and PG. Also, the mean dissolved Pb concentration in the coastal seawater (4 sampling locations to the north and south sides of the factory) (Table A1.1[3]) has been found to be 0.902 µg/L a value much higher than what is normally found in the Eastern Mediterranean Sea (Béthoux et al., 1990). The higher salinity and temperature of the Mediterranean Sea, however, could increase the metal mobility and its ecological hazard; the affinity of metals to bind with finer

[3] See Annex 1

particles could in addition help their dispersion to areas further than the local contamination site (Zhao et al., 2013).

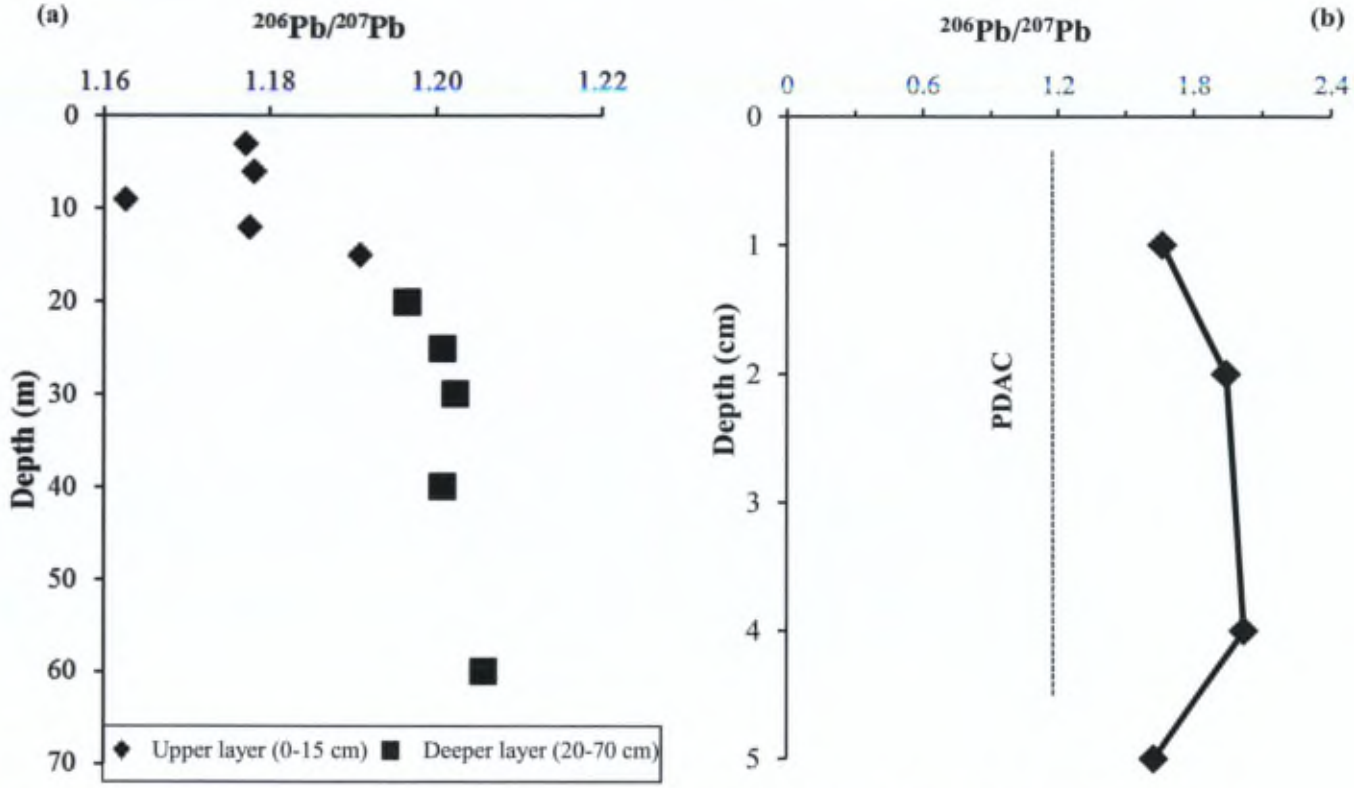

Figure 4.4: Vertical distributions of $^{206}Pb/^{207}Pb$ in (a) an industrail soil core and (b) a marine sediment core.

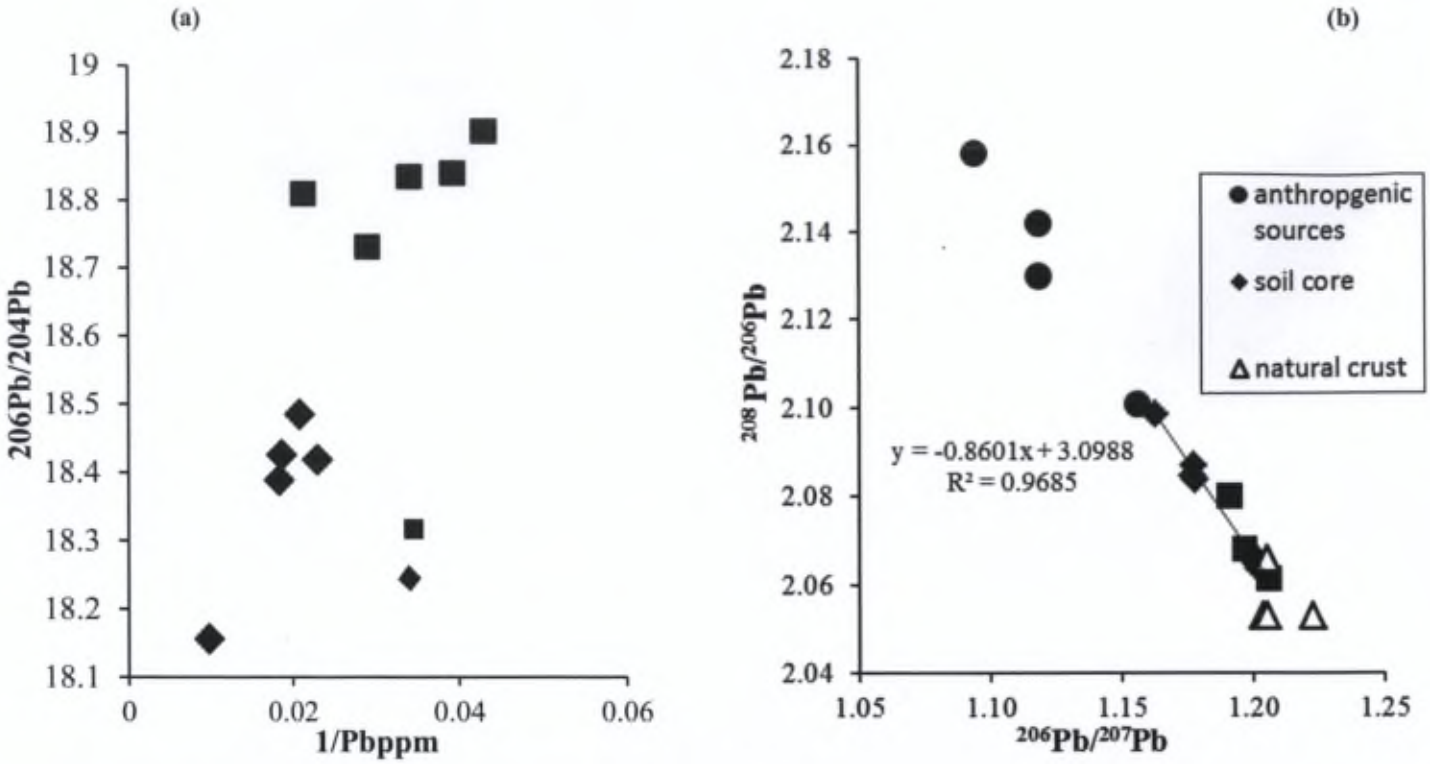

Figure 4.5: Plots of (a) $^{206}Pb/^{207}Pb$ vs.1/Pb content, and (b) $^{208}Pb/^{206}Pb$ vs. $^{206}Pb/^{207}Pb$ showing the mixing trend. All data refer to the industrial soil core.

4.4.2 Evolution of Pb pollution in an agricultural area

Particulate Pb content showed spatial and seasonal variations in lacustrine sediments where sediments collected at the river inlet during the rainy season exhibited the highest measured concentration (27 ppm) during all sampling seasons compared to other reservoir zones (Table 4.1). Pb concentration in sediments increased at all sampling sites during summer, but with the highest measured value observed in the Dz (20 ppm). However, the first flush diluted the particulate Pb concentration in the reservoir sediments with the highest concentration measured at the Ri (Annex 2). The reservoir sediments showed a moderate enrichment in Pb and the enrichment factors ranged from 2.2 to 2.9 respectively for dry season and wet period, with the reference values measured at 70 cm of a soil core retrieved nearby, 9.63 ppm for Pb and 28553 ppm for Al.

The river inlet brought sediments more enriched in metals to the reservoir and the highest $^{208}Pb/^{206}Pb$ ratio with the lowest $^{206}Pb/^{207}Pb$ signature were observed for all sampling campaigns (Figure 4.6). The highest $^{208}Pb/^{206}Pb$ value observed in the mid rainy season could be associated with the high particulate organic carbon content of the reservoir sediments (2.32%), possibly linked to the nature of agricultural practices. Soil tilling and application of agrochemicals to the cultivated land at the beginning of winter will cause the Pb to

accumulate in the topsoil that is more susceptible to erosion and its subsequent transport to the main river course and transfer to the reservoir sediments (Luck and Othman, 1998; Mikac et al., 2011). The distinctive behavior of Pb isotopes together with the Pb content of the sediments at the Ri compared to other zones of the reservoir (Figure 4.6) emphasizes the importance of hydrodynamics and the predominance of finer particles in the sediment matrix, where 50% of sediments have a grain size that ranges between 22.7-19.9 μm (Table 4.1). Also, Callender and Rice (2000) noted that the sediments trapping effect could play a role in the spatial variation of isotopic signatures. The structure of the Qaraaoun dam is trapping the sediments seasonally and annually, where no dredging events are taking place. Thus the accumulation of sediments can be one of the reasons to explain the seasonal variation of isotopic signatures in reservoir sediments.

The plot of calcium content against $^{206}Pb/^{204}Pb$ is used to reveal the impact of the local geological formation on the sediment composition (Hansmann and Köppel, 2000). Non contaminated soils are denoted with $^{206}Pb/^{204}Pb$ ratios above 18.8 (Hansmann and Köppel, 2000). As shown in Figure 4.7a, most reservoir samples have ratios below 18.8 and the positive correlation between calcium content and isotopic ratio support the assumption that carbonate rock is potential carrier of Pb in reservoir sediments. The abundance of carbonate minerals in the reservoir sediments could act as a diluting factor for Pb derived from other sources (Balkis et al., 2010). The first flush is reflected by direct increase of percolation from the watershed to the reservoir mainly in the Cz. The first flush event will result in increasing water turbulence and high input of sediments from the upper basin, which can influence the sediment composition. The positive correlation between $^{207}Pb/^{204}Pb$ and $^{206}Pb/^{207}Pb$ for reservoir sediments represented in Figure 4.7b shows clearly a mixing line. The identification of the samples on the mixing line indicates that the Ri brings suspended matter of the highest Pb content (Table 4.1) to the reservoir, where sediments collected during dry season are more polluted than those sampled during the rainy season. Data corresponding to the first flush event exhibit a transitional situation between the dry and the wet seasons, during which the contaminants are washed out from the upper basin to the reservoir and the Pb content of the sediments displays that of a mixture of both anthropogenic and natural sources.

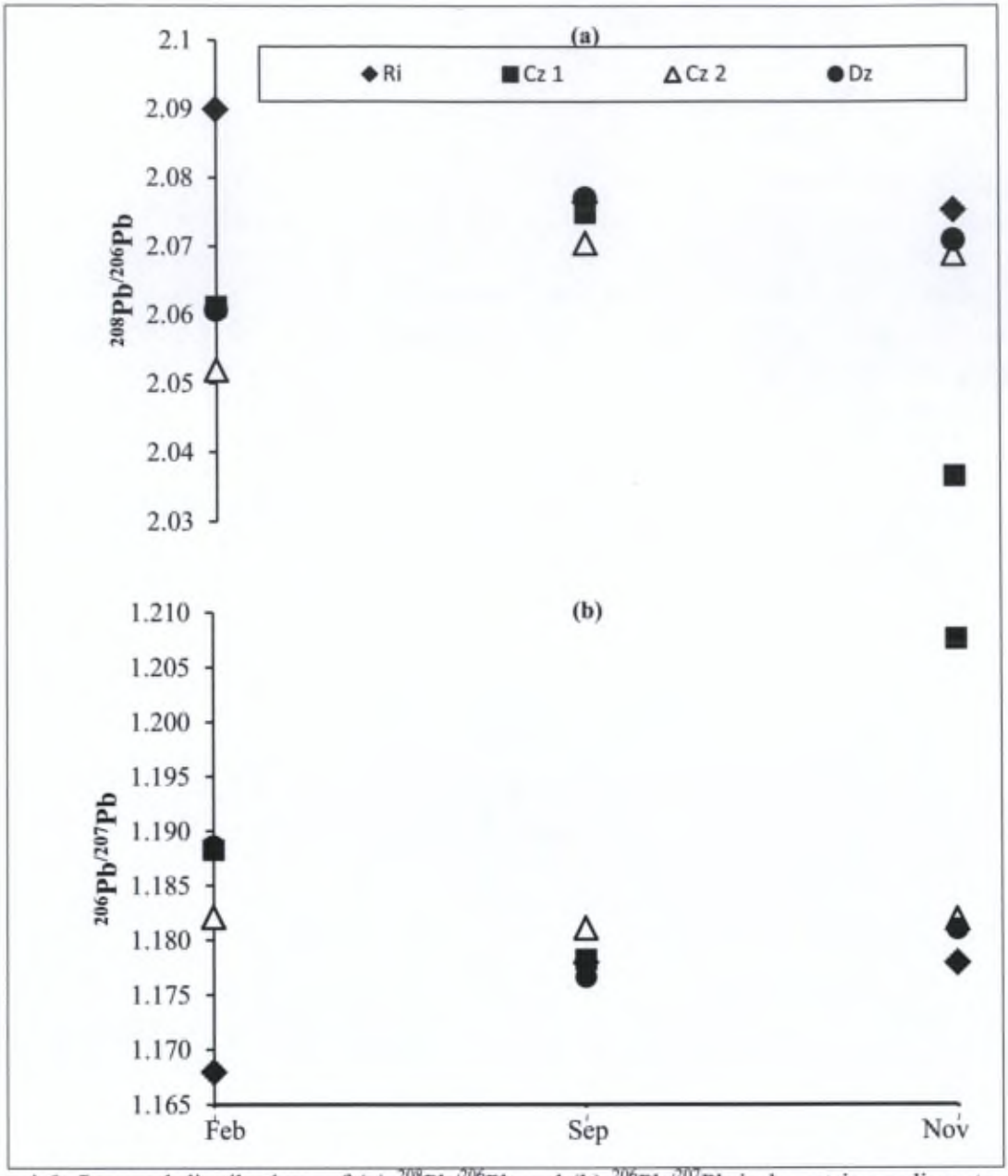

Figure 4.6: Seasonal distributions of (a) $^{208}Pb/^{206}Pb$ and (b) $^{206}Pb/^{207}Pb$ in lacustrine sediments of the agricultural watershed: Ri (river inlet), Cz (central zone) and Dz (dam zone).

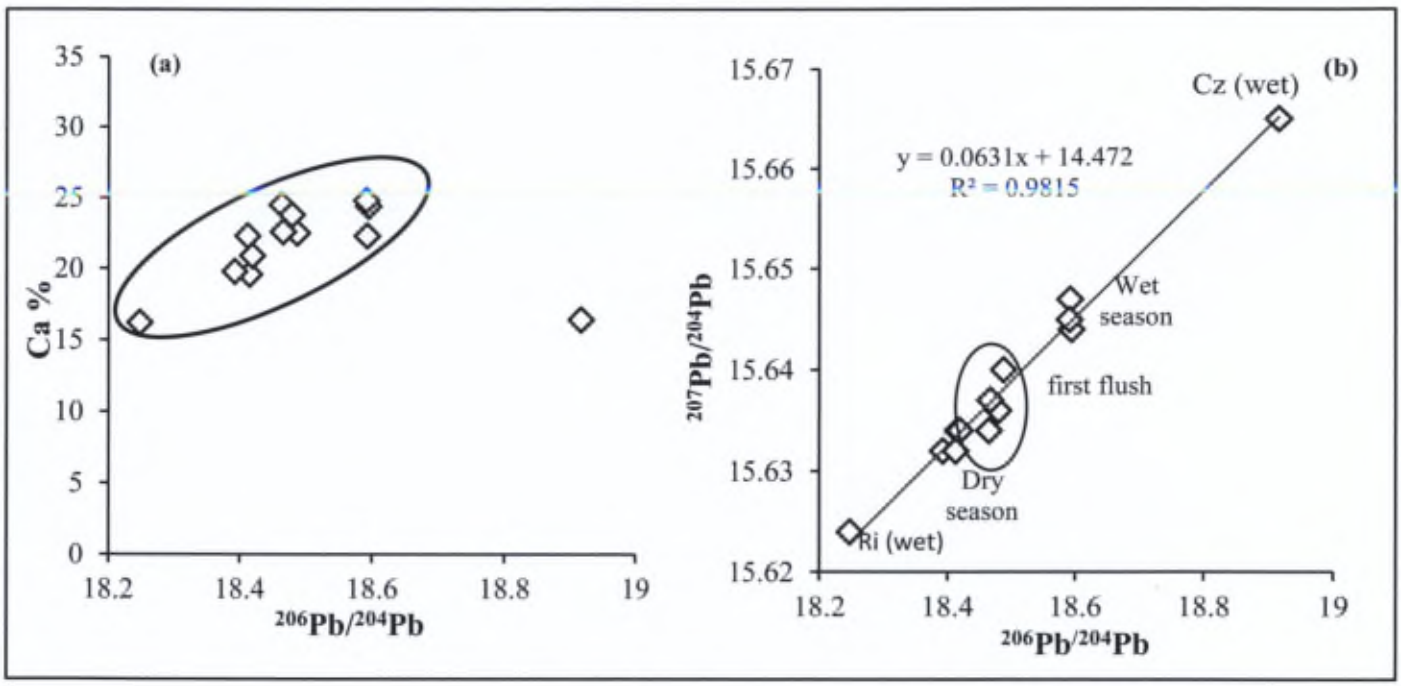

Figure 4.7: (a) Correlation of Ca content with $^{206}Pb/^{204}Pb$ ratio for the agricultural lacustrine sediments and (b) plot of $^{206}Pb/^{204}Pb$ against $^{207}Pb/^{204}Pb$ showing the binary mixing of two endmembers.

4.4.3 Comparison of the two contrasting watersheds

4.4.3.1 Excess Pb isotopic ratio

Excess Pb isotopic ratio has been used to implicate Pb anthropogenic source at a certain site using equation 4.2 (Farmer et al., 1997; Bindler et al., 2001; Wong and Li, 2004).

$$\left[\frac{^{206}Pb}{^{207}Pb}\right]_{excess} = \frac{\left([Pb]_s \; x \left[\frac{^{206}Pb}{^{207}Pb}\right]_s\right) - \left([Pb]_{ref} \; x \left[\frac{^{206}Pb}{^{207}Pb}\right]_{ref}\right)}{[Pb]_s - [Pb]_{ref}} \qquad (4.2)$$

Where $(Pb)_s$ and $(^{206}Pb/^{207}Pb)_s$ refers respectively to the total Pb content and Pb isotopic ratio of the sample at a specific site, while $(Pb)_{ref.}$ and $(^{206}Pb/^{207}Pb)_{ref}$ corresponds respectively to the Pb concentration and isotopic ratio of the background material. PDAC is used as the reference material, where $(Pb)_{ref}$ and $(^{206}Pb/^{207}Pb)_{ref}$ are 16 ppm and 1.20 respectively. Excess Pb isotopic ratios in riverine and surficial industrial samples (Table 4.1) indicates the

contribution of shales/limestones, local and regional contaminated aerosols in addition to industrial Pb derived from the European Pb ores. In the soil core, excess Pb isotopic ratio in the surface points towards the surcharge of industrial Pb sources from Pb ores, coal, dusts and contaminated aerosols where in the deeper layers limestone contributes to the isotopic signature. In contrast, in the agricultural lacustrine sediments and alluvial soils, excess Pb isotopic ratios reflect the collective signatures of European Pb ore, coal, regional contaminated aerosol (Turkey) and natural rock (carbonates and silicates).

4.4.3.2 Binary model

In order to investigate the land-use impact on each watershed, a binary isotopic model is used. Figure 4.8 shows the plot of $^{208}Pb/^{206}Pb$ against $^{206}Pb/^{207}Pb$, indicating a mixing trend of isotopic compositions of soils and sediments of the two studied watersheds. Data for both agricultural and industrial samples fall on a mixing line linking two endmember groups. The isotopic compositions of the natural crust correspond to those for carbonates and silicates of the Miocene and Paleocene ages in addition to those for sandstone and feldspar. The anthropogenic sources represent the leaded gasoline, fuel, emissions before 1992, contaminated local and regional aerosol and Saharan dust (Table 4.2).

Industrial soil samples are a mixture of natural crustal material, mainly sand feldspar, and anthropogenic sources (Figure 4.8). The emissions after 1992 indicate the importance of industrial Pb sources in the aerosols which have similar isotopic ratios to that found in the sample closest to the factory. Besides the contaminated regional aerosols, the isotopic composition of the Saharan dust emerges on the mixing line (Table 4.2, Figure 4.8). The more radiogenic values can be attributed to Saharan dust or industrial activities (Bollhöfer and Rosman, 2001). Previous studies indicate the contribution of Saharan dust to the Pb isotopic signature in Mediterranean sediments (Roussiez et al., 2005; Erel and Torrent, 2010). Lebanon is subjected to Saharan dust storms occurring mainly in spring with a few events in winter (Kutiel and Furman, 2003).

Agricultural samples have a Pb isotopic composition that is more affected by natural crust, mainly carbonates, as shown in Figure 4.8. They fall on a clear mixing line where some samples show ratios closer to the natural crust and others are impacted by anthropogenic sources. The two mixing lines for agricultural and industrial samples (Figure 4.8) exhibit slightly different slopes which could be related to different bedrock signatures (Hansmann and Köppel, 2000, Bollhöfer and Rosman, 2001; Erel et al., 2007).

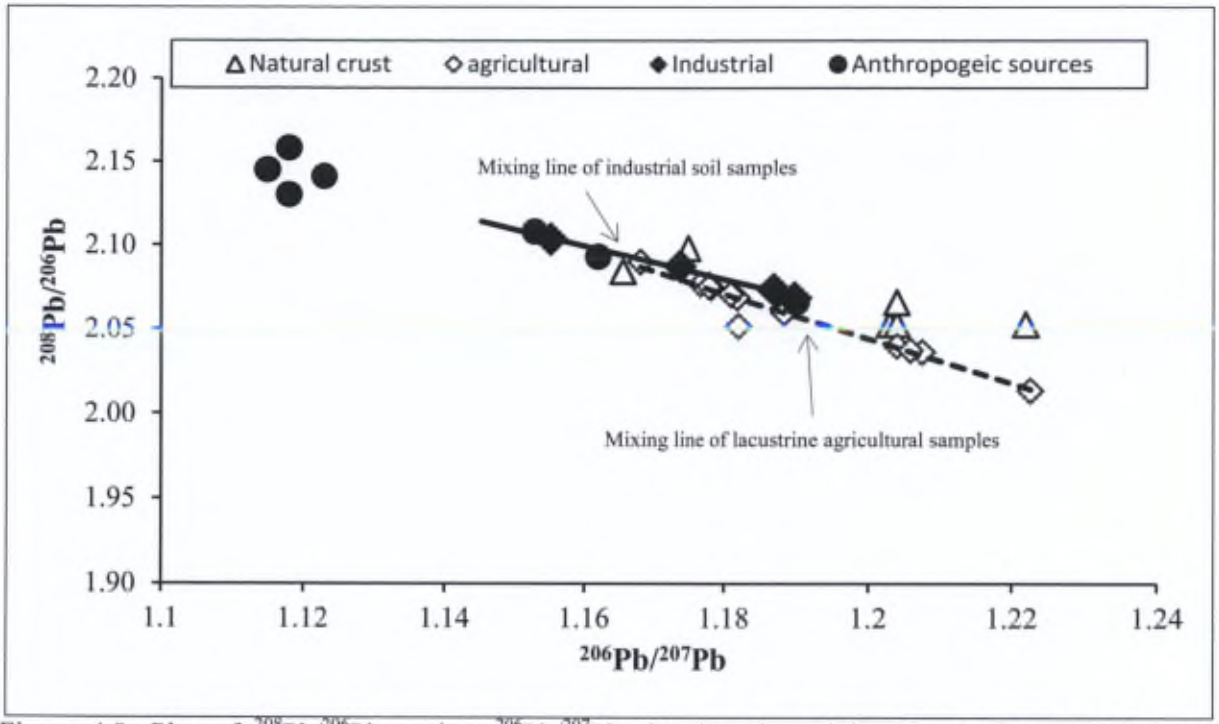

Figure 4.8: Plot of $^{208}Pb/^{206}Pb$ against $^{206}Pb/^{207}Pb$ showing the mixing trends for industrial and agricultural soils and sediments.

Table 4.2: Compilation of $^{206}Pb/^{207}Pb$ and $^{208}Pb/^{206}Pb$ isotopic ratios of anthropogenic and natural sources.

Sample		Pb 206/207	Pb 208/206	Reference
leaded gasoline	Anthropogenic sources	1.09-1.118	2.142-2.158	(Erel et al., 2007)
Aerosol North Lebanon (1994)		1.119	2.39	(Bollhöfer and Rosman, 2001)
Emissions before 1992		1.19	2.066	(Bollhöfer and Rosman, 2001, and the references in it)
Emissions after 1992		1.115	2.145	(Bollhöfer and Rosman, 2001, and the references in it)
Fly ashes		0.869	2.105	(Hansmann and Köppel, 2000)
Mean car emissions		0.899	2.1434	(Hansmann and Köppel, 2000)
aerosol Lebanon		1.118	2.13	(Abi Ghanem et al., 2009)
Aerosol ME		1.14- 1.156	2.1	(Erel et al., 2007)
Aerosol Turkey		1.123	2.141	(Bollhöfer and Rosman, 2001, and the references in it)
Aerosol Cairo		1.153	2.108	(Bollhöfer and Rosman, 2001, and the references in it)
Saharan dust		1.162	2.093	(Bollhöfer and Rosman, 2001, and the references in it)
European coal		1.16-1.21	2.451-2.464	(Hansmann and Köppel, 2000, and the reference within it)
Europe Pb ore		1.17-1.19	?	(Bollhöfer and Rosman, 2001, and the references in it)
Present day average crust PDAC	Natural sources	1.20	2.47	(Frostick et al., 2011)
Carbonates Miocene		1.203	2.053	(Luck and Othman, 1998)
Carbonates Paleocene		1.204	2.053	(Luck and Othman, 1998)
silicates Miocene		1.222	2.053	(Luck and Othman, 1998)
silicates Paleocene		1.204	2.066	(Luck and Othman, 1998)
Shale/lime stone		1.1848-1.2687	1.9386-2.075	(Hansmann and Köppel, 2000)
Sand stone feldspar		1.1655-1.1748	2.0843-2.0981	(Hansmann and Köppel, 2000)
Marine sediment core (Mediterranean coast)	Case studies	1.21	2.05	(Bollhöfer and Rosman, 2001)
Lake sed. (recent) West Greenland		1.218	?	(Bindler et al., 2001)
Tropical soil Brazil		1.09-1.35	2.438-2.559	(Schucknecht et al., 2011)
South china surface sea sed.		1.176-1.235	2.468-2.521	(Zhu et al., 2010)
Marine sediments France		1.17-1.19	?	(Roussiez et al., 2005)
Selaata marine sediment Lebanon		1.25-1.6	?	(Abi Ghanem et al., 2009)
mean sea sediments	Current study	1.816	1.321	Current study
mean river sediments		1.770	2.073	current study
mean lake sediments Feb.		1.182	2.065	current study
mean lake sediments Sep.		1.178	2.074	current study
mean lake sediments Nov.		1.187	2.062	current study
mean soil agricultural area		1.211	2.030	current study
mean soil industrial area		1.176	2.083	current study

4.4.3.3 Three-isotope plot

Pb isotopic compositions for all measured samples from both agricultural and industrial watersheds are compared to those of regional aerosols and main Pb ores in the world (Figure 4.9). Pb ores from Australia and Canada, leaded fuel in USA (1970) and Mexico and Peru Pb ores in addition to dust are represented by the triangle vertices A, B and C respectively. The present data are also compared to the regional Pb isotopic composition of aerosols (Bollhöfer and Rosman, 2001, 2002 and references therein; Erel et al., 2007). Coastal marine sediments from the industrial location are excluded from this diagram in order to represent more clearly the data, since they have high radiogenic signatures with high $^{206}Pb/^{207}Pb$ (1.63-2.02) and low $^{208}Pb/^{207}Pb$ (2.37 - 2.39) ratios compared to soils and lacustrine sediments. The supposed location of the coastal marine isotopic signatures to the upper right corner of line AB (Figure 4.9) confirms the uranium source of its high radiogenic composition (Bollhöfer and Rosman, 2001, 2002).

Industrial soil samples lie parallelly to the line AC and have a mixed Pb isotopic signature of leaded gasoline and industrial contaminants. The surficial soil samples extends on the mixing line of dust/Pb ore and leaded gasoline where they approach the values of aerosols from Egypt, Eastern Europe, Germany and France (Figure 4.9). For the time being, it is reasonable to expect the isotopic composition to deviate from that of the leaded gasoline after its banning from the global market, leading to the predominant influence of industrial signatures. The industrial samples are more affected by signatures from the leaded gasoline of USA, Eastern Europe, France and Germany. Thus, these convergent signatures could point towards a Pb ore source imported from France and Germany in 1997 as well as the fuel from the USA (Bollhöfer and Rosman, 2001). Additionally there is a possibility of industrial pollution transmitted via air masses from areas outside the Mediterranean region. Bollhöfer and Rosman (2001) evidenced the wind transmission of Chinese pollution reaching USA shores, but they did not show any transmission of pollution from Europe to North Africa. However, Erel et al., (2007) indicated the possible transfer of European contaminants to the Eastern Mediterranean by cooler air masses during the summer.

Pb isotopic compositions of agriculture soils and reservoir sediments are situated in the middle of the triangle ABC (Figure 4.9) revealing more than 2 sources of Pb in their mixed composition. Isotopic ratios of agricultural soil fall on line AB and decline to mingle with the lacustrine sediments in the center. Thus soil samples are less heterogeneous than the sediments and they show mainly a mixture of isotopic signatures of leaded gasoline and those derived from industrial and agricultural contaminants. Lacustrine sediments have an anthropogenic Pb mixture that could be composed of multivariate sources. In order to trace the origin of Pb we rely on a wide range of sources since the sediments contain also various allocthonous particles (Östlund and Sternbeck, 2001).

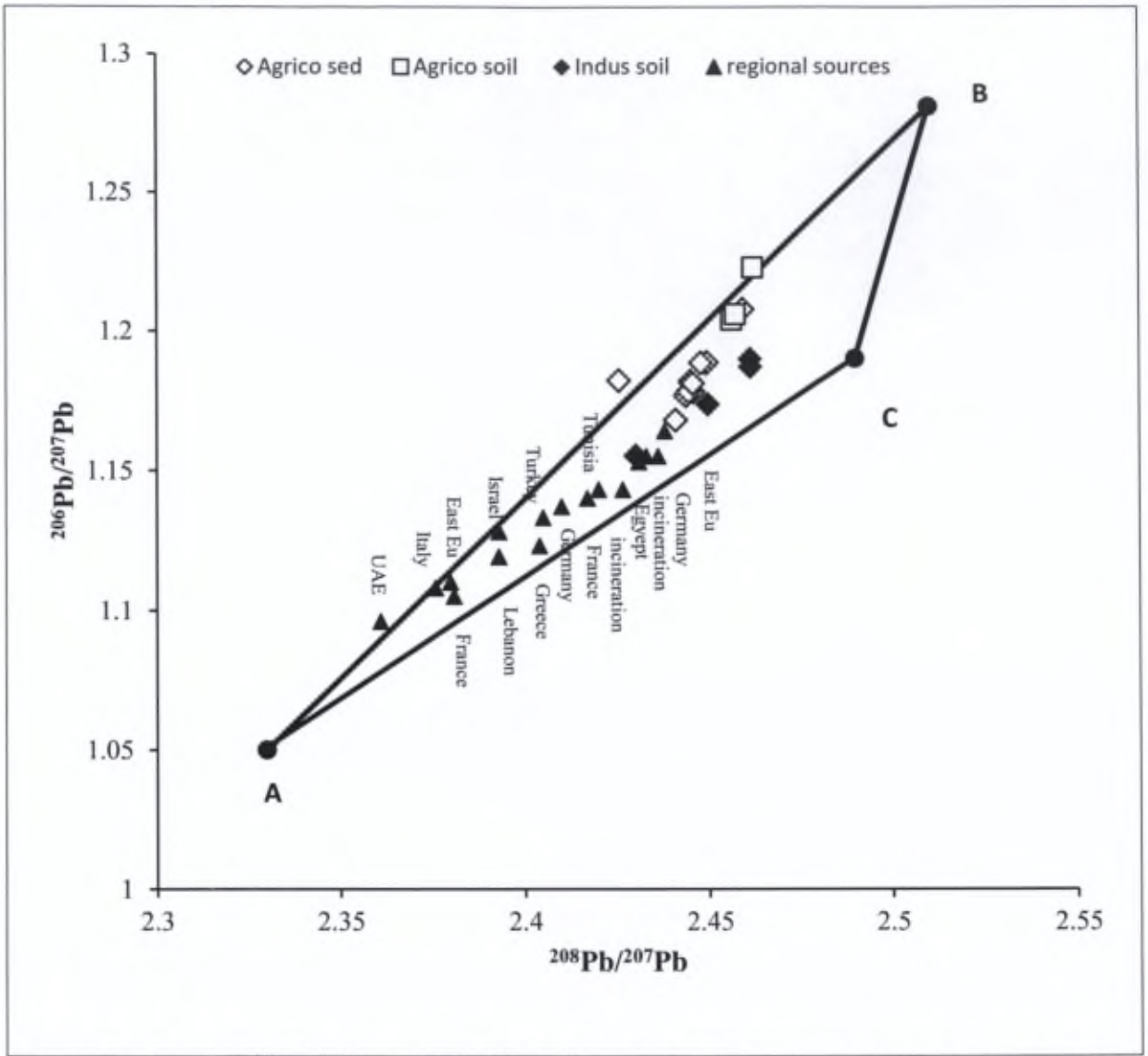

Figure 4.9: Plot of $^{206}Pb/^{207}Pb$ vs. $^{208}Pb/^{207}Pb$ for samples from the agricultural and industrial watersheds, in comparison with values found in major Pb ores and leaded fuels (A, B, C) and regional aerosols.

The agricultural sediments have isotopic signatures similar to those of particles from sand storms (Crocket et al., 1981; Mikac et al., 2011), European waste incineration, aerosols from Eastern Europe, Germany and France ((Bollhöfer and Rosman, 2001), phosphate fertilizers and pesticides (Grezzi et al., 2011; Escobar et al., 2013; Wang et al., 2013), granites (Juteau et al., 1986), paints and batteries (Wijaya et al., 2012). Thus the Pb isotopic composition of the samples could be derived from waste incineration, agricultural practices, industries such as paint and batteries manufacturing, granite industries and tailing and rock cutting activities. In addition, they can be influenced by the industrial usage of Pb ores imported from France and Germany, and even more by a possible transmission of European contaminants to the

basin or by the combustion of coal. The agricultural reservoir sediments are subjected to continuous mechanical movement and accumulation with time, as a result revealing a mixed composition of different Pb signatures of different ages. In consequence lacustrine sediments can be used to reconstruct the land-use activity and atmospheric deposition record (Kylander et al., 2005).

4.5 Conclusion

Contamination in the studied industrial area is strongly associated with the fertilizer factory and traffic. Pollution magnitude is high near the proximity of the factory and wind helps its dispersion to regions 3 km away from the industrial source. Socio-economical impacts are reflected on the deterioration of the soil quality where Pb penetration reaches a depth of 15 cm in the industrial watershed soils. Industrial activity affects strongly the coastal sediments that bear high radiogenic signatures due to the manufacturing process taking place. Thus, the coastal marine sediments act as a secondary point source of Pb pollution for the Mediterranean Sea. Multivariate sources of Pb are detected in the agricultural watershed, such as fuel, agrochemicals, waste incineration, industrial effluents (mainly paints and batteries), Saharan dust and contaminated aerosols, which are accumulated in the lacustrine sediments as revealed by their isotopic compositions. Seasonally dependent human activities such as farming, in addition to weather conditions, affect the Pb source thus inducing seasonal and temporal variations in Pb isotopic signatures. The continuous weathering of carbonate outcrops in the Litani basin results in the dilution of contaminants in the lacustrine sediments. The river inlet brings the most anthropogenically contaminated suspended matter to the reservoir during the wet season. However, the first flush washes out the pollutants from the upper basin, which are transported to the reservoir. Both watersheds are impacted by leaded gasoline, waste incineration, phosphate fertilizer and contaminated aerosols from Europe and North Africa. The magnitude of pollution is higher in the industrial watershed whereas the particularity of the agricultural receiving media amplifies the risk of Pb pollution and its tendency to infiltrate to the groundwater ultimately and to bioaccumulate in the food chain.

After the acknowledgment of pollution source, magnitude, distribution, and dynamics, it is crucial to understand the contaminant mobility in soil and sediments in the studied watersheds. The axiomatic question is "what are the factors that control metals behavior and design their fate in soil and sediments?" Each watershed is characterized by different land topography, geomorphology, soil type, and of course land-use cover, thus it is interesting to study the synoptic effect of all these factors on contaminants behavior. Furthermore, the matching date of the factory establishment and the dam construction in late 1950s can be of great interest, since this coincidence will allow the pollution flux chronology to be referred to the same period and to interrogate the contaminants behavior in different environmental contexts. Undisturbed soil cores give a clear stratigraphic idea about the flux record of pollutants' deposition, distribution, and age. As a consequence, the reconstruction of metal fluxes in undistributed cores will draw the land-use timeline and provide insights for water basins evolution. Correspondingly, soil type, texture, morphology, and constitution may interfere in contaminates distribution and transport. Therefore and in order to cover the treated issue from all angles, soil analysis should be conducted for soils collected from each watershed that will improve our understanding and strengthen the study outcome. Moreover, the impact of each factor controlling the metal behavior in soil should be discretely studied, purposing to develop a wider understanding that could be applied on different soil types rather than the studied case. In order to achieve this aim, a leaching column experiment represented by soil packed column approach spiked by contaminants of interest should be conducted. In our case, PG and fertilizers are the contaminants of interest due to their environmental significance in both watersheds. Mimicking natural soil cores by implementing packed column experiment will clarify the findings in the intact soil cores. Furthermore, testing each contaminate on different soil type may determine the factors influencing contaminant behavior and predict its fate in different contexts. As a consequence, linking the natural behavior of contaminants in intact cores from one side, to metals mobility induced by regulated factors in the packed columns from the other side, will enhance our comprehension of metal behavior and prediction of its fate in nature. Eventually, the awareness of metal behavior and fate in different receiving media will result in efficient pollution management plans.

Chapter 5

Metal behavior in intact cores and packed columns: Comparison between industrial and agricultural watersheds in eastern Mediterranean

Abstract[4]

Soils and sediments can preserve geomorphological changes and pollution records from point and non-point sources derived from multi-land use activities in hydrographic basins. Core samples give a clear stratigraphic idea about the flux record of pollutants' deposition, distribution, and age. The aim of this study is to document land-use impact on soil quality and to assess metal behavior and chronology in undisturbed soil cores. In addition, metal fate is predicted in column leaching experiments for two contrasting watersheds soils in Eastern Mediterranean. Sedimentation rates are influenced by land-use, land topography, soil pedology and climate. They also increase cumulative metal hazard risks. Dam construction promotes socio-economic development where this development could pose a great pollution risk in agricultural watersheds and hence requires specific management plans to sustain the hydropower projects and soil fertility. Similarly the establishment of industrial and manufacturing bases on the Mediterranean coast could exert high environmental stress on soil and water, through collective geomorphological, geological and climate factors resulting from hazardous metals leachability to groundwater and sea water. Contaminants nature and dose in addition to receiving media characteristics may alter metal bearing phases to more labile forms thus increasing its mobility and bioavailability. Land use, precipitation, land topography, intrinsic soil properties, pollutant type and magnitude are important factors for controlling metal fate in the environment. Thus all these factors should be taken in consideration to achieve efficient pollution management plans.

[4] Adapted from the article to be submitted (Ammar R, Kanbar H, Kazpard V, Wazne M, El Samrani AG, Amacha N, Schmidt S, Roveros N, Saad Z, Chou L. Metal behavior in intact cores and packed columns: Comparison between industrial and agricultural watersheds in eastern Mediterranean).

5.1 Introduction

Natural and anthropogenic activities, such as soil erosion, urbanization, industrial and agricultural activities, result in an increase in the rate of sedimentation and thus deterioration of the quality of environmental compartments, namely soils, sediment and water (Newman et al., 2006; Clark et al., 2014). Open water bodies are more susceptible to erosion and sediment flux that is enriched with contaminants derived from the upper watershed in the form of suspended matter. Consequently, lacustrine sediments act as sink for contaminants which reflect land use (Balogh et al., 2010; Hiller et al., 2010; Clark et al., 2014). Any geomorphological change on the land surface is well preserved in soils and sediments. It is critical not only to investigate superficial soils and sediments, but also deeper layers as well. This will give a clear stratigraphic idea about the flux record of pollutants' deposition, distribution, and age. Core studies determine land-use alternation in the watershed, sediment accumulation rates, and contamination loads in order to reconstruct the history of basins (Benoit and Rozan, 2001; Dabous, 2002; Balogh et al., 2010; Clark et al., 2014). Soil and sediment cores are able to preserve pollution records from point sources (direct reject), non-point sources (surface runoff) as well as atmospheric deposition (Balogh et al., 2010). The lack of atmospheric metal deposition data could be compensated by analyzing soil profile. Soil profile gives information about metals input and output records and metal distribution processes (Herndon et al., 2011). Accordingly, the behavior of metal in the soil profile and its potential leachability poses a great interest to many researchers (Syrovetnik et al., 2007; Lesven et al., 2010; Thevenon et al., 2013). Metal behavior in soils could be assessed by using soil columns leaching tests in order to predict potential leachability to ground water (Alvarez, 2007; Maszkowska et al., 2013). Packed columns system allows the investigation of metal mobility in different environmental contexts relative to soil and pollutant nature and dose. Leaching columns can predict the metal bioavailability and asses its hazard on microhabitat and groundwater quality (Zhao et al., 2009; Maszkowska et al., 2013).

Pb isotope dating is the most commonly used method to study the anthropogenic signature in a sediment or soil profile. Radioactive ^{210} Pb dating is able to reconstruct pollution history, whereas ^{137}Cs dating is used in parallel to constrain sediment accumulation rates in soil and sediment cores (Appleby and Oldfield, 1983; Benoit and Rozan, 2001; Dabous, 2002; Ruiz-Fernández et al., 2007; Liang et al., 2014). ^{210} Pb is a naturally occurring radionuclide decayed from ^{238}U with a half-life of 22.3 years. There are two types of ^{210}Pb, the supported and unsupported. The supported type is naturally found in soil from decayed ^{222}Rn and ^{226}Ra. While the unsupported type or so called excess is derived from atmospheric deposition. Following the decaying law, unsupported ^{210}Pb declines with age in sediment layers of a core, thus it allows sediment accumulation rate estimation (Appleby and Oldfield, 1983).

There are diverse factors and processes that impact metal behavior in soil and sediments profiles, which rely on the metal characteristics and its encompassing matrices. The mobility of metals is influenced by its speciation form, sorption capability, specific electronegativity and ionic radius, incubation time, potential contaminant type and dosage. This in turn is

correlated to the physico-chemical properties of soils, such as pH, redox potential, cation exchange capacity (CEC), mineral composition, particle size and nature, surface charge, soil structure and texture, permeability, organic content and vegetation cover (Jacksont et al., 1980; Alvarez, 2007; Balkis et al., 2010; Hiller et al., 2010; Herndon et al., 2011; Maszkowska et al., 2013).

Previous studies compared anthropogenic impacted watersheds (from industrial and agricultural uses) to natural undisturbed ones such as forest (Dabous, 2002; Balogh et al., 2010; Clark et al., 2014; Liang et al., 2014). This study compares an industrially active watershed (Levantine (Al Jouz) basin) to an agricultural dominated one (Litani Basin). The historical data deficiency in Lebanon regarding metal waste discharge can be compensated by investigating soil and sediment cores, which represent a robust tool to recreate the historical record of metal emission and atmospheric deposition in both watersheds (Azoury et al., 2013; Balogh et al., 2010). The objectives of the current work is to couple ^{210}Pb chronology to geochemical analysis in two different soil cores and investigate metal contamination magnitude, metal flux and pollution history in two contrasting watersheds. Correspondingly, the hydro-project impact on watershed ecology is evaluated by studying sediment cores at the reservoir banks. Furthermore, this study aims to understand the behavior of metals in intact soil cores, by investigating the influence of soil nature, contaminant type, and dose on metal mobility by conducting column leaching experiments, thus assessing the risk of socio-economic activities on a specific soil type.

5.2 Materials and methods

5.2.1 Study area:

The study area comprises of two contrasting watersheds in Lebanon, where they have different micro-environments, socio-economical context, land-use, climate, geology and geography. The first is an industrially dominated watershed (Al Jouz basin) located on the North Mediterranean coast in Batroun district. The geology of the watershed is mainly composed of middle Cretaceous and Eocene strata layered by Neogene marine strata, with a sandy-marly limestone in addition to partially marly rocks interbred with basalt, which could range in thickness from 100 to 400 m on the coast (Edgell, 1997; Walley, 1997). The industrial area is highly influenced by coastal Mediterranean climate of heavy winter and dry summer. The mean annual precipitation ranges between 1000 and 1100 mm, and the mean annual temperature is 20 °C (UNDP/MoE, 2010). It represents an active passage from the North to the capital Beirut; it also exhibits one of the largest chemical industries in the country and one of the most polluting factories in the Mediterranean region, a phosphate fertilizer factory established on the sea shore since 1956 (Bridgen et al., 2002; Fakhri et al., 2008). The chemical factory manufactures phosphate fertilizers and phosphoric acid by treating phosphate rocks with sulfuric acid and rejects hemi-hydrated calcium sulfate, or so called phosphogypsum (PG), as a byproduct (Rutherfors et al., 1994; Al-Masri et al., 2004). Both, raw parent material and the byproduct, are rich in radioactive elements and metals (Aoun et al., 2010 Ammar et al., 2013). Thus the factory exerts an immense environmental

stress on the watershed's ecology by its wet and dry deposits, stock-piles and direct rejects into the sea and the atmosphere as detailed in Chapters 3 and 4 (Fakhri et al., 2008; Abi Ghanem et al., 2009; Yammine et al., 2010; Ammar et al., 2013). As for the second watershed, Litani basin, it is dominated by agricultural practices, located in the continental Bekaa valley and bordered by two mountainous chains. The geology of the watershed is comprised of Quaternary alluvium limestone with a chalk and marly chalk outcrop that ranges in thickness from 150 to 900 m (Edgell, 1997; Walley, 1997). The inland Litani basin tolerates a continental semi-arid climate affected by the Mediterranean, where the mean annual precipitation ranges between 700 and 1000 mm, and the mean annual temperature is 16 °C (UNDP/MoE2010). The Litani basin is the major national agricultural producer in Lebanon. After the establishment of the Qaraaoun dam in 1956, multi industrial institutions were founded in the basin, in addition to hospitals, farms and touristic facilities (El Fadel et al., 2003). The Litani river acts as a collective funnel for domestic effluents, agricultural and industrial wastes in addition to earth crust erosions and transmits all these potential contaminants of suspended matter, solvents and chemicals to the reservoir (El Fadel et al., 2003; Korfali et al., 2006)

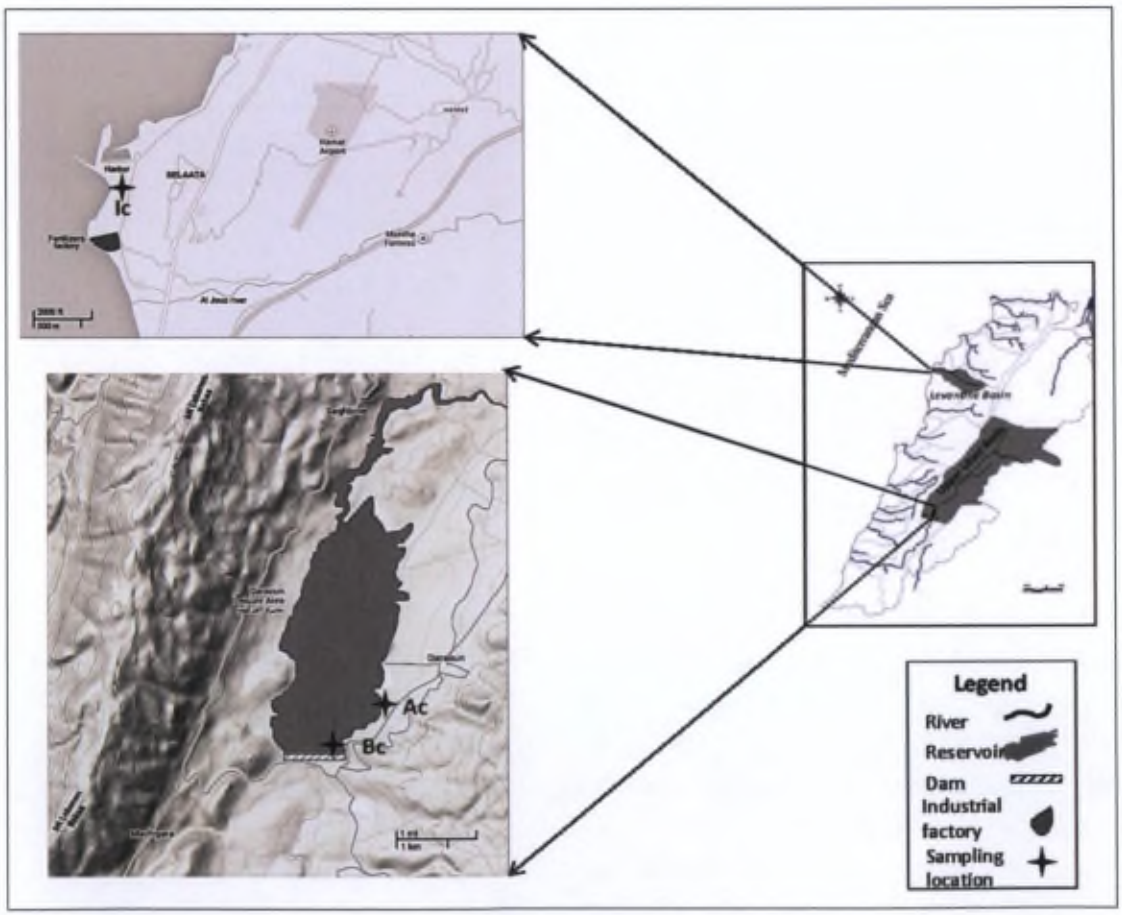

Figure 5.1: Study areas, where the industrial soil core (Ic) and agricultural soil core (Ac) and the bank core (Bc) localities are shown in the studied watersheds.

5.2.2 Intact soil cores

Undisturbed intact soil cores were retrieved from both watersheds, the industrial watershed (Ic) and agricultural one (Ac) during wet season in 2012. Furthermore, additional core (Bc) was collected from reservoir bank during the spill hydrological mode (summer 2012) (Figure 5.1). The bank core (Bc) samples became accessible due to the dramatic drop of water level during the dry season where parts of the reservoir that are usually completely submerged during wet seasons were revealed. Cores were extracted via a motorized core drill (COBRA TT, Carottage à Percussion- SDEC) with a stainless steel coated core of 7 cm inner diameter. The sample core of 70 cm length was partitioned into layers of increasing thickness with respect to the surface (5 x 3 cm, 7 x 5 cm and 2 x 10 cm layers). Samples were stored in polyethylene bags in a fridge, then freeze-dried using an Alpha 1-4 LD plus freeze drier.

5.2.3 Leaching soil columns

In order to understand metal behavior in the intact cores, and to study the soil type impact and the influence of contaminant type and its concentration; packed soil leaching column experiments were prepared in the laboratory in parallel to the field study. Soil designated for the packed columns were collected from the A-horizon from both watersheds right next to where the intact cores were collected. Soil for the agricultural packed columns experiments was comprised of a mixture of soils collected from lateral sides of the reservoir in order to have a better representative soil sample.

A total of 28 packed columns were divided into two groups, where each group was designated for each watershed. The first set of packed columns contains soil from the Industrial watershed (Ip, n=14) whereas the second set of soils came from agricultural watershed (Ap, n=14). The air dried samples were sieved over 2 mm mesh and were homogenized and used to pack the PVC columns (L= 40 cm; r = 4.75 cm) up to a depth of 36 cm. The columns were placed over a Büchner funnel connected to polyethylene bottle and supported by a wooden rack, and a filter paper was placed on the top layer of each column to guarantee the homogeneous distribution of added/irrigated water. The column tests were conducted according to the OECD norms (OECD 312, 2004). Volumetric and gravimetric water holding capacities (Θv and Θg) were determined, and 70 % of soil water capacity was reached in all 28 columns by adding ultrapure water to mimic natural conditions and allow biological growth. Fertilizers and PG were chosen as potential contaminants to be applied in the column tests, due to the presence of these contaminants in the agricultural and industrial studied areas respectively. PG was collected from a slurry of the industrial factory, and two concentrations were chosen for the treatment, PG 1x and PG 2x. The two dosages represent the saturation phase (2 g/l) and double saturation phase (4 g/l) in ultrapure water, respectively as shown in Chapter 3 (Ammar et al., 2013). A local survey was conducted to investigate a very common fertilizer in the agricultural area. The survey suggested the widespread use of NPK 20, 20, 20 which is a mixture of nitrogen, phosphate and potassium nutrients. In order to resemble fertilizer's application in the field, we have calculated the concentration of applied fertilizer with regard to the surface area of the column. The application rate of NPK 20-20-20

is 10 pounds/acre, thus the required fertilizer concentration for each column was determined at 7944.82 µg (1x) and 15889.65 µg (2x). Each set was further divided into subsets of Blanks (n = 2), columns spiked by NPK 1x (n = 4), columns spiked by NPK 2x (n = 2), columns spiked by PG 1x (n = 4), and columns spiked by PG 2x (n= 2). The soil columns tests were run for 72 days including 50 artificial raining events, where the total applied water volume was similar to the relative volume produced by the average annual precipitation in Lebanon (900 mm) (Shaban, 2014).

5.2.4 Analytical methods

- Leachate analysis

Leachates were collected on daily basis and were filtered through 0.45 µm filters stored at 4°C for later analysis. Major ions Cl^-, NO_2^-, NO_3^-, PO_4^{3-}, F^-, and SO_4^{2-} were measured using Ion Chromatography (Shimatzu - shim pack IC-A3), where Na^+ and K^+ were measured using flame photometer model 420 from Sherwood. However samples targeted for metal analysis were acidified using concentrated HNO_3 to reach pH 1 once they were collected, and later subjected to heavy metals measurements using Atomic Absorption Spectrometry (Rayleigh WFX-210 AA Spectrophotometry equipped with a WF-10A auto-sampler with flame and graphite furnace modes)

- Characterization of soil in cores and packed columns

The grain size distribution of the sediment cores, and soils used for packed columns were measured via laser scattering particle size distribution analyzer (Patrica LA-950V2 Horiba) equipped with a laser diodes of 1.6 mW with λ= 405 nm – 650 nm. Sample dry weight ranging from 10 mg to 5 g per 100-160 ml MQ water volume was used for analysis. The method relies on the Mie scattering theory with measuring size ranging from 0.01 µm to 3000 µm and an ultrasonic probe was used to break aggregates at 20 kHz frequency. Chemical functional groups were determined by FT-IR-6300 (Fourier Transform Infrared Spectrometer) from JASCO. A mixture of the powdered samples with potassium bromide (1% wt/wt) was prepared and compressed into a pellet of 0.7 cm diameter for measurement. Additionally total organic carbon content in sediment and soil cores of agricultural watershed were measured using CNS analyzer form Interscience FISONS (NA-2000; series 2), and values were calculated according to a calibrated reference material (stream sediments reference material STSD-2 with 1.6% of carbon content). In addition, mineralogical phases in the samples were determined using a D8 Bruker X-ray diffractometer (copper anticathode of wavelength $\lambda K\alpha$ = 0.154060 nm). A 2θ window ranging from 10° to 60° was chosen with each leap at 0.02° and 1 sec designed for measurement. Collected diffractograms were analyzed using the software EVA and the powder diffraction files provided by the International Centre for Diffraction Data.

Collected sample layers either from intact cores or scarified packed columns were freeze-dried and homogenized using pestle and mortar, sieved over 63 µm acid-cleaned nylon mesh, and extracted for particulate metals using a microwave acid digestion method. An amount of

50 mg of 63 µm sieved samples was digested in Teflon bombs along with suprapur acids: 1 ml of 10 N HCl, 2 ml of concentrated HNO_3 and 250 µl of 40% Hydrofluoric acid (HF). Samples were analyzed by Graphite Furnace Atomic Absorption Spectroscopy (GFAAS) with Zeeman-effect background correction (Varian AA-400) and Inductively Coupled Plasma Atomic Emission Spectroscopy (ICP-AES) (Varian Liberty series II). Certified standard materials (UN 3264 from MERCK) along with blanks were measured with sample batches, and the limit of detection was respected.

- Dating of cores

Lyophilized solid samples of the intact cores were ground by agate mortar and sieved over 63 µm acid clean nylon mesh, and aliquots of 2 g fine solid fractions were used to measure ^{210}Pb, ^{226}Ra and ^{137}Cs activities by gamma spectrometry, using a low-background, high-efficiency, well-type germanium detector (Canberra, Ge volume 280 cm^3). The radioactivity for ^{210}Pb, ^{226} Ra and its decay product were determined by 46.5 keV, 295 keV and 352 keV respectively. Standard materials were used for the calibration of the g-detector in accordance with IAEA reference materials (RGU-1, RGTh-1). Unsupported ^{210}Pb ($^{210}Pbxs$) was calculated from the total Pb after the subtraction of ^{226}Ra activity. Furthermore, counting errors of $^{210}Pbxs$ were computed by propagation from ^{210}Pb total and ^{226}Ra (Ruiz-Fernández et al., 2007; Schmidt et al., 2009; Azoury et al., 2013).

- Characterization of soil used for packed columns

pH and electric conductivity were measured in 1:5 (w:v) of dried soil: ultrapure water ratio using ADWA pH bench meter AD1000 coupled with a temperature electrode and conductivity meter Cond 330i according to NF ISO 10390 and NF ISO 11265 respectively. Bulk density, particle density, soil void % and porosity were calculated in the dried solid samples as detailed by Thien and Graveel, 2003. Soil texture was determined by the Bouyoucos hydrometer method using an ASTM-E-100 Soil solution hydrometer, and the soil type was determined referring to the United State Department of Agriculture (USDA) texture triangle according to NF X31_107 (as detailed in Chapter 2). While particles surface charge was measured by zeta potential using a Zeta-Meter System 4.0 unit, equipped with an electrophoresis cell (type GT-2) of 10 cm long and 4 mm in diameter with K factor and two platinum electrodes. Cation exchange capacity was determined by filling all the negative sites of the soil by copper acetate and then leaching adsorbed copper by ammonium acetate. The content of copper was certified by SP 2000 UV Spectrophotometer VWR (Thien and Graveel, 2003). In addition, the organic content percentage of the soil was estimated by the dry combustion method using wise thermo furnace/oven calcinatory (ASTM D 2974). The active calcareous content of the soils was determined by titration with potassium permanganate ($KMnO_4$) according to NF X-31-106 norm, while the total calcareous content was determined by Calcimeter Bernard method (NF ISO 10693). The available fractions of potassium (K^+) and sodium (Na^+) in the soils were determined using Protocol P05-001A. K^+ and Na^+ were extracted from the soil by a 0.5 M extracting solution of ammonium acetate and glacial acetic acid, and the dissolved portions of K^+ and Na^+ were measured using a

Flame photometer model 420 from Sherwood. At the end of the experiment the soil profile in each column was partitioned into increasing thicknesses as function of depth (2, 2, 2, 4, 5, 5, 5, 5 and 6 cm), stored in polyethylene bags at -80°C, and freeze-dried by Lyophilizator prior to analysis.

5.3 Results and Discussion

5.3.1 Reservoir impact on watershed

The geographical location of the dam enhances collection of surface runoff where the dam receives accumulated deposits derived by the river from the upper watershed. In order to investigate the land-use impact on soil, and the potential hazard of transported contaminants from the watershed, a soil core (Ac) was retrieved (Figure 5.1). The location of the soil core was chosen according to previous findings, since it has been reported that the eastern side of the reservoir is a hot spot due to contamination from anthropogenic effluents (Shaban and Nassif, 2007). An additional core was also collected from the reservoir eastern bank (Bc), which is frequently submerged during wet season, to estimate the dam influence on the watershed ecology and to assess pollution flux from multivariate land use activities.

Iron over aluminum ratio in the agricultural area cores was used to evaluate the continental input and metal behavior (Lyons et al., 2003). Fe/Al ratio in core Ac indicates an increase from 0.46 in the topsoil to 0.63 at a depth of 30 cm, thereafter Fe/Al ratio remained constant in the lower 40 cm (Figure 5.2a). Correspondingly, Fe shows a strong correlation with Al in the top 30 cm of the core Ac ($r= 0.99$) (Figure 5.2b). However Fe/Al ratio in the core retrieved from the reservoir bank (Bc) fluctuates in the top 40 cm where the maximum ratio was observed at 40 cm depth (0.75) and remains constant thereafter (Figure 5.2c). Iron indicated a strong correlation with Al in the whole profile of the core Bc ($r=0.99$) (Figure 5.2d). The Fe/Al ratio trends in both cores may suggest a diagenetic mobility of iron (Xia et al., 2013). The increase in the Fe/Al ratio in the vertical profiles may indicate Fe transition from oxic to anoxic zone (López et al., 2006). While the scattering observed in Fe/Al ratio in core Bc could be due to fluctuation of redox conditions caused by the reservoir active hydrodynamics. The submerged core (Bc) is exposed in the dry season thus shifting its redox condition, as a consequence changing iron distribution and remobilization in the profile as shown in Figure 5.2c (Lyons et al., 2003; López et al., 2006).

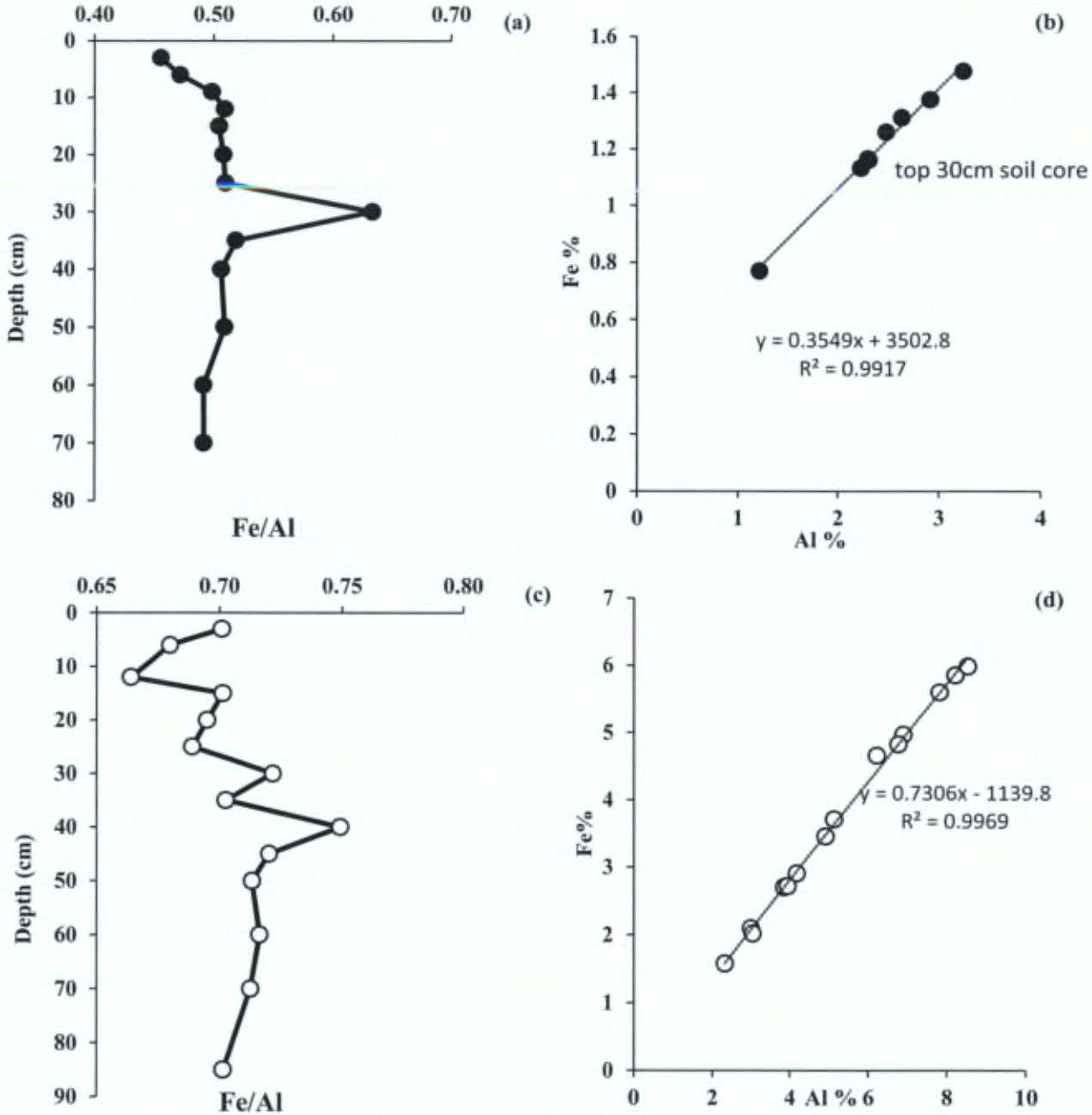

Figure 5.2: Plot of Fe/Al ratio and the plot of Fe vs. Al in agricultural soil (Ac) core (a and b) and core Bc retrieved from the reservoir bank (c and d respectively).

Total organic carbon (TOC) shows a gradual decrease with depth from 5 to 1.25% at the top 35 cm of core Ac, thereafter it remains constant with depth (Figure 5.3a). While in core Bc, the TOC was maximum in the top core layer (3.77%), and fluctuates with depth where it shows an increase at 15 cm (3.32%) and 40 cm (2.7%) depths, respectively (Figure 5.3a). The scattering of TOC in core Bc could be caused by the reservoir hydrodynamic changes impacting primary production, or reflecting records of nutrient load from the upper

agricultural watershed (Clark et al., 2014). TOC in both cores indicates antagonistic trends to Fe/Al ratios, thus organic carbon bearing phases may be dominated by phyllosilicates over iron oxides as a result of soil surface loss from the upper watershed (Kögel-Knabner et al., 2008). Similar to TOC, Cu, Cd, and Pb indicated higher concentrations in the top layer of the core Ac then decrease gradually with depth, while the trends for the corresponding metals in core Bc have opposite behavior (Figure 5.3b, 5.3c, and 5.3d). The highest Cu concentration (104 ppm) was observed at 70 cm, while Pb and Cd peaks were observed at 2.16 ppm and 31.4 ppm, respectively, at a depth of 60 cm in core Bc. The metal enrichment occupying the top soil layers are correlated with organic matter in core Ac as a result of soil weathering and geomorphological changes in the upper watershed (Van Griethuysen et al., 2005; Louri˜no-Cabana et al., 2011). Metal enrichment in the lower layers of the core Bc maybe referred to specific anthropogenic incidence (Louri˜no-Cabana et al., 2011), such as the dam construction and industrial development in Litani watershed. Metal behavior in the top layers of core Bc can be explained by their oxidation due to hydrodynamic changes of the reservoir, thus they may liberate their metal content with the transported dissolved organic content (DOC) to the reservoir when the banks are submerged during fill hydrological mode. However, when the water level drops, it induces biological activity which leads to metal precipitation and as a consequence its immobilization (Van Griethuysen et al., 2005).

Pearson correlation analysis (PCA) is utilized to link metal content in the studied cores with their possible source, and potential bearing phases (Xia et al, 2012, Clark et al., 2014). The calculated PCA coefficients between the elemental content of core Ac[5] are shown in Table 5.1. A positive correlation between Al and major elements (K, Si, Mn, and Fe) was observed, which indicates the affinity of these metals to mineral phases such as aluminum silicates, and Fe/Mn oxides (López et al., 2008; Xia et al., 2012). Nevertheless, Mg, Zn, Pb and Cd show a weak correlation with Al suggesting an anthropogenic source for these metals such as fertilizers and pesticides which is extensively applied in the agricultural watershed and could be associated with organic matter (Xia et al., 2012). Furthermore, Ca and Cu data indicate a negative correlation with all tested metals except with each other, which may be due to a solitary Cu source possibly associated only with carbonates. This could be related to massive application of copper sulfate in the agricultural area and its particular utilization as an algaecide to minimize algal growth in the reservoir and the irrigating canal (BAMAS, 2005). Copper from copper sulfate can precipitate with natural carbonates found in the watershed (Zhizhaev et al., 2007). A significant correlation was observed between Zn and each of Cd and Pb with ($P < 0.01$), which can reflect the common origin of these metals either from rocks, or anthropogenic practices, such as vehicles exhaust emissions and paper industries (Dabous, 2002; Clark et al., 2014).

[5] Metal content of core Ac are presented in Annex 3 (Table A3.2).

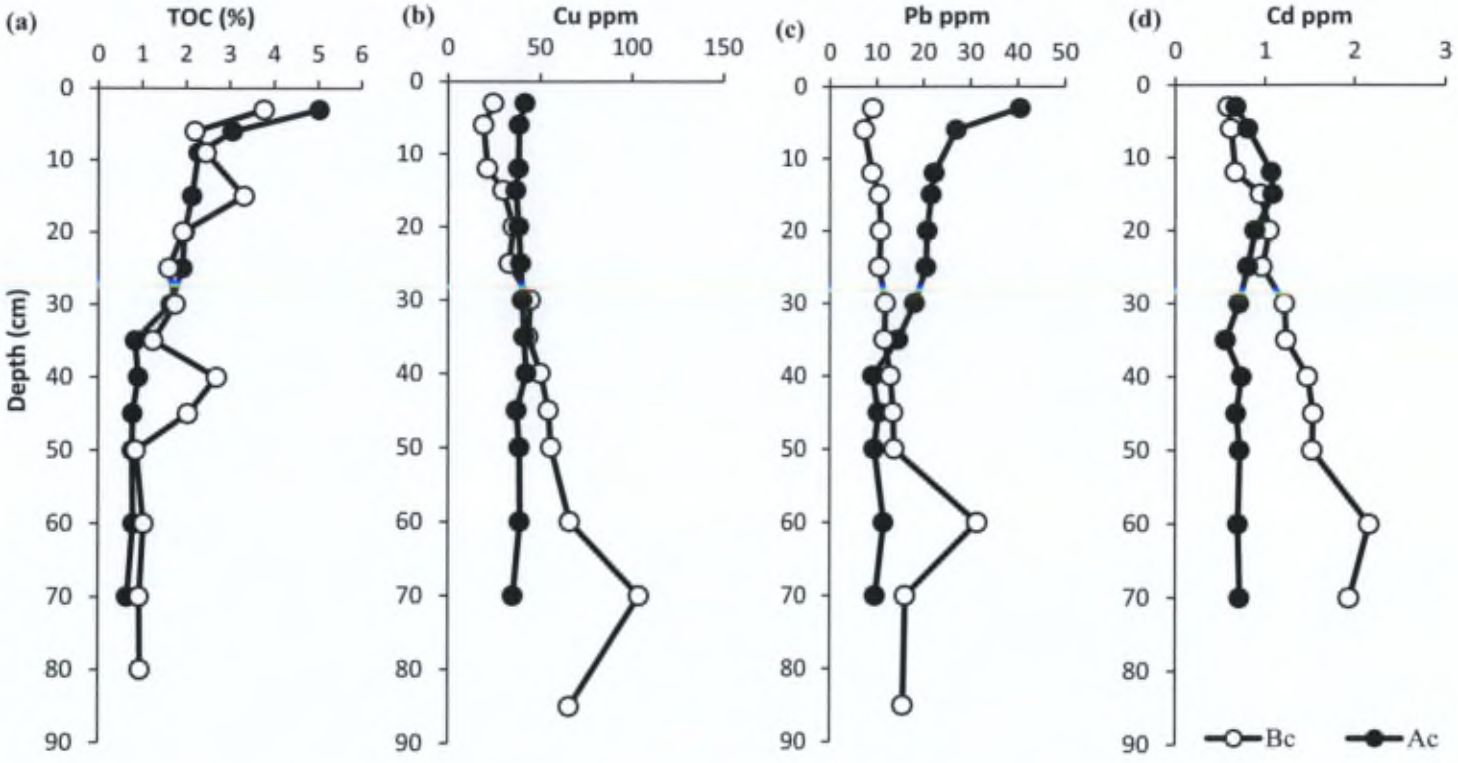

Figure 5.3: The comparison of (a) total organic carbon, (b) Cu, (c) Pb, (d) Cd content in the profiles of cores retrieved from soil (Ac) and reservoir banks (Bc) in the agricultural area.

Table 5.1: Pearson correlation coefficient between metals for soil core in agricultural watershed (Ac).

Element	Al	Ca	K	Mg	Si	Zn	Fe	Mn	Cu	Pb	Cd
Al											
Ca	-.920**										
K	.814**	-.776**									
Mg	.556*	-.590*	.830**								
Si	.746**	-.770**	.919**	.912**							
Zn	.414	-.490	.120	-.333	.001						
Fe	.990**	-.931**	.863**	.641*	.802**	.351					
Mn	.911**	-.873**	.923**	.739**	.850**	.224	.947**				
Cu	-.273	.497	-.432	-.496	-.520	-.138	-.327	-.356			
Pb	.353	-.268	-.141	-.518	-.271	.720**	.232	.037	.254		
Cd	.207	-.417	.119	-.160	.051	.810**	.222	.168	-.410	.253	

There are 10 paper mills and paper pulps industries in the studied area distributed over less than 40 Km from the reservoir and around 3 km from the river main course. On the contrary, Pearson correlations show a strong positive correlation between Al and all measured major,

minor, and trace metals in the core Bc[6] (Table 5.2). Metals in the core are correlated with each other at the same period of time, which means that they are referenced to same contamination source or time era as industrial development and as a result of important geomorphological change such as the dam establishment (Balogh et al., 2010). The strong correlation between all metals in core Bc and mainly the significant correlation between Fe and Mn ($P < 0.01$) (Table 5.2) suggests diagenetic processes, moreover metals in core Bc could be associated with Fe/Mn oxides fraction (Ruiz-Fernández et al., 2007; Clark et al., 2014). However in core Bc, Pb reflects a weak correlation with Mn and Cu (Table 5.2) which may be due to additional sources of Pb such as atmospheric deposition and effluents from paints, papers and plastic industries in the watershed (El Fadel et al., 2003).

Table 5.2: Pearson correlation coefficient between metals for sediment core in agricultural watershed (Bc).

Element	Al	Ca	K	Mg	Si	Zn	Fe	Mn	Cu	Pb	Cd
Al											
Ca	-.994**										
K	.995**	-.990**									
Mg	.872**	-.852**	.880**								
Si	.990**	-.991**	.984**	.871**							
Zn	.993**	-.995**	.988**	.828**	.989**						
Fe	.998**	-.997**	.993**	.872**	.990**	.994**					
Mn	.864**	-.840**	.866**	.700**	.826**	.840**	.854**				
Cu	.911**	-.897**	.874**	.783**	.906**	.907**	.908**	.693**			
Pb	.708**	-.719**	.737**	.575*	.719**	.751**	.707**	.456	.612*		
Cd	.977**	-.978**	.976**	.808**	.975**	.987**	.974**	.927**	.892**	.836**	

To the best of our knowledge, there is no dating or sediment sequencing for the reservoir or the agricultural area. Core chronology and metal fluxes are reconstructed using radioactive ^{210}Pb and ^{137}Cs isotopes, since each radiogenic isotope is derived from different source and reports a different measurement for sediment burial in the same core (Ruiz-Fernández et al., 2007; Liang et al., 2014). Radioactive $^{210}Pb_{xs}$ activity decreases monotonically with depth in core Ac, where the maximum activity observed on the top of the core layer (93 mBq/g) and decreases to 1 mBq/g at a depth of 20 cm (Figure 5.4a). The constant flux-constant sedimentation rate (Cf/Cs) model was used to graphically determine the sedimentation rate from a plot of $^{210}Pb_{xs}$ activity versus depth using semi-logarithmic scale (Appleby and

[6] Metal content in the core Bc are presented in Annex 3 (Table A3.3).

Oldfield, 1983). Specifically, the CF/Cs model was used to date the core, where the corresponding age for the top 20 cm are dated back to 1887.5. Anthropogenic radionuclide ^{137}Cs activity was observed at the top 12 cm which is dated back to 1953 (Figure 5.4a), which in turn corresponds to the onset of nuclear weapons testing (Ruiz-Fernández et al., 2007; Liang et al., 2014) and the dam establishment in late 1950s. As a consequence we have investigated metal fluxes in core Ac only for the top 25 cm with regards to the sedimentation rate (S= 0.18 cm/yr) as presented in Figure 5.5a. Al, Fe, Mn, and Pb fluxes indicated a monotonic increase to the surface (by 1.5, 1.3, 1.5, and 2.2 folds respectively) which may be correlated to continuous natural weathering, anthropogenic activities and atmospheric deposition (Azoury et al., 2013). While Mg, Si, K, and Zn data indicates two trends possibly relating to two periods, the first period/trend relates to the flux increase from 25 cm to 12 cm depth (before dam construction), and the other one relates to the flux fluctuation with slight decrease in the top 12 cm (post dam construction) of the core Ac. However, Cu and Cd showed an antagonistic behavior before dam construction where Cu flux indicated an increase with depth and Cd flux indicated a decrease with depth. Conversely, post dam construction Cu decreased whereas Cd flux increased, with depth (Figure 5.5). The recorded change in metal flux post dam construction can be related to land-use change in the watershed upon dam construction (Clark et al., 2014), where more agricultural and industrial practices are reported as indicated in Chapter 4 (El Fadel et al., 2003; Ammar et al., submitted). For example, the increased fluxes of K, Cu, Mn, Zn and Fe post dam construction in core Ac could be a result of disposal of olive oil mill wastes near the dam (Kavvadias et al., 2010). However the slight decrease in the top surface for K, Mn and Zn fluxes (Figure 5.5a) could be due to forcing the olive oil processing factory by the Litani River Authority (LRA) to dispose wastes in impermeable evaporative pond.

In the core Bc, radioactive $^{210}Pb_{xs}$ activity decreases with depth, but fluctuates mainly at the top 40 cm of the core, where the maximum activity was observed at surface (30 mBq/g) (Figure 5.4b). This ^{210}Pb anomalous distribution could be related to perturbation due to water dynamics (aggressive water drop during dry season), soil physicochemical changes and biological activity (Xia et al., 2012). Moreover, ^{137}Cs maximum activity (27 mBq/g) was observed at 60 cm depth and corresponds to the year 1987 that denotes the Chernobyl nuclear accident in 1986 (El Samad et al., 2007).

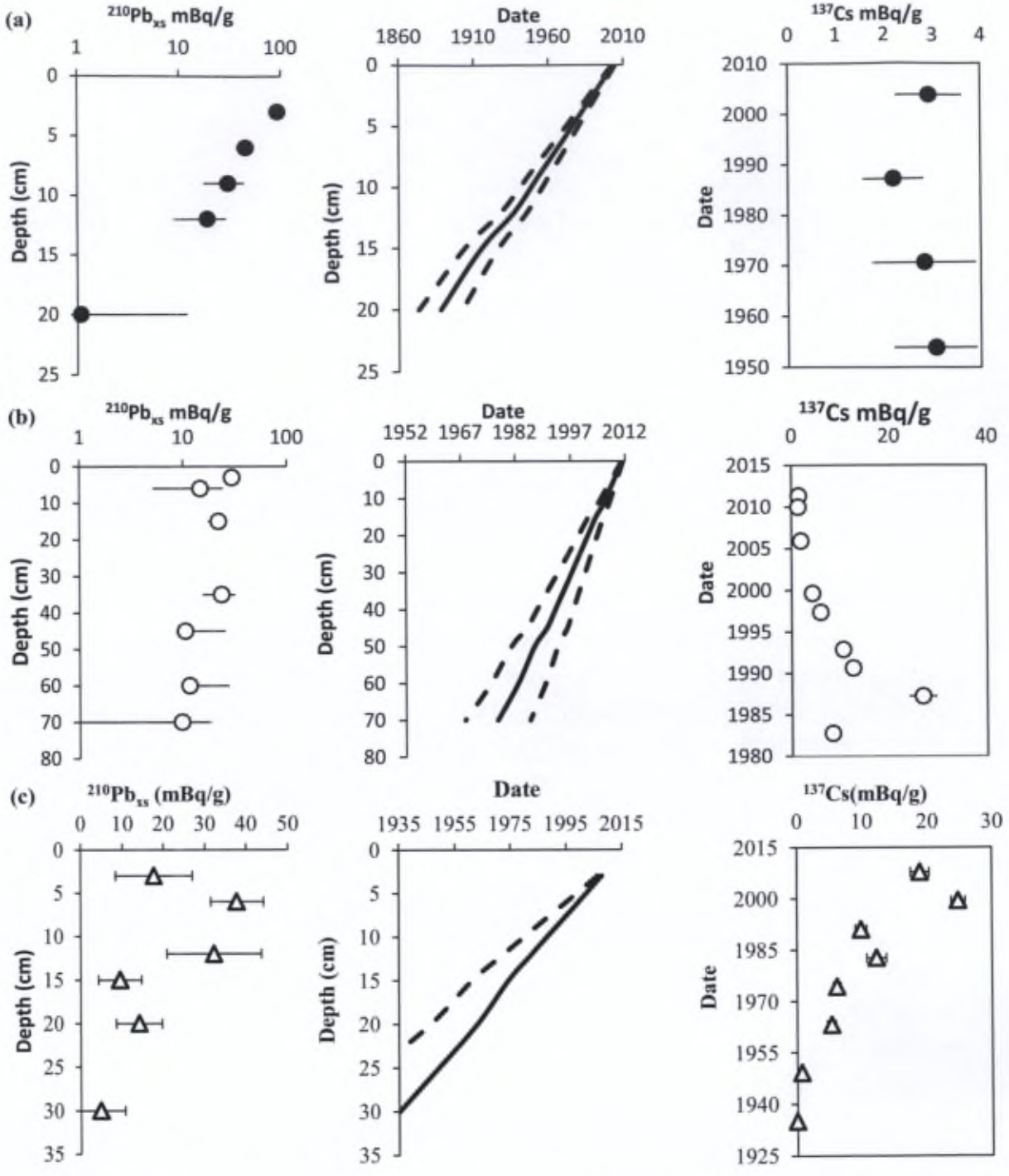

Figure 5.4: Chronology of old core Ac (a) and modern core Bc (b) in the agricultural area, and core Ic (c) retrieved from the industrial area.

Indeed, a study on a marine sediment core in front of the Lebanese shore dated back the maximum ^{137}Cs activity to 1987 (Azoury et al., 2013). Core Bc is composed of local atmospheric deposition, and eroded soil from the upper watershed which may explain the higher ^{137}Cs activity compared to core Ac. This could be also due to better preservation of ^{137}Cs in reservoir sediments (Ruiz-Fernández et al., 2007). The Cf/Cs model indicted that Bc core is younger than Ac core where the 70 cm depth of core Bc is dated back only to the year 1977. Evidently, core Bc is formed as a result to the dam construction in late 1950s, which is further indicated by the high sedimentation rate 2.22 cm/yr. Metal fluxes in core Bc were calculated for the whole column and presented in Figure 5.5b. Al, K, Mg, Si, Zn, Fe, and Mn fluxes decreased toward the surface (by 3, 2.3, 1.4, 2.5, 2.5, and 3 folds respectively), while Ca flux increased in the core Bc by 4 folds. However, Cu, Pb and Cd indicated a spike in their fluxes at 60-70 cm depth similar to ^{137}Cs behavior, which could be linked to the nuclear accident. Flux trends can be strongly associated to land-use changes and geomorphological alterations in the upper watershed, by which the constructed dam induces a rise in anthropogenic practices (Ruiz-Fernández et al., 2007). Calcium is originated from continuous crust erosion and effluents from quarries and rock cutting industries that are distributed widely in the watershed, which is reflected by the flux increase in Bc core unlike Ac core. However, the higher ^{210}Pb activity at the top layers of both studied cores can be related to dry deposition of building materials that have naturally occurring radioactivity (El samad et al., 2013). Noteworthy, building material industries are distant 2 km only from the core location. Furthermore, the high ^{210} Pb activity observed for core Ac at the top layer (Figure 5.4a) could be related to recent dry deposition of ^{210}Pb from the atmosphere (Pham et al., 2013) , hence core Ac was retrieved during a raining event in the wet season unlike core Bc that was collected in dry season. While trace elements such as Cu, Cd and Pb are originated from constant anthropogenic activities, reflected by their insignificant change regarding sedimentation rates. However the detected slight decrease mainly at the top core could be related to environmental management plans forced by ministry of environment (MoE), such as banning of leaded gasoline and some agrochemicals that are rich in trace elements, establishing waste water treatments plants, and closing numerous quarries (El Fadel et al., 2000; Kouzayha et al., 2013).

High sedimentation rate recorded by core Bc highlighted the risk of soil erosion from the upper agricultural basin by which soil tilling are majorly the result of increasing sedimentation rates (Matisoff et al., 2002). If the estimated sedimentation rate well presents the actual sedimentation rate taking place in the reservoir, we can assume that after 50 years the banks will be raised by 1 meter, thus decreasing the reservoir water capacity and increasing the area of flood plains (Newman et al., 2006).

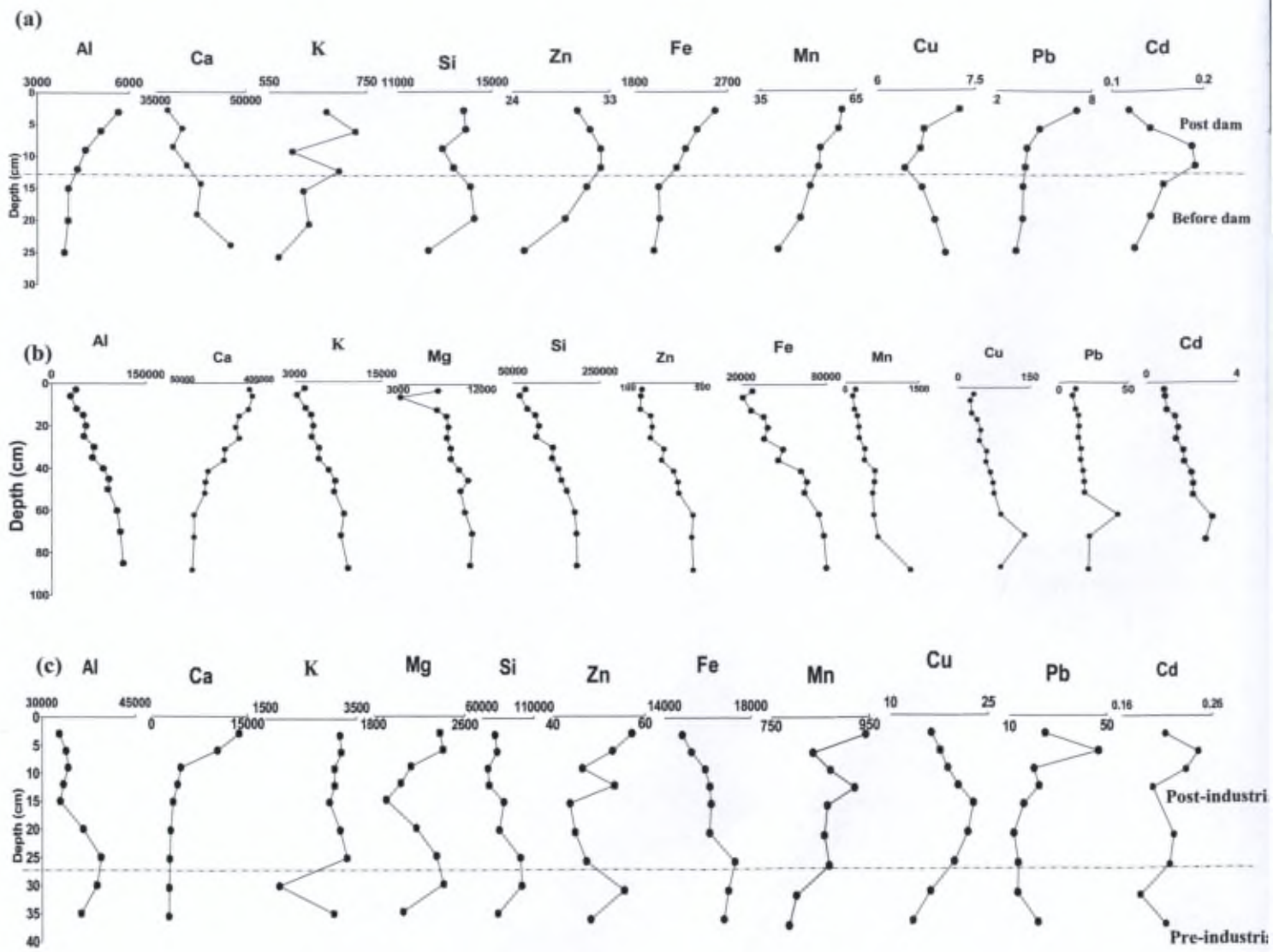

Figure 5.5: Metal fluxes in the core Ac (a), core Bc (b) collected from the agricultural watershed and in core Ic (c) collected from the industrial watershed.

5.3.2 Comparative analysis between agricultural and industrial watersheds

The PCA data between metals for core Ic[7] are presented in Table 5.3. A week and negative correlations were observed for metals in the industrial core which may indicate their allocthonous origin and multiple sources (Xia et al., 2012). However, significant correlation was observed between Al and Fe, Si, and Mg ($p < 0.05$), which could be due to the association of these metals with aluminum silicates. On the other hand, Pb shows a strong correlation with Ca and Cd which could be related to phosphate fertilizer wastes (phosphogypsum and phosphate rocks) (Ammar et al., 2013 (Chapter 3)). The highest radiogenic activity $^{210}Pb_{xs}$ was observed at 6 cm (38 mBq/g) and 9 cm (32 mBq/g) depths in the soil profile (Ic) retrieved near the industrial factory, then after radioactivity decreases with depth (Figure 5.4c). Anthropogenic ^{137}Cs activity resembles ^{210}Pb activity where the highest radioactivity is observed at 6 cm depth (25 mBq/g) and the lowest radioactivity was measured at 25 cm depth (1 mBq/g) (Figure 5.4c). Pb activity could be due to decaying chain of uranium naturally present in phosphate rocks and PG associated with the industrial process as described in Chapter 4 (Aoun et al., 2009; Ammar et al., submitted). The higher activity observed for ^{137}Cs in the top layers of the core could be due to post-deposition of ^{137}Cs fallout. ^{137}Cs radioactivity was documented in northern soil between 2 and 113 Bg/kg which is associated with atmospheric deposition after nuclear weapons testing in the 1960s succeeded by Chernobyl nuclear accident in 1986 (El Samad et al., 2013). The higher radiogenic activity of ^{137}Cs detected in core Ic (1-25 mBq/g) in the industrial area (Figure 5.4c) compared to that in core Ac (2-3 mBq/g) (Figure 5.4a) could be due to Lebanese topography and variant soil type and precipitation rates that can influence atmospheric deposition of ^{137}Cs from radioactive cloud resulting from the Chernobyl nuclear accident (El Samad et al., 2007). This further agrees with the previous findings that soil in the Lebanese Northern coast contain more ^{137}Cs compared to Bekaa soil (El Samad et al., 2007).

The measured radioactivity at 6 cm depth is dated back to 1999, while the date at 25 cm corresponds to the year 1949 (Figure 5.4c). Thus we can consider the top 25 cm of the core Ic as archives for postindustrial period (of Phosphate fertilizer factory). The sedimentation accumulation rate in the industrial soil core Ic (0.4608 g/cm/yr) is higher than the core Ac (0.1746 g/cm/yr). The northern coast exhibits more runoff potential due to land slope and soil type which is susceptible to more erodibility compared to the Bekaa region agricultural plain (Bou Kherir et al., 2006). As a consequence, the high sedimentation rate in the industrial area is associated with land-use, soil type, land topography and higher precipitation rates (Alemaw et al., 2013). Al and Fe metal fluxes indicated a decrease toward the surface in core Ic (Figure 5.5c). However, Ca and Mn fluxes increased toward the surface by 5 and 1.2 folds, respectively, while K flux indicated a constant increase after the industrial revolution in the1950s (Figure 5.5c). Mg, Si and Zn fluxes indicated a scattered trajectory by which a slight increase was observed in the top core layer (Figure 5.5c), the observed heterogeneous distribution of these metals may indicate their multiple sources (Clark et al., 2014). Pb and

[7] Metal content of core Ic are presented in Annex 3 (Table A3.1)

Cd fluxes indicated a scattered increase toward the surface and a sharp decrease (by 2 folds for Pb) was observed at the top layer which corresponds to the date of banned leaded gasoline usage in Lebanon in 2002 (El Fadel et al., 2000). In the contrary, Cu fluxes show two stages by which Cu flux increases by 1.7 fold from 35 cm depth to 15 cm depth, then decreases by 1.4 fold toward the surface which could be related to implementation of environmental management plans not only in Lebanon but also in Europe, since European pollution can reach the Lebanese coast (Azoury et al., 2013).

Pb is clearly derived from multiple sources in the two investigated watersheds, where the contribution of each potential anthropogenic endmember can be calculated according to equation 5.1 (Komárek et al., 2007, Monna et al., 1997):

$$X_s = \frac{\left[\frac{^{206}Pb}{^{207}Pb}\right]_s - \left[\frac{^{206}Pb}{^{207}Pb}\right]_{ref}}{\left[\frac{^{206}Pb}{^{207}Pb}\right]_{anthropogenic} - \left[\frac{^{206}Pb}{^{207}Pb}\right]_{ref}} \quad X \quad 100\% \qquad (5.1)$$

Where X_s is the % contribution of a particular anthropogenic source in the total Pb isotopic ratio of the studied sample, and $[^{206}Pb/^{207}Pb]_s$, $[^{206}Pb/^{207}Pb]_{ref.}$, $[^{206}Pb/^{207}Pb]_{anthropogenic}$ correspond respectively to the isotopic ratio of the sample, the natural background ($^{206}Pb/^{207}Pb$ PDAC=1.20), and the anthropogenic endmember. In the vicinity of the industrial factories, the leaded gasoline ($^{206}Pb/^{207}Pb = 1.11857$) isotopic ratio contribution (Östlund and Sternbeck, 2001) to the Pb isotopic ratio in core Ic increased with time from factories' establishment date (66.71%), to present (28.08%) (Figure 5.6a). Similarly, fertilizers ($^{206}Pb/^{207}Pb = 1.159$) (Wang et al., 2013) contribution increased from 22.12 to 55.77% after the factories' establishment (Figure 5.6a). Evidently the phosphate fertilizers factory is contaminating the local soil by dry deposition of fertilizers; moreover the traffic activity on the nearby highway is clearly reflected by the increased Pb contamination in the core. However in the agricultural area, isotopic ratios of universal Pb ores (1.19-1.25) (Bollhöfer and Rosman, 2001) highly contributed with the soil signature in core Bc during the dam establishment (83.3%) which may be referred to the construction period. Thereafter, it decreases down to 13.3% in the present as a result of banned leaded gasoline, and strict environmental limitations of Pb usage in industries. Eroded calcareous crust in the agricultural watershed represented by Ca flux (Figure 5.5b) can play as a dilution factor for anthropogenic Pb signatures (Ammar et al., submitted). This is further confirmed by the location of Bc core samples between the $^{206}Pb/^{207}Pb$ signatures of Pb ore and natural rock of silicates and carbonates (Figure 5.6b). While the top 20 cm of the industrial soil core (Ic) that pronounced the factory age is positioned between universal Pb ore, European Pb ore and coal, and oil of 20th century (Figure 5.6c), indicating the high industrial stress exerted on this area, in addition to traffic and atmospheric deposition.

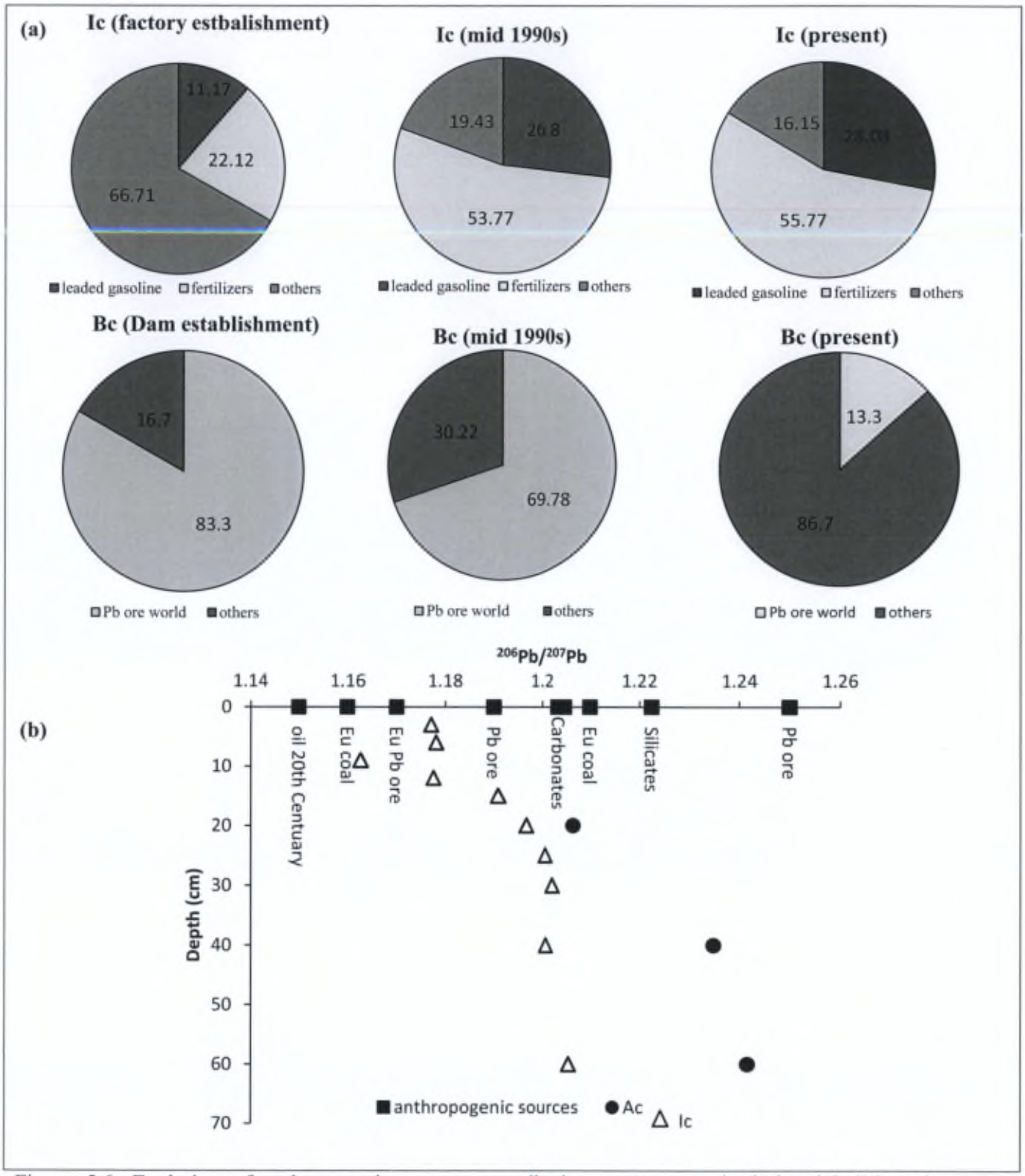

Figure 5.6: Evolution of anthropogenic sources contribution percentages in industrial (Ic) and agricultural (Bc) cores (a), and the $^{206}Pb/^{207}Pb$ distribution in regard to anthropogenic and natural sources.

Table 5.3: Pearson correlation coefficient between metals for soil core in industrial watershed (Ic).

Element	Al	Ca	K	Mg	Si	Zn	Fe	Mn	Cu	Pb	Cd
Al											
Ca	-.612*										
K	-.071	.179									
Mg	.568*	.260	.039								
Si	.580*	-.349	-.451	.364							
Zn	-.352	.555*	.116	.267	-.230						
Fe	.817**	-.809**	-.024	.158	.590*	-.431					
Mn	-.482	.401	.437	-.152	-.356	.498	-.493				
Cu	-.417	-.067	.243	-.484	-.091	-.098	-.173	.416			
Pb	-.610*	.719**	.146	.048	-.370	.442	-.653*	.137	-.061		
Cd	-.607*	.462	.392	-.205	-.464	.198	-.654*	.264	.336	.663*	

As a result, land use activity implication on metal behavior and fate in the two soil cores retrieved from the two contrasting watersheds (Figure 5.1) can be compared using metal enrichment factors as indicated in Figure 5.7. Metal enrichment factor was calculated to assess metal contamination magnitude and its potential hazard in each watershed by normalizing it to Al content according to equation 4.1 (Ruiz-Fernández et al., 2007; Clark et al., 2014).

$$EF = \frac{[M/Al]_{sample}}{[M/Al]_{ref}} \qquad (4.1)$$

Where M and Al stand for the concentration of metal M and Al, respectively, in the particulate phase; $[M/Al]_{sample}$ and $[M/Al]_{ref}$ denote the concentration ratio of M to Al, respectively, in the sample and in a reference material representative of the natural background of the studied area. The reference level relies on the measured values in the deepest layer of the studied core that can be considered as the local natural background which are presented in Table 5.4 (Renberg, 2002).

Natural enrichment ratios were observed for Al, Mg, Si, Fe, and Mn for both cores with slightly higher ratios for Al, Mg, and Mn indicated for core Ic (data not shown). However, the magnitude of metal fluxes in the industrial area (Figure 5.5c) are greater than those of agricultural soil core Ac (Figure 5.5a). Moderate enrichment (> 2) was observed for Ca in the top 10 cm of core Ic and in core Ac with more significant enrichment detected at 30 cm depth

* correlation is significant at 5%
** correlation is significant at 1%

and higher flux (Figure 5.5a, 5.7b). Industrial core Ic indicate an enrichment in K and a higher flux (Figure 5.7c, 5.5c) compared to core Ac that shows a moderate enrichment in Zn at 30 cm depth (data not shown). However Pb represents a significant enrichment in the top soil layer (6 cm) in the industrial soil up to 4.5 then decreases to <2 down the core Ic. Where Pb enrichment ranges between 3.7 and 2.4 in the top 30 cm depth of core Ac (Figure 5.7d). Both Cd and Cu show slight enrichment in both cores where more enrichment was observed for Ac at 30 cm depth for both Cd (Figure 5.7e) and Cu (Figure 5.7f). In the industrial core Ic, higher Cu, Pb and Cd fluxes (Figure 5.5c) were observed compared to core Ac (Figure 5.5a). The higher metal fluxes in the industrial soil are associated with intense industrial activities due to the fertilizer factory, higher rates of vehicles activity, and atmospheric deposition. The Mediterranean coast receives higher rates of atmospheric deposition compared to the continental valley (El Samad et al., 2007). Louri˜no-Cabana et al., (2011) observed a high enrichment factor for certain metals at a specific depth, so they related this enrichment to specific industrial incidence during the industrial revolution. Similarly, the spike of metal enrichment (Ca, K, Zn, Fe, Pb, Cd, and Cu) at 30 cm depth of the soil core taken from agricultural area (Ac) is referred to the period before 1860s that was denoted by Ottoman Empire era. The industrial incidence was represented by establishing of a train railway from Beirut to Syria passing through the Bekaa, that was later removed out of service during the civil war (Bernier, 2010), where the increased coal combustion and military activities increased the metal content in soil.

The contribution coefficient of anthropogenic signatures and the distribution of samples between potential polluting sources, suggest that the coastal industrial area is under the influence of the industrial factory, traffic and atmospheric deposition from allocthonous pollution sources. While in the agricultural area, Pb contamination is originating from different Pb sources and its corresponding fluxes are sensitive to land use changes.

Table 5.4: Coordinates of the retrieved cores and the reference value (at 70 cm depth) used for normalization for each metal

Sample	coordinates		Depth	Ref Al	Ref Ca	Ref K	Ref Mg	Ref Si	Ref Zn	Ref Fe	Ref Mn	Ref Cu	Ref Pb	Ref Cd
Industrial soil core	34.280264°N	35.659654°E	70 cm	8.05 %	0.83%	0.3%	0.4%	18.6%	86.6 ppm	3.4 %	1585.8 ppm	33.9 ppm	27.2 ppm	0.38 ppm
Agricultural soil core	33.331601°N	35.421696°E	70 cm	2.8 %	20.6%	0.4%	1.1%	10.2%	132.2 ppm	1.4 %	342.8 ppm	35.2 ppm	9.6 ppm	0.72 ppm

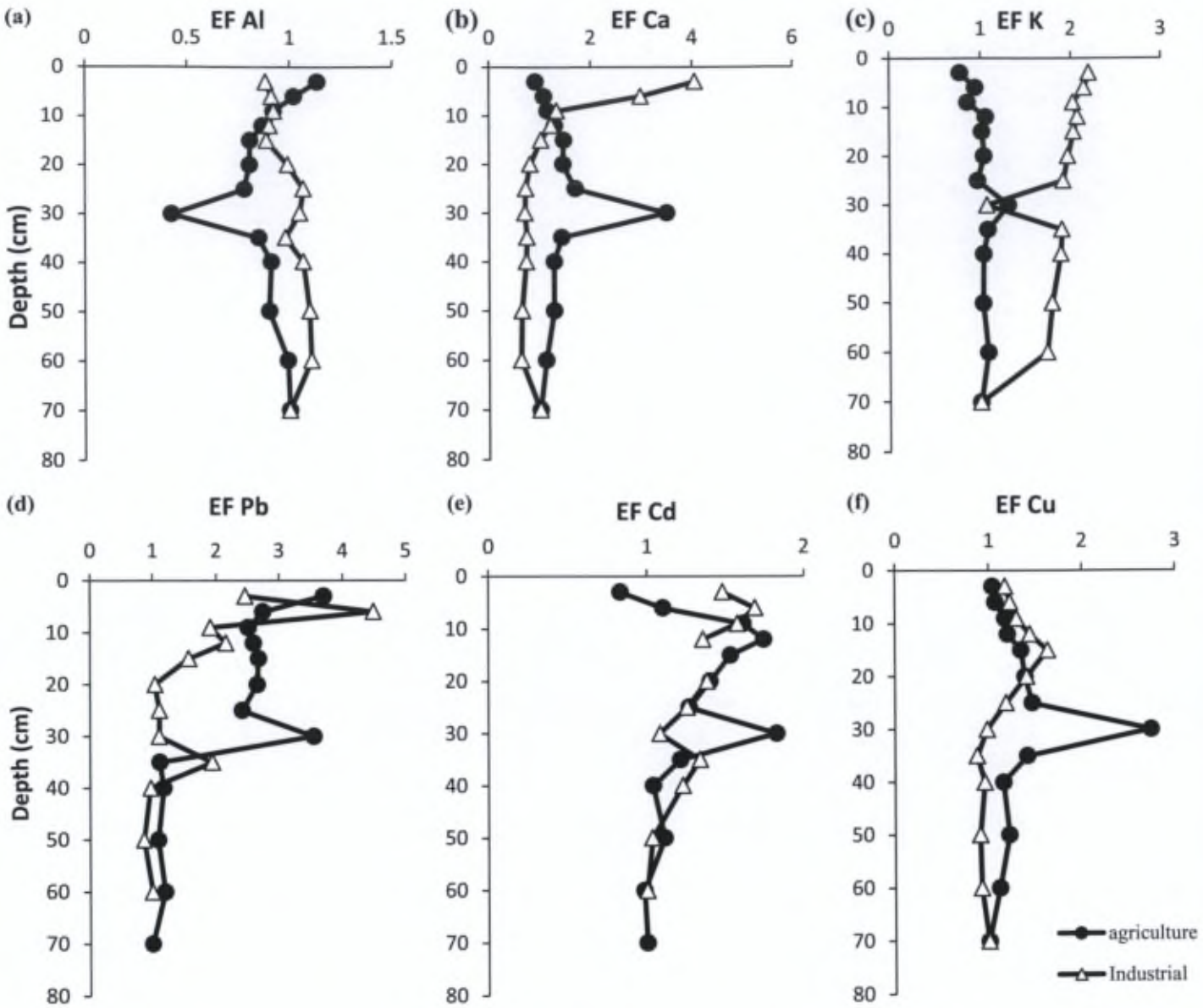

Figure 5.7: Enrichment factor profiles for metals in soil cores retrieved from industrial (Ic) and agricultural (Ac) watersheds.

5.3.3 Factors that control metal behavior in soil

5.3.3.1 Soil characterization

Nutrients and metal adsorption to particulate phase are controlled by multiple factors such as pH, temperature, EC, redox state, sediment texture, cation exchange capacity (CEC), contamination magnitude, and organic matter content (Greenwood and Kendall, 1999; Mortimer and Raeà, 2000; Hiller et al., 2010). As a consequence, it is very important to investigate the physiochemical characteristics of the soils in packed columns tests to understand metal behavior.

The physical and chemical properties of the two soils used in the packed columns are summarized in Table 5.5. The pH of both industrial and agricultural soils is slightly basic, reflecting the calcareous soil type that possess negative charge (ΔpH= -0.4) (INRA, 1995). Measured EC of industrial and agricultural soils showed moderate and weak conductivities, respectively, however the measured EC upon saturation extract and TDS are very high for both thus reflecting high salinity content (NF ISO 11265). Higher values of TDS and EC observed for industrial soil (3.2 ppm) are due to sea spray since this site is located a few tens of meters from the sea shore (Gomes et al., 2003). Bulk and particle density of industrial soil lies in the average range of soils (1.28-2.22 g/cm^3), whereas that of the agricultural soil indicates either high content of OM or clayey soil (0.97 - 1.92 g/cm^3) (Thien and Graveel, 2003). The two soils show high porosity, but when comparing the relatively high values of porosity and solid space of agricultural soil (49.51 – 50.48% respectively), inadequacy of large pores and high water retention capacity can be concluded (Luo et al., 2010). A rich content of organic matter and carbon is found in agricultural soil (OM 14.18 - OC 8.22%), while those of industrial soil (OM 4.69 - OC 2.72) are medium, but both values of OM estimate a high content of clay (>30%) according to AFNOR X 31-109. Referring to active and total calcareous percentages, agricultural soil is more alkaline compared to the slight calcareous industrial soil (AFNOR X 31-106). The content of Na^+ and K^+ indicates that the two soils have very low cations content (P05-001A). The high negativity of ζ-potential (I: -88.79 mV and A: -76.63 mV) of both soils point out excellent stability and strong repulsion forces between the colloids; thus they rarely dissociate and flocculate (Greenwood and Kendall, 1999). Furthermore, the CEC of the agricultural soil is very high (30.67 cmol/kg) compared to the industrial soil (26.46 cmol/kg) (Pleysier and Jou, 1980). Regarding the soil texture, industrial soil is sandy clay loam since it possesses higher percentage of soil fraction and agricultural soil is of clay loam type (Table 5.5), which is further confirmed by the finer grain size of the agricultural soil (70% of soil < 63 μm) compared to the industrial soil (55% of soil < 63 μm) (Figure 5.8a). In addition, few visual inspections of the soils were done. The red to brown color of the industrial soil indicates good aeration, while the gray color of the Qaraoun soil reveals poor aeration (Thien and Graveel, 2003). Agricultural soil possesses higher amounts of clay, and thus is able to hold water (Θg) approximately 50% of its mass, while that of industrial soil is able to hold only 27.67% (Table 5.5). Correspondingly, organic composition obtained by IR spectroscopy for soils (Figure 5.8b) reflects various functionalities. The agricultural soils exhibit intense peaks corresponding to abundant O-H,

C=C, and C-O stretches compared to the industrial soils which contain organic compounds such as aldehydes, alkenes and carboxylic acids. X-ray diffraction analysis shows different soil mineralogy in both watersheds. Quartz is the dominant mineral in the industrial soil samples; in contrast, calcites and montmorillonites are the prevailing phases of the agricultural soil (Figure 5.8c). Therefore, the agricultural soil has a possibility of poor internal drainage and high metal retention ability due to fine clay soil texture (Pathak, et al., 2004; Bou Kheir et al., 2006). In addition, the mean metal content values in the initial soil (blanks) of the industrial area for Zn, Cd, and Pb are 128.1, 0.72, and 27.9 ppm respectively, while those for agricultural soil were 96.6, 0.74, and 32.2 ppm respectively.

Table 5.5: Physicochemical parameters for soil used in the Leaching columns experiment from both watersheds.

Soil Parameters	**Soil from Industrial Area**		**Soil from Agricultural Area**	
	Value	**Significance**	**Value**	**Significance**
pH	7.5	Slightly basic	7.7	Basic
pH(KCl)	7.1	Slightly basic	7.28	Slightly basic
Salt Effect (ΔpH)	-0.4	Net negative charge of soil	-0.42	Net negative charge of soil
EC (mS/cm)	0.5	Moderate	0.275	Weak
Saturated EC (mS/cm)	3.2	Very high	1.76	Very high
TDS (ppm)	3.2	Very high	1.76	Very high
Bulk ρ (g/cm^3)	1.28	Average for soils	0.97	Rich in OM and clay
Particleρ (g/cm^3)	2.22		1.92	
Porosity %	42.3	High porosity	49.51	High porosity
Solid space %	57.69	-	50.48	Low amount of large pores
OM %	4.69	Medium	14.18	Rich
OC %	2.72		8.22	
Active Calcareous %	1.18	Weak	2.81	Weak
Total Calcareous %	1.38	Weak (slightly calcareous)	31.07	High (very calcareous)
Cations (ppm)	Na^+ 23 K^+ 28.6	Very low	Na^+ 21.6 K^+ 57.6	Very low
ζ-potential (mV)	-88.79	Excellent stability	-76.63	Excellent stability
CEC (cmol/Kg)	26.46	High	30.67	Very high
50% of population < (μm)	51.471	Lesser small-sized particles	39.234	More small-sized particles
Texture	55.31% sand 12.5 % silt 32.18% clay	Sandy clay loam	39.06% sand 26.25% silt 34.68% clay	Clay loam
whc ($height_{water}$ /$height_{soil}$)	13.1/36		18.75/36	
Θ_v (%)	36.40		48.20	
Θ_g (%)	27.67		48.54	

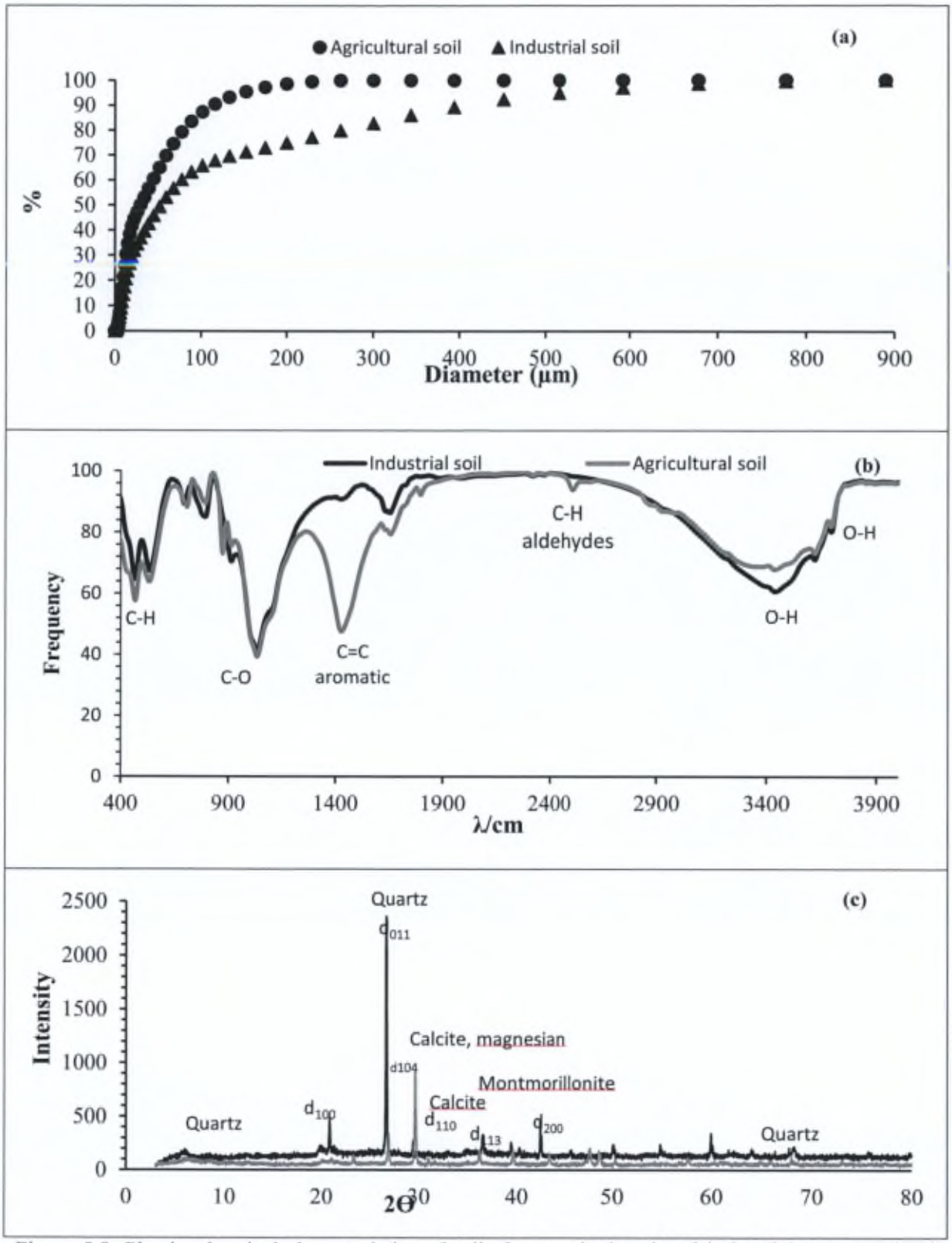

Figure 5.8: Physicochemical characteristics of soils from agricultural and industrial areas, grain size (a), functional groups (b) and mineralogy (c).

5.3.3.2 Leaching columns experiment

The leaching trends in all columns (Figures 5.9, 5.10) follow a decreasing trajectory by which the first flush or leaching event mostly carries along the soluble fraction of the ions (Mclean

and Bledsoe, 1992), and it may contain the highest concentrations of the leachate ions. Sodium content of the leachates from industrial packed columns (Ip) (Figure 5.9a, 5.9b) showed a peak at the fourth leaching event (after 20 days of incubation). Since Na in the blanks behaves in the same manner as in the spiked columns after 20 days of incubation, the explanation of Na^+ mobility could be only referred to the impact of artificial raining. Sodium has slow infiltration rates in soil, and may form insoluble complexes with other ions in the matrix such as Ca, Mg, and K, however under more alkaline conditions Na could be leached from the soil (Hodges, 2010). Thus due to increasing volumes of continuous artificial rain during the treatment period, sodium leachates reaches its peak at the 20th and followed by the 30th day of incubation in the industrial soil columns. Soil columns spiked with NPK and PG show an increased Na^+ mobility compared to the blanks. Gypsum application is recommended to extract sodium from soils with sodium excess, by which the free Ca ions liberated from PG dissolution will replace Na causing its leaching (Hodges, 2010). The first raining event flushes out most of Cl^- from Ip column (Figure 5.9c, 5.9d). Where the Cl^- content in the blank's leachate (1016.6 ppm) exceeds the leachates from columns spiked by fertilizers (839 ppm) and those spiked by PG 1x (736.6 ppm) and 2x (579.3 ppm), respectively. The negatively charged Cl^- ion is repelled from the soil and leached with the first water contact (Hodges, 2010). Potassium content in Ip columns indicates the highest leachability at the first flush in the blanks (159 ppm), followed by columns spiked with NPK 1x (92 ppm), NPK 2x (56.2 ppm), PG 1x (42.5 ppm), and PG 2x (28.7 ppm), respectively. However, after the second leaching event in both sets of columns, potassium content was quasi-stable. Potassium competes with bivalent ions like Ca^{2+} and Mg^{2+} for soil negative sites, thus explaining most quantified potassium ions in the leachates of the blank columns in calcareous soil blanks (Hodges, 2010). However, K^+ was subjected to complexation with anions released from NPK and PG, thus retarding its mobility in those spiked columns. Nitrate was detected only in leachates of the blanks and for the first leaching event in the column spiked with NPK 1x (Figure 5.9g); this could be a result of ammonia assimilation by soil micro flora, and when water passes through the negatively charged soil, the NO_3^{2-} anion was readily repelled with the leachates (Hodges, 2010). Sulfate was only detected in the leachates from the industrial soil (Figure 5.9h, and 5.9i). The columns spiked with PG 2x flushed the highest concentration of sulfate (2710 ppm), followed by the blanks and the columns spiked with fertilizers. Hence the PG ($CaSO_4.0.5H_2$) has high solubility and SO_4^{2-} will dissociate and be readily released from the columns spiked with PG. Moreover, industrial soil may receive sulfates residues produced during the manufacturing process by which phosphate rocks are treated with sulfuric acid, and leachate form PG stockpiles (Ammar et al., 2013). The same explanation for sulfates could be used for fluoride behavior that was only liberated from the columns at the 6th and 9th leaching events. The retarded leaching of ions in columns spiked with PG can be explained by calcium ions release from PG that will form aggregates with soil particles thus decreasing the porosity and as a consequence water permeability (Jaakala et al., 2012). Moreover PG crystals are able to grow by complexing available ions as shown in Chapter 3, thus limiting their mobility in the soil column (Ammar et al., 2013).

Sodium content of the leachates from agricultural packed soil columns (Ap) showed a direct increase of the cation content after the first flush, and the maximum values were reached for blank, NPK 1x, and NPK 2x, at the second leaching event (Figure 5.10a). While for columns spiked with PG 1x and 2x, the maximum values were reached at the third leaching event (1 week of incubation) according to the treatment (Figure 5.10b). The sodium behavior in the Ap blank columns can be explained by the high calcareous agricultural soil type that contain more Ca^{2+} ions (Table 5.5), which will cause faster Na^{+} liberation compared to the Ip columns (Hodges, 2010). PG dissolution may liberate ions that will form complexes with Na^{+} in the soil thus retarding its release until the third leaching event (Figure 5.10a). Chloride content was the highest in the blank (2521.3 ppm) after the first flush, followed by columns spiked with PG and the lowest concentration was observed in the columns treated with NPK fertilizers (51.7 ppm) (Figure 5.10e, and 5.10f). The high Cl^{-} content in the soil blanks from the agricultural area could reflect land-use activities where irrigation and waste water effluents from the watershed (Shaban and Nassif, 2007) are able to increase chloride content in the soil. The fertilizers application in the agricultural soil could form complexes with chloride ions prohibiting its leaching. The same phenomenon could also be observed in the leached potassium ions of the agricultural soil (Figure 5.10e, and 5.10f), where potassium is highly leached in the blank column (62.5 ppm), followed by PG (52.5 ppm) and NPK (32.5-42.5 ppm) treated soils for the first flush and the same trend was repeated in the successive leaching events in the same order. The similar behavior of Na^{+}, K^{+} and Cl^{-} in the agricultural packed columns spiked with NPK fertilizers suggested their complexation in the soil that has high cation exchange capacity and clay content (Table 5.5). Furthermore, they can form salts (KCl or NaCl) thus increasing soil salinity (Hodges, 2010). Nitrate was readily leached in the blank column (397 ppm) after the first flush, followed by columns spiked by PG 1x and 2x (252.3-263.7 ppm) respectively (Figure 5.10g). However the lowest concentration of nitrate was observed in the leachates of columns treated with NPK fertilizers 2x (115 ppm) and 1x (97.3 ppm) and it decreased with continuous leaching (Figure 5.10h). The agricultural soil could be enriched by nitrates due to anthropogenic effluents from intensive agricultural practices and waste effluents from domestic households and nearby industries. This observation agrees with a previous study that indicated nitrate contamination at the eastern side of the reservoir where the agricultural soil was collected (Shaban and Nassif, 2007).

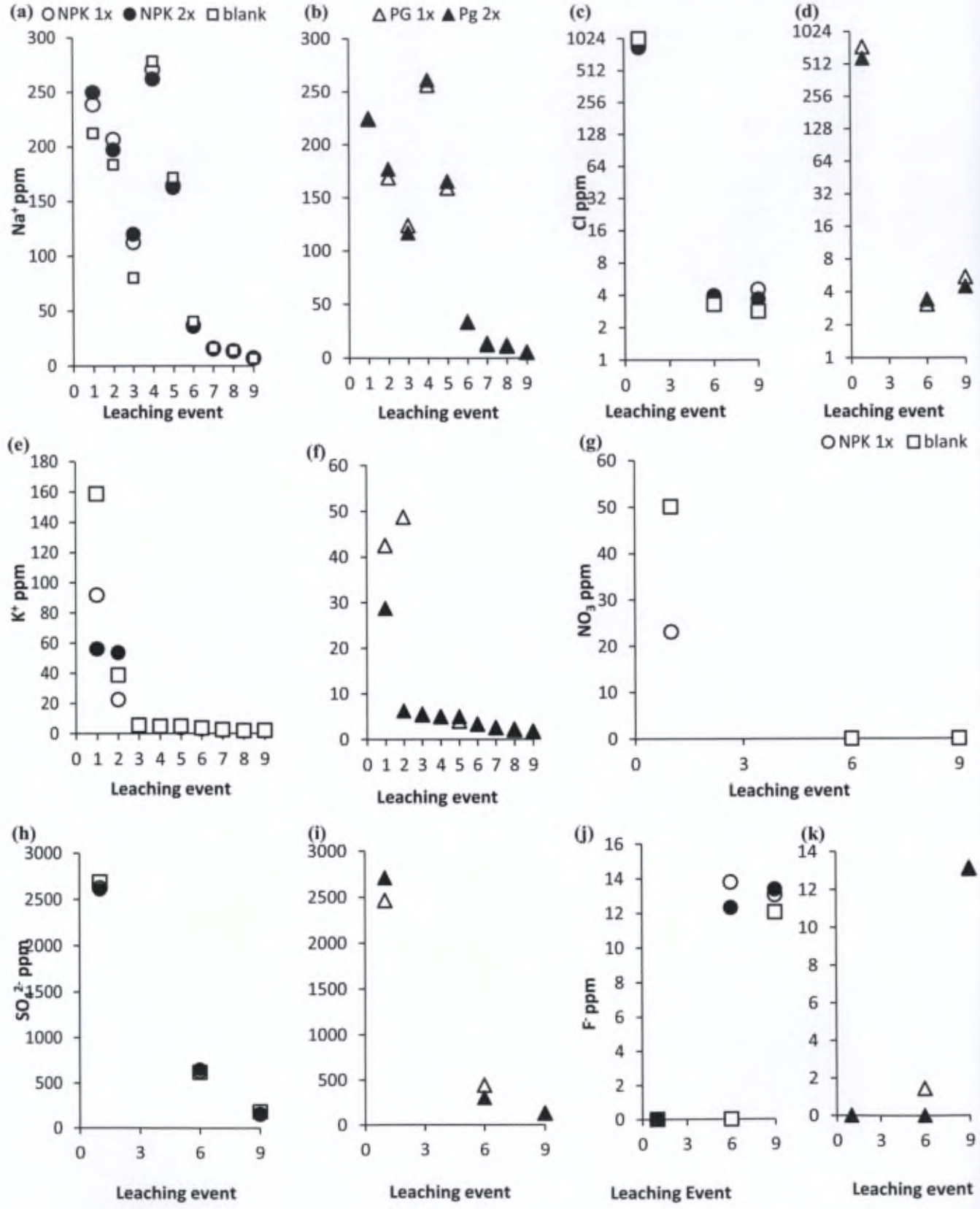

Figure 5.9: Cations and anions concentration in the leachates of soil packed columns of industrial soil (Ip).

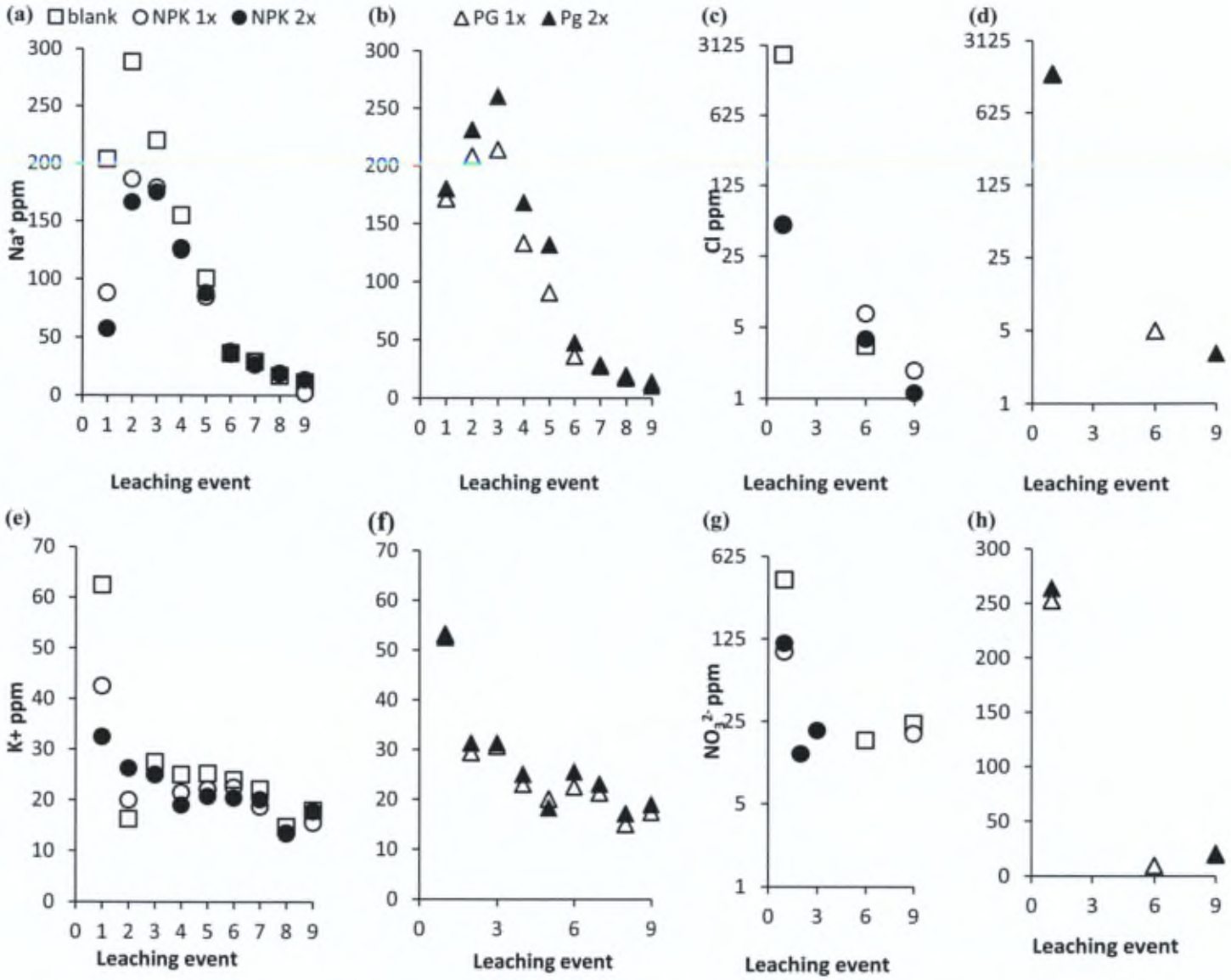

Figure 5.10: Cations and anions concentration in the leachates of soil packed columns of agricultural soil (Ap).

Cadmium mobility in the packed soil columns from both watersheds was investigated. In the packed columns of soils collected from the industrial site, the highest Cd concentration was observed in the column spiked with NPK 1x leachates (0.12 ppm) at the 4th leaching event after 2 weeks of incubation (Figure 5.11a). Correspondingly, residual Cd in the packed columns (Figure 5.11c) indicated the lowest concentration in the column spiked by NPK 1x and the highest residual concentration detected in the top 2 cm of the column spiked with PG 2x. We showed in Chapter 3 that Cd is irreversibly mobilized to the aquatic medium and accumulate in the soil when PG is added (Ammar et al., 2013). Furthermore, a study on red Mediterranean soil indicated the fast Cd mobility after PG amendment compared to Pb

(Kassir et al., 2012c). On the contrary, the agricultural blank column readily flushes Cd (0.33 ppm) that decreases with the successive leaching events (Figure 5.11d), followed by columns spiked by PG 1x (0.11 ppm), and PG 2x (0.04 ppm), respectively (Figure 5.10e). The Cd content in the blank columns of Ap columns exceeds that in Ip columns, which is more bioavailable that may be derived from agrochemical applications in the watershed. The Cd mobility in columns spiked with PG could be induced by the presence of more organic matter ligands in the agricultural soil (Table 5.5). The behavior of Cd in both industrial and agricultural soils spiked with PG indicates a distinct trend (Figure 5.11b, and 5.11e), by which Cd concentration in the leachates increases slightly after the 6^{th} leaching event suggesting an increased mobility due to alteration in metal bearing phase to more labile fractions (associated to organic matter or sulfates) in addition to continuous watering (Kassir et al., 2012c). However, Cd content in the leachates of agricultural soil spiked with fertilizers shows very low concentrations during the whole incubation period (Figure 5.11d). This behavior was further confirmed in the particulate Cd content in the columns spiked with NPK fertilizers that exhibits the highest concentration (Figure 5.10f). While the soil columns spiked with PG 2x exhibits the lowest Cd content thus inducing its mobility. Columns of industrial soil spiked with NPK 2x exhibits the highest recorded particulate Pb content on the top surface of the treated columns then declines with depth from 117 to 45 ppm (Figure 5.11g). However the lowest Pb content was observed for the Ip column spiked with PG 2x (Figure 5.11g). Similarly, Pb behaves in the same manner in agricultural soil columns where NPK treated columns exhibits higher Pb content compared to PG treated ones (Figure 5.11h). In agreement with our recent study (Chapter 3), by which Pb mobility to the aquatic phase increases with increasing PG mass load (Ammar et al., 2013). Application of fertilizers increases metal content of Cd and Pb in red Mediterranean soil (Kassir et al., 2012b), where nitrogen fertilizers have an important influence on metal leaching and speciation in soils (Zhao et al., 2009). Cd in the agricultural soil column (Figure 5.11f) shows a higher concentration than in the industrial soil (Figure 5.11c) after NPK fertilizer application; in contrast, particulate Pb content in the Ip columns (Figure 5.11g) spiked with NPK indicates a higher concentration compared to the Ap columns (Figure 5.11h).

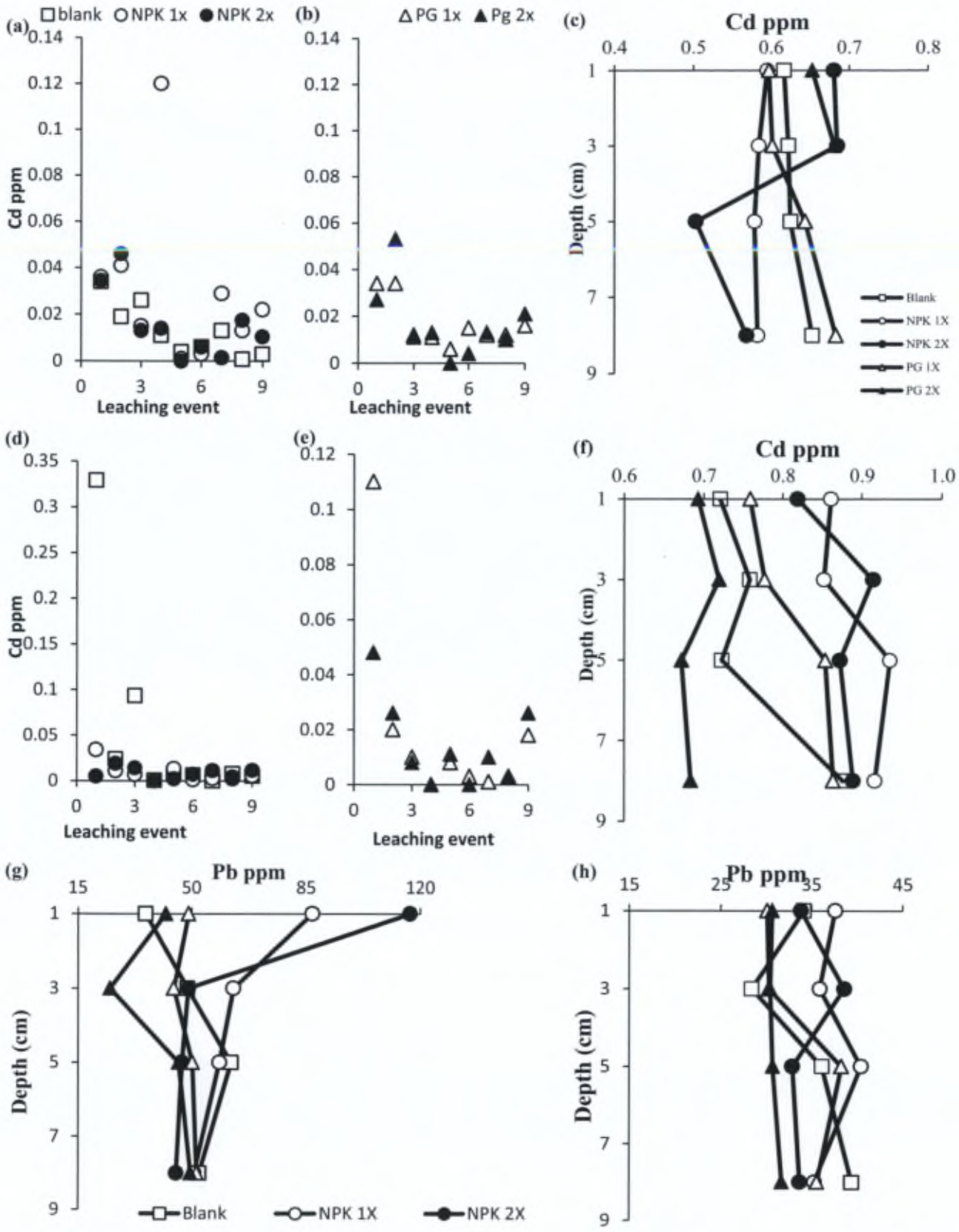

Figure 5.11: Cd concentration in the leachates and the residual content in the top 10 cm of the packed soil columns of industrial soil (a, b,c) and agricultural packed columns (c,d,e); and the Pb behavior in the packed soil columns in industrial soil (g) and agricultural soil (h).

Land use activity could affect soil composition by which soil collected from the industrial area contained sulfides and fluorides but insignificant amounts of nitrate. The contrast is true for the soil collected from the agricultural area. Most of the studied elements indicate higher mobility in industrial soil compared to agricultural soil and this could be referred to the soil physiochemical characteristics. The synergetic effect of higher clay and organic matter content, higher cation exchange capacity, and finer grain size of the agricultural soil will induce higher affinity, and thus possess higher retention potentials (Alvarez, 2007, Balkis et al., 2010). As a result, pollutants will accumulate in agricultural soil and will have higher tendency to bioaccumulate in the food chain, and the fine fraction could be mechanically transport to open water bodies. This can further explain the behavior of Pb and Cd in the undisturbed soil in core Ac, where their enrichment extent in the soil is deeper compared to core Ic (Figure 5.7d, and 5.7e). While groundwater in the industrial area is under the risk of contamination, due to higher soil permeability of the sandy clay loam. Furthermore, the subsurface flow which is a common hydrological feature in the Lebanese coast where water percolates to the Mediterranean sea as a subsurface flow (Awad and Darwich, 2009), could be enriched by metals leached from PG stockpiles when subsurface flows crosses under the waste stockpiles near the factory and possess contaminated plumes to the Mediterranean Sea. Additionally, this agrees with our recent finding of enriched coastal sediment sub-layers by Pb compared to the top layer explained in Chapter 4 (Ammar et al., submitted). Type of contaminate and dose have different behaviors on each soil type, by which NPK fertilizers increased soil salinity in agricultural soil unlike PG. Thus treated PG could be used as a soil amendment in agricultural plain instead of fertilizers for later fertilizers application phases to prevent soil salinity, and in order to achieve sustainable agricultural production. Metals such as Zn and Cu that have similar behavior to Pb (Ammar et al., 2013), will be a potential hazard in PG stockpiles leachates that will contaminate both groundwater and the Mediterranean Sea. Since their mobility in industrial soil will be enhanced upon addition of PG in increasing mass content (Figure 5.11g). In addition to the permeable soil type in the industrial area (Table 5.5) that will facilitate metal leachability. Particular care should be given to areas subjected to heavy rain, since precipitation show an increase in chemical mobility thus increasing their hazardous on the receiving environment.

5.4 Conclusion

Reservoir active hydrodynamics shift redox conditions thus altering metals behavior and increase metal lability during fill hydrological mode. In the agricultural watershed, metals are derived from soil erosion and intensive agricultural activities (mainly for Cu and Cd) in addition to several industrial practices by which metals are associated with organic matter and Fe/Mn oxides. However, Pb has multi-sources in the agricultural watershed, including industrial sources from plastic, paper and paints manufacturing, agrochemicals, vehicle emissions, and atmospheric deposition. Dam establishment induces a geomorphological change in the upper basin thus increases metal contamination and fluxes. Sediments show a better preservation mechanism of historical time line of the watershed ecology compared to soil. Furthermore, the modern core retrieved from reservoir banks, indicates a high sensitivity to watershed changes by which recent environmental management plans were positively reflected on metal fluxes. Sediments risk assessment plans should be firmed up in the agricultural watershed to limit sedimentation rates that decreases the reservoir water capacity and increasing the area of flood plains. Evidently the phosphate fertilizers factory is contaminating the local soil by dry deposition of fertilizers; moreover, the vehicular activity on the nearby highway and atmospheric deposition contribute greatly to soil pollution. The potential cumulative damage of the fertilizer factory threatens the soil, gorundwater, and sea in Al Jouz basin. Land use, precipitation, land topography, intrinsic soil properties, pollutant type and magnitude are important factors that control metal fate in the environment. Thus of all these factors should be taken into consideration to achieve effective pollution management plans.

Evidently the dam construction alters the geomorphological practices in the upper watershed, thus amplified contaminants load are arriving to the reservoir in the form of suspended matter. Then after, seasonal and annual dam hydrodynamics has a great impact on sedimentation rate and on metal mobility either in depth or its transport to the open water of the reservoir or to the ultimate groundwater. The changing of water level in the reservoir induces a redox shift at the water-sediment interface which in its role will influence metal behavior. Evaluation of chemical loads entering to the reservoir must be documented and further characterized in the water column spatially and seasonally. For our knowledge the influence of the active hydrodynamic dam on pollutants partitioning between the water column and at the water-sediment interface was not identified previously in Qaraaoun reservoir. Thus exploring the biogeochemical cycles of potential contaminants and relating it to the hydrological setting of the reservoir is an utmost necessity to evaluate dam functioning and its influence on the watershed scale. Nutrient transport and its fate under variant environmental conditions can assess the risk of sediments, and evaluate the actual environmental situation of the dam. The environmental significance is located in the water quality withdrawn from the reservoir bottom layer used for crop irrigation and hydropower production. Therefore the evolution of water quality in the reservoir must be examined and it is essential to identify the role of the contributing factors. In the previous chapter, it was shown that the modern sediments accumulated as a result of dam establishment indicate a high sensitivity to the socio-economical practices in the upper watershed. Thus the interaction of the reservoir with the upper basin and the extent of the hydrological connectivity must be explored. Investigating the respond of reservoir to seasonal fluxes that is associated with human life style and hydrometeorological aspects is of great interest to understand hydrogeochemical processes that are taking place. Surface ground water interaction is an important concern for environmentalist and governmental stakeholder. Thus, characterizing the groundwater, and testing the possibility of groundwater recharge by the reservoir can be achieved by environmental isotopic applications. Multi analytical approaches must be utilized including classical measurements, limnology, elemental analysis, characterization and isotopic application to attain overall interpretation of the study. This in its role will aid in implementing regulations to sustain hydropower projects and sediments risk assessment plans.

Chapter 6

Reservoir sediments: A sink or source of chemicals at the surface water-groundwater interface

Abstract [8]

This study delineates the physical, chemical, and biological effects resulting from anthropogenic and endogenic activities in a sensitive dammed reservoir situated in a semi-arid region. The reservoir is characterized by two major flow regimes: a wet fill hydrologic regime and a dry spill one. A seasonal sampling campaign was carried out over a period of two years (2011-2013) where water samples were collected across the water column and from piezometers just outside the perimeter of the reservoir. Similarly, sediments were collected from the corresponding areas beneath the water column. The water samples were analyzed for environmental isotopic ratios, elemental composition, physical, biological and chemical parameters, whereas the sediment and algal samples were subjected to physical, mineralogical, spectroscopic, and microscopic analyses. This investigation indicated that the dam had resulted in the alteration of the biogeochemical cycle of nutrients as well as the degradation of the sediment and water quality. The hydrological and biogeochemical processes were found to induce vertical downward transport of chemicals towards the fine grained calcareous sediments during the fill mode, whereas the sediments acted as a source of a chemical flux upward through the water column and downward towards the groundwater during the spill mode. The geomorphological characteristics of the reservoir enhanced the strong hydrological connectivity between the surface water and the groundwater where the reservoir responded quickly to natural and anthropogenic changes in the upper watershed. The water and sediments in the sensitive spill mode were of poor quality and should receive more attention due to the potential hazard for the associated hydro-project and the sustainability of the agricultural soil in the long term. Thus a safe water and sediment management plan should be implemented in order to improve the dam functionality and to safeguard the precious water resources.

[8] Adapted from the submitted article (Ammar R, Kazpard V, Wazne M, El Samrani AG, Amacha N, Saad Z, Chou L. Reservoir sediments: A sink or source of chemicals at the surface water-groundwater interface. Submitted to Journal of Environmental Monitoring and Assessment; EMAS-S-14-01467).

6.1 Introduction

Dams are major tools for water management where they are used for irrigation and hydropower production. They also contribute significantly to the industrial activity and socio-economic development (Wei et al., 2009; Delsontro et al., 2010, Wildi, 2010). However, the environmental cost of dam constructions manifests in the modification of the hydrological regime, alteration of the biogeochemical cycles, and degradation of both sediment and groundwater quality. The degradation results from the accumulation of chemical contaminants in the sediments and the potential leaching of the contaminants to groundwater due to the long residence time of water (Wei et al., 2009, Wildi, 2010, Akin et al., 2010, Mikac et al., 2011, Kraus et al., 2011, Yang et al., 2012). Reservoirs are considered as a transitional zone between rivers and lakes. They reveal complex hydrodynamics and shorter water residence times as compared to lakes (Wall et al., 2005). They also have higher water temperature as compared to rivers, which could result in a decrease in the level of dissolved oxygen thus reducing the rate of decomposition of pollutants and potentially enhancing the hazard of these pollutants in the aquatic system (Wei et al., 2009). The increase in the concentration of nutrients in reservoirs during flushing events could induce high primary production leading to reservoir eutrophication. As a consequence, the nutrient biogeochemical cycle will be altered (He et al., 2008, Wildi, 2010, Yuan et al., 2011).

The fate of chemicals in lacustrine systems is dependent on their transport mechanism, solute mixing and redox environment (Peretyazhko et al., 2005). Despite the fact that some chemicals, mainly metals, are essential for growth, they are able to denature cell proteins therefore increasing their hazards for living organisms (Balkis et al., 2010). However, binding of these metals with organic matter and minerals, mainly clay, can minimize their toxicity (Gadd and Griffiths, 1987). Blais and Kalff (1993) classified the reactions being able to remove elements from aquatic systems into two categories, adsorption reactions (cation/ligand exchange) and precipitation reaction (with oxides, and carbonates). Korfali and Davies (2004) reported that limestone lining had the capacity of buffering pollutant concentrations in aquatic systems. Heavy metals could partition between dissolved phases in the water column and solid phases in the suspended matter and entrapped in the sediments (Korfali and Davies, 2004). Delfino (1976) described the lack of attention to sediments in environmental studies and their impact on aquatic systems in the past as out of sight-out of mind (Delfino, 1976). However, researchers have recently intensified their efforts to develop innovative approaches to understand the implications of sediment contamination. Sediments reflect the varied land-use of the watershed and act as historical archives of land-use alteration and geomorphological changes (Miller et al., 2003, Tuna et al., 2007, Balogh et al., 2010, Mikac et al., 2011). Thus in order to trace contaminants and their fate in the aquatic environment, scientists rely on sediments as a tool to document their chemical behavior under different aquatic conditions (Duman et al., 2007, Alaoui et al., 2010, Yuan et al., 2011).

Sediments represent a potential reservoir for contaminants brought in by rivers, surface runoff and atmospheric deposition (Callender and Rice, 2000, Roussiez et al., 2006, Yuan et al., 2007). Thus, lake bottom-sediments act as sink for contaminants derived from the upper

watershed in the form of suspended matter (Skoulikidis et al., 2008, Hiller et al., 2010, Akin et al., 2010). Nutrient retention and metal adsorption to sediments are controlled by various factors such as pH, temperature, redox state, sediment texture, and organic matter content. Any change in these factors, could release the sorbed chemicals to the water system (Hiller et al., 2010). The physiochemical properties of the water column and sediments in addition to the metrological and hydrodynamic particularities of the watershed may cause the sediment to be resuspended and act as a source of contaminants thus impacting the overlying water quality (Miao et al., 2006, Atkinson et al., 2007, Yuan et al., 2007, Chon et al., 2012). In other words, the geochemical interaction at the sediment-water interface may trap chemicals in the sediments, or it could also release them upward to the overlying water column or downward ultimately to the groundwater (Wildi, 2010, Krau et al., 2011, Banks et al., 2012).

The hydrological settings of the Qaraaoun reservoir in a sensitive semi-arid watershed provide a particular example of sediment behavior under different environmental conditions. This study aims to identify the sediment behavior in the reservoir and the fate of various contaminants in an oxic/anoxic hypolimnion altered by different hydrological regimes. Moreover, it will assess the impact of the sediments at the water-sediment interface on the overlying water column and the ground water quality. The objectives of this work are to understand the sediment behavior in the reservoir under various hydrodynamic regimes, to investigate the biogeochemical processes in a sensitive semi-arid and strongly hydrologically connected reservoir, and finally, to pinpoint potential sediment management plans for the onsite hydropower project.

6.2 Materials and Methods

6.2.1. Study area and sampling

Qaraaoun reservoir is an artificial dammed lake established in 1956 that captures the flow of the Litani River (170 km) in a 2.2 km^2 lake for hydropower production and irrigation purposes. The Litani basin is the largest watershed in Lebanon known for its farming lands and characterized by a semi-arid climate. This basin has an important socio-economical value. It constitutes about 15-20% of the total area of the country, 20% of the total population, 20-30 % of the total national water budget, more than 60% of the agricultural industry and about 30% of the total energy production. The Litani basin is of karstic structure characterized by high infiltration capacity to a shallow groundwater table and it has an estimated capacity of 104 million cubic meters (MCM) (El Fadel et al., 2003, BAMAS, 2005, Saad et al., 2006, Saadeh et al., 2012).

The lacustrine sediment samples in this study were obtained from 3 different zones (Table 6.1) crossing the center of the reservoir longitudinally north to south (River inlet [Ri], Central Zone [Cz], and Dam zone [Dz]). The samples were collected using a stainless steel sediment grabber during both spill and fill modes over a period of two years from 2011 to 2013 (Fieldmaster Mighty Grab II Dredge). Water samples were collected from the water column above the location of the sediment samples using a depth dependent sampler at successive

depths of 5 meters. More samples in the top 5 meters were collected to investigate the biological activity at the level of epilimnion (0, 1, 3, 5, 10, 15, 20, and 25 m). Furthermore, in order to understand the hydrological connectivity between the main components of the watershed comprised by the river, reservoir and groundwater, additional samples were also collected from piezometers around the dam during the study period as shown by the work of Tuna et al., (2007). The coordinates of all samples are presented in Table 2.3.

6.2.2. Characterization of water samples

Water pH, temperature, electric conductivity (Ec), total dissolved solids (TDS), and dissolved oxygen (DO) were measured simultaneously onsite using a pH meter (HANNA pH211 microprocessor pH meter), conductivity-meter (WTW cond i), a portable LaMotte pocket multi Tracer-1766, and an oxymeter (JLO30 Jeulin) respectively. In addition, alkalinity and dissolved ammonium were measured by colorimetry (smart3 Lamotte) onsite. Water samples were filtered directly onsite using 0.45 µm minisart filters and stored in two divided batches of 50 ml polyethylene tubes. First group of water samples were filled to the rim with no head space to avoid aqueous air exchange prior to environmental isotopic analysis, whereas the other samples were acidified using concentrated HNO_3 to reach pH 1 for metal analysis. All collected samples were stored at 4°C until analysis. The acidified samples were analyzed for (Ca), magnesium (Mg), cadmium (Cd) and copper (Cu) using Atomic Absorption Spectrometry (Rayleigh WFX-210 AA Spectrophotometry with flame and graphite furnace mode), whereas aluminum (Al), zinc (Zn), nickel (Ni), cadmium (Cd), cobalt (Co), chromium (Cr), and lead (Pb) were analyzed using ICP-MS (Thermo Scientific). The major anions Cl^-, NO_2^-, NO_3^-, PO_4^{3-}, and SO_4^{2-} were measured using Ion Chromatography (Shimatzu - shim pack IC-A3). Oxygen and hydrogen stable isotopes in the water samples were measured using a laser detection for isotopic ratios (Liquid Water Isotope Analyzer - LWIA-24d) with precision <0.1‰ for $\delta^{18}O$ and <0.3‰ for δ^2H. The isotopic ratios were expressed as delta ($\delta^{18}O$-δ^2H) according to a standard calibration curve using V-SMOW certified standards in consistency with the international atomic energy agency (IAEA) norms. Two additional water samples at 0 m and 3 m depth below the water surface were also collected and directly frozen for dual isotopic approach ($\delta^{15}N$ and $\delta^{18}O$) in order to delineate the nitrate source in the reservoir (Liang et al., 2013). Denitrifier method was used to measure the isotopic signature of nitrogen and oxygen at the Vrije University of Brussels (VUB) according to Sigman et al., (2001) and Casciotti et al., (2002). Briefly, nitrate is biologically converted to N_2O gas by *P. aureofasciens* bacterial strain, which is later purified by gas chromatography and measured by isotopic ratio mass spectrometer (V IRMS- ThermoScientific) coupled with open split interface. The method of bacterial culture, and nitrate conversion to nitrous oxides, purification and measurement is detailed in Mangion (2011).

For chlorophyll–a, water samples (100 mL) were filtered on glass fiber filters and then extracted with acetone according to the method described by Arnon (1949). The extracted chlorophyll was measured using a photometer (SP 2000 UV Spectrophotometer VWR) over

two wavelengths, λ= 645 and 663 nm. The total chlorophyll was calculated according to equation 2.1:

$$\text{Chlorophll (total)} = 20.2\ (A645) + 8.02\ (A663) \qquad (2.1)$$

where A645 and A663 are the absorbance values detected at λ= 645 and λ= 663 nm, respectively.

6.2.3 Characterization of sediments and algae

The grain size distribution of the lacustrine sediment samples was measured using a laser scattering particle size distribution analyzer (Patrica LA-950V2 Horiba) equipped with a laser diodes of 1.6 mW with λ= 405 nm – 650 nm. An ultrasonic probe was used to breakup any aggregates at 20 kHz frequency before analysis. The chemical functional groups were determined using FT-IR-6300 (Fourier Transform Infrared Spectrometer) from JASCO. The FT-IR samples were prepared by mixing the powdered samples with potassium bromide (1% wt/wt) and compressed into 0.7 cm diameter pellets. The total and particulate organic carbon content in sediment samples were measured using a CNS analyzer from Interscience FISONS (NA-2000, series 2). The mineralogical phases in the sediment samples were determined by X-ray Powder Diffraction (XRPD) using a D8 Bruker X-ray diffractometer (copper anticathode of wavelength λKα = 0.154060 nm). The data were collected in the 2θ range of 10° to 60° with a step size of 0.02° per sec. The collected diffractograms were analyzed using the EVA software and the powder diffraction files provided by the International Centre for Diffraction Data. Sediments were also examined by scanning electron microscopy (SEM) using a JEOL JSM 6360LV, accompanied by a silicon drift detector (SDS), PGT Sahara.

The sediment samples were digested in concentrated acid before elemental analysis using a microwave digestion oven. The samples were first homogenized using pestle and mortar and sieved through 63 μm acid-cleaned nylon mesh. An amount of 50 mg of the 63 μm sieved samples was digested in Teflon bombs along with suprapur acids: 1 ml of 10 N HCl, 2 ml of concentrated HNO_3 and 250 μl of 40% Hydrofluoric acid (HF). The filters, used for sample filtration of the water column and containing thus the suspended matter, were stored and digested following the same method used for the sediments. Digested sample solutions were analyzed for major, minor and trace element contents by Graphite Furnace Atomic Absorption Spectroscopy (GFAAS) with Zeeman-effect background correction (Varian AA-400) and Inductively Coupled Plasma Atomic Emission Spectroscopy (ICP-AES) (Varian Liberty series II). Certified standard materials (UN 3264 from MERCK) along with blanks were measured with sample batches.

Algae material collected from the eutrophicated reservoir water was examined by SEM. The algae samples were prepared for SEM analysis in a similar way to the preparation of the sediment samples as described in §6.2.3. In addition, the morphology of algae samples and the presence of chlorophyll was examined by Epifluorescence microscopy (Leica - DMRXA) equipped with a brightfield and darkfield inspection and coupled with motorized sextuple type nosepiece and HC PL Fluotar BD objectives: 5x/10x/20x/50x/100x. The tilting

trinocular viewing head with 10x/25 eyepieces is associated with a 12V/100W lamp and automatic Koehler illumination. Finally, a DAPI staining analysis was performed with chlorophyll filter as described by Sherr et al., (1993) to investigate the nature of the material.

6.3 Results and discussion

6.3.1 Characterization of reservoir sediments

The sediments showed a fine grain size distribution composed entirely of particles with diameters less than 230 μm (Figure 6.1a). Moreover, about 50% of the sediment particles have a diameter less than 63 μm (Figure 6.1a), such sediments are expected to have dominant clay and silt textures (Roussiez et al., 2006). Fine grain particles have higher affinity to metals and higher tendency to be resuspended under active hydrodynamics; furthermore researchers found that clay fraction control the distribution of chemical species (Taher and Soliman, 1999, Roussiez et al., 2006). Since metals are retained through particle surface actions, it is expected that fine particles with high surface area to exhibit higher surface actions (Balkis et al., 2010).

XRPD analysis showed that calcite and montmorillonite are the prevailing mineral phases in the lacustrine sediments (Figure 6.1b). In addition, chemical characterization of sediments using SEM indicated enrichment of the sediments with trace metals such as Cr (Figure 6.1b). Conversely, the FT-IR spectra for the reservoir sediment organics (Figure 6.1d) exhibited various functionalities. They showed strong peaks corresponding to abundant O-H and C=C and C-O vibrations linked to various organic compounds with weak intensities as reflected by their corresponding narrow absorption bands (Figure 6.1d).

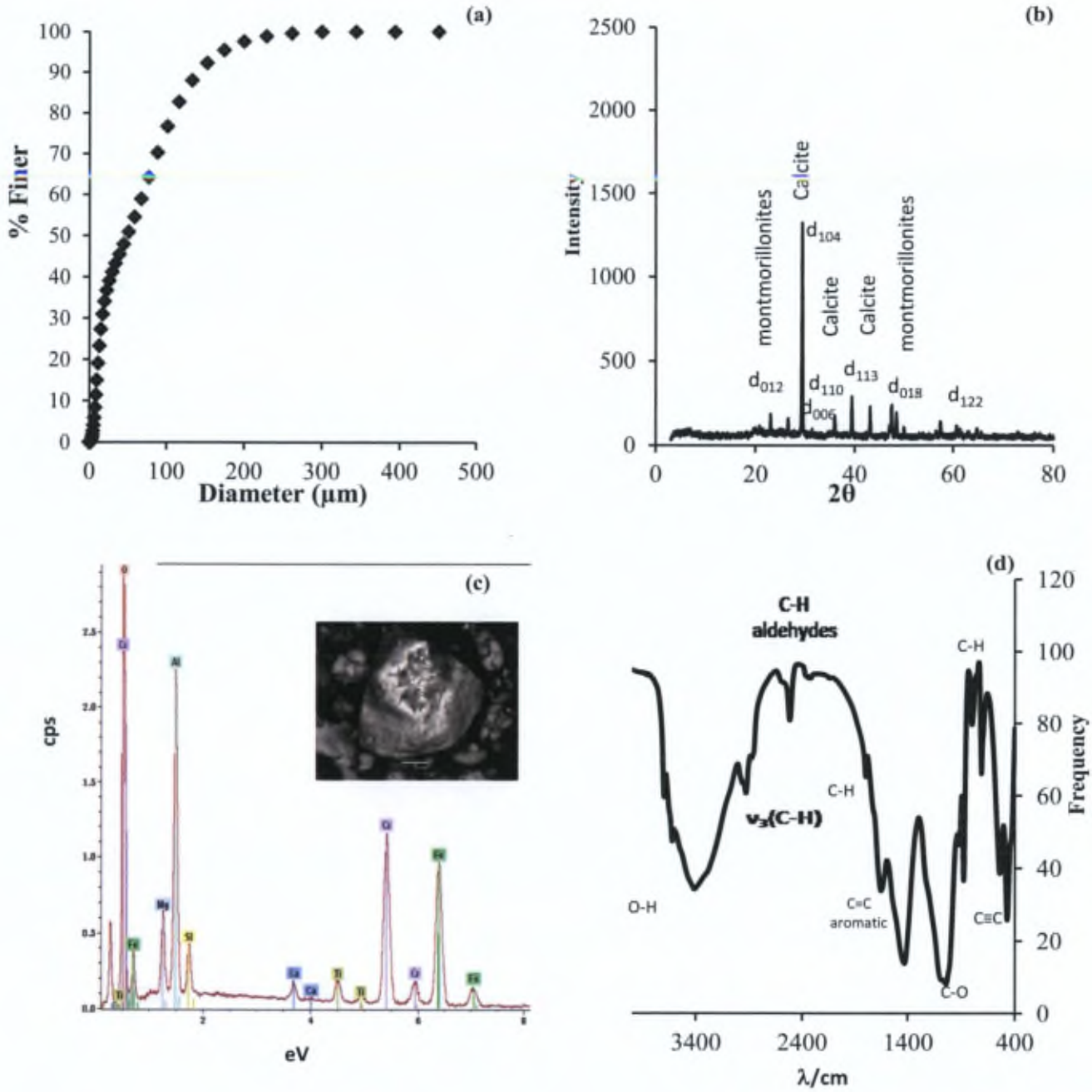

Figure 6.1: Characterization of reservoir lacustrine sediments, (a) grain size, (b) mineralogy, (c) elemental analysis, and (d) functional groups at the dam zone (Dz) during spill hydrological mode (September 2011).

The sediments at all locations (Ri, Cz, and Dz) showed some variations in the concentration of the major elements (Figure 6.2). However, all sediments exhibited the same abundance for major elemental contents in the order Ca>Si>Al>Fe>Mg>K. For different sampling sites, sediments collected at the river inlet exhibited the highest Al, Fe, K and Mg contents and the lowest Ca value. In contrast, sediments in the central zone showed the highest Ca content and lowest Al, Fe, K, Mg and Si concentrations. The high calcium content (about 20%) in the reservoir sediments of the agricultural watershed (Figure 6.2) could be due to limestone bedrock weathering and rock cutting industries prevalent in the drainage basin. The Ca concentrations in the central zone of the reservoir are relatively high as compared to other major elements and to other zones (Table A2.2)[9]. The high Ca concentration in the central zone of the reservoir could be due to the low turbulence in that zone allowing the deposition of carbonate phases as reflected by the sediment composition. In addition, some of the calcium carbonates could be endogenic or could be trapped in a particular zone through endogenic means. Martín-Puertas et al., (2009) used the ratio of Ca/Al to address the nature of carbonates in lacustrine sediments and to delineate the origin of sediments where a high Ca/Al ratio indicated an endogenic source. In our case, the Ca/Al ratio registered the highest values in the central zone (10.2) as shown in Figure 6.2 for samples collected in spill mode, suggesting the in-situ origin of Ca and the importance of the biogeochemical cycle of weathered Ca and its precipitation taking place in the reservoir (Martín-Puertas et al., 2009). In contrast, the dam zone reveals more contaminated sediments that have the highest content of aluminum silicates (Figure 6.2), with the highest metal content observed during dry season and low river flow (Table 6.1). This may suggest more lithogenic and anthropogenic sources of metals which may have been transported with the fine fraction to the dam zone especially during the low river flow.

The particulate organic carbon in the sediments ranged between 2% and 3% which corresponds to an organic matter content of 5 – 7.5%, assuming a converging factor of 2.5 (Broadbent, 1953). Delsontro et al., (2010) reported that agricultural watersheds are important sources of carbon and nutrients for reservoirs, inducing biological growth. Furthermore, methane emissions are expected to register the highest values at the dam zone during summer (Delsontro et al., 2010). Thus, in our discussion we will focus on the Dz because of its sensitive location with regard to the reservoir, and the potential hazardous impact of this zone on the utilized water drawn from the reservoir.

The presence of carbonate phases, such as calcite in lacustrine sediments may dilute metal enrichment in the reservoir sediment bed, whereas the presence of clays may aid in trapping trace metals such as Pb and Cu, through sorption and precipitation (Korfali and Davies, 2004). Conversely, the formation of metal-organic complexes may mobilize the metals (Balkis et al., 2010).

[9] See Annex 2

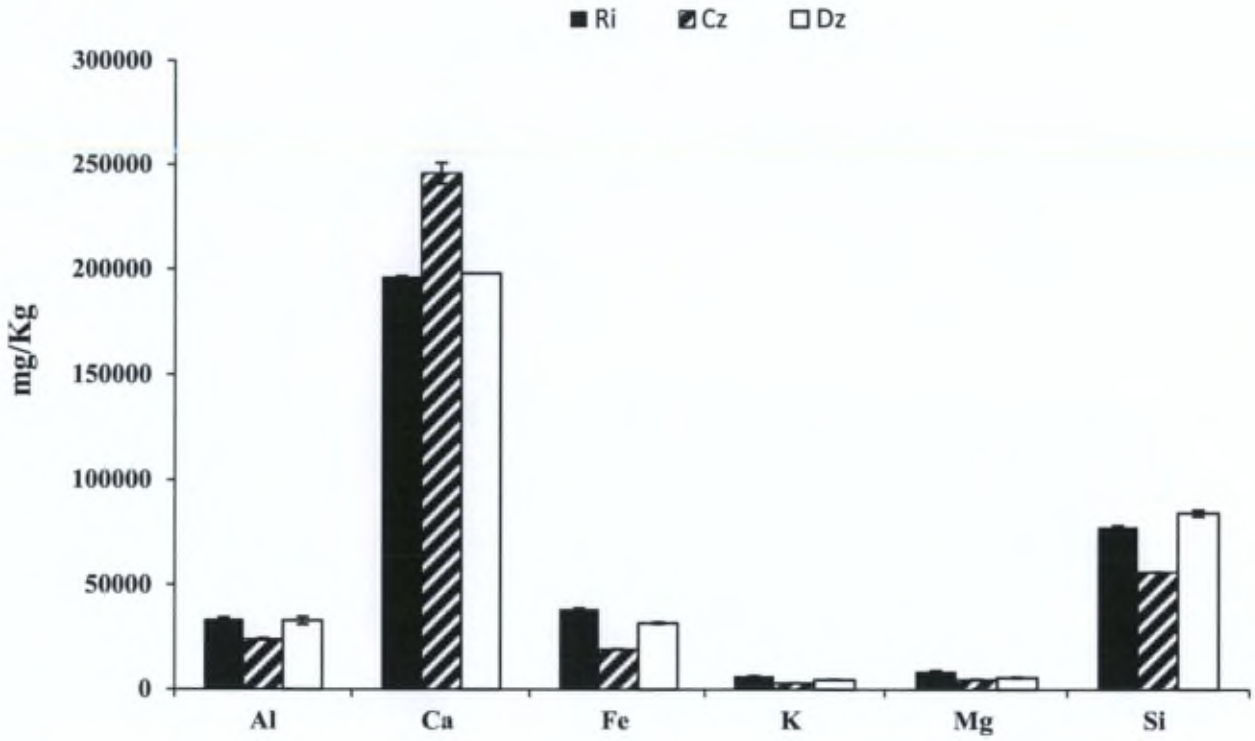

Figure 6.2: Geochemical characterization and spatial variation in lacustrine sediments at Ri, Cz, and Dz during spill hydrological mode (November 2011).

Table 6.1: Spatial variation of metal contents in the reservoir sediments during dry season.

Zone	Pb (mg/L)	Cd (mg/L)	Mn (mg/L)	Zn (mg/L)
Ri	24.08588	0.627146	414.8493	76728.17
Cz	15.68978	0.505517	280.9001	55930.69
Dz	24.15436	0.609844	446.0104	84109.76

6.3.2. Reservoir hydrodynamics

The reservoir hydrodynamics is characterized by two major flow regimes: the fill hydrologic regime and the spill hydrologic regime. During the wet fill mode water flows to the reservoir from surface and road runoff, springs and the main river course, whereas during the dry spill mode the river flow decreases and water level in the reservoir is lowered due to water withdrawal for various usages. Similarly, the reservoir is characterized by three distinct spatial zones, the dam zone (Dz), the central zone (Cz), and the river inlet zone (Ri). The Dz is subjected to weak hydrodynamic regime in the winter season where settling of suspended matter are expected to be more favored. However, the Dz is expected to be under more active hydrodynamics in the summer season due to the turbine flux that is installed at the bottom of

the dam, where the withdrawn water is expected to be used for irrigation and hydropower purposes (Ammar et al., a submitted). The Cz exhibits a similar hydrodynamic behavior as the Dz but it is subjected to weaker hydrodynamic influence since it is situated in a transient zone between Ri and Dz in the river pathway prior to the construction of the dam. Nonetheless, the river inlet zone is where the reservoir connects with the Litani River and it serves as the major inlet of water to reservoir. Sediments in this zone are expected to bear the highest metal content in both spill and fill modes (Korfali et al., 2006, Ammar et al., b submitted) as explained in Chapter 4.

6.3.2.1 Fill hydrological mode

6.3.2.1.1 Physicochemical characteristics and transport direction of chemicals

The physicochemical characteristics of the water column above the retrieved sediments collected in the fill hydrological mode of the reservoir are shown in Figure 6.3, (Tables A4.1, A4.2, and A4.3)[10]. During the fill mode and as a result of high river flow and surface runoff, the water column is alkaline and shows a decrease in pH from 8.79 at the surface to 8.17 at the bottom (Figure 6.3a). Like pH, the temperature decreased along the water column by about 2.5 degrees (Figure 6.3b). However, the total dissolved solids (Figure 6.3c) and conductivity (Table 6.2) increased by 13 mg/l and 19 µS/cm with depth, respectively. Measured alkalinity fluctuated in the water column where it reached its maximum concentration (167 mg/l as CaCO3) at 3 m below the surface, and then decreased along the water column (Figure 6.3d).

Table 6.2: Physicochemical characteristics of the water column at Dz during fill mode, showing the electrical conductivity and the concentration of certain dissolved elements.

Dz depth (cm)	Ec (µS/cm)	Cl^- (mg/L)	SO^{2-}_4 (mg/L)	Ca^{2+} (mg/L)	Mg^{2+} (mg/L)	Ni^{2+} (µg/L)	Mn^{2+} (µg/L)
0	501	28.45	31.77	58.59	15.45	1.848	0.537
1	504	22.05	31.1	59.52	15.47	1.541	0.362
3	501	23.92	31.34	59.51	15.49	1.496	0.518
5	509	26.38	31.42	57.43	15.57	1.39	0.218
10	508	22.22	30.98	65.07	15.72	1.266	0.241
15	517	22.22	31.69	60.61	15.78	1.78	0.264
20	517	22.28	32.64	61.76	15.32	1.602	0.618
25	520	22.1	32.8	61.71	15.37	5.713	0.31

The ambient temperature and the mineralized water with increased loads of nitrogen enhanced the photosynthetic production of organic matter which was then degraded via oxic respiration, causing oxygen depletion in the reservoir as indicated by the anoxic epilimnion

[10] See Annex 4 for detailed water chemistry data in wet season.

(Figure 6.3e) (Peretyazhko et al., 2005). Dissolved oxygen level is minimum in the epilimnion (top 5 meters) ranging from 1.6 to 4.8 mg/l, which then increases with depth reaching maximum levels in the hypolimnion (Figure 6.3e). Vertical profiles of dissolved inorganic nitrogen are shown in Figure 6.3 where ammonium levels decreased with depth (Figure 6.3f) and nitrites and nitrates increased mainly between 5-10 meters as shown in Figures 6.3g and 6.3h. The profile of heavy metals concentrations along the water column (Figures 6.3i, 6.3j, 6.3k, and 6.3l), mainly in the top 5 meters, resembled the trend observed for alkalinity and nitrate/nitrite. The sharp fluctuation of chemical concentration at 3 meters indicates the presence of an additional biological community such as phytoplankton which could be responsible for this fluctuation. A drop in the concentration of DO in the water column accompanied by a drop in pH, as that observed during the fill mode at 5 m below the surface, could be a result of proton release from aerobic respiration of organic matter and/or oxidation of reduced species such as NH4, known as the nitrification, that decreases with decreasing DO according to equation 6.1 (Peretyazhko et al., 2005).

$$NH_4^+ + 2O_2 \leftrightarrow NO_3^- + 2H+ + H_2O \qquad (6.1)$$

In the epilimnion, NO_3^- (33.71 ppm) and Mn^{2+} (0.54 ppb) concentrations (Table 6.2) in the lake are relatively high thus indicating that nitrification and Mn reduction are taking place when O_2 levels are low (Peretyazhko et al., 2005). EC gradient increasing from 501 µS/cm at the surface to 520 µS/cm at 25 m depth (Table 6.2) supports the presence of biogenic meromixis (Taillefert et al., 2000). This biogenic meromixis may induce a density gradient which may slow down the transport of dissolved species from monimolimnion to epilimnion, where chemical species accumulate at a depth of 5 meters from the surface. The general vertical direction of water in the fill mode is expected to be from the top to the bottom, as groundwater has not yet developed enough pressure head in the aquifer at the bottom of the reservoir to force an upward flux (Ammar et al., a submitted). Moreover, diffusive transport in general is very slow and is not expected to result in large gradients over relatively short time intervals; so the chemical and temperature gradients, if any, would be due to advective-dispersive flow (Boehrer and Schultz, 2008). The water temperature gradient decreasing from approximately 14.7°C at the surface to approximately 12.3°C at the bottom supports the top down transport. Similarly, the concentration profiles of Cr, Cu and Zn (Figures 6.3i-6.3k) show an increase in concentration with depth also indicating transport direction from top to bottom during the fill hydrological mode. Thus, the river is expected to exert the most chemical stress on the epilimnion during the fill hydrological mode, which was also reported by Ammar et al., a (submitted) (detailed in chapter 7).

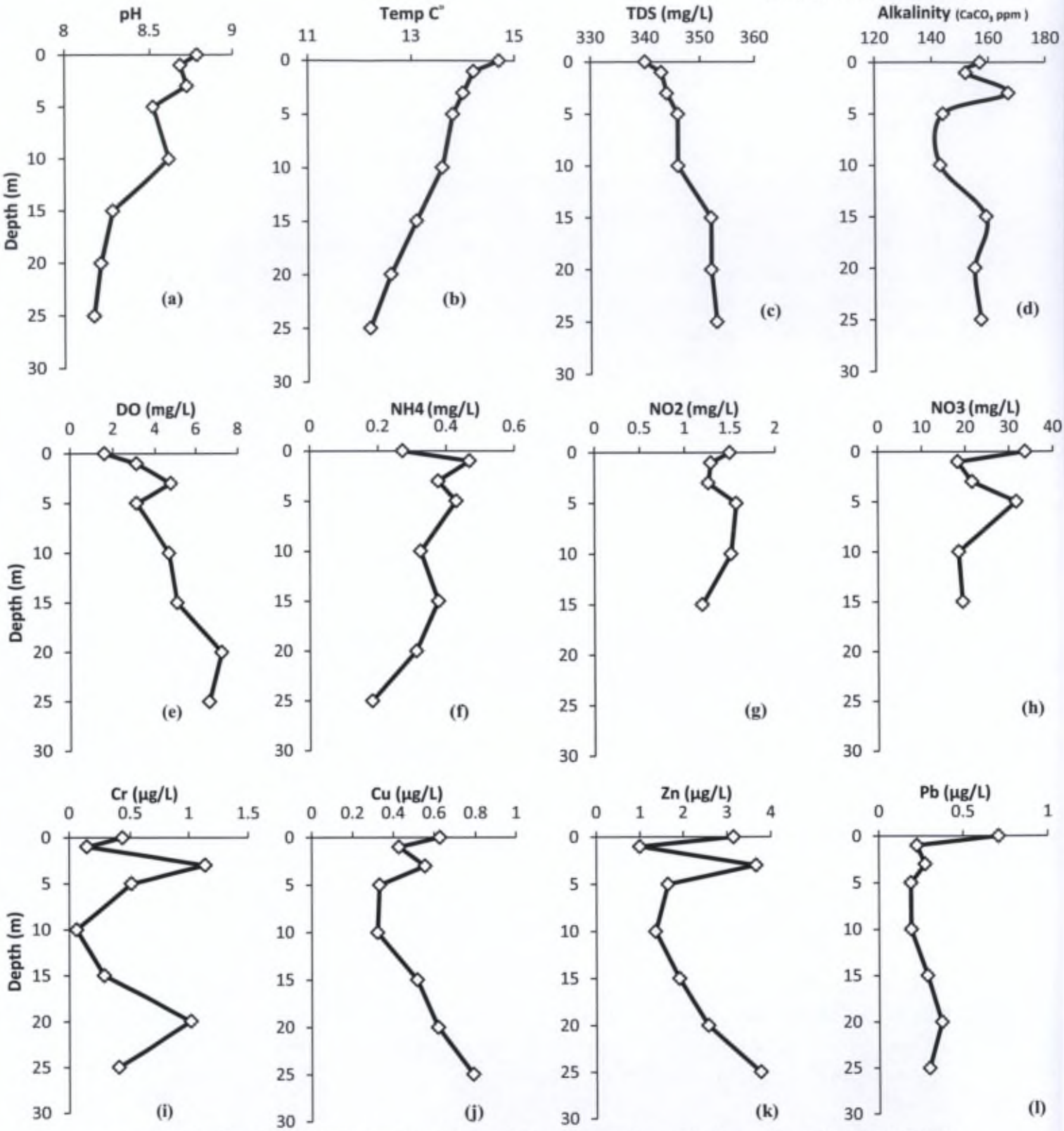

Figure 6.3: Physicochmical characteristics of the water column during fill mode (April 2013), showing chmical stratification and the bottom water enriched by chemicals at the level of oxic hypolimnion at Dz.

6.3.2.1.2 Sediments act as a sink for chemicals

The chemical stratification or enrichment in the water column can be expressed as:

$$e\% = \frac{(\bar{x}_{hypolimnion} - \bar{x}_{epilimnion}) * 100}{\bar{x}_{epilimnion}} \qquad (6.2)$$

Where x stands for the concentration of the chemical species of interest, and, epilimnion and hypolimnion are taken at the water surface and bottom, respectively. The TDS enrichment of approximately 3% clearly indicates an ongoing chemical stratification in the dam zone in the reservoir during the fill hydrological mode (Table 6.3). The calcium enrichment, estimated to be approximately 4.3%, could be due to surface and groundwater flows. During the fill mode, the surface runoff and groundwater inflow from Karst springs and the corresponding calcite dissolution are reported as factors in calcium enrichment (Jeelani et al., 2011). Thus the high calcium concentration in the water column mainly found at the bottom (Table 6.1), in addition to the high Ca content in the sediments (Figure 6.2) suggest more alkaline conditions which may scavenge metals from aquatic systems and precipitate them as insoluble oxyhydroxides at the water-sediment interface (Gadd and Griffiths, 1987, Korfali and Davies, 2004). However, the sorbed metals may be later released in the spill mode when the environmental conditions change in the sediments.

Similarly, the enrichment percentage of Ni, Cr, Cu, Zn, and Cd increased by 5.5, 24.1, 31.0, 21.5 and 46.5%, respectively, from surface to bottom, in the water column (Table 6.3). This enrichment confirms the presence of heavy water layer at the bottom. Metal input such as Cd and Zn could have originated from various industries such as paint manufacturing, agricultural application of phosphate fertilizers that are extensively applied in the watershed during the fill hydrological mode, in addition to domestic and industrial effluents. The higher enrichment observed for Cd compared to other metals, mainly Zn, and the unexpected negative enrichment for Pb (Table 6.3), is consistent with higher particulate Pb concentration and lower Cd concentration in the reservoir sediments during the fill mode (Figure 6.4). This difference in partitioning behavior of Cd and Pb between the dissolved and the particulated phases at the water-sediment interface could be attributed to their different behavior in response to water physicochemical characteristics. Pb is more influenced by dissolved oxygen changes, salinity, conductivity and redox state in the water column; thus it may effectively be adsorbed to finer grained particles and transferred to the sediments (Ekpo and Ibok, 1998). The transport of chemicals downward to oxygenated hypolimnion (Figure 6.3e) may further allow the entrapment of these chemicals by sediments at the sediment-water interface. Oxidizing conditions will lead to metal immobilization and its entrapment by its adsorption to sediment (Miao et al., 2006).

As discussed above, and as a consequence of the reservoir hydrological setting and the water physiochemical characteristics, sediments can act as sink for chemicals during the fill hydrological mode. Furthermore, the thermal gradient in the water column, accompanied with the chemical stress exerted by the river on the surface of the reservoir can cause an indwelling water movement of water molecules enriched in chemicals toward the bottom.

The thermal gradient and the enriched water movement toward the bottom will result in a heavier water layer at the level of hypolimnion where it can resist the water turn over during the fill hydrological mode (Boehrer and Schultze, 2008, Ammar et al., a submitted).

Table 6.3: Physicochemical parameters and mean concentration of dissolved elements in the epilimnion and hypolimnion, and the calculated execs % in Dz for both fill and spill modes.

Hydrological mode		TDS ppm	EC µS/cm	DO mg/L	Alkalinity mg $CaCO_3$/L	Ca mg/L	Ni mg/L	Cr mg/L	Cu mg/L	Zn mg/L	Cd mg/L	Pb mg/L	NH_4^+ mg/L
Fill	Epilimnion	342.33	502	3.16	158.66	59.20	1.52	0.57	0.53	2.60	0.014	0.40	0.37
	Hypolimnion	352.5	518.5	6.9	156	61.73	1.60	0.71	0.70	3.16	0.021	0.33	0.247
	e%	+2.97	+3.29	-6.2	-1.68	+ 4.3	+5.49	+24.11	+31.01	+21.52	+46.51	- 17.06	-33.7
Spill	Epilimnion	234	343	6.3	211	36.62	0.91	0.68	1.02	1.11	na	0.105	0.39
	Hypolimnion	281.5	412	3.35	284.5	46.83	0.97	0.08	0.41	2.42	na	0.245	1.36
	e%	20.3	+20.1	-46.8	34.8	27.9	7.67	-88	-59.3	118.8	na	132.7	250

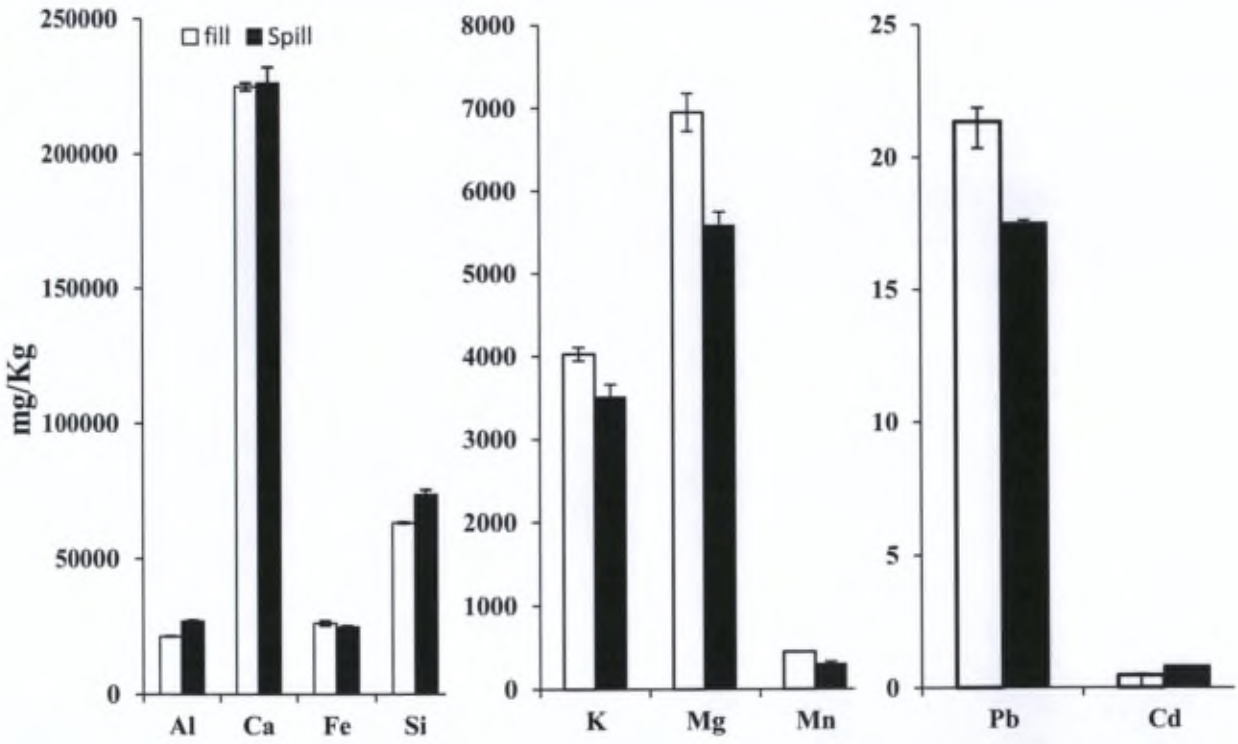

Figure 6.4: Sediment characterization in fill (March 2012) and spill (November 2011) hydrological r at dam zone (Dz).

6.3.2.2 Spill hydrological mode

6.3.2.2.1 Physicochemical characteristics and transport direction of chemicals

The water column exhibits chemical profiles in the spill mode different from those observed in the fill mode[11]. The chemical stress exerted by the river is weak due to low river flow and the absence of any surface runoff, which is reflected by the reservoir's limnology. The reservoir water remained alkaline (Figure 6.5a), but the pH was lower than that exhibited during the fill mode, and the surface water temperature increased by 5°C ; nevertheless, the water column still exhibited a thermal stratification (Figure 6.5b). The TDS concentration increased with depth, where the recorded concentration at the level of hypolimnion was 308 mg/l (Figure 6.5c). The same trend was observed for alkalinity where the hypolimnion was more enriched than the upper water column by almost one fold (Figure 6.5d). The dissolved oxygen and nitrogen species in the water column are affected by increased temperature and the presence of favorable conditions for biological growth. The DO (Figure 6.5e) showed an opposite trend to that exhibited in the fill mode by which oxygen level decreased with depth and the water at the bottom of the reservoir was depleted in oxygen. Denitrifying bacteria could explain the higher concentration of NH_4^+ in the hypolimnion (Figure 6.5f) (Krivtsov and Sigee, 2005). In addition, the lower ammonium level in the epilimnion (Figure 6.5f) could be due to its assimilation by photosynthetic phytoplankton which explains the high levels of DO, NO_2^- and NO_3^- (Figures 6.5e, 6.5g, and 6.5h).

Anthropogenic effluents are reported to be the major source of trace metals in the aquatic system (Roussiez et al., 2006, Callender and Rice, 2000, Chon et al., 2012). The metal contamination is manifested in the higher concentration of dissolved Cr and Cu in spill mode and the corresponding fluctuation in the water column as shown in Figures 6.5i and 6.5j. The high metal concentration in the top layer could be related to the usage of algaecides in the upper watershed where irrigation is active during the dry season. Moreover, industrial effluents are more concentrated dissolved metals when the river flow is low. However, dissolved Zn (Figure 6.5k) and Pb (Figure 6.5l) concentrations increased with depth, thus in the spill hydrological mode the water at the hypolimnion level was highly enriched with chemicals as compared to the upper water layers, and to the water column during the fill mode. The vertical distributions of dissolved elements indicate an opposite trend to that exhibited during the fill mode. These profiles agree well with the vertical water mixing exerted by groundwater influx as reported by (Ammar et al., a submitted) (further explained in chapter 7).

[11] See Annex 5, 6, and 7 for detailed water chemistry data during dry season and first flush (spill mode).

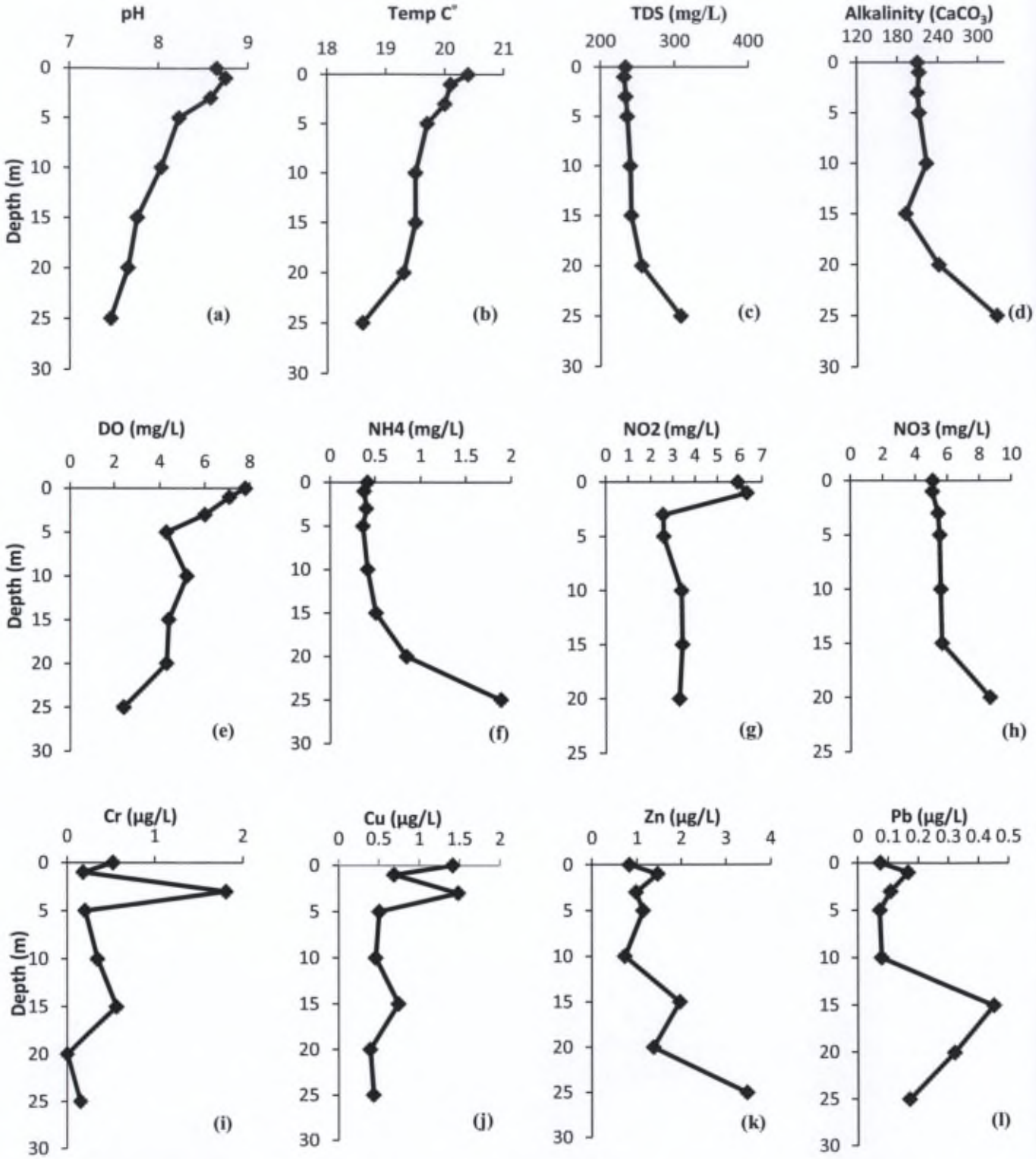

Figure 6.5: Physicochmical characteristics of the water column during spill mode (October 2012), showing the presence of an anoxic hypolimnion and a flux of nutrients from resuspended sediments upward the water column at Dz.

6.3.2.2.2 Sediments act as a source for chemicals

The enrichment of dissolved chemical species in the water column during the spill mode is relatively high at the bottom layer where EC, TDS, alkalinity, and Ca increased by 20%, 20%, 34.8 and 27.8 %, respectively. Similarly, dissolved Ni, Zn and Pb were enriched by 7.6%, 119% and 133%, respectively (Table 6.3). The high enrichment in Zn and Pb suggests a flux of chemicals from the sediments beneath the water column. Due to the physicochemical changes in the overlying water column in the spill mode as compared to the fill mode (Figures 6.3 and 6.5), and the change in the redox state at the sediment water interface, metals may be subjected to exchange fluxes between sediments and the overlying water column (Argese et al., 1997). Metals are expected to form complexes with the abundant carbonate ions in the reservoir during the fill mode, and as pH decreases during the spill mode (Figure 6.3a and 6.5a) at the level of hypolimnion, the carbonate/metal complexes are expected to liberate the metals to the water column. Witness observation of gas bubbles in the spill mode during sediment sampling supports possible dissolution of $CaCO_3$ by fugitive CO_2 gas emanating from methanogenic reactions in the hypolimnium. The dissolution of $CaCO_3$ will result in an increase in the concentration of Ca^{2+} and metals as shown in Figure 6.5 and Table 6.3. Similarly the high enrichment of dissolved Pb at the level of hypolimnion (Table 6.3) can be explained by the high affinity of Pb complexes for residual oxide phases and the possible dissolution of these oxides due to physicochemical changes at the sediment-water interface. Similarly, ammonium levels in the hypolimnion increased by 2.5 folds whereas dissolved oxygen decreased by 46.8% at the dam zone (Table 6.3). This is in agreement with Wall et al., (2005) who reported that sediment denitrification is highest in the deep dam zone during summer. In their study, they found that nitrate concentration was high in the spring and low in the summer.

The reducing conditions in the sediments in the spill hydrological mode may allow bacteria to reduce sulfate and release sulfides according to equation 6.4. This is further confirmed by the increased alkalinity with depth along the water column (Figure 6.5d) concomitant with a decrease in sulfate concentration in the epilimnion from 54.4 ppm to 22.8 ppm in the hypolimnion (Table 6.4) suggesting the degradation of organic matter according to equation 6.3 (Peretyazhko et al., 2005).

$$2CH_2O + SO_4^{=} \rightarrow H_2S + 2HCO_3^{-} \quad (6.3)$$

The anoxic conditions may facilitate reduction reactions where metals can be released from sediments and transferred to the overlying water to be later transported by the vertical mixing induced by groundwater influx through the water column at Dz (Ammar et al., a submitted). Studies show that Pb, Cu, Zn, and Cd are easily exchanged between sediments and the overlying water; the sediments are mostly anoxic whereas the overlying water is in an oxidized state. Metals which are associated with labile phases such as oxides and organic matter are easily resuspended and solubilized in the water column (Argese et al., 1997, Xue et al., 1997). In addition to the favorable conditions for metal release from sediments created by the variation in redox state between sediments and the overlying water column, the sediment texture is composed mostly of fine grains (Figure 6.1a) which will aid in their resuspension.

The sediment resuspension and the consequent metal release are further helped by the active hydrodynamic conditions caused by turbine suction during the spill mode, and the seasonally dependent groundwater influx (Argese et al., 1997, Ammar et al., a submitted).

Table 6.4: Physicochemical characteristics of the water column at Dz during spill mode, showing the electrical conductivity and the concentration of certain dissolved elements.

Dz depth (cm)	Ec (µS/cm)	Cl^- (mg/L)	SO^{2-}_4 (mg/L)	Ca^{2+} (mg/L)	Mg^{2+} (mg/L)	Ni^{2+} (µg/L)	Mn^{2+} (µg/L)
0	342	20.307	54.398	37.84	13.23	0.86	0.369
1	341	20.223	55.069	36.57	13.04	0.947	0.141
3	343	21.41	26.78	39.27	13.25	0.911	1.060
5	346	21.47	26.8	32.83	13.36	0.915	0.183
10	349	21.83	26.71	35.71	13.19	0.917	0.245
15	352	21.89	26.61	38.28	13.25	1.242	0.164
20	374	21.78	25.9	36.41	13.17	0.98	0.516
25	450	21.53	22.85	57.25	13.75	0.976	0.586

The low inflow into the Litani river during the warm spill mode and the reservoir bathymetry in addition to reservoir hydrodynamics influenced by water exploitation for irrigation and hydropower production lead to dramatic decrease in the water level which could induce intense biogeochemical reactions (El Fadel et al., 2003, Saadeh et al., 2012). They are more favored in larger surface areas with weak water currents such as those featured near the dam zone, which is the largest and deepest part of the reservoir (Taillefertet al., 2007, Figueiredo et al., 2011). Two possible factors could explain the metal enrichment at the sediments-water interface in the dam zone: the mechanical transport of sediments from the river towards the dam and the subsequent sedimentation of finer clayey sediments, and the precipitation of pollutants due to biogeochemical processes in the alkaline water and/or its resuspension from sediments as a result of redox reaction. Reservoir sediments in the dam zone are composed of fine grains where approximately 50% of the total sediments consist of grains with size less than approximately 20 µm, these fine fractions could be easily resuspended with the water current. As a consequence of the increase of particulate metal content in finer fractions, the bioavailability and hazardous impacts of metals increase significantly (Callender and Rice, 2000, Ebrahimpour and Mushrifah, 2008).

6.3.3 Reservoir eutrophication and biological processes

The physicochemical properties of the reservoir water indicate high mineralization during the fill hydrological mode (Figure 6.3). Under this condition, the river is enriched with nutrients and chemicals derived from crustal erosion during the winter, and anthropogenic activities such as land-use in the upper watershed where fertilizers and agrochemicals are applied in the agricultural plain (Bamas, 2005, Darwish et al., 2011). The nutrient enrichment is clearly shown in Figure 6.6, where PO_4^{3-}, NO_3^- and SO_4^{2-} concentrations are relatively high during the fill mode as compared to the spill mode. These nutrients are brought in by the river at the level of epilimnion (Figure 6.6) during the fill mode and may induce the algal blooms when the favorable conditions are provided during the spill mode. The algal proliferation provokes a new biogeochemical cycle in the reservoir (Ocampo et al., 2006). Moreover, the alkaline

pH (Figures 6.4a and 6.5a) may reflect photosynthetic assimilation of nutrients and higher primary production in the spill mode compared to fill hydrological mode (Hart et al., 2002).

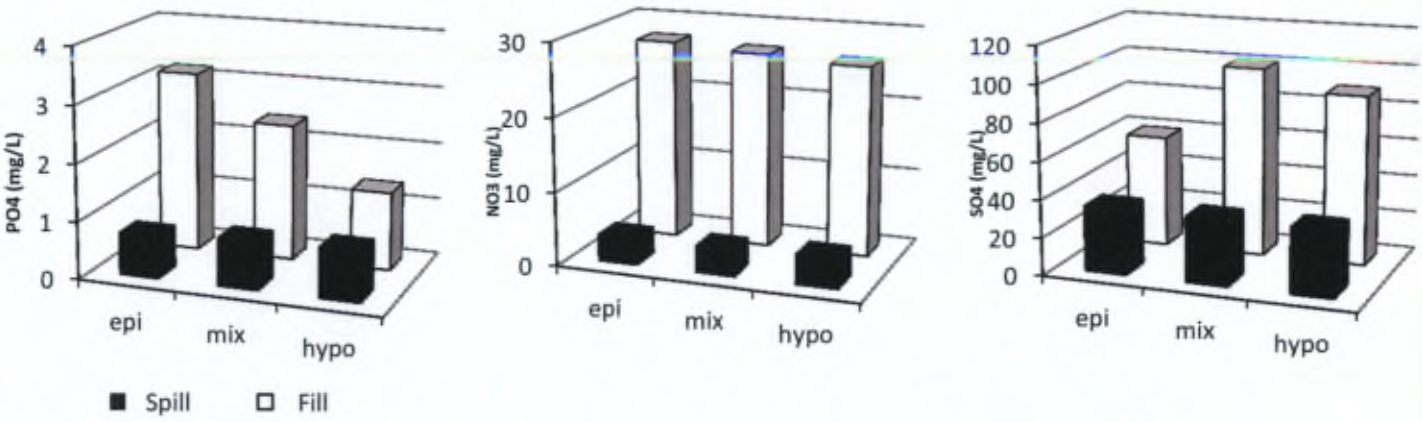

Figure 6.6: Anthropogenic influence on the nutriens concentration in the reservoir during fill mode (March 2012) and their assimilation by primary productivity during spill mode (September 2012) at Dz. Epi denotes epilimnion (top 5 m), mix is mixilmnion (5-15 m), and Hypo is hypolimnion (the bottom water).

The eutrophic conditions in the reservoir have recently led to a massive proliferation of algal blooms. These blooms are wreaking havoc with the reservoir and the associated hydro-project. Optical and scanning electron microscopy examination of these algal materials indicated the presence of diatoms, and other photosynthetic phytoplankton that share the characteristics of cyanobacteria (Figure 6.7e). Cyanobacteria are photoautotrophic prokaryotes, able to fix atmospheric nitrogen and enrich sediments with organic matter (Taher and Soliman, 1999, Kremer et al., 2008). However, the SEM images indicated the presence of carbonate aggregates with perfect dodecahedral crystal morphology (Figure 6.7e). This observation suggests the possibility of in-situ precipitation of calcite in the reservoir by cyanobacteria mats, since the photosynthetic cyanobacteria are able to fix CO_2 thus concentrate the bicarbonate ions in the reservoir and as a result increase the calcite saturation state during the spill mode (Merz, 1992, Kremer et al., 2008, Kamennaya et al., 2012). The dense biological community could result in the creation of an anoxic layer, whereas the activities of the photosynthetic species may result in an increase in the concentration of dissolved oxygen in the water column (Singh et al., 2008, Lenzi et al., 2013). This may explain the sharp decrease in DO in the upper 5 meters as shown in Figure 6.5.

During bacterial respiration and denitrification, oxygen and nitrogen molecules fractionate by the preferential consumption of the lighter isotopes ^{16}O and ^{14}N leaving the water column enriched by ^{18}O and ^{15}N (Brandes and Devol, 1997). The measured ^{15}N ratio during the spill mode in the reservoir at the 0 m and 3 m levels are 8.27‰ and 8.48‰ respectively, whereas the ^{18}O ratio was measured at 6.04‰ and 5.9‰, at the same levels, respectively. This

indicates that the source of nitrogen in the reservoir is most likely farming and agritainment practices (Liang et al., 2013).

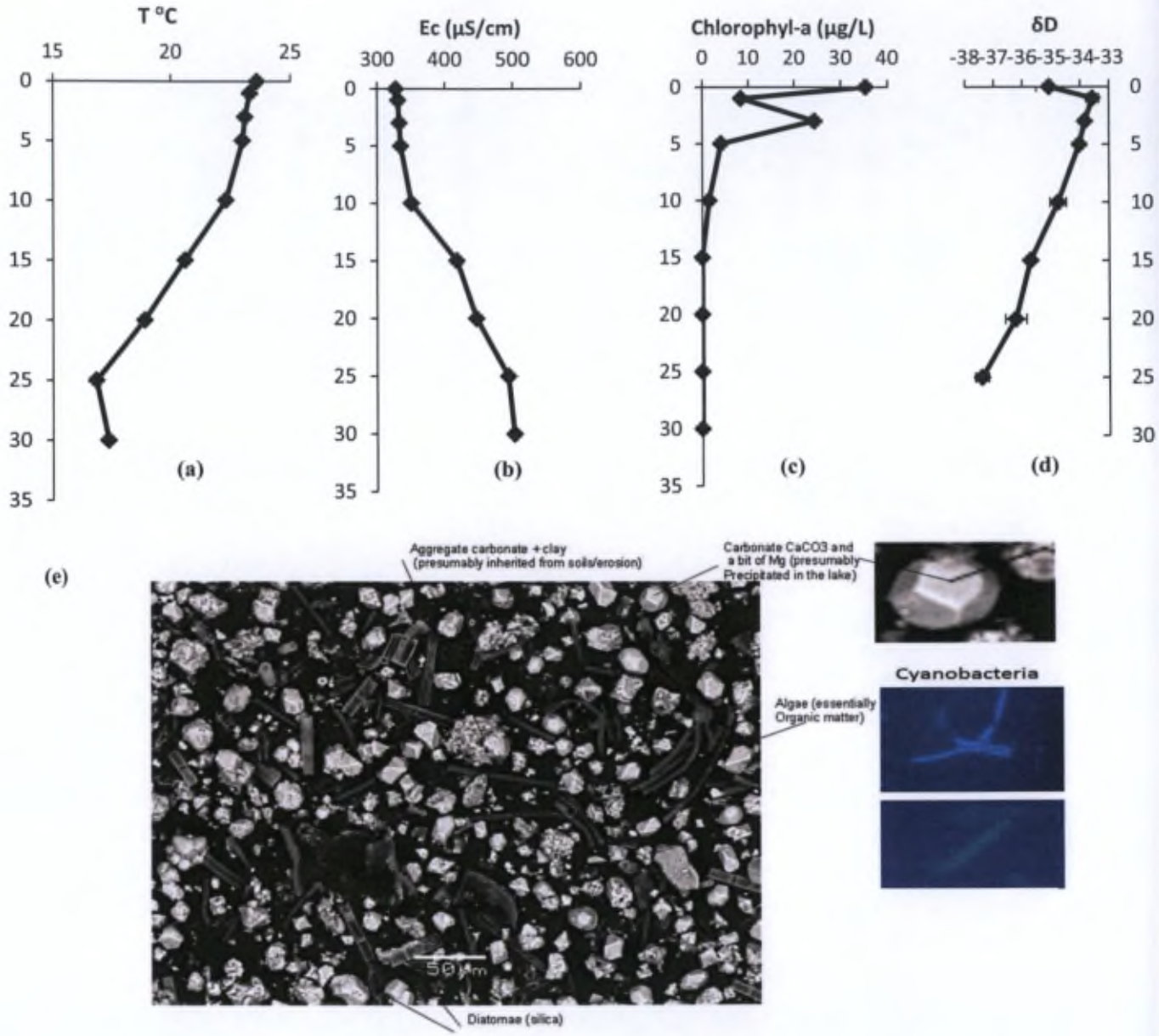

Figure 6.7: Vertical distributions of (a) temperature, (b) electrical conductivity, (c) chlorophyll-a, (d) dD, showing respectively thermal, chemical, biological and isotopic stratification, (e) reservoir eutrophication leading to biogenic preciptaion and alternation in the biogeochmical setings of the dam.

6.3.4 Hydrological and chemical connectivities of the system

6.3.4.1 Hydrologic connectivity

Environmental isotopic ratios of oxygen and deuterium were used to investigate the water infiltration from the reservoir to the surrounding piezometers during both hydrological modes. The hydrological setting of the reservoir was explained in details in a previous work (Ammar et al., a submitted); however, the interaction of the reservoir with groundwater is presented in this work. The environmental isotopic investigations in both fill and spill modes in the reservoir and the adjacent piezometers denote the strong hydrological connectivity between surface water and groundwater (Figure 6.8). The plot of water samples between global meteoric water line (GMWL) (Siebert et al., 2009, Develle, 2010) and local meteoric water line (LMWL) (Saad et al., 2006) signifies the seasonal influence of precipitation and evaporation on the reservoir. In Figure 6.8, samples located to the right of GMWL are subjected to evaporation enrichment during spill hydrological regime (Halder et al., 2013), and those located on the GMWL and/or LMWL are more influenced by precipitation (Cartwright et al., 2012). As a consequence, samples located between the two lines are the mixing results of the mentioned groups which will be further explained in Chapter 7 (Ammar et al., a submitted). In addition, samples located to the left of LMWL indicated by circles and squares in the same figure characterized by the lightest isotopic signature are the result of snow melting and recharge from higher altitudes during the transition season (June 2012)[12] (Cartwright et al., 2012). However, the variation in isotopic signature of groundwater in the investigated hydrological mode shows their recharge by multisources, and their rapid response to the changes in the reservoir. During fill mode, piezometers are influenced mainly by precipitation. However in spill mode, the data on piezometers are plotted close to that of the reservoir signatures in Figure 6.8, which indicates the important impact of the reservoir on their isotopic signature. The isotopic compositions confirm the water infiltration from the reservoir to surrounding piezometers thus aggravating the hazard of metal behavior in sediments during spill mode. Therefore, the mobilized metals from the reservoir sediments during the spill mode pose a potential hazard for the groundwater quality.

[12] See Annex 5 for reservoir water chemistry during transition season.

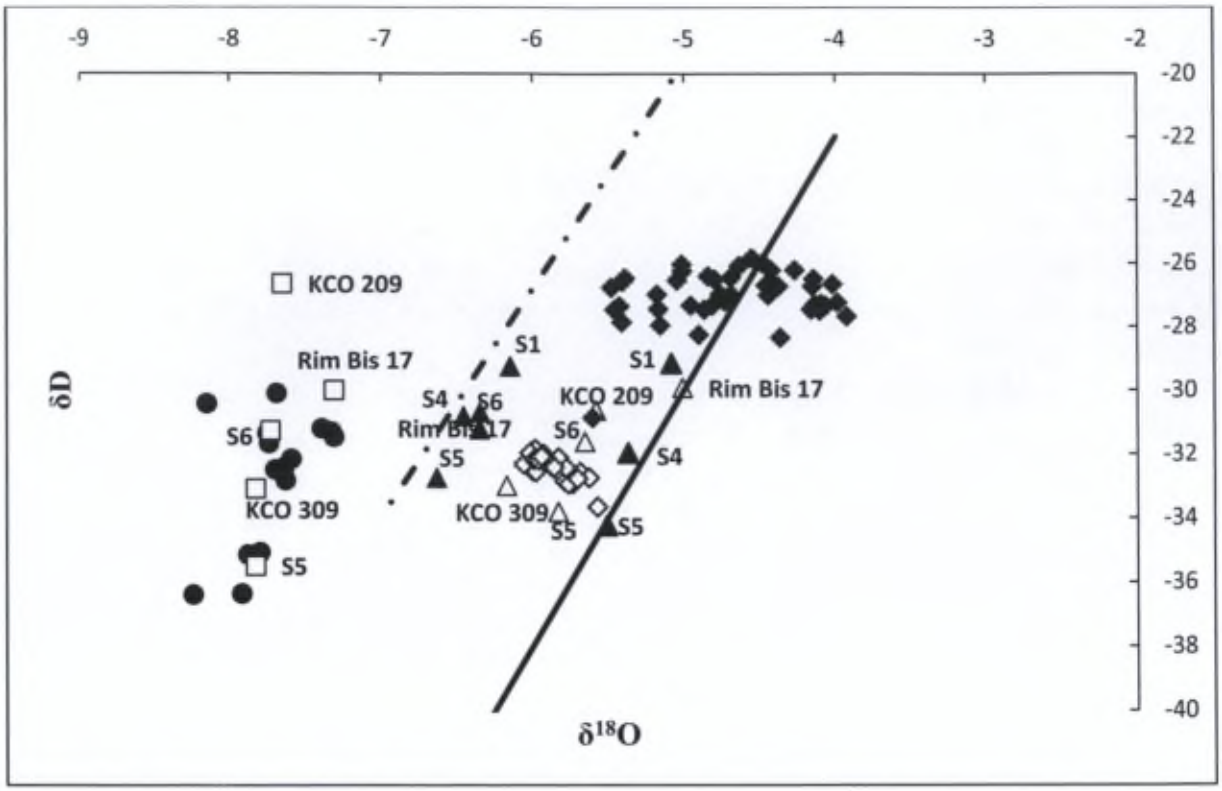

Figure 6.8: Strong hydrological connectivity between reservoir (diamonds) and piezometers (triangles) during both fill (open symbols) and spill (filled symbols) and their rapid response to changes in the upper watershed (2011-2013). Data on piezometers (□) and reservoir water (●) during transition season in June 2012 are also shown.

6.4.3.2 Chemical connectivity

In the fill hydrological mode, the hypolimnion is depleted in heavy isotopes and has a similar isotopic ratio to groundwater represented by both $\delta^{18}O$ and δD (Figures 6.9a and 6.9b). Groundwater inflow can change water quality in the hypolimnion; even more, it can breakdown stratification (Krivtsov and Sigee, 2005). Contrary to the conditions in the fill mode, water at the hypolimnion level in the spill mode is enriched with heavier isotopes where certain piezometers are affected by the reservoir water (Figures 6.9e and 6.9f). Furthermore, the limnology of the piezometers (Table 6.5) reflects a similar water composition as observed for the reservoir water[13]. For example, similar TDS values are found in piezometer S6 (315 mg/L) and RM Bis 7 (283 mg/L) as compared to those for the reservoir hypolimnion (308 mg/l) in the spill mode (Figure 6.5c). High altitude springs owe their high TDS loads to the sediments (Jeelani et al., 2011). This agrees well with a previous study which reported that the Qaraaoun reservoir is recharging the surrounding piezometers (Saad et al., 2009).

During the fill mode, the concentration of dissolved Pb fluctuated in the water column but showed an increasing trend with water depth (Figure 6.9c). Similarly, particulate Pb

[13] See Annex 8 for detailed physicochemical data of piezometers

increased at depth but with larger fluctuations (Figure 6.9d). The dissolved Pb concentration in the water column above the retrieved sediments ranged between 0.2 to 0.4 µg/L. The Pb content in the suspended matter increased from 45 µg/g at the water surface to 354 µg/g at 30 m depth, suggesting the enrichment of Pb close to the sediment-water interface in the dam zone. The dam zone in the fill mode is expected to have a quiescent hydrological regime favorable for deposition of fine particles. This partitioning of Pb between the dissolved and particulate phases and the similar concentration gradients along the water column suggest a downward transport direction where particulate Pb will precipitate out and deposited at the water-sediment interface. The low concentration of Pb measured in the piezometers as compared to those measured in the hypolimnion exclude the possibility of Pb leaching from the sediment with the infiltrated water (Figure 6.9c). It appears that particulate Pb deposition at the sediment surface is the main transport process of Pb from the water column to the sediment bed similar to other reported results (Chon et al., 2012). However, in the spill mode, dissolved Pb concentration in the hypolimnion is higher than that in the epilimnion (Figure 6.9g) whereas the particulate Pb is still enriched in the hypolimnion with higher concentrations than those measured in the fill mode. The concentration of dissolved Pb in the groundwater in the spill mode is higher than that in the fill mode (Figures 6.9c and 6.9g). Moreover, it is higher in the groundwater than in the hypolimnion during the spill mode. This could be explained by the fact that dissolved Pb may originate from the resuspended sediments, enriching the hypolimnion, but it may be ultimately transported by the infiltrated water to groundwater.

Table 6.5: Limnology of hypolimnion at Dz and the surrounding piezometers during spill hydrological mode.

Piezometer	pH	Ec (µS/cm)	TDS (mg/L)	CaCO3 (mg/L)
S1	7.91	200	136	157
S4	7.59	220	150	193
S5	8.29	119.6	81	101
S6	7.24	463	315	361
RM Bis 17	6.91	416	283	330
Dz Hypolimnion	7.47	450	308	328

Finally, the transition between the fill and spill hydrological modes is characterized by groundwater influx at the bottom of the reservoir as reported by Ammar et al., a (submitted). Low river flow accompanied with water withdrawal by the hydropower turbines under high temperature conditions will result in high primary productivity. It appears that the reservoir is subjected at this stage to stratification as indicated by the thermal and chemical trends shown in Figure 6.7. The thermal gradient manifests in 7 degrees difference from surface to bottom (Figure 6.7a), whereas the chemical gradient manifests in an increase in electric conductivity by about 175 µs/cm along the depth (Figure 6.7b). The thermal and chemical downward gradient trend is opposed by an upward gradient trend for both biological and isotopic indices. The intense biological activity is revealed by the high chlorophyll-a concentration in the top 5 meters with the highest level of 35.4 µg/L at the water surface (Figure 6.7c). The

environmental isotopes analyses using deuterium show unexpected isotopic ratios; the highly heavy isotope-depleted water at the bottom can only be explained by an external recharge from either high altitude or snow thawing at the bottom of the reservoir (Cartwright et al., 2012). As a consequence, the water column appears to be under chemical stress exerted by the river inflow and phytoplankton in the top layer, and subjected to vertical water mixing induced by the groundwater influx (Figure 6.7d) (Ammar et al., a submitted).

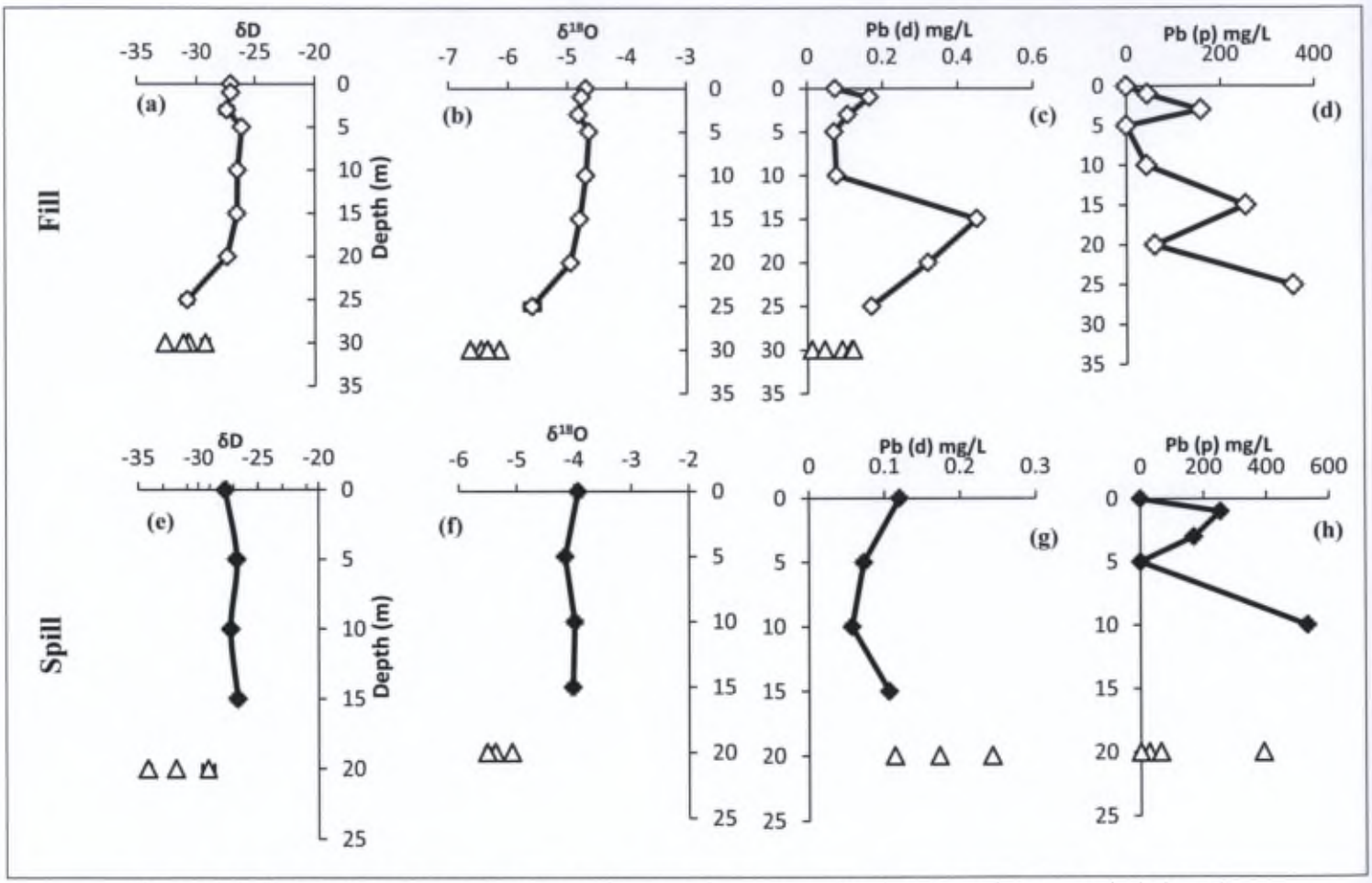

Figure 6.9: Enviromnetal isotopic ratios indicating the water infiltraion from the reservoir (♦) to the adjacent peizometers (Δ) where Pb is remobilized from the sediment and migrates with reservoir water to groundwater in spill mode (October 2012) in Dz.

6.3.5 Reservoir vulnerability and capacity to retain and liberate chemicals

The collected historical data over a period of five years reveal the capacity of the reservoir to retain chemicals (Figure 6.10). The electric conductivity measured a few km away from the reservoir at Jeb Janinne, which is a representative point for the collective water quality brought up by the Litani river main course, nine (9) tributaries and surface runoff, is higher than the measured Ec at the reservoir (Figure 6.10). The drop in the measured Ec in the reservoir could be a result of precipitation in the more alkaline water of the reservoir and the

reservoir hydrodynamics. It appears that the reservoir sediments are responsible for this retention capacity and they show the ability to control reservoir physicochemical settings.

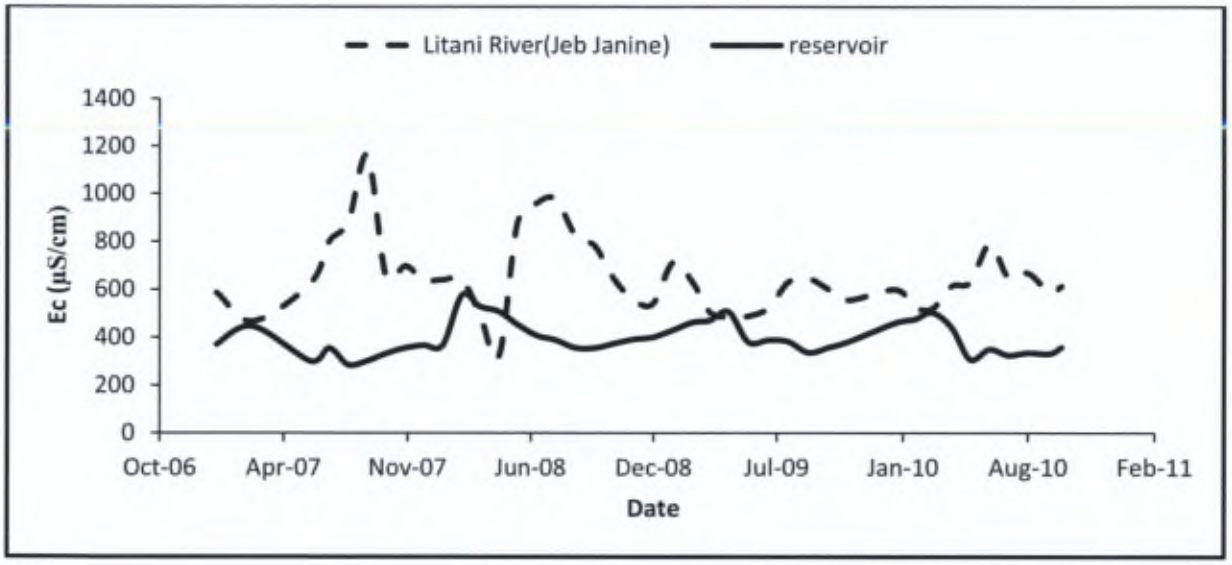

Figure 6.10: Reservoir vulnerability at the watershed scale and its capacity to retain and liberate chemicals, showing that endogenic process dominates over the watershed impact. Data were provided by the Litani River authority.

Table 6.6 summarizes the water quality data for water entering and exiting the reservoir for the fill and spill hydrological modes. The water entering the reservoir at the level of epilimnion is labeled (in) whereas the water exiting the reservoir at the level of the turbines at the hypolimnion level in the dam zone is labeled (out). In the fill mode, a slight increase was observed in the concentration of Ca, Mg, Al, Ni, Cu, Zn and Pb in the hypolimnion as compared to the concentration of the same chemical species in the water entering the reservoir. Even though during the fill mode the incoming water is more mineralized as compared to the incoming water in the spill mode, the incoming water during the spill mode is more enriched in anthropogenic heavy metals such as Cu, Zn, and Pb. Furthermore, the water exiting the reservoir during the spill mode is more enriched in chemicals and heavy metals as compared to the incoming water in the spill mode and the exiting water during the fill mode. The exiting water in the spill mode is enriched in metallic pollutants as a result of chemical accumulation in the heavy water layer at the hypolimnion and the leaching of chemical species from the resuspended sediments (§ 6.3.2.2.2).

We can estimate mass fluxes of chemical species exiting the reservoir by multiplying the dam outflow (10.05 m^3/s) by the concentration of chemical species at Dz hypolimnion (below 10 m) during the spill mode (Peretyazhko et al., 2005). This indicates that water used for irrigation has the following fluxes for metals: Co (3.43 kg/day), Ni (1.02 kg/day), Cu (1.01 kg/day), Zn (5.21 kg/day), and Pb (0.4 kg/day). Furthermore, the nutrient fluxes are estimated to be 1.4 tons/day for NH_4^+, 3.4 tons/day for NO_2^-, and 7.2 tons/day for NO_3^-. Finally, 3.4 tons

of Cl/day are exiting from the reservoir during the spill mode which threatens to salinize the agricultural soil and increase metal bioavailability.

Table 6.6: Physico-chemical parameters and dissolved metal concentrations in the incoming water and outgoing water of the reservoir during both fill and spill hydrological modes.

Parameters		pH	T °C	DO (mg/L)	Alkalinity (mg/l)	Ec (µS/cm)	Ca (µg/L)	Mg (µg/L)	Al (µg/L)	Mn (µg/L)	Co (µg/L)	Ni (µg/L)	Cu (µg/L)	Zn (µg/L)	Pb (µg/l)
Fill	In	8.1	15.2	5.1	176.2	511.2	60.0	15.28	26.15	1.85	3.94	1.16	0.54	2.96	0.19
	Out	8.2	12.4	6.9	156	518.5	61.7	15.34	31.41	0.46	3.93	1.60	0.70	3.16	0.33
Spill	In	7.9	25.8	6.3	208.7	344	37.5	15.2	4.23	0.52	3.94	0.84	0.89	3.3	0.43
	Out	7.7	25.3	6.4	211	337.5	38.3	15.9	3.53	0.62	3.95	1.18	1.17	6.0	0.54

The water quality in the spill mode should receive more attention since this water is used for irrigation during the dry months. In the long term, the concentration of anthropogenic fluxes of chemical species entering the reservoir will increase due to the increasing industrial and agricultural activities in the basin. This will threaten the quality of water exploited from the reservoir and the hydropower project sustainability. As a consequence, the water pumped from the reservoir to the irrigation canal (canal 900) will be enriched with contaminates leading ultimately to accumulation of toxins in the food chain. Furthermore, the increased nutrient flux during the warm spill hydrological mode will induce biofilm proliferation, menacing the turbine and the canal activity.

6.5 Conclusions

As a consequence of the reservoir hydrological settings and the water physiochemical characteristics, the hydrological and biogeochemical processes induced a vertical downward transport of chemicals towards the fine grained calcareous sediments during the fill mode. In contrast, during the spill mode the sediments acted as a source for a chemical flux upward through the water column and downward toward groundwater. The sediments behavior and reservoir eutrophication in the spill mode impacted significantly the quality of the water exiting the reservoir in the hypolimnion near the dam zone. However, local hydrodynamics and sediment behavior buffered partially the chemical and thermal stress on the reservoir water quality during the fill mode. The geomorphological features of the reservoir situated in a Mediterranean semi-arid area enhanced the strong hydrological connectivity between surface water and groundwater where the reservoir responded quickly to natural and anthropogenic changes in the upper watershed. The water used for irrigation is enriched in metals and nutrients such as nitrogen in addition to chloride, which threatens to salinize the agricultural soil and increases metal bioavailability and its potential to bioaccumulate in the food chain. Moreover, the nutrient enrichment in the water withdrawn from the reservoir will induce algal growth that may lead to turbine biofouling thus disturbing irrigation canal activity and hydro-project sustainability. The water quality in the spill mode should receive more attention due to its potential hazard for the hydro-project and the sustainability of the agricultural soil in the long term.

According to chapter six, the reservoir is not acting as an entity of one hydrological unit but it is divided into different sections vertically and transversely. Where the water quality entering the reservoir is different from that is exiting due to biogeochemical interferences. It is also evident that hydroclimatological impacts have a great influence on the reservoir hydrodynamics. Furthermore, the reservoir indicated a strong hydrological connectivity with groundwater by which water is infiltrating from the reservoir and recharging the surrounding piezometers. In parallel, a groundwater source might exist, and disturbing the chemical and thermal gradient of the reservoir which was never been detected before. Thus, a detailed hydrological study is needed to explore the water cycle, trace hydrological routes, and address water recharging area for the sensitive reservoir. The influence of geomorphological terrain and the complex microenvironment that bears tough orographic structure in a continental basin, creates an interesting study area that join the Mediterranean semi-arid climate and the impact of mountains on water cycle. Consequently, the natural geomorphological facts and the findings of the previous chapter are motivating to explore the internal hydrological settings of Qaraaoun reservoir, and its response to seasonal meteorological and anthropogenic changes. Water environmental isotopes will guide us to delineate groundwater interaction in both ways from the reservoir and into the reservoir. Coupling isotopic study to water physicochemical characteristics will assist in designing the water mixing lines, and assigning the major hydrological units and layers in the reservoir that have an environmental value. The acquired knowledge of lake type, nature and behavior under different environmental conditions and in different sectors of the reservoir will be essential for risk assessment plans. This investigation should give indications of the water quality and its variation spatially and seasonally thus curators in LRA can control the periods and locations of water withdrawn from the reservoir. Thus efficient and particular management plans can be dedicated for hydropower project sustainability. The outcome of this study could be extrapolated to similar basins in the world either situated in semi-arid climate or under the influence of orographic effect.

Chapter 7

Hydrodynamic influence on reservoir sustainability in semi-arid climate: physicochemical analysis coupled to an environmental isotopic study

Abstract[14]

Water scarcity and the increasing demand lead to the necessity of developing water management plans, such as establishment of artificial lakes and dams. However, the uprising challenges are to improve the water quality and the sustainability of hydro-projects in the long term. In order to understand the water cycle and to assess the geomorphological and environmental impacts on a reservoir located in an intensively used agricultural watershed under a Mediterranean semi-arid climate, environmental isotopes coupled to physicochemical studies were investigated over biannual cycle. The particularity of semi-arid climate and the diverse topography generates both continental and orographic rain effect on the isotopic composition of precipitation and recharged sources. The reservoir responds quickly to land-use activities and climatic changes where its isotopic composition responds to seasonal and spatial variations. Based on chemical stress and internal hydrodynamic processes, the reservoir can be divided into different water sectors that undergo temporal and spatial variation and highlight its interaction with groundwater. River inlet exerts a chemical stress on the upper 5-10 m of the reservoir and dominates over lateral runoff. Based on environmental isotopic signatures, this study demonstrates for the first time the occurrence of groundwater inflow to the central and dam zones of the Qaraaoun reservoir inducing vertical mixing. Thus river flow and groundwater influx could modify the hydrological settings of the reservoir where groundwater acts as a dilution factor by renewing the bottom layer and minimizing the reservoir response to internal biogeochemical reactions and external hydrological variations. A great attention should be devoted to the hydrogeological location of planned reservoirs that should be constructed in the vicinity of shallow water table to insure water quality and sustainability.

[14] Adapted from the submitted article (Ammar R, Kazpard V, El Samrani AG, Amacha N, Saad Z, Chou L. Hydrodynamics influence on reservoir sustainability in semiarid climate: physicochemical analysis coupled to environmental isotopic study. Submitted to Journal of Hydrology; hydrol16716, under review).

7.1 Introduction

Lakes and reservoirs are a key player in hydrological water cycle; these water bodies denote the interaction between surface water and groundwater and act as a sink of natural and anthropogenic fluxes that will affect the total nutrient budget in hydrographic basins (Froehlich et al., 2005). As a consequence, scientists have established the foundations of environmental applications of isotopes in the past 60 years in order to understand the hydrogeochemical cycles and regulate enactments for both water and waste management (Masson and Meilliez, 2008; Wei et al., 2009; Hoefs, 2009; Meredith et al., 2009; Akin et al., 2010). Water Stable isotopes became a robust tool to investigate hydrological processes such as addressing water source, tracing water flow dynamics, and defining mixing patterns under seasonal and spatial variations. Water isotopic signature is the outcome of evaporation and mixing of rain water with the composition of water body present (Petelet-Giraud et al., 2007). Small lakes and reservoirs are much more sensitive to climate and anthropogenic changes, where water stable isotopes are used to fill hydrological gaps to trace the origin of water source and to track its pathway over a specific watershed (Butler, 2007; Kumar et al., 2008; Singh et al., 2010). Furthermore, it is a promising approach to study lakes and groundwater recharge due to its conservative behavior and resistance to water-rock interactions (Grünberger et al., 2004; Froehlich et al., 2005; Petelet-Giraud et al., 2007; Gibson and Reid, 2010; Wassenaar et al., 2011; Al-Charideh, 2012).

Isotopic fractionation is strictly associated to open water systems such as lakes and reservoirs (Huang and Pang, 2012). Since lakes are more subjected to evaporation, as a result they are more enriched in heavier isotopes (^{18}O and ^{2}H) compared to rivers, tributaries and precipitation. Seasonal overturns and wind induce lake mixing; some undergo a complete mixing, others are subjected to seasonal stratifications (Froehlich et al., 2005; Boehrer and Schultze, 2008). In the contrast, groundwater preserves its isotopic composition unless it is recharged by different sources (Froehlich et al., 2005). Recharge sources in aquifers are precipitation, snow melting, surface runoff and water used for irrigation (Butler, 2007; Develle, 2010). Surface-ground water interaction is magnified in desiccated watersheds due to increasing water demand and intensive groundwater withdrawal. As a consequence in arid and semi-arid areas, both surface water and groundwater are subjected to salinization due to increasing land-use changes, exploitation, irrigation and land-use activities. In addition, soil salinization due to plant evapotranspiration and fertilizer application will mobilize minerals that will be transferred ultimately to groundwater (Huang and Pang, 2012). Furthermore, slight climatic fluctuations has a noticeable impacts on semi-arid water catchments (Wassenaar et al., 2011); therefore isotopic composition of surface water in these areas is in disequilibrium with evaporation, thus enriched in heavier isotopes.

Numerous studies were conducted to investigate both natural and anthropogenic impacts on the evolution of water quality worldwide. Surface-groundwater interaction was observed in global basins (Petelet-Giraud et al., 2007; Singh et al., 2010; Yin et al., 2011; Cartwright et

al., 2012; Diaw et al., 2012), and many studies focused on hydrological cycles in arid and semi-arid watersheds (Bouchaou and Michelot, 1997; Meredith et al., 2009; Gibson and Reid, 2010 Wassenaar et al., 2011). While few investigations were devoted to study the hydrochemical processes in the semi-arid areas of the Eastern Mediterranean regardless its particularity and environmental complexity in Egypt, Turkey, Jordan, Palestine, Syria and Lebanon (Sultan et al., 2000; Schemmel et al., 2013; Siebert et al., 2009; Khayat et al., 2009; Al-Charideh, 2012; Saad et al., 2005, 2006, 2009).

Mediterranean rain is subjected to evaporation and thus has high d-excess values of around 22‰ compared to Global Meteoric Water Line GMWL: $\delta D = 8\delta^{18}O + 10$ (Siebert et al., 2009; Develle, 2010). However, the Lebanese local meteoric water line was delineated as $\delta D = 7.13\delta^{18}O + 15.98$ (Saad et al., 2005), where evaporation enrichment of rainfall is taking place in November. Furthermore, the rain isotopic fractionation is influenced by altitude effect, where rain is isotopically depleted in $\delta^{18}O$ in the inland semi-arid areas compared to the coast (Saad and Kazpard, 2007). Previous studies on the Litani River have focused on water quality evaluation in river, reservoir, and adjacent piezometers. Saad et al., (2006) have stated that Qaraaoun reservoir is a warm Monomictic lake isotopically enriched compared to the river by 3 ‰ in $\delta^{18}O$ and 10 ‰ in $\delta^{2}H$, which is well mixed in winter and stratified only in summer with no spatial variation observed. Furthermore, artificial infiltration from the reservoir to groundwater was observed and estimated to be 28.5 % at the reservoir entrance compared to 20.7 % at the dam (Saad et al., 2006). Additionally, altitude thermal gradient influence highly the isotopic fractionation in the Bekaa (Develle, 2010). As δD and $\delta^{18}O$ composition of aquifers in the area are altitude dependent, more negative values were observed in Cenomanian aquifers compared to Jurassic and Eocene (Awad, 2011, 2013). Upper cretaceous groundwater has typically depleted isotopes (Al-Charideh, 2012).

Qaraaoun reservoir is a delicate hydrogeochemical system which is directly impacted by alternations of the microclimatic conditions and evolution of the drainage basin. It has comparable features with natural and artificial lakes located in arid and semi-arid areas with complex topography and under increasing environmental stress. Few studies investigate the isotopic response of both natural and anthropogenic changes in semi-arid artificial lakes either temporally (seasonal short and/or annual long terms) or spatially. Studying hydrogeochemical cycles in dammed reservoirs is crucial for the determination of water recharge areas and the assessment of potential contamination sources and fate in order to preserve groundwater sustainability, dam functioning, and efficient management plans in the basin.

Thus, stable isotopic ratios of $\delta^{2}H$ and $\delta^{18}O$, in addition to physicochemical parameters, coupled to hydrological and meteoric data were studied in the Qaraaoun reservoir of the Litani basin (Lebanon) over two annual cycles (2011-2013). This study aims (1) to investigate hydrochemical processes in a reservoir in semi-arid areas and to evaluate their impact on water quality and sustainability in long term, (2) to understand the isotopic response of a Fill and Spill system represented by the seasonal variation of the Dam Lake, and (3) to identify the spatial interaction of the reservoir with the upstream flow from both

river and lateral seepage in addition to groundwater inflow, and (4) to highlight the longitudinal and transversal mixing zones and to characterize the different hydrological components in the system. This study was conducted to build a solid background for future water management plans and dam functioning sustainability with the purpose of improving water quality in countries suffering from scarce water resources.

7.2 Background

7.2.1 Geographic location, Geology and Topography:

Litani Basin is the largest water basin in Lebanon, where the non-transboundary Litani River (170km) crosses it longitudinally from the North-East to South-West, and drains into the Mediterranean Sea (Figure 7.1). Litani watershed or so called Bekaa plateau stretches over a surface area of 2.17 km^2 with a mean altitude of 800 m above sea level (a.s.l). The basin is fringed by rain shadow flanks of Lebanon Mountainous chain from the west (highest summit 3087 m) and Anti-Lebanon chain from the east (highest summit 2800 m) (El Fadel et al., 2003; FAO, 2008; Develle et al., 2010; Awad, 2011). The orographic structure of high steep slopes induces crustal erosion from soil superficial strata. The geological age of Litani watershed dates back to Mid Eocene, where the plain is overlaid by a Quaternary alluvium limestone with a chalk and marly chalk outcrop that ranges in thickness from 150 to 900 m; also, alluvial soils are covering the central and western reaches of the basin (Edgell, 1997; Walley, 1997; FAO, 2008).

Both surface and groundwater serves to fulfill the needs of 160 communities composed of 350000 habitants, almost 10% of the total Lebanese population (BAMAS, 2005; Saad et al., 2009). Bekaa Valley serves 40% of the total national cultivated area (FAO, 2008). According to a statistical study conducted by ministry of agriculture (1998), the Litani basin is the major producer in the country regarding industrial agricultural yields (62 %), cereals and legumes (57 %), vegetables (57 %), fruit and olive trees (37 %). However, this basin is subjected to enormous environmental stress, since it is historically known as a major agricultural area but now witnesses multi industrial practices expansion after the dam construction. The zone of the watershed extending from the natural source to the dam is called upper Litani basin (ULB) representing 70% of the total watershed area (Ramadan et al., 2013) (Figure 7.1), where 67 dumpsites are found in the basin with a total surface area that equals 429150 m^2. Dumping leakage reaches the river banks and the lake boundaries. In addition, both river and reservoir receive untreated wastes from more than 288 industrial factories, hospitals, and farms in addition to its historical practices of agricultural activities.

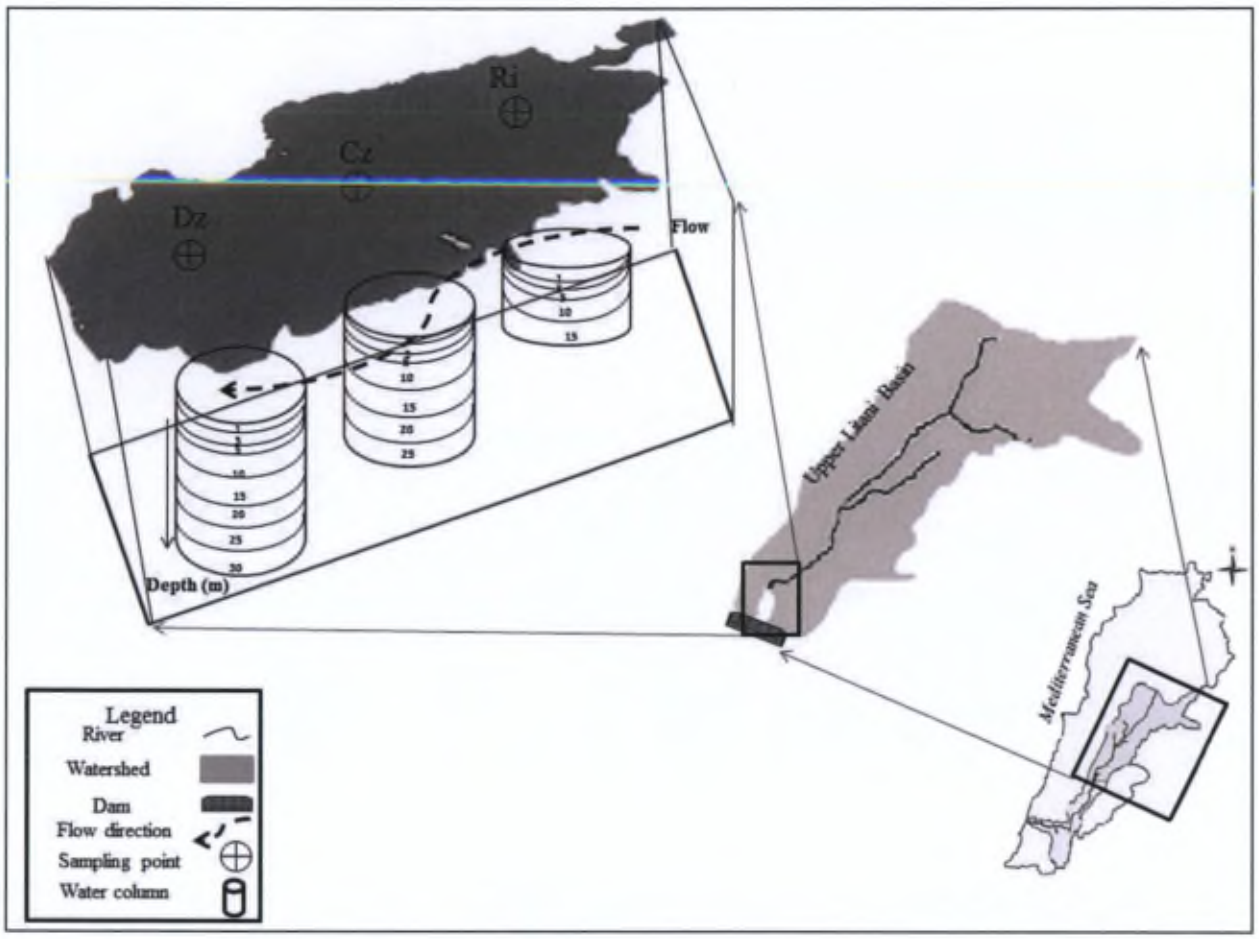

Figure 7.1: Sampling locations of the water columns collected in the river inlet (Ri), central zone (Cz) and dam zone (Dz) in the Qaraaoun reservoir, Upper Litani Basin.

7.2.2 Climate and Hydrology:

The Mediterranean Sea is the origin of precipitation in the studied area, by which the basin receives between 700 and1000 mm/y as mean annual precipitation (Develle et al., 2010; Awad, 2011). The inland Litani basin tolerates a continental semi-arid climate affected by the Mediterranean. The collective impacts of the Bekaa diverse topography, its proximity to Mediterranean influence from west, in addition to Syrian Desert in the north-eastern reaches, create specific microclimates with drastic varying temperatures, humidity values and precipitation distribution in the region (FAO, 2008; Ramadan et al., 2013). The rainy season extends from November till May by which 90 % of the precipitation falls in winter, followed by a severely dry season from May till September. The temperature ranges mainly from 5°C to 26°C in winter and summer respectively with an average annual temperature of 16°C. However the mean annual evaporation in the Bekaa plain is 1200 mm/y with maximal

recorded values in July (FAO, 2008, Ramadan et al., 2013). Humidity is high at the coast and decreases toward the Bekaa plain ranging thus between 35 and 75 %. Orography plays an important role in micro-climate changes, where snow falls 30 days/y on the mountains flanking the basin (El Fadel et al., 2003; Develle et al., 2010).

The Litani River has an annual average discharge of 9.34 m^3/s and a volume of 750 million cubic meters (MCM). As part of the national water management plan, the Qaraaoun Dam was constructed in 1955 to terminate Litani river flow in a 2.2 km^2 reservoir, for hydropower production and irrigation. The dam in Qaraaoun village is 110 m long and 61 m wide and stores water delivered by the Litani main river, nine tributaries, surface runoff, and groundwater discharges from the upper drainage area which is estimated to be 2180 km^2. The reservoir has a minimum allowed volume of 40 MCM, though 70 % of the total water volume (220 MCM) is used to produce electric power via al Zahrani electric power plant during full capacity (El-Fadel et al., 2003; Saad et al., 2006; Assaf and Saadeh, 2008; FAO, 2008; Saad et al.,2009). Furthermore, the Qaraaoun reservoir is aiming to supply more than 22000 hectares of cultivated land with irrigating water (30 MCM/y) via Canal 900.

7.3 Materials and Methods

7.3.1. Data source

Dam hydrology data, including the Litani River inflow, water level in the reservoir, and water outflow to Markhaba electric power station, were monitored and provided by the Litani River Authority (LRA) for the past years. Air temperature, relative humidity, and precipitation were measured at the nearest station to the reservoir in Kherbit Kanafar on a daily basis during the study sampling period.

7.3.2 Sampling program

Sampling schedule was chosen to cover both temporal and spatial variations in order to distinguish potential sources that could contribute to the isotopic fractionation of reservoir. Therefore, field surveys were conducted over two annual cycles (2011 – 2013) during which 4 sampling campaigns were carried out each year: at the end of the dry season (September), first flush (October/November), mid of the rainy season (February/April), and at transient season (May-June). In order to trace the water source and to follow the recharge pathway in the lake water column, hydrogen and oxygen water isotopes were utilized due to their accuracy and specificity. Water samples were taken from the Qaraoun reservoir (33.5° N and 35.6° E), from three fixed sampling locations that passes latitudinally across the middle of the lake (N-S) using the LRA Zodiac boat. Additionally, 2 minor locations at the central transversal cross-section of the reservoir on both eastern and western sides were sampled to identify the possible lateral runoff. The first sampling point Dz is located near the dam zone, sampling point Cz is in the center of the reservoir and point Ri is in the river inlet zone which is the entrance of the reservoir as shown in Figure 7.1. Water samples were collected using a

depth dependent sampler along the water column at successive distances of 5 meters each, with a higher sampling frequency at the top 5 meters to investigate the biological activity at the level of epilimnion. Water level increased up to 16 meters during the winter of 2012 compared to summer, where full capacity of the dam was reached. Water pH, temperature, electric conductivity (Ec) and total dissolved solids (TDS) were measured simultaneously on board using respectively a pH meter (HANNA pH211 microprocessor pH meter), conductivity-meter (WTW cond i), and a portable LaMotte pocket multi Tracer-1766. Water samples were filtered directly onboard over 0.45 µm ministart filters. The filtrates were stored at 4°C in 50 ml polyethylene tubes filled to the brim to avoid any water evaporation prior to analysis. Oxygen and hydrogen stable isotopes in water samples were measured using a Liquid Water Isotope Analyzer (LWIA-24d) with a precision of <0.1 ‰ for $\delta^{18}O$ and <0.3‰ for $\delta^{2}H$. Isotopic ratio was expressed as delta notion ($\delta^{18}O$-$\delta^{2}H$) and six measurements are performed according to a standard calibration curve using V-SMOW certified standards in consistency with IAEA norms.

7.4 Results and discussion

7.4.1 Closed system (no groundwater inflow: Ri zone)

According to the river discharge data of the Litani (Figure 7.2a) two phases are observed for the river flow regime: high flow rate during the wet season (Jan-Feb-March) and low flow rate during the dry season (July-Aug). River high inflow in addition to maximal recorded precipitation from November till March (Figure 7.2b) exhibits an increase in the reservoir water level (fill mode) that reaches its full capacity during April and May (855-860 m a.s.l.). Reservoir's water level decreases to its minimal allowed capacity (spill mode) during November-January (835-840 m a.s.l) as a result of low precipitation, high evaporation and increasing water pumping during the dry summer (Figures 7.2a and 7.2b). In response to river inflow behavior, reservoir water salinity obtained by measured electric conductivity and total dissolved solids shows a similar trend and increases in rainy season. In this case, water mineralization as shown by the high electric conductivity and the TDS measurements (Figure 7.3) is induced by intensive runoff in the Basin reaching the reservoir either by river course or by direct lateral flows (Singh et al., 2010). The chemical stress was exerted not only on the surface water, but also on the water column during the wet season where Ec increased by almost 200 µS/cm compared to the dry season at the Ri (Table 7.1).

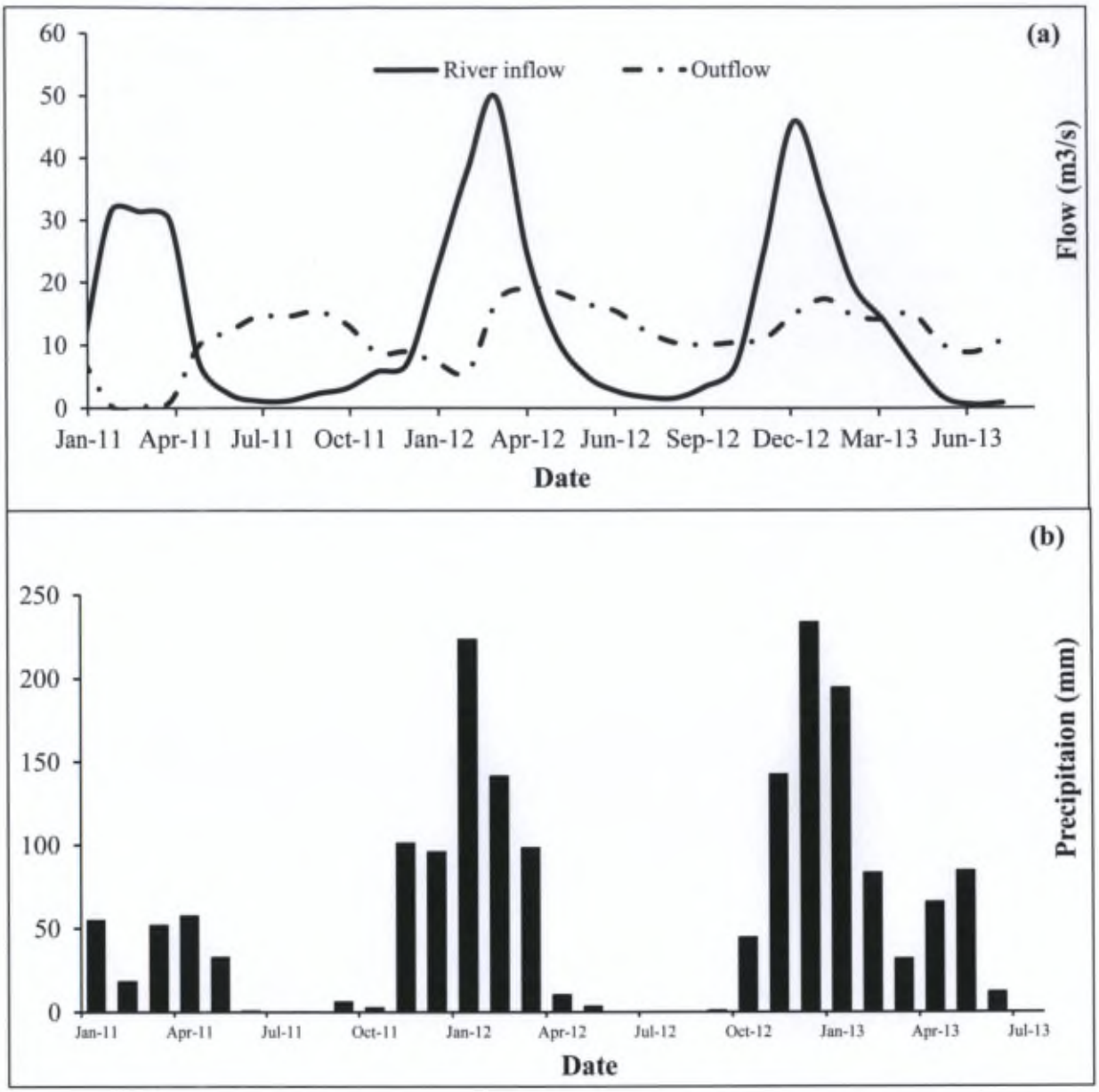

Figure 7.2: (a) Seasonal river inflow and water outflow from the reservoir during the study period (2011-2013), (b) Seasonal precipitation during the study period (2011-2013).

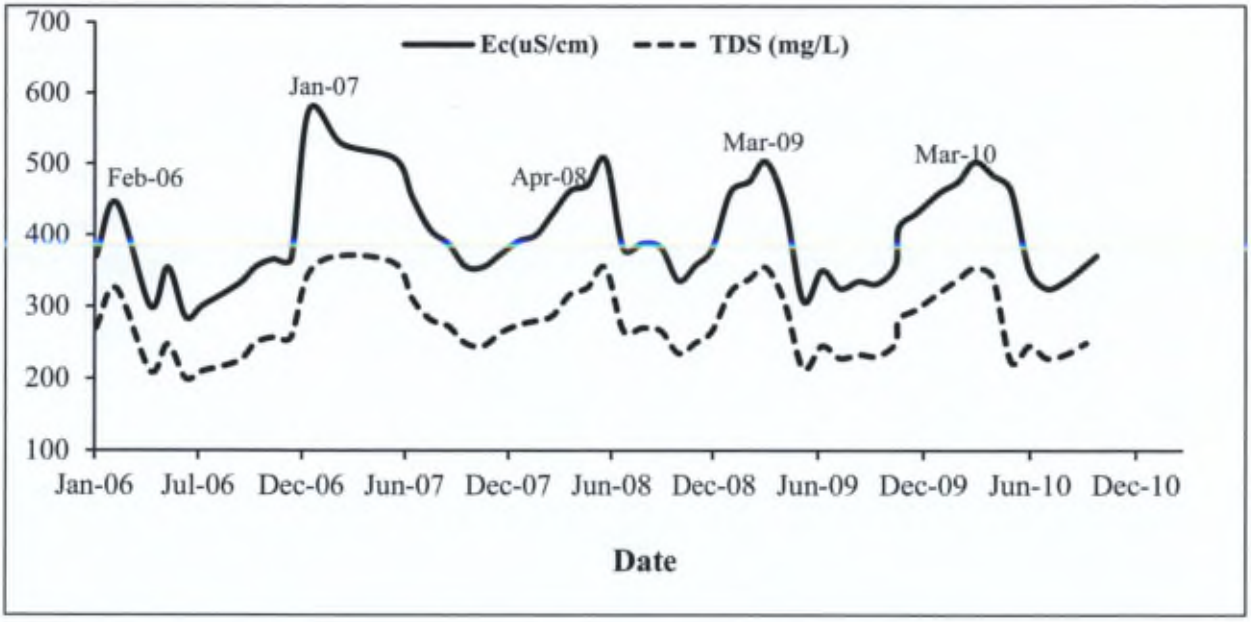

Figure 7.3: Historical annual records of electrical conductivity (Ec) and total dissolved solids (TDS) of surface water in the reservoir showing mineralization during the wet season.

Table 7.1: Physicochemical parameters and environmental isotopes ratios at Ri during dry and wet season[15].

Sample		Depth m	pH	Temp °C	Ec µS/cm	$\delta^{18}O/^{16}O$	σ ($\delta^{18}O/^{16}O$)	$\delta^{2}H/^{1}H$	$\sigma\ \delta^{2}H/^{1}H$	d-excess
Sep 2012	Ri 0	0	8.47	na	337	-4.71	0.034034	-28.22	0.236291	9.44
	Ri 1	1	8.30	na	340	-4.7	0.02	-28.9	0.08165	8.70
	Ri 3	3	7.93	na	343	-4.62	0.053151	-28.62	0.204939	8.36
	Ri 5	5	6.99	na	356	-4.63	0.025	-28.3	0.08165	8.80
	Ri 10	10	7.87	na	349	-4.60	0.025	-29.27	0.095743	7.59
April 2013	Ri 0	0	8.14	15.70	513	-6.12	0.017321	-34.75	0.250383	14.24
	Ri 1	1	8.05	15.10	512	-6.27	0.02	-33.57	0.181475	16.58
	Ri 3	3	8.08	15.10	512	-6.26	0.017321	-33.41	0.14	16.67
	Ri 5	5	8.23	15.10	508	-6.16	0.0263	-32.84	0.045826	16.50

The particular position of river inlet (Ri zone) that merges the river with the reservoir, renders this area to be under the direct influence of the main river. Furthermore, the shallow water level at Ri induces its vulnerability to increased turbidity brought by the river to the reservoir. Figure 7.4 summarizes the seasonal variation of Ec and environmental isotopes on the epilimnion (top 5 m) at the Ri during the study period, where high electric conductivity (500-

[15] All isotopic data during the study period are presented in Annex 9.

550 µS/cm) is conjugated with depleted $\delta^{18}O$ (-5.82 & -6.21 ‰) and depleted $\delta^{2}H$ (-32.51 and -33.65 ‰) during the wet season. Precipitation in the studied area is subjected to seasonal variation due to the mountainous topography and the varying air temperature. Secondary evaporation under cloud level is more pronounced during precipitation in warmer spring and fall compared to rainfalls during colder seasons, which results in heavier isotopic signatures of the first flush (October and November) (Develle et al., 2010; Wassenaar et al., 2011). The depleted isotopic signature in the reservoir is related to the low isotopic signatures of the continental precipitation, and snow thawing recharge that increases the river flow during winter which is subjected subsequently to evaporation and as a result to enrichment during dry summer for both $\delta^{18}O$ (from -4.3 to -4.6 ‰) and $\delta^{2}H$ (from -25.92 to -27.24 ‰) isotopes. The observed seasonal and annual isotopic variation in the reservoir reflects environmental changes and due to the limited catchment area the $\delta^{18}O$ in the reservoir responds rapidly to minor changes in $\delta^{18}O$ in the precipitation (Teranes et al., 1999).

The measured Ec was the highest at Ri during both dry and wet seasons compared to Cz and Dz at the top 5-10 m (Figures 7.5a and 7.5c). This salinity is acquired by Ri due to its vicinity to river inflow, which transport all the dissolved ions and transmit them progressively to the Cz and later to the Dz as a result of dam hydrodynamics. The water current is forced to follow the old river course at the bottom of the reservoir, in addition to the suction force of the turbine that creates a preferable flow direction towards the dam. At Ri during the dry season, Ec increases from 337 µS/cm at the surface to 356 µS/cm at a depth of 5 m while pH decreases from 8.47 to 6.99 (Table 7.1). Vertical profiles of the isotopic signatures indicate an isotopic stratification accompanied by the chemical layering, where $\delta^{2}H$ signatures decrease from -28.22 ‰ to -29.32 ‰ (Figures 7.5b and 7.5d). Correspondingly, computed d-excess values ($= \delta^{2}H - 8\delta^{18}O$), used to define the hydrological process, decrease from 9.44 to 7.59 from surface to 10 m depth (Table 7.1), indicating evaporation (Mayr et al., 2007; Diaw et al., 2012). In attempt to assess the contribution of evaporation to environmental isotopic signatures scientists rely on deuterium excess values in relation to salinity, where the increased salinity due to mineral dissolution and evaporation induces chemical and isotopic stratification as a result of evaporative enrichment in heavier isotopes during summer (Meredith et al., 2009). In the current case study, during the wet season at Ri Ec decreases with depth while $\delta^{2}H$ isotopic ratios and d-excess increases (Figures 7.5c and 5d, Table 7.1). The contrasting behavior of $\delta^{2}H$ during the wet season results from water recharge rich in dissolved ions but depleted in heavier isotopes due to continental precipitation that is impacted by orographic rain from the upper basin (Jonsson et al., 2009; Singh et al., 2010).

Ri zone is a regular hydrological unit which resembles a closed water system immune to groundwater inflow, but sensitive to seasonal variations subjected to mixing during winter and stratification during summer thus creating heavier water rich in ions at the bottom. As a consequence, if water used for irrigation is pumped from a reservoir of a closed system such as Ri, then the water will be of poor quality and a risk of salinization will occur, followed by

soil degradation that could threaten ultimately the groundwater by its deterioration in the long term.

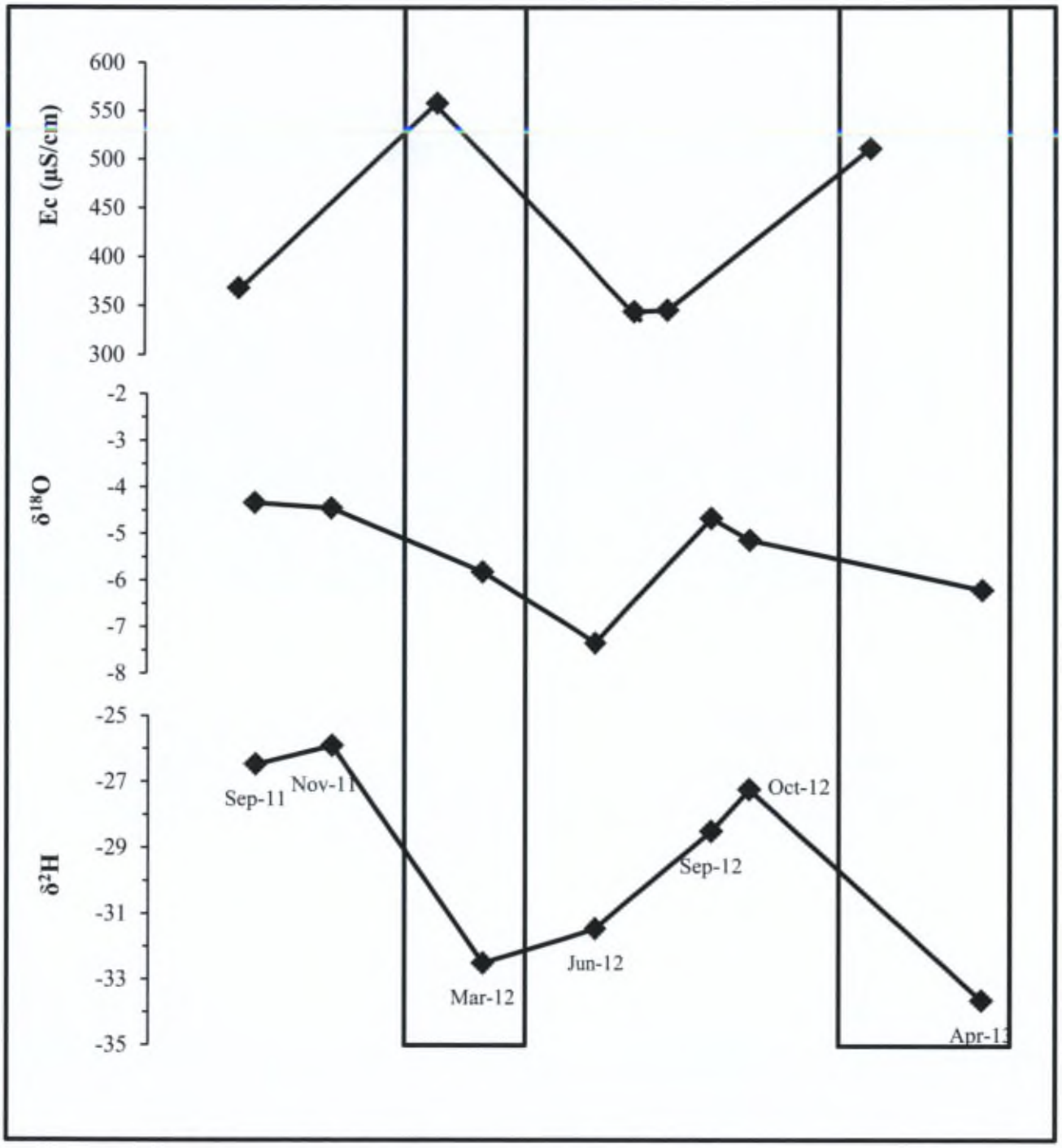

Figure 7.4: Temporal variation of electrical conductivity and water isotopic signature of surface water, showing anti-correlation in between water mineralization and $\delta^{18}O$ and $\delta^{2}H$ during dry and wet seasons.

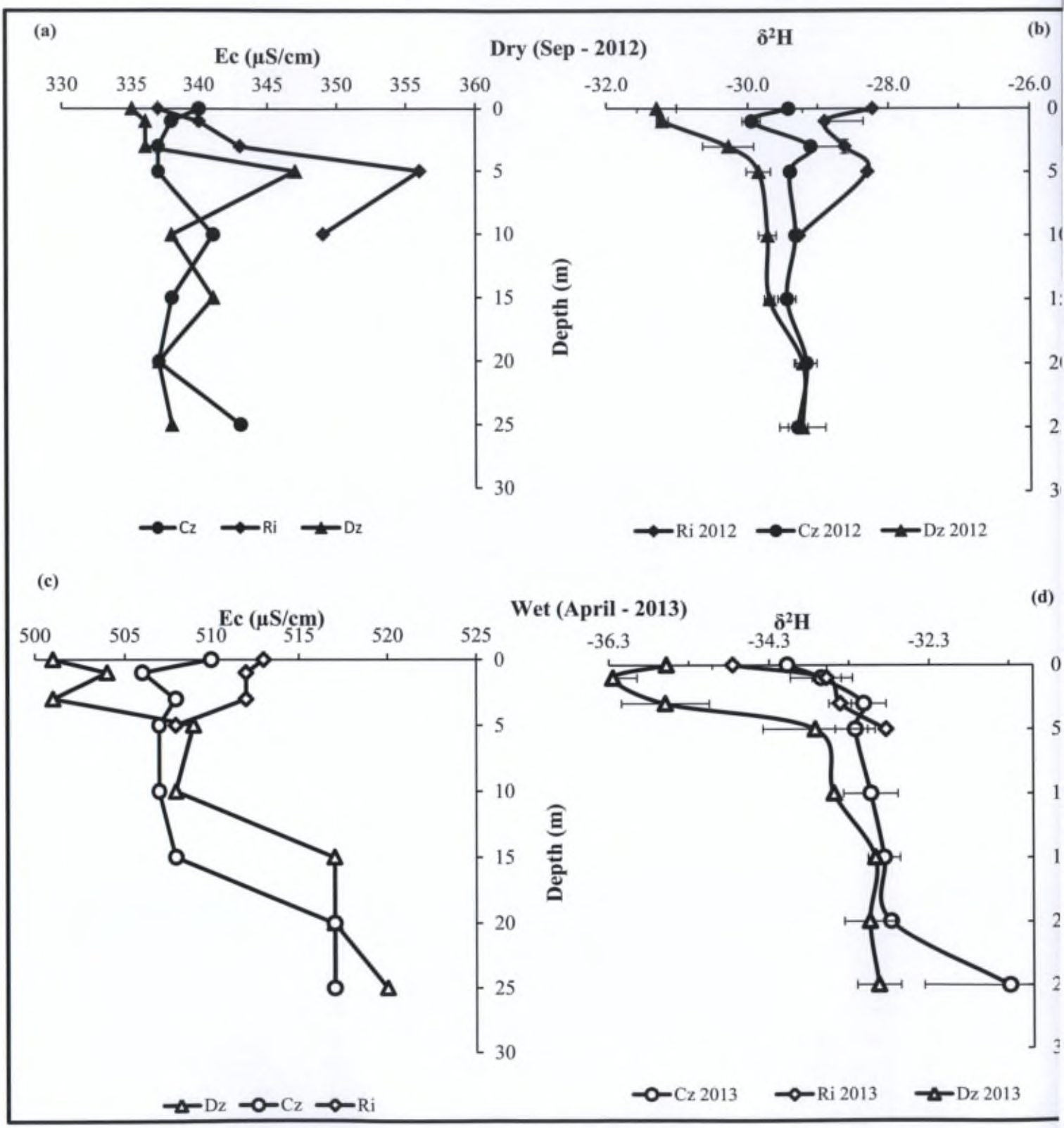

Figure 7.5: Seasonal and spatial variation of Ec and hydrogen isotopic signature in the reservoir during second annual cycle 2012-2013.

Physicochemical parameters and environmental isotopic ratios for both dry and wet seasons at east and west sides of the reservoir in the Cz and Dz zones show insignificant lateral variation (Table 7.2). In contrast to the Ri (Table 7.1), east and west sides of the reservoir exhibit similar Ec values and isotopic ratios for both seasons. When compared to Cz and Dz (Tables 7.3 and 7.4), waters of the lateral sides of the reservoir exhibit similar properties of the surface water at Cz or Dz. Thus impact of the lateral flow on reservoir is of minor importance compared to the dominant influence of Ri, especially in dry season. As a result Ri is under the influence of the river and responds quickly to any climatic or land-use changes. Furthermore, it acts as a second point source and exerts a chemical stress for the upper 10 m of central and dam zones of the reservoir.

Table 7.2: Physicochemical parameters and environmental isotopes ratios at lateral slides of the reservoir during dry and wet seasons.

Sample		Depth m	pH	Temp C°	Ec µS/cm	$\delta^{18}O/^{16}O$	σ ($\delta^{18}O/^{16}O$)	$\delta^{2}H/^{1}H$	$\sigma\ \delta^{2}H/^{1}H$	d-excess
Sep 2012	Es	0	8.20	na	339	-5.3125	0.078049	-28.62	0.377492	13.88
	Ws	0	8.37	na	339	-4.6	0.040415	-28.08	0.109545	9.24
April 2013	Es 0	0	8.53	15.70	508	-5.85	0.005	-34.71	0.175309	12.15
	Es 1	1	8.60	14.30	507	-6.02	0.011547	-32.27	0.341858	15.89
	Es2	2	8.59	14.10	505	-5.96	0.066833	-32.92	0.290803	14.76
	Ws0	0	8.70	16.10	492	-5.75	0.175119	-30.09	0.793788	15.91
	Ws1	1	8.68	14.60	507	-5.79	0.140089	-35.34	0.214321	11.00
	Ws2	2	8.58	14.20	507	-6.11	0.02708	-33.62	0.484458	15.26

7.4.2 Open system (groundwater inflow: Cz and Dz zones)

During the dry season (spill mode) in September 2012 (Figure 7.5) and October 2012 (Table 7.3), Cz shows no significant changes in measured Ec and pH values, also only a weak thermal stratification is present. Unexpectedly there is no isotopic stratification due to evaporation in summer, both hydrogen and oxygen isotopic ratios in the water column exhibit comparable ratios. The fairly homogenous water column at Cz observed during low river flow in summer has an isotopic signature more depleted in $\delta\ ^{18}O$ compared to what is brought by Ri, thus suggesting a possible groundwater influx at the bottom which leads to a vertical mixing throughout the water column (Jonsson et al., 2009; Merdith et al., 2009). This is consistent with the fact that the aquifers in the studied area are karstic and the water table is shallow (Saad et al., 2009; Awad, 2013). In contrast, in the wet season during the reservoir fill mode period, Ec is higher at the bottom (517 µS/cm) compared to the water layer above (508 µS/cm), and a weak thermal stratification is also observed. In addition, hydrogen and oxygen isotopes show an isotopic stratification but in an unexpected sense by which lighter water is present at the top, and heavier water at the bottom coupled with higher ion content (Figure 7.5d). Thus the mixing process observed in summer is disrupted during winter due to

chemical stress exerted by the Ri on Cz. The local precipitation with a more negative isotopic signature has an impact on the top layer (5-10 m) of the water column, while the groundwater inflow characterized by higher Ec and TDS values with cooler water temperature dominates the water nature at the bottom (20-25 m). The water at the bottom layer of Cz in winter is isotopically heavier compared to the water column above. This enrichment could be due to its recharge during the summer and/or to the infiltration through the flood plains of the return flow of water used for irrigation (Diaw et al., 2012), creating a heavier water layer at the bottom level that prevents its mixing with the upper water layers.

The water at Dz is less mineralized but contains a higher alkalinity than that of Cz and Ri in the upper 5-10 m during both seasons (Figure 7.5). This depth may represent the intrusion of the river inflow layer through the reservoir, where Cz is more impacted by Ri and acts as a transition zone to Dz. The dam zone acts as a barrier for the water flow due to the presence of the dam which influences also the hydrodynamics. Chemical stratification was observed at Dz as shown by a rapid increase of Ec and decrease of pH in the upper water column during the spill mode in late summer (Figure 7.5a, Table 7.3). The Dz exhibits also a week thermal stratification (Table 7.3), in addition to an isotopic stratification with lighter isotopes at the surface and heavier ones at the bottom (Figure 7.5c). Nonetheless, the isotopic signatures in the upper 20 m of the water column at Dz are more negative compared to those observed at Ri and at Cz. The same phenomenon of groundwater influx may also occur at Dz, in addition to the likely biological interference owning to the calm water flow in this zone. The favorable conditions in the top layer of Dz may allow the proliferation of the algal blooms, which consume preferably the lighter isotopes for the photosynthesis of organic matter in the top layer (Hofes, 2009). The dam zone receives the groundwater inflow from the bottom which is more representative during late summer (Table 7.3). In the rainy season (fill mode), chemical stratification as shown by the increasing Ec and H^+ concentration from the surface to bottom is accompanied by a slight thermal stratification (Table 7.4). There is however no isotopic stratification at the Dz and the groundwater influx induces a vertical mixing (Figure 7.5d) (Halder et al., 2013). Water resources are highly impacted by climate fluctuations in the Levant region (Develle et al., 2010). Thus, during the wet season the groundwater nourishing Cz and Dz owed its more depleted nature, compared to the dry season, to the depleted isotopic recharge from orographic impacted rain and snow thawing (Wassenaar et al., 2011; Halder et al., 2013), which flowed spontaneously into the reservoir. However during water scarcity in summer, the groundwater exhibits less depleted signatures and this might be due to the multivariate sources. These inputs include the return flow of irrigated water (Diaw et al., 2013), rapid infiltration of heavy precipitation to the fractured karstic aquifer (Bouchaou and Michekot, 1997; Develle et al., 2010; Yin et al., 2011), and infiltration and mixing of groundwater with isotopically heavier wastewater (Singh et al., 2010) since the Bekaa valley is characterized by shallow groundwater table that is vulnerable to land-use impact (Bulter, 2007; Awad, 2013). Therefore, the groundwater is flowing into the reservoir as a result of hydrostatic processes of turbine water withdrawal and decreasing water level in the reservoir (Kumar et al., 2008). Similar observations have been made where old aquifers recharge shallow ones due to extensive water pumping for hydropower production and irrigation

during dry summer, and groundwater flows to the reservoir from the karstic aquifers in order to establish the hydrostatic equilibrium (Al-Charideh, 2012).

Table 7.3: Physicochemical parameters and environmental isotopes of Cz and Dz at the end of Summer (Oct 2012).

Sample		Depth m	pH	Temp C°	Ec µS/cm	$\delta^{18}O/^{16}O$	σ ($\delta^{18}O/^{16}O$)	$\delta^{2}H/^{1}H$	$\sigma\ \delta^{2}H/^{1}H$	d-excess
Cz	Cz0	0	8.58	14.5	510	-6.84	0.085264	-34.07	0.498899	20.63
	Cz1	1	8.66	13.8	506	-6.74	0.091104	-33.64	0.38863	20.24
	Cz3	3	8.60	13.7	508	-6.40	0.033665	-33.12	0.277549	18.08
	Cz5	5	8.66	13.8	507	-6.17	0.042426	-33.22	0.247167	16.14
	Cz10	10	8.60	13.7	507	-6.11	0.136717	-33.03	0.340135	15.83
	Cz15	15	8.48	13.9	508	-6.08	0.110868	-32.86	0.199729	15.79
	Cz20	20	8.16	12.7	517	-6.21	0.038341	-32.78	0.078049	16.91
	Cz25	25	7.93	12.6	517	-5.96	0.15327	-31.29	1.07677	16.37
Dz	Dz0	0	8.79	14.70	501	-7.45	0.097767	-35.58	0.065574	24.00
	Dz1	1	8.69	14.20	504	-7.04	0.041932	-36.25	0.30348	20.09
	Dz3	3	8.73	14.00	501	-7.34	0.080416	-35.595	0.548969	23.13
	Dz5	5	8.52	13.80	509	-7.24	0.045092	-33.7233	0.654243	24.17
	Dz10	10	8.62	13.60	508	-6.96	0.046458	-33.49	0.008165	22.21
	Dz15	15	8.28	13.10	517	-6.96	0.017321	-32.9767	0.020817	22.70
	Dz0	20	8.21	12.60	517	-6.91	0.051235	-33.0475	0.314788	22.25
	Dz25	25	8.17	12.20	520	-6.95	0.030957	-32.935	0.27258	22.69

Table 7.4: Physicochemical parameters and environmental isotopes of Cz and Dz during Winter (April 2013).

Sample		Depth m	pH	Temp C°	Ec µS/cm	$\delta^{18}O/^{16}O$	σ ($\delta^{18}O/^{16}O$)	$\delta^{2}H/^{1}H$	$\sigma\ \delta^{2}H/^{1}H$	d-excess
Cz	Cz0	0	8.22	21.2	345	-5.01	0.012583	-26.05	0.04	14.05
	Cz1	1	8.36	20.4	344	-5.01	0.021602	-26.25	0.148885	13.83
	Cz3	3	7.93	20.0	347	-4.86	0.017321	-27.47	0.150555	11.45
	Cz5	5	7.77	19.7	348	-4.9	0.06245	-28.27	0.442267	10.93
	Cz10	10	7.80	19.8	348	-4.72	0.033166	-27.21	0.049244	10.58
	Cz15	15	7.83	19.6	346	-4.84	0.017078	-26.41	0.032016	12.28
Dz	Dz0	0	8.65	20.4	342	-4.68	0.025	-27	0.174165	10.50
	Dz1	1	8.75	20.1	341	-4.75	0.028723	-26.99	0.286647	11.07
	Dz3	3	8.58	20.0	343	-4.81	0.01633	-27.34	0.527857	11.14
	Dz5	5	8.23	19.7	346	-4.63	0.031091	-26.09	0.044347	10.99
	Dz10	10	8.03	19.5	349	-4.69	0.065955	-26.47	0.157348	11.05
	Dz15	15	7.76	19.5	352	-4.79	0.023805	-26.52	0.089582	11.84
	Dz0	20	7.66	19.3	374	-4.95	0.03304	-27.34	0.202052	12.27
	Dz25	25	7.47	18.6	450	-5.60	0.133167	-30.87	0.502046	13.96

The dam zone received a great attention due to its critical position as tailwater or the source of water used for irrigation, where the turbine is located at the bottom. Figure 7.6 summarizes the evolution of environmental isotopes at Dz through the study period. The enriched isotopic

values presented during summer 2011 are homogeneous through the shallow water column (Profile 1), which is subjected to depletion during winter 2012 (Profile 2) due to isotopically depleted continental rain. However, the most depleted values were observed during June 2012 (Profile 3), which could be attributed to the groundwater inflow with depleted isotopic ratios related to snow melting and precipitation at high altitude. Water is subsequently subjected to evaporation during summer (Profile 4), which is reflected by the enriched isotopic ratios, and the 2nd cycle starts thereafter. Oxygen isotopic ratios are homogeneous, while hydrogen isotopes exhibit a slight stratification by which lighter isotopes are enriched at the surface. As mentioned in the previous paragraph, there is a groundwater influx leading to vertical mixing of the water column. This is further confirmed by the clear groundwater inflow at the bottom of the reservoir by the end of the dry season during which an accumulation at the surface of evaporated residual water with heavier isotopic signatures is also observed (Profile 5). Finally the reservoir water is depleted again in heavier isotopes (Profile 6) after receiving isotopically more depleted river water which represents the local rain in addition to groundwater inflow from the bottom. As a result of the groundwater inflow, which is more representative during the dry season due to low flow from Ri, the water column at the Dz is subjected to vertical mixing leading to a homogenized water body where the groundwater influx dilutes the residual water, thus decreasing its potential hazard (Profiles 1 and 4). However, at the end of the dry season, the groundwater table is lowered, and as a consequence its impact on the reservoir decreases allowing the thermal stratification to develop, inducing an isotopic stratification (Profile 5). This stratification is broken down after receiving precipitation and groundwater recharge with depleted isotopic signatures (Profiles 2 and 6). The transitional seasons between summer and winter reflect the lag period of groundwater recharge from snow melting and nourishing from precipitation at high altitude. The heavy water enriched in dissolved ions in summer 2011 represents the common dry years in semi-arid areas, where the enriched isotopic signature reflects the scarce raining events and low groundwater inflow of the preceding year. Hence, the residual water in the reservoir will not be suitable for irrigation in the long term and if not succeeded by heavy winters then management plans should be considered.

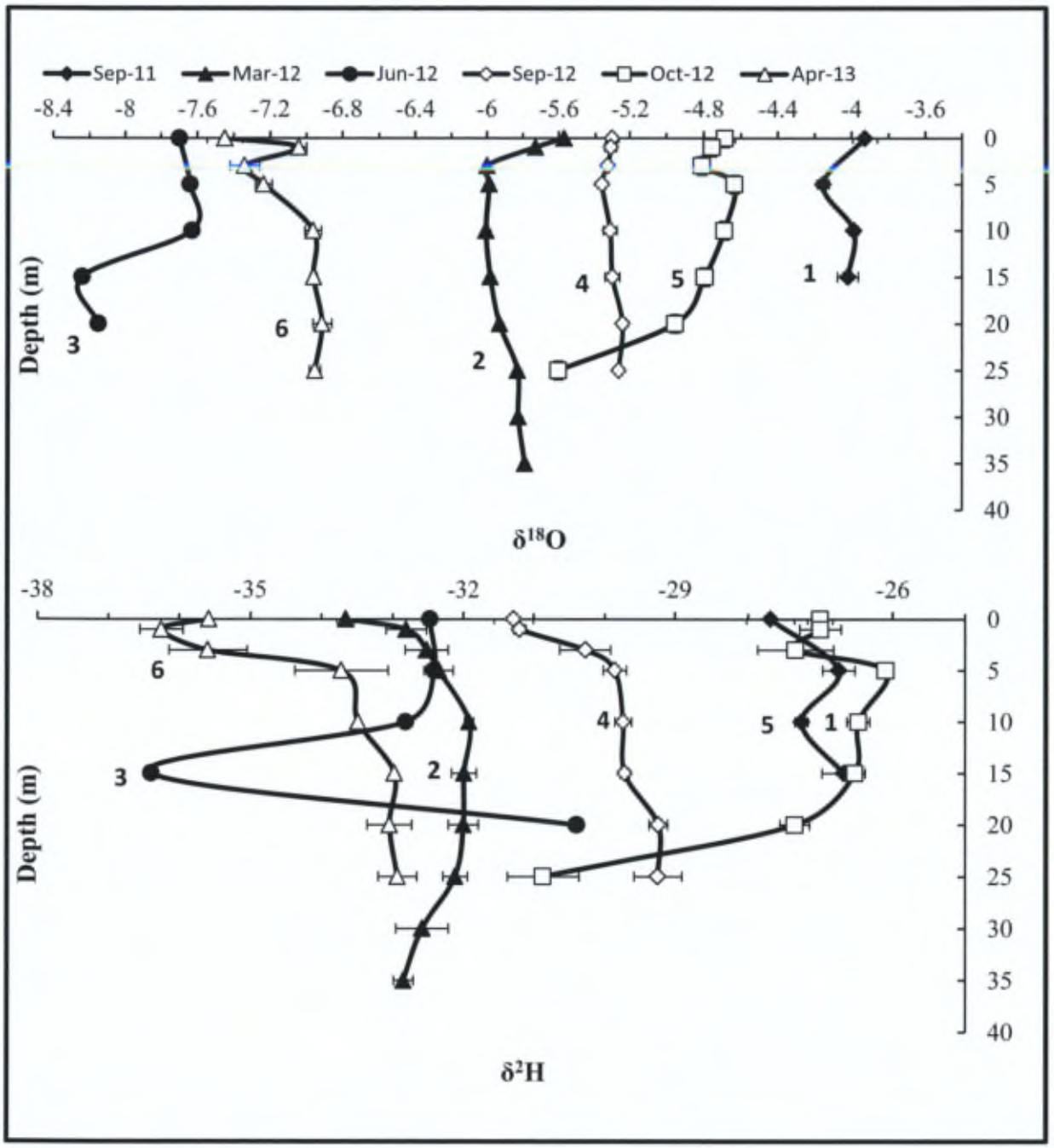

Figure 7.6: Evolution of environmental isotopes in the calm zone of the reservoir (Dz) over 2 annual cycles. The numbers indicate the profiles of various sampling campaigns (see text).

7.4.3 Isotopic response of the reservoir to climatic and land-use changes

Each lake has a different response to environmental change forcings and climatic aspects which are accurately recorded by lake isotopic compositions (Jonsson et al., 2009). Thus isotopic signatures of collective sampling locations and campaigns are presented in Figure 7.7. For the sake of clarity, GMWL ($\delta D = 8\delta^{18}O + 10$) and Lebanese LMWL ($\delta D = 7.13\delta^{18}O + 15.98$) (Saad et al., 2005) are not shown on the graph. The position of the isotopic signatures of samples in regard to the meteoric water line could reveal the hydrological settings of the reservoir (Jonsson et al., 2009), where water samples collected during the dry season locate below the GMWL would indicate their evaporation and/or recharge by evaporated sources (Halder et al., 2013). Isotopic signatures of samples collected during wet season 2012 and 2013 are scattered between the GMWL (left) and LMWL (right), except for samples taken in the transition season (June 2012 and July 2013). During storm events light isotopes would enter the water system and d-excess would be shifted to LMWL values as shown in Tables 7.1 and 7.2, compared to d-excess values in summer (Meredith et al., 2009). Nevertheless, certain samples of winter 2013 and transition season (June/July) are located above LMWL on the left. This position reflects the climatic difference between the continental rain effect in semi-arid areas and the coast (Cartwright et al., 2012) and the recharge from precipitation at high altitude where isotopes are subjected to orographic rain effect (Bouchaou and Michekot, 1997).

Isotopic signature of the reservoir water shows a strong variation between dry and wet seasons for both studied years, by which hydrogen and oxygen isotopes are depleted by 6 and 2 ‰ respectively (Figure 7.7). Then a further depletion in both isotopes by 2 ‰ range was observed at transition season between winter and summer. This depletion is caused by rainfall and thus depleted water recharge from high altitude and snow thawing reaching the reservoir form river main course, tributaries surface runoff and groundwater influx. Previous studies have found that snow thawing in the west flank of the Mount Lebanon melts and recharges directly the karstic groundwater without subjecting to evaporation (Develle et al., 2010; Awad, 2013). Thus, the increased depletion detected in transition season (June-July) where no rain events were recorded (Figure 7.7) is a proof of activated runoff of depleted water recharge from high altitudes and snow melting, which characterizes the groundwater inflow in karstic area (Gibson and Ried, 2010). The depleted isotopic ratios were compensated during the second dry season in 2012 where hydrogen and oxygen isotopes were enriched by 6 and 2 ‰ respectively as a result of evaporation and scarce raining events during summer. Thus, seasonal climate affects precipitation over the studied area, resulting in a seasonal and spatial variation in d-excess values (Tables 7.1-7.4) as revealed by the position of the isotopic composition of the reservoir water regarding to LMWL (Wassenaar et al., 2011). The increasing heavier isotopic signature during summer 2011 in the reservoir creates an unsteady state of the water system, which enhances the seasonal variation of the succeeding seasons; this variation underlines the importance of reservoir water exchange with groundwater (Froehlich et al., 2005 and references therein; Jonsson et al., 2009).

The environmental isotopic ratios of water determined during the first annual cycle (2011-2012) are more enriched compared to those of the second yearly cycle (2012-2013) that are much more depleted. A shift of -2 ‰ for δD and -1 ‰ for $\delta^{18}O$ was detected during the second annual cycle for each sampling campaign. This depletion was probably due to a heavy winter (Mayr et al., 2007) accompanied by several snow events during 2012, where the mean annual precipitation was 898.4 mm compared to 2011 (422.4 mm). Furthermore, the isotopic ratios of water collected during the 2nd annual cycle are more scattered, suggestion a variation in their isotopic nature. This variation may reflect different end member water sources; both local rain and river could contribute to the isotopic signature of the reservoir water, in addition to a third sources represented by the groundwater influx that is influenced by the recharge from high altitude and snow thawing (Halder et al., 2013). This large seasonal and annual variation reflects the rapid isotopic response of the reservoir to topographic, climatic and hydrodynamic changes in the basin.

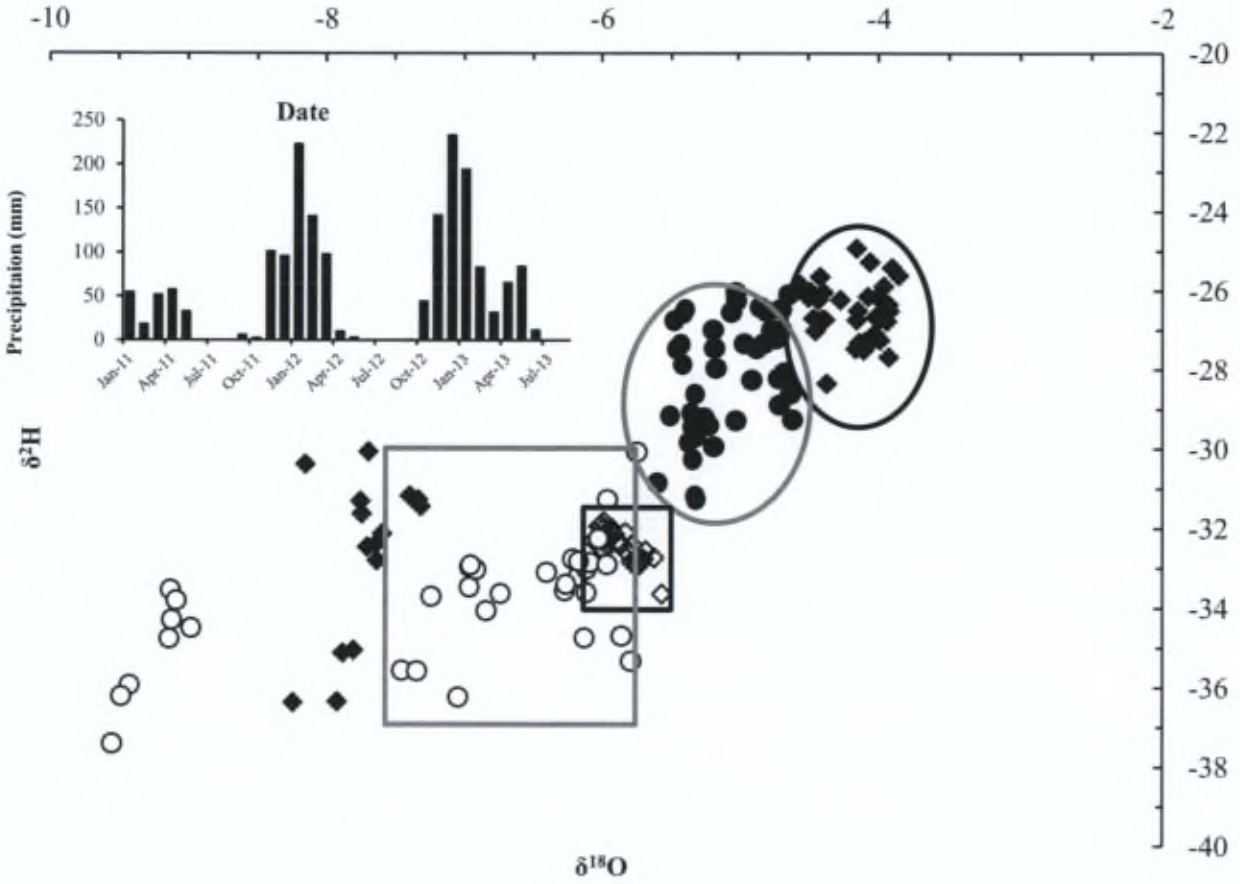

Figure 7.7: Isotopic response of the reservoir to changes in precipitation (histogram) and hydrodynamics, same characters represent the samples for each annual campaign, where closed and open characters resample samples in dry and wet seasons respectively.

7.4.4 Hydrological units and mixing depths

The meteorological characteristics of the studied area in addition to the hydrodynamic regime of the dam shows that the river flow responds to annual and seasonal climatic variations, where rainy winter followed by long dry summer characterizing the semi-arid climate is reflected on Litani River discharge. A period of one month is the lag time between precipitation and the response of increased river flow, and it requires 2 months to be reflected on the reservoir water level (Figures 7.2a and 7.2b). Water residence time in the reservoir is conditional and strictly linked to precipitation and reservoir hydrological settings, by which more water is pumped during years experiencing heavy winter (spill mode) as shown in Figure 7.2a for 2012 and 2013. Therefore, when the turbine starts pumping water from the dam zone, one can consider it as the transition stage during which the outflow is greater than the inflow. As a result, water has a residence time in the reservoir of about 4 to 5 months during wet seasons, which is fairly short (fill mode). The isotopic compositions of some sampling points fall on the GMWL during summer (Figure 7.7) indicating that evaporation does not affect significantly the reservoir water due to short water residence time and groundwater inflow. Water residence time is affected by two factors: the ratio of the lake area over the total watershed area and the elevation of the hydrographic basin; smaller basins with higher elevation are more subjected to intensive runoff with a shorter lag period influencing the water residence time (Jonsson et al., 2009). The Qaraaoun reservoir comprises 18 % of the Litani basin area and is situated at 800 m a.s.l where rain effected by elevation and snow melting reaches the reservoir fast enough to reduce the residence time of water in the reservoir which in its role reflects a seasonal variation of isotopic composition as shown by their position with respect to LMWL in Figure 7.7 (Jonsson, 2009).

The different zones (Ri, Cz and Dz) of the reservoir are presented schematically in Figure 7.8 where the various layers for each zone are also indicated. The river inflow was observed in the top layer (5-10 m) dominating Ri (Ri1 and Ri2), then water flows to Cz3 and further to Dz6 following the hydrodynamic flow and dam structure. The Epilimnion (upper 5 m) is the primary contact layer subjected to evaporation and local precipitation in addition to the chemical stress exerted by Ri. According to the physicochemical characteristics and environmental isotopic data, the top layer indicates the presence of biological activity. Nutrient discharge from agricultural and industrial activities in the basin, warm water surface and increasing light intensity in addition to calm water dynamics at Dz trigger the proliferation of living organisms (Teranes et al., 1999). The phytoplanktonic activity appears to be limited to the top 5 m where the photosynthetic organisms consume preferentially lighter isotopes leaving the water column more enriched in heavy environmental isotopes (Li et al.,, 1997; Teranes et al., 1999). Beneath the epilimnion, a mixolimnion is present (Cz4 and Dz7) where water is mixing and reflecting similar physicochemical characteristics (Tables 7.3 and 7.4) and environmental isotopic signatures that is situated between 10 and 15 m depth in summer (Figure 7.5b) and between 10 and 20 m depth in winter (Figure 7.5d). Temperature and salinity gradient through the column will help to trace the renewal water

body (Hohmann et al., 1997) where the bottom water or Hypolimnion is principally influenced by the groundwater inflow of higher salinity and cooler water masses (Cz5 and Dz8).

Studying mixing processes and indicating mixing lines will delineate the path and fate of contaminants in the reservoir (Froehlich et al., 2005; Halder et al., 2013). During the dry season, Ri is stratified and not subjected to mixing where heavy water may be created at the bottom. The dam zone is stratified only during late summer (Figure 7.6 and Table 7.3) due to accompanied chemical and thermal stratifications with isotopic stratification resulting from cumulative heavy isotope enrichment of evaporated residual water. However, in wet season, Cz is not totally mixed (Figure 7.5d) since the water in the Hypolimnion is enriched by heavier isotopes and bears higher Ec than the water column above as shown in Table 7.4. This heavy water with increased water density prohibits its mixing with the lighter layer above (Boehrer and Schultze, 2008) that is impacted by the depleted isotopes brought by Ri. This enrichment at the bottom of Cz could be attributed to a recharge of a different water source feeding the Dz, whose isotopic signature is subjected to evaporation or return flow of water used for irrigation. In contrast, a vertical mixing due to groundwater inflow is taking place at Cz during dry season and at Dz during wet season. Groundwater influx is renewing water in the bottom layer, which minimizes the lake response to both internal biogeochemical reactions and external hydrological variations on a specific time scale. A horizontal mixing may take place as well between Cz and Dz at 20 m and 25 m depth as shown in Figure 7.5 where water at these depths exhibits similar Ec values and isotopic ratios. Two water masses with different properties could mix when they meet horizontally (Hohmann et al., 1997). Thus, the varying nature of the bottom waters at Cz and Dz of different groundwater sources and the magnitude of chemical stress could allow their horizontal mixing. As a consequence, latitudinal mixing is caused by seasonal variations, while horizontal mixing is caused by seasonal flow (Froehlich et al., 2005). Stratification is due to short water residence time in a "box" which is not sufficiently homogenized due to water flow in a certain direction (Froehlich et al., 2005). The chemical stress exerted by the river inlet at the water surface (Figures 7.3 and 7.5) will induce a chemical stratification in the top layer. When epilimnion will be enriched in dissolved ions, water density will increase and indwelling trajectory in the water column will take place to reach 10-20 m. If the bottom water is denser, the mixing will not reach hypolimnion which is the case due to groundwater inflow with heavier isotopic composition and ion content in wet season. Thus, the reservoir has a partial overturn and an ectogenic meromixis will take place. However, when the reservoir is in spill mode during summer, the groundwater influx dominates over river flow thus a crenogenic meromixis will occur (Boehrer and Schultze, 2008).

Sectored lakes have varying water currents and evaporation ratios resulting in different water budgets and in turn different physicochemical and isotopic compositions (Froehlich et al., 2005). The current observation of the Qaraaoun reservoir shows a sectored lake by which natural hydrological factors divide the reservoir into two different water bodies with different

physiochemical and isotopic characteristics. Ri acts as a closed system (§7.4.1) and Cz and Dz can be considered as an open system for groundwater inflow (§7.4.2). As a consequence, utmost attention should be paid to reservoir design by which the dam location and establishment must respect specific hydrogeochemical characteristics in the vicinity of shallow groundwater table in order to allow the reservoir to compensate for the anthropogenic stress by hydrological dilution.

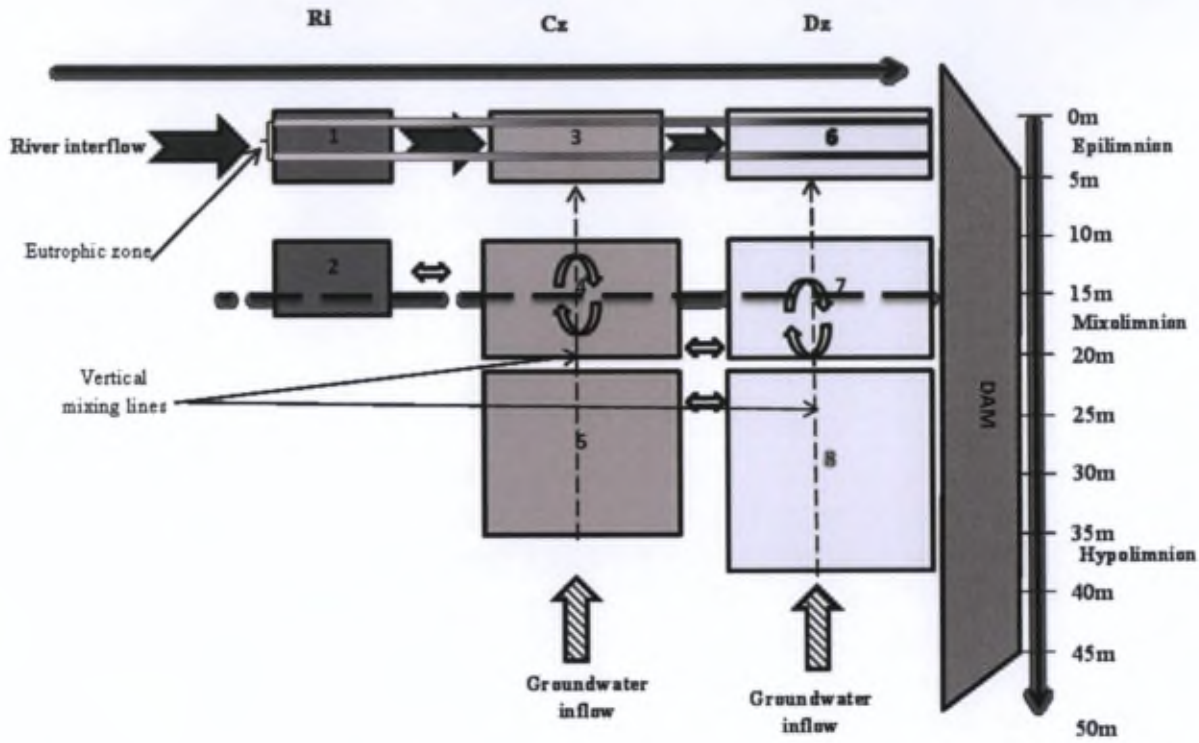

Figure 7.8: Schematic diagram showing different hydrological zones and layers, and mixing depths in the reservoir.

7.5 Conclusions:

Diverse topography and semi-arid climatic variations are reflected on dam hydrology. The short residence time minimizes evaporation impact on isotopes where no annual equilibrium is reached during fast climatic and hydrological changes of seasons thus the response is directly reflected on the isotopic composition of the reservoir. The dam lake reacts rapidly to cyclic variations of climatic changes (both continental and orographic rain effects) and land-use activities. The particularity of the reservoir is represented by two modes: the fill mode of high river flow during the rainy season combined with high mineralization and depleted isotopic composition versus the spill mode of high outflow and less mineralization with heavier isotopic composition during the dry season. The varying isotopic composition in time and space allows the identification of different water sectors in the reservoir. The river inlet acts as a closed system without groundwater intrusion where heavy water accumulates, which may act as a sink for contaminants during dry season. The Cz and Dz can be considered as an open water system subjected to dilution by groundwater inflow that causes vertical mixing and reverse stratification. Thus, the location of planned reservoirs should be established in characterized hydrogeological areas with shallow water table permitting the groundwater inflow to the reservoir. Anthropogenic stress should be compensated by hydrological dilution and the environmental impacts of artificial reservoirs should be assessed to ensure the sustainability of hydro projects in the long term. This study could be extrapolated and applied to similar areas due to its socio-economical importance and the particularity of its geographical location in a semi-arid region bearing diverse topography.

In order to complement the findings of chapter seven by modeling the reservoir hydrodynamics, to estimate the water budget and assess the possibility of reservoir self-purification or the induced hazard by contaminating the groundwater by infiltration. Previously there was a poor knowledge of hydrological routes and climatological implications on Qaraaoun reservoir water budget, thus it have not been evaluated before. Meanwhile it is feasible to estimate reservoir water budget by relying on the hydrological and meteorological data provided by Litani river authority. Furthermore, modeling the water fluxes entering and exiting the lake in a simple box model will allow us to prove the source flux to the lake and estimate its volume and assess its role on reservoir water balance. Coupling environmental isotopes from the field study with mass balance box model will allow us to reconstruct reservoir hydrological regime and estimate the impact of hydrometeorological aspects on both water cycle and water balance. Water environmental isotopes are well known for their preservative characteristics and their resistance to geochemical alternation, thus they can be used as a pioneer element to constrain the model which can be easily validated. The model robust indication will fill the gap in our knowledge regarding the hydrological routes in the Litani basin, the lagging time for groundwater recharge, and the sensitivity of reservoir response to hydrometeorological changes at the watershed scale. This simulation will further provide the quantification of groundwater source entering the reservoir, which is impossible to measure and evaluate in any other way. Further the model outcome will indicate the delta notion of the source and possible mixing processes which in its role can give evidence about the recharging zones. This model will explore the reservoir behavior in heavy rainy years and dry years typical in semi-arid areas which in its role will predict the water sustainability at the long term. The principal purpose of hydrological modeling is to provide a reliable database, simple to read by stakeholders, and aiming to create an appropriate water management plan to preserve the water sources and sustains the hydro-project. This study will be the leading example that can supply the decision makers with solid data to extrapolate this study to designed dams in order to preserve national water resources. In addition this model can be applied on similar case studies suffering from gaps in hydrological knowledge of the basins, and used as a tool to evaluate unmeasurable sources.

Quantification of groundwater fluxes using hydrological box model: Balancing the water budget of a semi-arid reservoir

Abstract[16]

Dams and artificial reservoirs are widely used as water management tools and often are characterized by strong surface-groundwater interactions. The environmental cost of dams' construction stems from alternations in hydrological regime and biogeochemical cycles as well as degradation of groundwater quality. The hydrological routes and meteorological implications on water budget can be traced by applying environmental isotopic methods, while reliable scenarios for hydrological water models can achieve efficient water management plans. Thus we will couple hydrometeorological data with the $\delta^{18}O$ water isotopic signatures to build a water budget and estimate surface-groundwater interaction with the reservoir. This study will present for the first time a simple box model derived from mass balance equations for Qaraaoun reservoir. The hydrological box model allows quantifying the seasonal surface-groundwater interaction intensity studied over a 3 years period in a sensitive semiarid basin. Results provide new insights on both surface and groundwater quality, water exchange quantity, and the isotopic signature of the source. Surface-groundwater interaction reflects a strong hydrological connectivity and quick response to hydrometeorogical changes at the watershed scale. The yearly integrated net source inflow to the reservoir is estimated to be 27% of that of the river and can trigger water purification. While average water loss from the reservoir to the underlying ground water is estimated to be 17% and could potentially threaten the groundwater table. Similar modeling approaches can be applied to other lakes and reservoirs subjected to subsurface inflow which is unapproachable for direct measurement and to be hydrologically evaluated and characterized.

[16] Adapted from the article to be submitted to Journal of Hydrology. Ammar R, Laruelle G G, Kazpard V, El Samrani AG, Amacha N, Regnier P, Saad Z, Chou L. Quantification of groundwater fluxes using hydrological box model: Balancing water budget in semi-arid reservoir.

8.1 Introduction

Dams and artificial reservoirs are widely used all over the globe as water management tools which can be designed for hydropower production purposes or water supply projects such as irrigation (Wei et al., 2009; Wildi, 2010). Fifty thousand operating dam worldwide provide 30% of all available global water resources, contribute to 40% of irrigation water and yields 20% of universal electric hydropower (Berga, 2008). Reservoirs are key components of the hydrological water cycle which, similarly to lakes, increase the water residence time in the fluvial system, thus modifying sedimentation rates and affecting nutrient transport (Akin et al., 2010; Wildi et al., 2010). These water bodies are also often characterized by strong interactions between surface water and groundwater, thus potentially affecting the chemical composition of the aquatic system. Additionally, lakes and reservoirs act as a sink of particulate material through enhanced sedimentation as a consequence of increasing residence time and trapping significant amounts of natural and anthropogenic fluxes. These modifications can lead to ecological perturbations of hydrographic basins in general and of reservoirs in particular (Froehlich et al., 2005). Dams' constructions will induce geomorphological changes, land-use transition, and demographic redistribution (Ignatius and Jones, 2014). Moreover, dams can alter nutrients loads (C, N, S, P, and Si), dissolved oxygen, and water thermal state thus triggering algal proliferation (Friedl and Wüest, 2002). Damming can also alter nutrient ratios such as Si/N or Si/P and, as a consequence, affect phytoplankton succession by favoring the growth of certain species over others (Friedl and Wüest, 2002). Most of the environmental cost of dams' construction stems from alternations in both hydrological regime and the biogeochemical cycle, and degrades groundwater quality (Wildi, 2010). During dry weather, the watershed responds quicker to hydrological changes and groundwater becomes a major source of surface flow (Fenicia et al., 2006). Surface-ground water interaction is magnified in desiccated watersheds due to increasing water demand and intensive groundwater exploitation (Huang and Pang, 2012; Meredith et al., 2009). Thus minor climatic changes have a significant influence on semi-arid water catchments (Wassenaar et al., 2011). The investigation of these systems using conservative tracers is thus required to better understand the potential effect of dams on groundwater.

Environmental applications of isotopes are a promising approach to study lakes and groundwater recharge, due to their conservative behavior and resistance to water-rock interactions (Froehlich et al., 2005; Wassenaar et al., 2011). In regions characterized by small lakes and reservoirs that are highly sensitive to hydroclimatic and anthropogenic changes, $\delta^{18}O$ and $\delta^{2}H$ isotopes are used as pioneer tool to fill hydrological gaps and denote water recharging areas and further trace water hydrodynamics at the watershed scale (Kumar et al., 2008). Previous studies used isotopic mass balance approach to characterize the water origin from the input source flowing into a lake. The isotopic signature of the source can determine whether the water comes from precipitation, rivers, groundwater inflow, and or from snow thawing (Sacks et al., 2013; Turner et al., 2010; Yi et al., 2008). Scientist used to conceptualize steady state mass balance budgets to reproduce mass isotopic balance which

ignores the variable groundwater fluxes under variant hydrostatic conditions (Sacks et al., 2013).

Mass balance equations are a projection of conservative laws of matter and energy that allow reproducing the hydrological conditions in water bodies under the assumption of homogeneity within the studied system (Edlshtein et al., 2010). Models derived from such equations are simplified representations of highly complex watershed dynamics based on geometric properties (i.e. volume) and measurements or so called hard data such as river flow, water level, meteorological data etc. (Seibert and McDonnell, 2002). In addition, such models allow estimating fluxes that cannot be measured directly. Models are able to estimate unmeasurable values and the simulation outcome can cover study compartments difficult to be sampled on field (Edlshtein et al., 2010; Seibert and McDonnell, 2002). Monthly water balance models were extensively applied and developed over the past 60 years to resolve hydrological problems and assess meteorological and topographical influence of hydrological regimes on watersheds (Xu and Singh, 1998). The popularity of this approach also comes from its flexibility, ease of use and limited data requirement (Xu and Singh, 1998). Box models are useful for solute transport in a preferable flow route, and typically used to explore water mixing processes (Seibert and McDonnell, 2002). Mathematical box models are used to investigate hydrological settings, biogeochemical processes, and flow dynamics of water bodies such as lakes, rivers, seas and even aquifers (Edlshtein et al., 2010; Fenicia et al., 2002; Nuttle, 2002; Xu and Singh, 1998). Coupling of diagnostic modelling with field studies is performed in order to reconstruct the hydrological regime of reservoirs and set management plans to sustain hydro-projects at the long term (Edlshtein et al., 2010).

Qaraaoun reservoir is a significant water supply project in Lebanon, located in the Litani watershed, which is characterized by a complex topography and endures high environmental stress. Sustainability and preservation of this hydro-project is an utmost necessity due to its national value and its role in socio-economical development. Lebanon is well known to be affected by climatic oscillation which is assumed to witness an increase in temperature and thus reduction in precipitation rates (Shaban, 2014). Litani basin will respond to the hydroclimatological alternation in the area by decrease in its runoff at the long term (Ramadan et al., 2013). Major water challenges are facing Lebanon, including geomorphological, hydrological and climatic aspects. Shaban (2014) have summarized the previous models conducted on Lebanon to investigate hydrological and climatic changes, and highlighted the deficiency of these models and their output unreliability due to lack of sufficient data. Correlation of precipitation-flow data and water balance are not available for Lebanon to demonstrate projection of water regimes at the long term. Poor knowledge of hydrological routes and meteorological implications on water budget can be solved by applying isotopic tracing methods and reliable scenarios for hydrological water models to achieve efficient water management plans (El Fadel et al., 2001; Shaban, 2014).

In this study, we present a simple box model derived from mass balance equations for the reservoir. It allows understanding the hydrological regime of the reservoir and evidences the major contribution of ground-water exchange between the bottom waters of the lake and the

water table. Conceptual box modeling utilized for hydrographic basins can be built and developed using both hard qualitative and soft quantitative data (Seibert and McDonnel, 2002). Thus in this study we will couple hydroclimatic data with the $\delta^{18}O$ water isotopic signatures to build water balance and delineate groundwater interaction with the reservoir. Due to the robust $\delta^{18}O$ indication and its more resistant to error, it was chosen instead of deuterium isotopes in the model. Using $\delta^{18}O$ isotopic measurements, the two exchanging ways between the lake and the ground water source are quantified and their seasonal dynamics is studied over a 3 years period, including fill and spill water regimes under variant meteorological conditions in a sensitive semiarid basin. These results will provide new insights regarding the water quality in surface water, which is used for irrigation in the surrounding region, replenished groundwater quality, and the isotopic signature of the source that will allow in its role to define groundwater recharging areas during different metrological conditions and through seasonal variations typical to areas situated in semi-arid climates.

8.2 Methodology

8.2.1 Study site

The Litani Basin is the largest hydrographic basin in Lebanon and the Litani River (170 km) has an annual average discharge of 9.34 $m^3 s^{-1}$. The reservoir has a volume of 220 million cubic meters (MCM) and is largely used for irrigation over the entire region. This basin has an important socio-economical value. It constitutes about 15-20% of the total area of the country, houses 20% of the total population, represents 20-30% of the total national water budget, and provides more than 60% of agricultural industry and about 30% of the total national energy production (BAMAS, 2005, El Fadel et al., 2003, Saad et al., 2006, Saadeh et al., 2012). Thus, it has both socio-economical and environmental significance at the national scale. As part of the national water management plan, the Qaraaoun Dam was constructed in 1955 to collect Litani River flow into a 2.2 km^2 reservoir, for hydropower production and irrigation. The dam in Qaraaoun village is 110 m long and 61 m wide and stores water delivered by the Litani main river, nine tributaries, surface runoff, and groundwater discharges from the upper drainage area which is estimated to be 2180 km^2. The reservoir is subjected to dramatic hydrological changes seasonally and annually, by which the hydrological regime can be divided into two modes spill and fill as described in Chapter 7. The reservoir reaches its full capacity during fill hydrological mode as a result of increased river flow due to precipitation and subsequent increased river discharge (winter, 210 MCM). The lowest water volume is reached during spill hydrological mode (end of summer, 49 MCM) due to lower river flow, increased evaporation, and water pumping from the reservoir. The geographic extent and bathymetry of the reservoir are displayed under spill and fill conditions on Figure 8.1. The reservoir has a minimum allowed volume of 40 MCM, though 70% of the total water capacity (220 MCM) is used to produce electric power during full capacity (El-Fadel et al., 2003). Furthermore, the Qaraaoun reservoir is aiming to supply more than 22000 hectares of cultivated land with irrigating water (30 MCM yr^{-1}) via

irrigating Canal 900. The Litani watershed is situated in the Bekaa valley between two mountainous chains at a mean altitude of 800 m above sea level (m a.s.l), and is known for its karstic geological outcrop that enhances fast water percolation (Shaban et al., 2014). The synoptic impacts of the Bekaa diverse topography, its proximity to Mediterranean influence from west, in addition to Syrian Desert in the north-eastern reaches, create specific microclimates with drastic varying temperatures, humidity values and precipitation distribution in the region (FAO, 2009; Ramadan et al., 2013). As a result, orography plays an important role in micro-climate changes, where snow falls 30 days per year on the mountains flanking the basin over an area estimated to be 550 km^2 (Develle et al., 2010; El Fadel et al., 2003; Shaban et al., 2014). The mountainous chains flanking the continental Litani basin has an average slope gradient ranging between 15-17% from the west and 7-10% from the east toward the valley (Shaban, 2014). The Mediterranean Sea is the origin of precipitation in the studied area, by which the basin receives between 700 and 1000 mm yr^{-1} as mean annual precipitation (Awad, 2011; Develle et al., 2010). The rainy season extends from November till May by which 90% of the precipitation falls in winter, followed by a severely dry season from May till September. The temperature ranges mainly from 5 °C to 26 °C in winter and summer respectively with an average annual temperature of 16 °C. However the mean annual evaporation over the Bekaa plain is 1200 mm yr^{-1} with maximal recorded values in July (FAO, 2009, Ramadan et al., 2013). Humidity is high near the coast and decreases toward the Bekaa plain ranging thus between 35 and 75% (Awad, 2011, Develle et al., 2010; El Fadel et al., 2003; FAO, 2009).

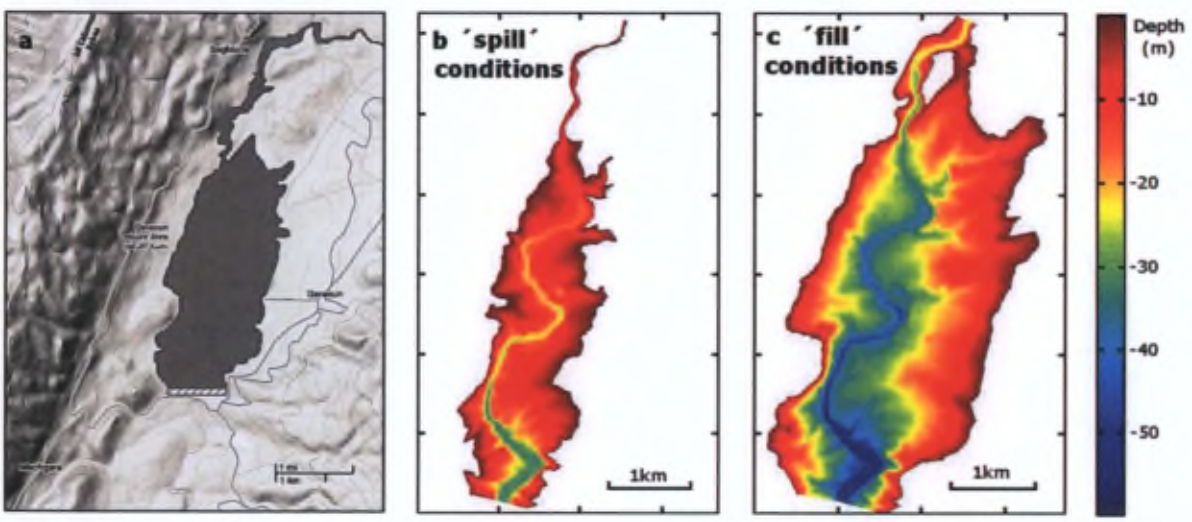

Figure 8.1: Topography of the surroundings of Qaraaoun reservoir (a) and bathymetry of the reservoir under spill (b, 836 m a.s.l) and fill conditions (c, 858 m a.s.l).

8.2.2 Model description

The model presented here is a single box model treating the Qaraaoun reservoir as a homogeneous entity of volume V (Figure 8.2). The sources of water to the lake are the discharge of the Litani River (*Fr*) and the direct precipitation over the lake surface (*Fp*). Lateral surface runoff is considered negligible in the reservoir because of its insignificant influence on the reservoir water chemistry and isotopic signature as shown in Chapter 7 (Ammar et al., submitted). Water is removed from the lake through the direct output from the dam's turbines (*Fo*), evaporation at the lake surface (*Fevp*) and, in case of extremely high water levels, an evacuator (*Fevc*), which only gets activated when the water level exceeds 858 m a.s.l. All these fluxes are either monitored or can be directly measured. Additionally, water exchange between the lake and ground waters have been identified in Chapter 7 (Ammar et al., submitted) but never yet quantified. These are represented by two fluxes: *GWi* corresponding to the ground water input towards the lake and *GWo*, corresponding to the output of lake water towards the groundwater. The mass balance equation governing the water budget of the lake can be written as:

$$\frac{dV}{dt} = F_r + F_p - F_o - F_{evp} - F_{evc} + GW_i - GW_o \qquad (8.1)$$

From equation (8.1), the net water exchange between groundwater and the lake can be expressed as:

$$(GW_i - GW_o) = \frac{dV}{dt} - F_r - F_p + F_o + F_{evp} + F_{evc} \qquad (8.2)$$

Under the assumption of a strict unilateral flow at the ground-surface water interface over a given period of time, the sign of (GWi-GWo) determines the direction of the flow such as way that:

$$GW_i = \frac{dV}{dt} - F_r - F_p + F_o + F_{evp} + F_{evc} \quad \text{and} \quad GWo = 0 \qquad (8.3) \text{ and } (8.4)$$

when (GWi-GWo) > 0 and

$$GW_o = +F_r + F_p - F_o - F_{evp} - F_{evc} - \frac{dV}{dt} \quad \text{and} \quad GWi = 0 \qquad (8.5) \text{ and } (8.6)$$

when (GWi-GWo) < 0

Alternatively, a term GW_m can be added to both GW_o and GW_i to account for the two-ways mixing between the lake and the groundwater.

Using the symbols described in Figure 8.2, the balance equation governing the isotopic signature of the lake (δ_Q) can be expressed as:

$$\frac{d(V\delta_Q)}{dt} = F_r\delta_r + F_p\delta_p - F_o\delta_Q - F_{evp}\delta_{evp} - F_{evc}\delta_Q + GW_i\delta_s - GW_o\delta_Q \qquad (8.7)$$

Following Gupta and Deshpande (2004), the above equations can be re-written as recurrence equations assuming a discrete time interval $\Delta t = dt$ corresponding to the time elapsed between time (t) and time ($t+1$). The volume V of the lake at times t and t+1 are then written as $(V)_t$ and $(V)_{t+1}$, respectively. Equation (8.1) leads to:

$$(V)_{t+1}(\delta_Q)_{t+1} - (V)_t(\delta_Q)_t = \left[(F_r)_t(\delta_r)_t + (F_p)_t(\delta_p)_t - (F_o)_t(\delta_Q)_t - (F_{evp})_t(\delta_{evp})_t - (F_{evc})_t(\delta_{evc})_t + (GW_i)_t(\delta_s)_t - (GW_o)_t(\delta_Q)_t\right] \quad (8.8)$$

From equation (8.8), δ_s can be isolated:

$$(\delta_s)_t = \frac{(V)_{t+1}(\delta_Q)_{t+1} - (V)_t(\delta_Q)_t - \Delta t(F_r)_t(\delta_r)_t - \Delta t(F_p)_t(\delta_p)_t + \Delta t(F_{evp})_t(\delta_{evp})_t + \Delta t[(F_o)_t + (F_{evc})_t + (GW_o)_t](\delta_Q)_t}{(GW_i)_t \Delta t} \quad (8.9)$$

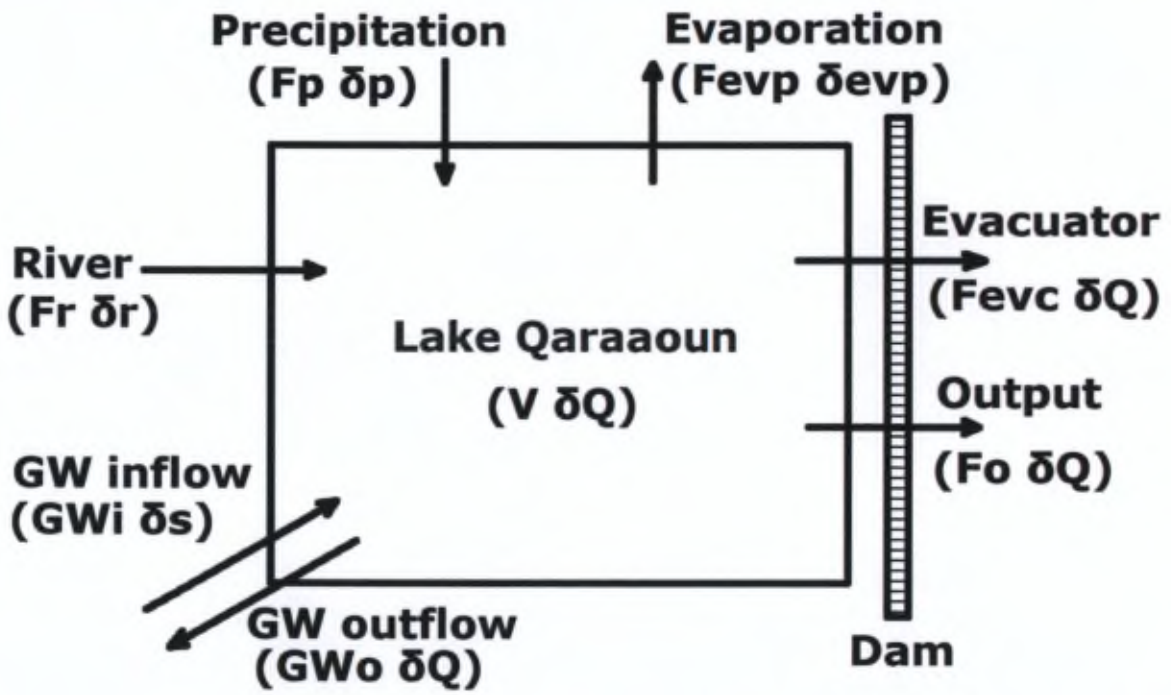

Figure 8.2: Conceptual scheme of the Qaraaoun reservoir box model. All fluxes are reported with their corresponding symbol and that of their isotopic signature.

8.2.3 Forcings and isotopic values

The data used to constrain the model were derived from local measurements performed by local agencies for hydrological parameters of field studies for isotopic data[17] (Ammar et al., submitted). Hydrological data, including the Litani River inflow, water level in the reservoir, and water outflow to Markhaba electric power station, were monitored daily and provided by the Litani River Authority (LRA). A high resolution (i.e. 5 meter) bathymetric file provided by LRA was used to calculate the volumes as well as the water surface area of the lake from the daily water elevation data provided by the LRA (Figure 8.3a and 8.3b). Precipitation rates were measured at the nearest station to the reservoir in Kherbit Kanafar on daily basis during the three years of the study (2011-2013) and multiplied by the corresponding surface area of the lake to derive *Fp*. Reservoir surface evapotranspiration (*Fevp*) was estimated from air temperature and relative humidity measured at the same station using potential evaporation according to Thornthwaite method (Thornthwaite and Mather, 1955), following the assumption that evaporation over a water body can approximated by potential evapotranspiration (Zhang et al., 1996). Potential evapotranspiration (PET) is calculated according to equation (8.10).

$$PET = 16\,(10\frac{\theta}{ATI})^{\alpha} C\,(\lambda) \qquad (8.10)$$

PET is the potential evapotranspiration in millimeters per month, where θ is the monthly mean air temperature in °C. ATI is the annual thermal index that can be calculated from the sum of the 12 months thermal indexes (MTi), where $MTi = (\frac{Tm}{5})^{1.514}$ which in its role is based on average monthly temperature (Tm); while (α) can be derived from equation (8.11) as follow:

$$\alpha = 6.75\times10^{-7}\,ATI^3 - 7.71\times10^{-5}\,ATI^2 + 1.79\times10^{-2}\,ATI + 0.49239 \qquad (8.11)$$

Where the C(λ) is the correction coefficient estimated as a function of the latitude of the studied area and the corresponding month (Brochet and Gerbier, 1968). When the monthly PET (mm $month^{-1}$) value is computed it is multiplied by the surface area of the reservoir (km^2) for the corresponding month; thus we got the water evaporation flux (*Fevp*) in MCM $month^{-1}$.

The isotopic data used in this study for the river inlet and the lake are derived from experimental studies on Qaraaoun reservoir during the period extending from September 2011 to July 2013 as explained in Chapter 7 (Ammar et al., submitted). The values used are seasonal mean summarized in Table 8.1. The means are calculated from $\delta^{18}O$ measurements performed at several depths on two locations. For each season, the value of each depth interval (i.e. epilimnion, mixed layer and bottom waters) in both sub-sections of the lake was

[17] Complete isotopic data through the study period are presented in Annex 9.

calculated. The seasonal means used for the entire lake represent volume weighted averages of the $\delta^{18}O$ of each of these sub-compartments. Figure 8.4 presents the surface area and volumes of both epilimnion and hypolimnion (defined as mixed layer plus bottom waters) for the entire spectrum of water levels observed in the lake. To our knowledge, these data had never been presented prior to this study, in spite of their environmental significance. The increased water volume of the reservoir follows an exponential growth with the increased water level attained by the dam (Figure 8.4a). The hypolimnion follows the same behavior of the whole reservoir, while the epilimnion indicates a more sensitive change to increased water level in the dam compared to the hypolimnion. The epilimnion water volume follows a significantly more linear increase with the increased water level in the reservoir (Figure 8.4a). Similarly, the reservoir surface area expands linearly with increased water level in the dam. Evidently the reservoir responds quickly to hydrometeorological changes in the basin, and its topography induces active hydrodynamics. As a consequence the epilimnion layer is an environmentally significant hydrological unit in the reservoir, by which it receives the river flux and represents the first frontier of water-soil interaction with the surrounding lake banks. The subsequent active hydrodynamics caused by water expansion vertically and transversely in the reservoir will activate soil erosion, thus increasing the mechanical transport of soil from lake banks to the open water body (Van Griethuysen et al., 2005). Furthermore, the continuous alternating conditions of revealing and submerging the reservoir riparian zones will provoke a redox shift at the surface soil layer (Argese et al., 1997). As a result to the altering redox conditions at the soil-water interface, the metal biogeochemical cycles will be modified (as explained in Chapters 5 and 6), increasing their lability thus increasing their hazard on the aquatic system (Miao et al., 2006; Ocampo et al., 2006). Additionally the fast expansion of the reservoir surface area will increase the water loss via evaporation and triggers a quick biological proliferation, therefore inducing reservoir eutrophication (Taillefert et al., 2006).

The epilimnion and hypolimnion $\delta^{18}O$ for the entire lake were calculated as a volume weighted averages between the central and dam zone (see Ammar et al., submitted (Chapter 7) for more details about the sub-sections of the reservoir). The delta ^{18}O for rain was estimated from the local meteoric water line (LMWL) particularly for the local rain in the studied area as $\delta p = -8‰$ (Saad et al., 2005). While the delta notion of evaporated water was estimated from equation (8.12) (Gonfiantini, 1986; Majoube, 1971);

$$\delta_{evp} = \frac{(\alpha^{*}\delta L - h\delta a - \varepsilon)}{1 - h + 10^{-3}\Delta\varepsilon} \qquad (8.12)$$

α^{*} is the equilibrium fractionation factor, and for $\delta^{18}O$ fractionation it is calculated as follow:

$$\alpha^{*18}O = \exp\left(\frac{1.137}{T2} \times 10^{3} - \frac{0.4136}{T} - 2.06667 \times 10^{-3}\right) \qquad (8.13)$$

Where T is the average monthly air temperature and h is the relative humidity. ε is the total fractionation factor which is equivalent to the summation of ε^{*} and the kinetic fractionation factor ($\Delta\varepsilon$). However, $\varepsilon^{*} = (\alpha^{*}-1)$ and $\Delta\varepsilon$ for $\delta^{18}O$ is calculated according to equation (8.14):

$$\Delta\varepsilon^{18}O = \exp\left(\frac{0.35041}{T3} \times 10^{6} - \frac{1.6664}{T2} \times 10^{3} + \frac{6.7123}{T} - 0.007685 + 28.4\, n(1-h) \times 10^{-6}\right) \quad (8.14)$$

Where n is the turbulence taken as 0.5 for this type of open lakes (Gibson et al., 2008). While δL is the delta oxygen at the lake surface water at 1 m depth of the epilimnion, and $\delta^{18}O$ in atmospheric moisture (δa) is derived from equation (8.15):

$$\delta a = \alpha^{*18}O \times \delta p - \varepsilon^{*} \quad (8.15)$$

8.2.4 Model set-up

The model simulations are performed over the period extending from September 2011 to August 2013 using monthly average forcings. The volume of the lake and its isotopic signature are calculated by solving equations (8.1) and (8.7), respectively, using Euler's method with an integration time step of 0.01 month. The values of GWi, GWo and δs are updated 6 times over the simulation period, corresponding each to a sampling campaign.

8.3 Results and discussion

8.3.1 Hydrological regime of the reservoir

The Litani river flow is subjected to annual and seasonal variations correlated with annual changes in precipitation rates and the highest flow recorded over the study period took place during the rainy season extending from December to April (Figure 8.3a). Precipitation over reservoir surface area was heavy during February 2011 (1.18 MCM $month^{-1}$) which decreased to zero during dry summer (Figure 8.3b). As a typical semi-arid area the precipitation rate varies annually by which it increased during the succeeding wet seasons, for February 2012 it reaches 1.2 MCM $month^{-1}$, while the maximum precipitation flux was observed for January 2013 (1.5 MCM $month^{-1}$) during the study period. Correspondingly, the withdrawal of water from the reservoir is scheduled according to the accumulated water volume in the lake. As a result, the period of water pumping is strictly attributed with meteorological aspects. For instance, water pumping was almost terminated during February-April 2011, while the pumped water volume was the highest in April 2012 and February 2013 (Figure 8.3a). Moreover, heavy winter and high river inflow could lead to excessive water volume in the reservoir where it is evacuated through a security spill outlet that was observed only for March and April of 2012 (Figure 8.3a). Evaporation reaches its highest value during dry season mainly for July 2011 (1.33 MCM $month^{-1}$), June 2012 (1.37 MCM $month^{-1}$), and July 2013 (1.66 MCM $month^{-1}$) (Figure 8.3b). This is in agreement with the previous estimates which indicate that the highest evaporation takes place during July in the Bekaa Valley (Ramadan et al., 2013).

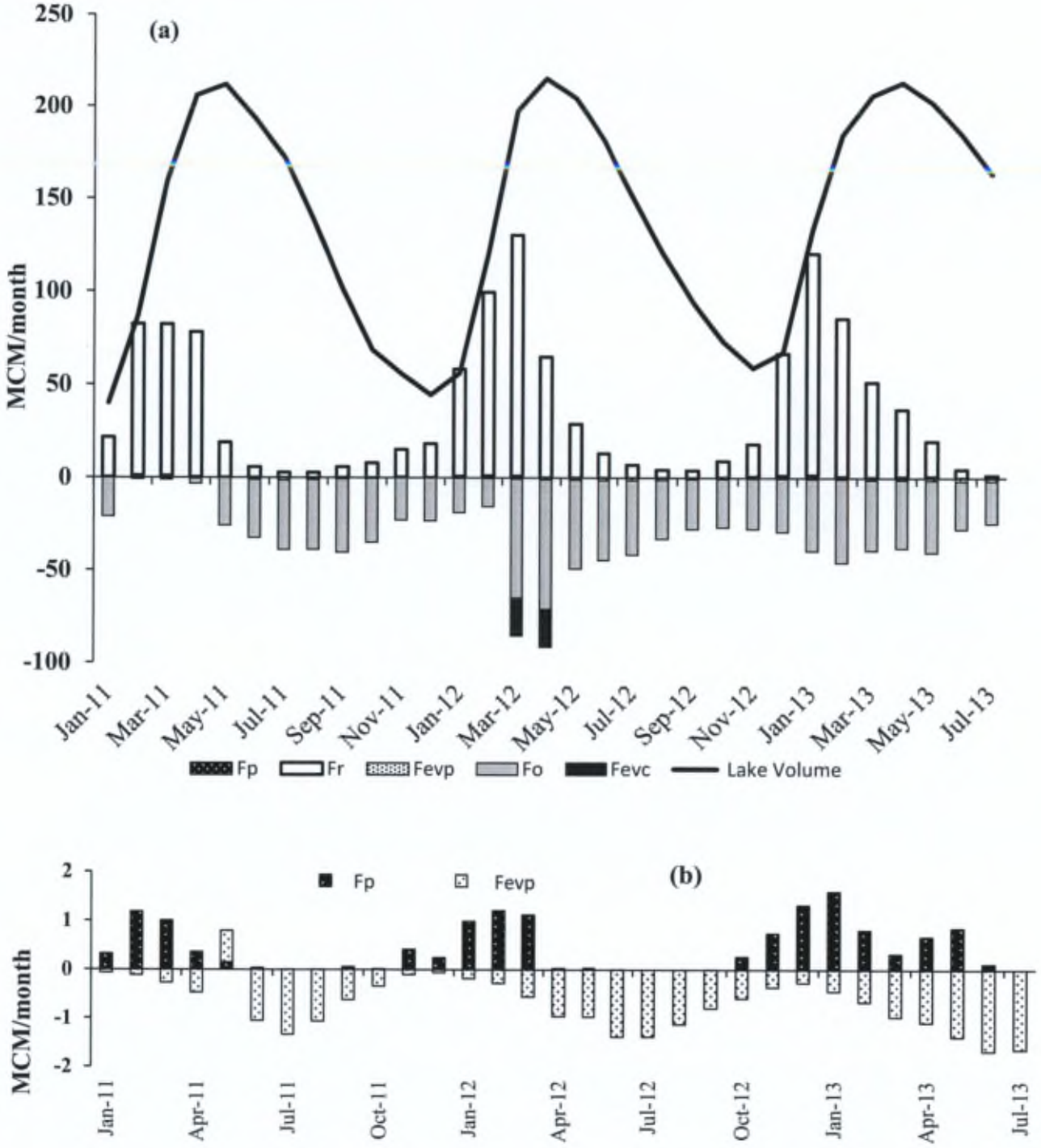

Figure 8.3: Hydrological water budget of the reservoir, ignoring all interaction between the lake and groundwater. Input are represented by river flow (Fr) and precipitation (Fp) while outflow comprises the water withdraw (Fo), potential evaporation (Fevp), and evacuated excess water (Fevc).

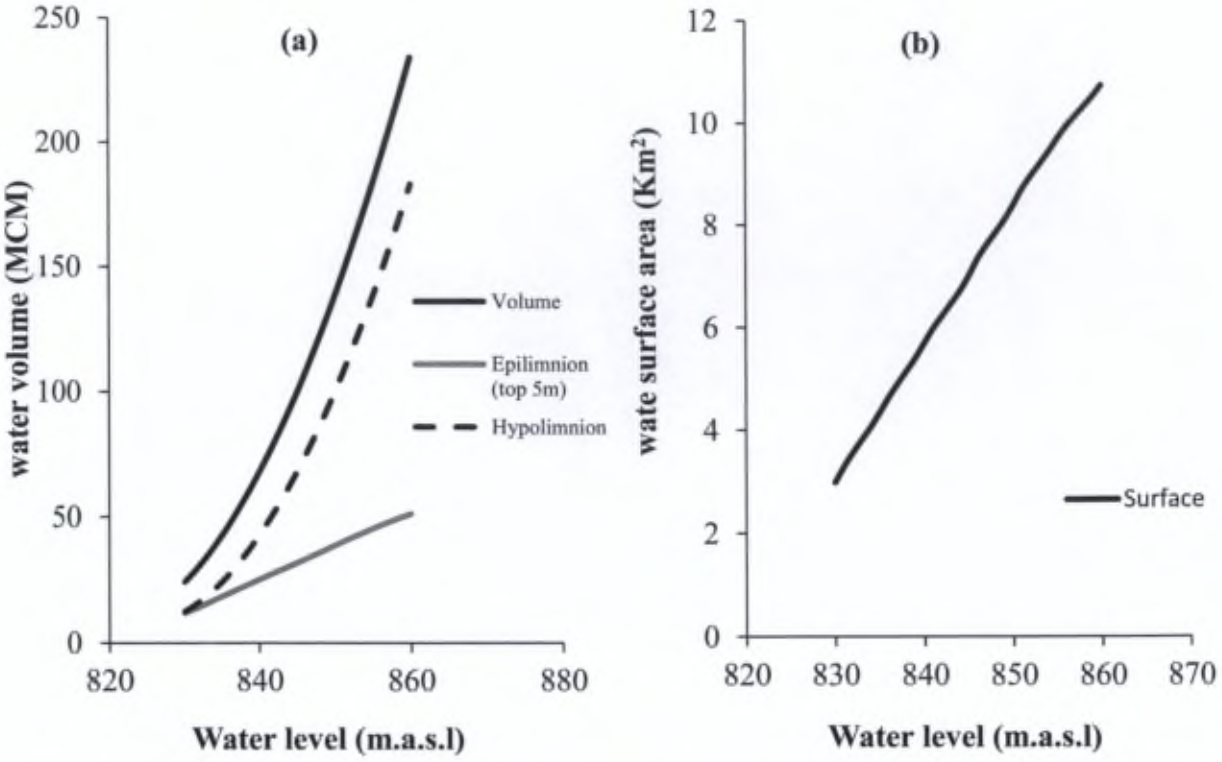

Figure 8.4: The extension of water volume in the reservoir and in both epilimnion and hypolimnion (a), and the surface expansion of reservoir surface area (b) upon water level increase in the dam.

Reservoir water budget computed according to total input fluxes (river flow and precipitation) and the output fluxes (evaporation, withdrawn water volume, evacuated excess water) should result in an expected water volume attained by the reservoir as shown in Figure 8.5.

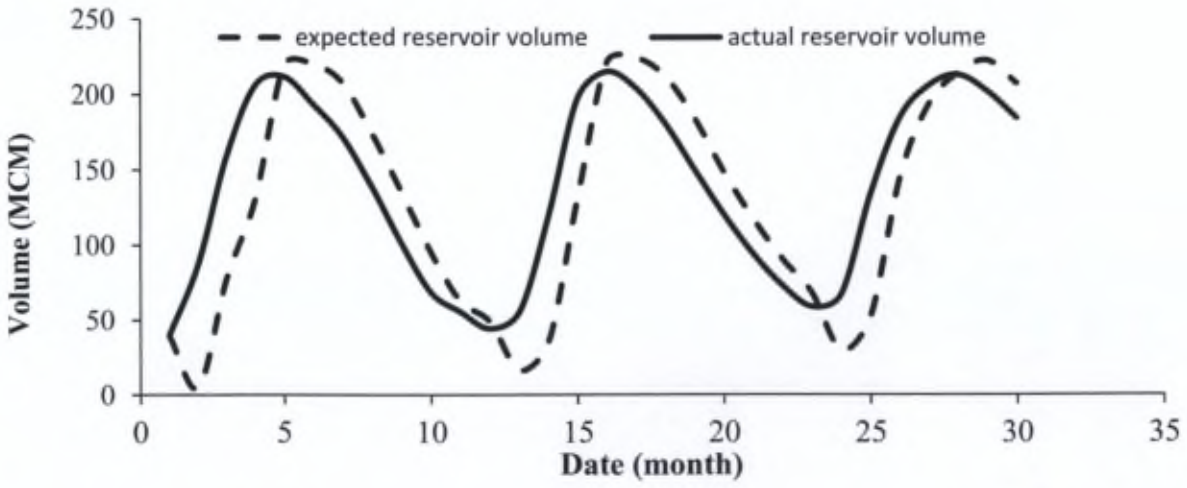

Figure 8.5: The imbalanced water budget represented by the difference in actual water volume in the reservoir and the expected volume.

However, comparing the expected reservoir water volume to the actual water volume indicates a big deviation and an imbalanced water budget. That can only be explained by a

significant exchange between surface water and groundwater. The existence of such process was already suggested by isotopic analysis in Ammar et al., (submitted). The observed water volume in the reservoir during raining season (December till March) exceeds the expected one (Figure 8.5), evidencing the presence of an additional input water source to the reservoir which will raises the water level. Correspondingly, during dry season extending from May untill October the actual reservoir water volume is lower than the expected one, thus supporting the idea of water loss from the reservoir via infiltration toward the ground water.

Figure 8.6 represents the seasonal evolution of volume difference between inputs and outputs to the reservoir (in-out) and reservoir monthly volume change (Figure 8.6a). The mismatch between those quanta indicates an additional flux corresponding to the water exchange at the surface/groundwater interface, as calculated by equation (8.2). These results indicate an alternating direction of the surface-groundwater net flux as input flux (from the source into the reservoir) and output flux (infiltration from the reservoir toward groundwater). The maximum inward flux (28.54 MCM $month^{-1}$ that corresponds to 11.01 m^3 s^{-1}) takes place in December 2012 (Figure 8.6b, 8.6c). Water infiltrates from the reservoir starting from February to July in 2011 and 2012, while in 2013 water infiltration starts earlier in January 2013 but also terminated earlier in May 2013 (Figure 8.6b). The highest infiltration during the study period was estimated for April 2011 (69.32 MCM $month^{-1}$ that corresponds to 26.7 m^3 s^{-1}) as shown in Figure 8.6b, and 8.6c. The hydrological connectivity between the reservoir and the source can vary as a result of water table elevation in the source and the water level reached by the reservoir (Barrett and Charbeneau, 1997). The source-reservoir hydrodynamics respects the hydrostatic laws, where the water source charges water into the reservoir when the water level in the latter is low, as shown for spill hydrological regime (October to January) (Figure 8.6c). While during the fill hydrological regime (February to May) where the water level in the reservoir reaches its maximum capacity, the water infiltrates from the reservoir and recharges the groundwater (Figure 8.6c). The seasonality of the source dynamics is hydrologically connected with the precipitation rate in the upper watershed. The lag period between precipitation and replenishment of groundwater table is conditional and related to annual precipitation rates and the successive raining months. Apparently the lag time between precipitation peak and the source influx into the reservoir can range between two to several months (Figures 8.3b and 8.6). This fast water infiltration can be referred to the steep land topography and the karstic geology in Litani basin (Shaban et al., 2014; Shaban, 2014). Furthermore, increased annual precipitation rates and snow thawing will enhance the ground water table and control the timing of the source influx to the reservoir. This may explain the increased early flux of the source detected in 2013 compared to 2012 and to 2011(Figure 8.6), because 2012 and 2013 experienced a heavy winter season compared to the dry year of 2011 (Figure 8.3b). As a result, the groundwater table in 2011 might be low, thus justifying the highest infiltration that was estimated for April 2011 (Figure 8.6b). The remarkable snow cover that engaged around two thirds of Lebanese territory in 2012 and 2013 (Shaban, 2014) certainly contributed in replenishing quickly the groundwater table. Moreover, a recent study indicated that the snow residence time on Lebanese mountain

chains decreased by 25 days (Shaban et al., 2014), thus potentially explaining the fast response of both the source and the reservoir to snow events.

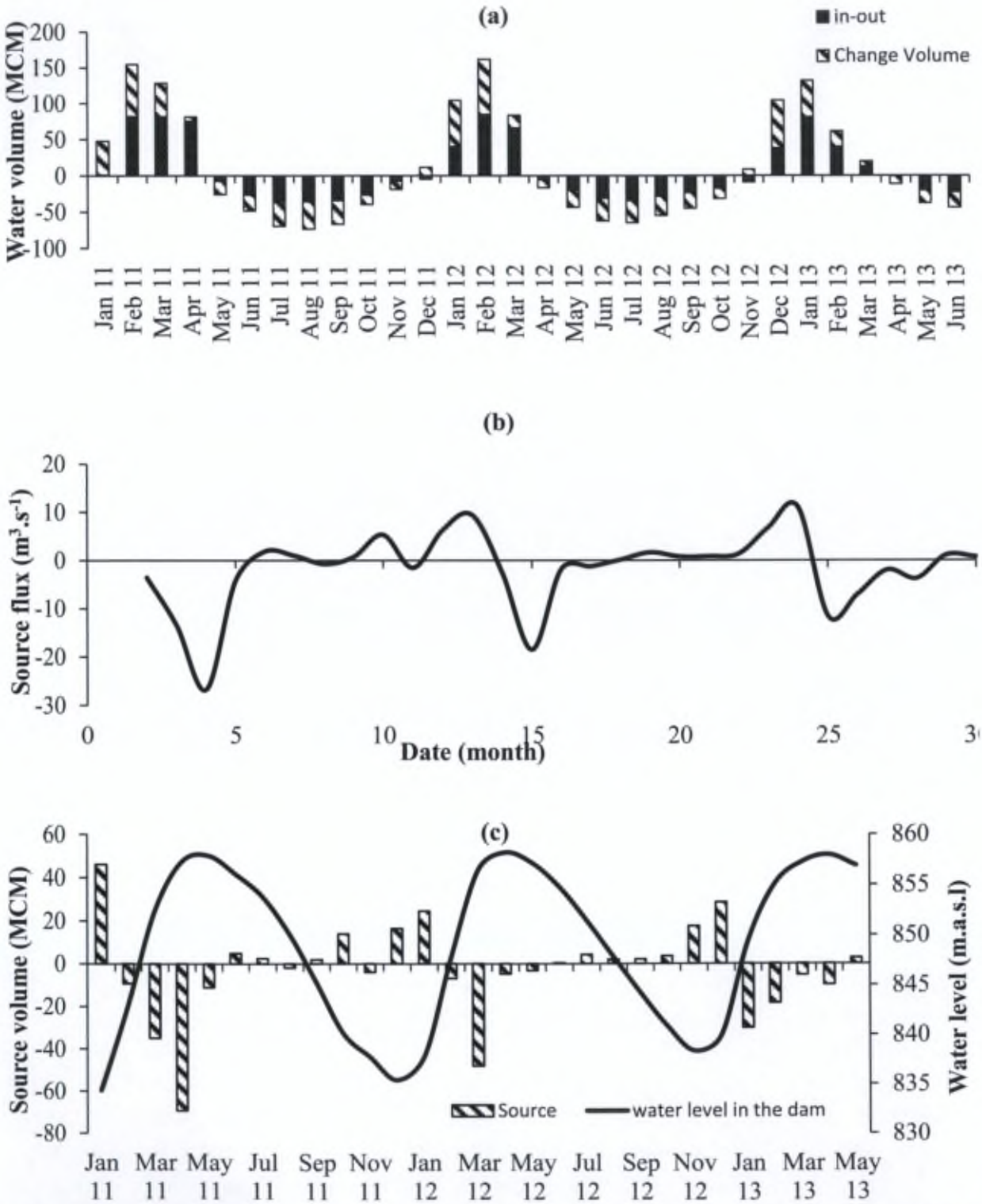

Figure 8.6: The fluxes difference (in-out) and the accumulated volume change in the reservoir (a), source flux (b), and the response of water dynamics to source volume and water level in the dam (c).

8.3.2 Identification and qualification of the source using isotopes

The delta notion of the water derived by the river into the reservoir varies seasonally as shown in Table 8.1. Where the most enriched waters are observed for September 2011 (-4.33 ‰), and start to be depleted by heavy isotopes during the wet season as a result of precipitation. The lightest water was measured in June 2012, even though there is no precipitation during this month of the year (Figure 8.3b). However this depleted isotopic ratio by heavy isotopes can be due to the recharge of snow thawing and water recharge from high altitudes (Halder et al., 2013; Wassenaar et al., 2011). Delta evaporation for the studied area was estimated as -8.1‰ which is in agreement with the local evaporation line (Saad et al., 2005). Theoretically, isotopic signature in the open lake should be enriched by heavy isotopes compared to the water brought by the river as a result of evaporation (Mayr et al., 2007). This is the case during dry months (September, October and November) when comparing the delta notion of the reservoir (δQ) to that of the river inlet (δr) (Table 8.1). Unexpectedly, δQ in June (the highest month of evaporation) is more depleted compared to δr (Table 8.1), this is an indication of mixing with more depleted water source. This is further confirmed by the source influx into the reservoir during June 2012 (3.8 MCM month^{-1}) as shown in Figure 8.6c. During the other studied months, the reservoir indicated a slight depleted isotopic ratio compared to the river, which could be explained by groundwater influx regardless the net flux of the source that does not indicate an inward movement.

Table 8.1: Environmental isotopic notion of water entering the reservoir by the river, precipitation, evaporation, in the moisture and the estimated delta 18O of Qaraaoun reservoir.

Sampling date	δr	δp	δevp	δa	δQ
Sep-11	-4.33594	-8	-8.14299	-8.09053	-4.10964
Nov-11	-4.45351	-8	-8.13807	-8.10036	-4.3107
Mar-12	-5.8212	-8	-8.11794	-8.10052	-5.89075
Jun-12	-7.35	-8	-8.07342	-8.08826	-7.88961
Sep-12	-4.66688	-8	-8.12595	-8.08936	-5.29453
Oct-12	-5.13588	-8	-8.13325	-8.09175	-4.85675
Apr-13	-6.20563	-8	-8.09814	-8.09669	-6.69068

The isotopic ratio of the source and as a consequence its origin have been determined by coupling water mass balance budget with isotopic mass balance using equation (8.7). The results of this simulation are presented in Table 8.2. The model output from the simulation only accounting the net surface-groundwater exchange (0 MCM month^{-1}) produces unreasonable isotopic ratios for $\delta^{18}O$; mainly for June and September 2012 represented by positive isotopic ratios. The resulted anomalous model output data can be explained by the usage of the net flux of surface-groundwater interaction to conduct the calculations of the isotopic ratio of the source. The model provides the source net flux, where one of the hydrological routes is dominating and concealing the other. The isotopic ratio of the reservoir must be affected by the groundwater influx for certain months; regardless the model output that shows an outward source net flux (Figure 8.6). However that does not prevent the fact

that the source is flushing water to the reservoir at the same time during water infiltration from the reservoir. Thus the groundwater minor contribution can alter lake's water budget, where the conventional water budget estimation can only distinguish groundwater net flux but can not distinguish the inflow from the outflow (Sacks et al., 2013).

Table 8.2: Estimated delta 18O of the source depending on the intensity of the two-ways mixing between the groundwater and surface waters

Sampling date	0 MCM month^{-1}	10 MCM month^{-1}	20 MCM month^{-1}	50 MCM month^{-1}	75 MCM month^{-1}
Sep-11	-4.83705	-4.42972	-4.31482	-4.20844	-4.17863
Nov-11	-11.1945	-7.78271	-6.63215	-5.47483	-5.13315
Mar-12	-	-34.5034	-20.1971	-11.6133	-9.70576
Jun-12	+26.81906	-1.56857	-4.41246	-6.4098	-6.88885
Sep-12	+6.565741	-3.20339	-4.14788	-4.80763	-4.96543
Oct-12	-10.7317	-7.51434	-6.57394	-5.68971	-5.4396
Apr-13	-4.83705	-4.42972	-4.31482	-4.20844	-4.17863

Based on the isotopic signature of both the reservoir and the source, they evidenced that there is an exchange between groundwater and surface water in both directions at the same time. Hence, with the intention of quantifying acceptable isotopic ratios for the source, a series of increasing mixing volumes (GW_m) was used to study their influence on the isotopic ratio of the source. The constant intensities of the monthly two-way mixing volumes between reservoir and groundwater source were chosen to be 10, 20, 50 and 75 MCM month^{-1}, and the outputs of the corresponding simulations are presented in Table 8.2 and illustrated in Figure 8.7. The measured isotopic ratios of the reservoir indicate an antagonistic trend to the reservoir water volume (Figure 8.7a and 8.7b). The simulation of the reservoir water volume changes over time result in a very good fit with the observation (Figure 8.7a). Enriched isotopic values (-4.3‰) are associated with lower water volume (55.7 MCM), and depleted isotopic values (-7.88‰) are associated with higher water volume reached by the reservoir (181.3 MCM). The isotopic response of the reservoir to hydrological settings is a result of evaporation and recharge from precipitation, river and ground water sources. Thus, the isotopic ratio of the reservoir is the output of mixing endmembers such as surface water and ground water. The model output for M0 produces a reservoir isotopic ratio very far from the measured one (Figure 8.7b). While upon increasing the mixing flux by 10 MCM month^{-1} (M10) the model gave isotopic ratios for the reservoir that approached the measured ones, mainly for September and November 2011 (Figure 8.7b). For the remaining months, the model gave an outlying isotopic matches compared to the measured reservoir isotopic ratios. This output configuration is attributable to the unrealistic isotopic ratios of the source, mainly for March (-34.5‰) and June (-1.5‰) (Table 8.2). Similarly, the simulations of M20, M50, and M75 resulted from increasing mixing fluxes by 20, 50 and 75 MCM month^{-1} respectively, improves the isotopic ratio of the reservoir compared to the measured ones. This

was applicable for the first four studied months (September 2011-June 2012), but not for the last three months (September 2012, October 2012, and April 2013).

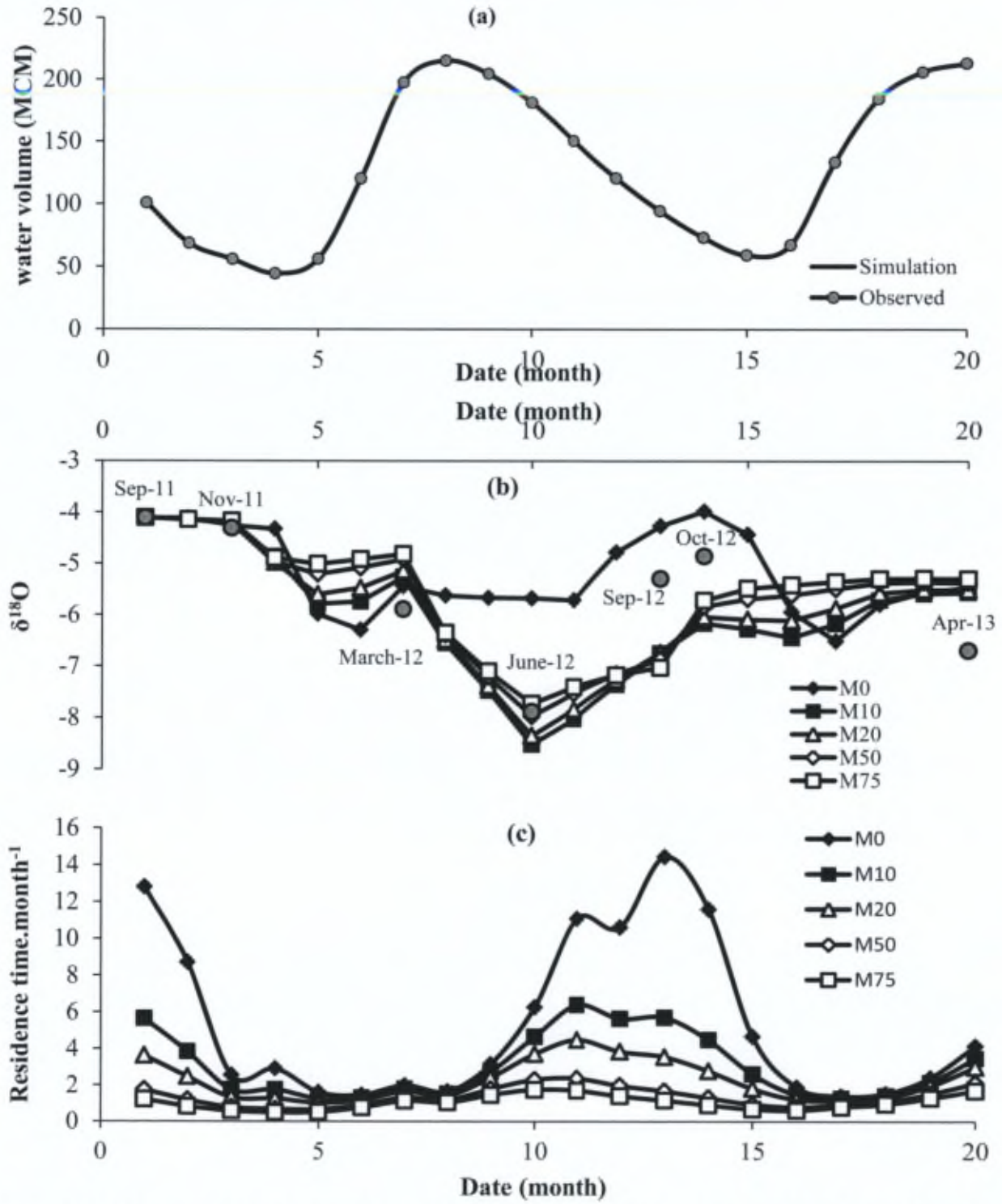

Figure 8.7: The model simulations of water level (a), and the resulted output from increasing the intensities of mixed volumes (*GWm*) of the source (b), and the water residence time in the reservoir (c).

If the reservoir retains a particular isotopic ratio and a hydrological setting for a certain month, it will lead to specific recession period identified as potential water residence time per month as shown in Figure 8.7c. Predictably, the increased mixing volumes of water exchange will result in a shorter water residence time. Where the water residence time decreased from 6 months to 1.5 months as the mixing flux increased from 10 to 75 MCM $month^{-1}$ (Figure 8.7c). Apparently during the period extending from September to December the reservoir might experience longer water residence time compared to other months as the mixing volume decreases (Figure 8.7c).

In order to overwhelm the weak isotopic match resulted from the first approach of presuming the addition of constant mixing volumes that were applied for the whole studied period. Another approach was tackled to quantify the isotopic ratios of the source by compatibility scenarios with possible isotopic values, and composed of specific mixing volume for each studied month.

The first scenario is characterized by calibrating the volume of water exchange between the groundwater and the reservoir for each season in order to match the isotopic ratio of the source with those of piezometers, which were measured in the same seasons as the reservoir. Isotopic ratios of the surrounding piezometers may represent a potential water origin for the source (Table 8.3). The mixing volume for each month produces an isotopic ratio for the source that fit in the piezometer range as shown in Table 8.3. The corresponding simulation for these values point toward seasonal reservoir isotopic ratios as represented in Figure 8.8a. Isotopic ratios for September and November 2011 indicate a strong match with the measured isotopic ratios in the reservoir. However the mixing volumes are very high, resulting a very short residence time that does not exceed 2 months except for September (Figure 8.8b). These high mixing rates up to 1000 MCM $month^{-1}$ are hardly ever attained *in situ*.

Table 8.3: Estimated flux intensity and delta 18O of the source for the best fit in 1st scenario, and the 2nd scenario relying on piezometers isotopic signature.

Sampling date	1st scenario			2nd scenario	
	Fgw	δs	piezometers	Fgw	δs
Sep-11	20	-4.83705	-5.09 to -5.50	8	-4.47009
Nov-11	1000	-6.63215	-6.62 to -6.26	6	-8.64124
Mar-12	150	-6.17687	-5.0 to -6.17	70	-9.97827
Jun-12	1000	-7.38191	-7.31 to -7.83	14	-3.12675
Sep-12	-	-5.2692	-6.14 to -6.63	100	-5.04598
Oct-12	-	-	na	2	-9.58648
Apr-13	0	-	na	0	-4.83705

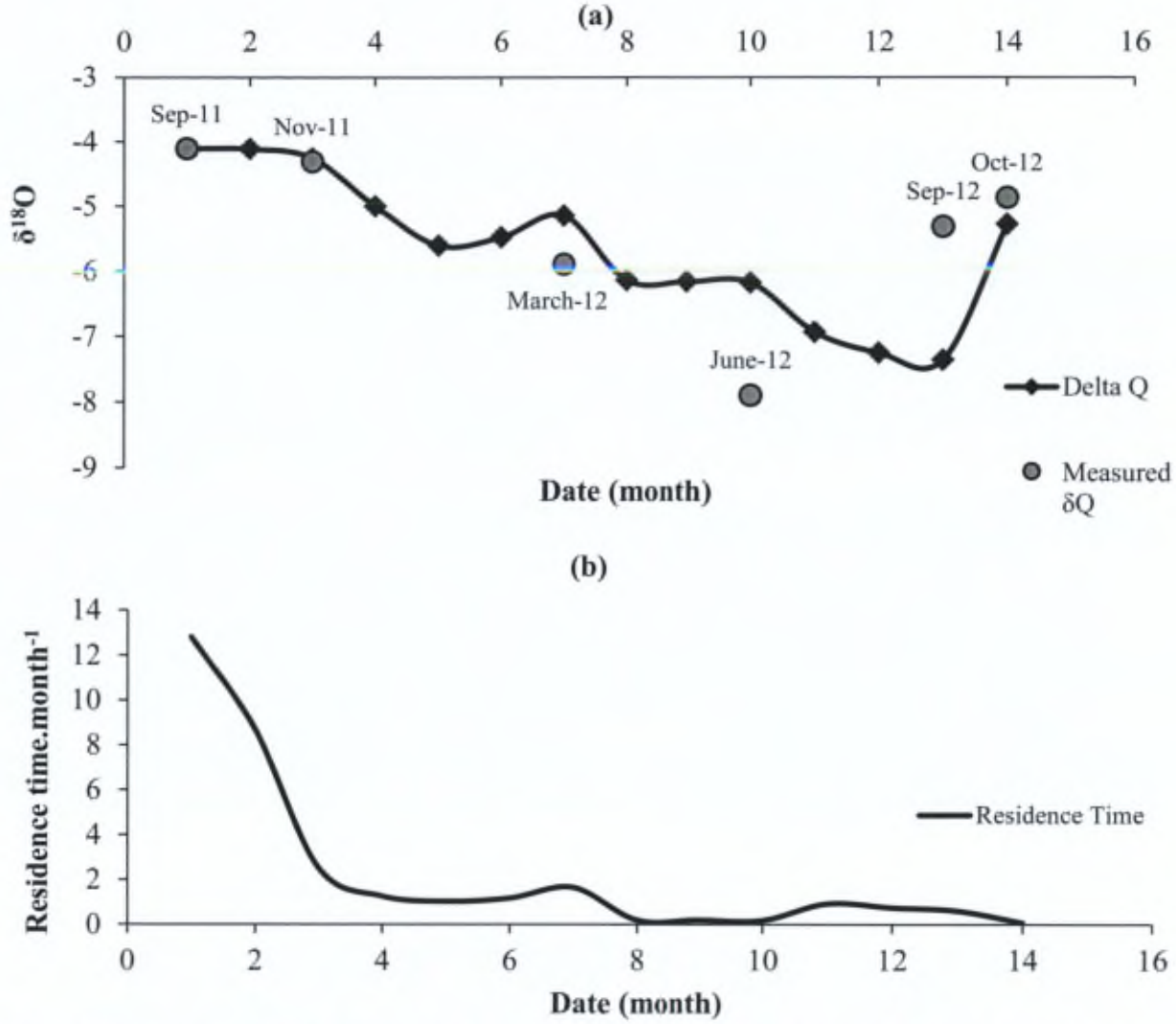

Figure 8.8: The isotopic response of the reservoir to the source flux intensities resulting from compatible isotopic signature with the surrounding piezometers (a), and the water residence time in the reservoir (b).

While the second scenario characterizes the best match between all the tested model outputs for the reservoir isotopic values that best fit the measured ones. The mixing volumes were restricted to a value less than 100 MCM, and the isotopic ratio of the source for $\delta^{18}O$ were forced to range between -3.1 to -9.9‰ (Table 8.3). The enriched isotopic ratios of the source estimated for September 2011, June 2012, September 2012, and April 2013 (Table 8.3) may indicate a water source influenced by water subjected to evaporation during dry period, or reflow of irrigated water (Diaw et al., 2012). In the contrary, depleted isotopic ratios for the source estimated during first flush and rainy season (November, October and March) directs toward the possibility of ground water source recharged from precipitation at high altitudes and/or influenced by snow thawing (Gibson and Ried, 2010; Halder et al., 2013). The best match model produces reservoir isotopic values close to the measured ones as indicated in

Figure 8.9a. The model output best fit the isotopic values that correspond to Sep-11, Nov-11, and June-12. However the divergence observed between the model and the observations for Sep-12 and Oct-12, which could be explained by the significance influence of evaporation on reservoir isotopic signature leading to more enriched values. Since the water level in the reservoir in 2012 was higher than 2011 (Figure 8.3a), thus the surface area subjected to evaporation was larger according to Figure 8.4b. Accordingly, evaporation in Sep-12 (0.8 MCM month^{-1}) and Oct-12 (0.6 MCM month^{-1}) were higher compared to that for Sep-11 (0.6 MCM month^{-1}) and Nov-11 (0.1 MCM month^{-1}) (Figure 8.3b). The model divergence from the observations of April 2013 can be explained by the fact that there are 6 months' worth of simulation between the measurement of October 2012 and April 2013, where the reservoir hydrological regime was subjected to important alternations during this period. Furthermore, the hydrological regime of the river in the wet season of 2013 is very active (Figure 8.3a), thus the river discharge will dominate over the source by indicating the reservoir isotopic ratio during the last three months of the simulation.

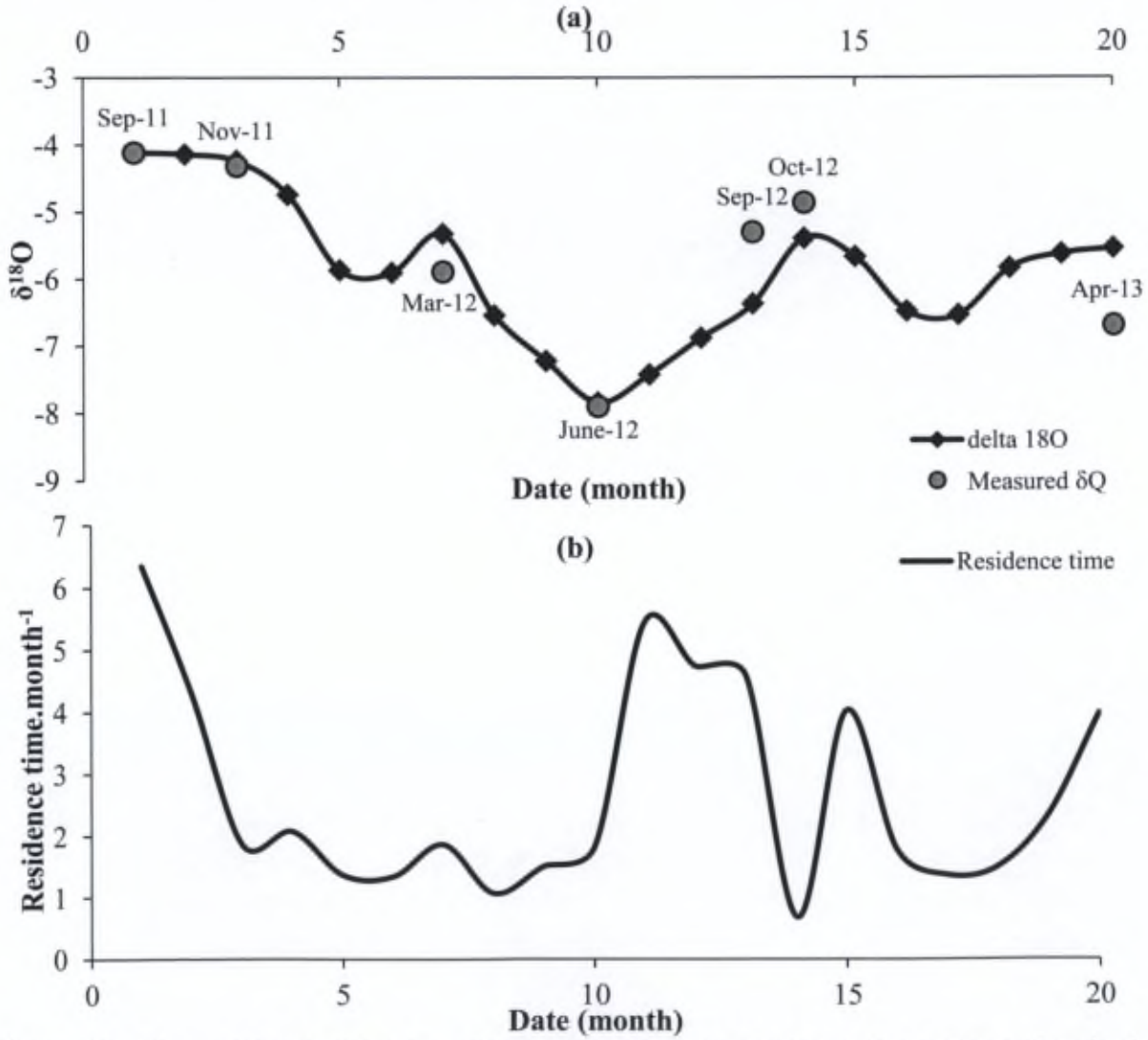

Figure 8.9: The model output that best fits the observation (a) and the water residence time in the reservoir (b).

The corresponding residence time for the best match model output is shown in Figure 8.9b, which reflects a short water residence time that never exceeds 7 months. Estimated residence time ranges between the longest period of 6.3 months for January 2011 to the shortest residence time of 0.7 months in February 2012. Furthermore, the estimated residence time during March 2012 (1.87 month) may result in the depleted isotopic signature of the reservoir for the following months until June. In other words, the depleted water by heavy isotopes flushed from the source into the reservoir during March (-9.97‰) will possibly have the adequate residence time to influence the isotopic ratio of reservoir water until June (-7.88‰). Even though the estimated source waters in June are heavy (-3.12‰) it might not impact the reservoir water mixing instantaneously but in the later months as shown in Figure 8.9.

8.3.3 Environmental implications and method limitations

The simulations of the model clearly evidence inward and outward surface-groundwater interactions in the reservoir. Consequently, several parameters controlling fluxes direction into and out from the reservoir. Thus the significance of the water exchange will be controlled by its direction and the physicochemical situation of the reservoir, and the hydrometeorological conditions. For instance, during dry years when there is less precipitation, low river inflow, and shallow water table; the dominating flux is the outward infiltration from the reservoir to the groundwater, thus threatening groundwater quality. While in rainy years addressed by heavy rain, high river flow and high groundwater table, an inward water exchange will dominate the net flux. Precipitation contributes only by 1% of the total incoming water to the reservoir, while the inward source net flux is significantly contributing in the total water income to the reservoir. The mean water input of the source during the study period is estimated to be 27% of the total water income. While during October 2011 and September 2012 the source flux represents almost half the water income to Qaraaoun reservoir other than Litani river inflow. Conversely, the mean water loss from the reservoir through evaporation is estimated to be 2.5%. Additionally 17 % of reservoir water is lost due to infiltration to groundwater.

Apparently the groundwater source contributes by a significant water income into the reservoir thus playing a crucial role in controlling the reservoir water budget which is equivalent in its importance that of the Litani River. Groundwater influx will serves as a diluting factor and adjusts the internal hydrological settings of the reservoir by attaining a self-purification process. Previous studies indicated a better water quality at the lower reaches of the dam compared to the river inlet (Korfali et al., 2006), but they have ignored the possibility of groundwater flux that improves the reservoir water quality. Furthermore, the bottom water of the reservoir will be renewed by the source influx, thus improving the water quality used for irrigation. In the other hand, this active water exchange will control the transport direction of nutrients in the reservoir according to the flux direction, and initiates the resuspension of sediments from reservoir bed mechanically. Additionally, the groundwater influx will aerates the bottom water layer thus altering the redox conditions at sediment water interface. As a consequence, metals will be released from the sediments to the above water column and deteriorate irrigation water quality (Argese et al., 1997). Thus, a

precise water management plans should be conducted to effectively minimize the hazardous of contaminates in reservoir bottom water and at the water-sediment interface. These observations can emphasize the importance of the geological contexts in future designed reservoirs and rain harvesting projects. The significance of surface-groundwater interactions must be taken in consideration on water quality and sustainability of water management programs.

There is an antagonistic relationship between the magnitude of surface-ground water interaction and the duration of water residence time in the reservoir, where the increased mixing volume will decrease the water residence time and vice versa is true. Short residence time will not provide the sufficient time to homogenize the water in the reservoir (Froelich et al., 2005), thus depriving the bottom layer to be renewed by surface water. As a consequence, increasing the hazard of contamination on the water pumped for irrigation and groundwater ultimately. Moreover, short residence time that is well pronounced in the studied reservoir (Figure 8.9b), will increase the reservoir vulnerability to seasonal variations (Jonsson et al., 2009), which explains the fast response to minor hydrometeorological changes. Nevertheless, longer residence time will enhance water evaporation (Jonsson et al., 2009). This further supports the explanation of model divergence from the observations for Sep and Oct 2012 (Figure 8.9a), that are associated with longer residence time compared to other months (Figure 8.9b).

The model outputs can suggest a seasonal water management plan, by which the Litani river authority can control the hydrological parameters, and harnesses the hydrostatic law in the benefit of the hydropower project sustainability. This can be simply achieved by monitoring meteorological conditions and linking it through the model to reservoir water capacity and the water level in the piezometers, in order to regulate the reachable water level in the reservoir. Water collected in the reservoir must be allowed to be diluted by groundwater influx and/or pumped for hydropower project and stored in the irrigating canals to prevent its infiltration to groundwater in accordance with the source flux.

Although insightful, the work presented here and its subsequent conclusions are limited by the restricted dataset available. A higher sampling rate would allow better constraining the model and ensure that the lake does not go through a change in hydrologic regime between two series of measurements. The use of another conservative isotopic ratio could strengthen the method by allowing performing a calibration of the hydrologic parameters based on one isotope and a validation on the other. The second limitation of the model is that this method only allows quantifying the net water exchange between the lake and the groundwater. The resulting isotopic ratios for the source clearly indicate that additional mixing occurs and the current version of the model can be used as a tool to run scenarios trying to establish the most realistic mixing rates. These methods remains however a significant step forward towards a better understanding of the hydrology of Qaraaoun reservoir and the simplicity of the approach, associated to its limited data requirement suggest that similar studies could be carried out in other similar system in the region.

8.4. Conclusions

The mass balance model described here brings a better understanding of the hydrological regime of Qaraaoun reservoir. In particular, it puts in evidence the significant role of a two ways exchange between the reservoir and the underlying groundwater. Qaraaoun reservoir is highly influenced by subsurface inflow by which source flux fluctuations are translated as an alternation in the reservoir water budget. The water volume going through this source exceeds, at times, those delivered by the Litani River and precipitations. However, depending on the season, a significant volume of water also infiltrates the groundwater, thus posing a potential threat for the quality of ground waters. Additionally, isotopic data provide insight on the origin of the water coming from the source which responds quickly to seasonal and annual hydrometeorological changes at the watershed scale. This suggests that the water provided to the lake via the source comes either from local precipitation and snow thawing, or recharged by surface water after a relatively short journey through the water table. These findings have ecological significance for the region because of the use of Qaraaoun reservoir water for irrigations purposes that contributes in the socio-economical development of the basin. Future studies of the Qaraaoun reservoir should focus on better understanding the dynamics of the groundwater-lake interactions and may help local authorities in the design of future water management plans able to take advantage, for example, of potential water purification via groundwater inputs during the rainy season. Similar modeling approaches can be applied to other lakes and reservoirs subjected to subsurface inflow which is unapproachable for direct measurement and to be hydrologically evaluated and characterized.

Chapter 9

Conclusions

In the intention of investigating the environmental implications of land-use on evolution of watersheds and pollutants dynamics, this research was conducted over a study period of three years (2011-2013) in two contrasting watersheds in Eastern Mediterranean (Lebanon). The contrasting aspects of the studied basins include variations of land-use type, geographical location, geomorphological features, geology, soil type, and climate. The synoptic influence of these factors controls pollutant behavior and its fate in nature. Consequently the pollutants behave differently according to the environmental context of each hydrographic basin. The studied watersheds are indirectly influenced by the same potential contaminant (fertilizers) derived from the phosphate fertilizer factory in the basin dominated by industrial land-use (Al Jouz Basin), and the intensive agricultural practices in Litani basin.

Characterization of the industrial byproduct (phophogypsum) indicated that this material have high solubility and rich in trace metals. Solubility of PG particles shows a decrease as its concentration increases, due to the cumulative ionic strength leading to the formation of stable aggregates. As a consequence, this will increase the environmental hazards linked to metal release from PG in stockpiles when later recycling actions are taken. This study addresses certain approaches to improve the quality status of aquatic environments exposed to industrial solid wastes. The aim is to remediate PG wastes and enhance their reusability as economically beneficial gypsum substitute. Subjecting PG wastes to alkaline treatment in order to encapsulate the hazardous contaminants within the matrix, or treating these wastes with acid will render them ecofriendly reusable. The magnitude and extent of industrial wastes discharge were explored in Al Jouz basin, by coupling geochemical analysis to Pb isotopic approach in both soil and sediment. Similarly, Pb isotopes were a selective and robust tool to distinguish the different pollution sources that were preserved in lacustrine sediments derived from multiuse land in the agricultural watershed. Contamination in the studied industrial area is strongly associated with the fertilizer factory and traffic. Pollution magnitude is high near the proximity of the factory and wind helps its dispersion to regions 3 km away from the industrial source. Socio-economical impacts are reflected on the deterioration of the soil quality where Pb penetration reaches a depth of 15 cm in the industrial watershed soils. Industrial activity affects strongly the coastal sediments that bear high radiogenic signatures due to the manufacturing process taking place. Thus, the coastal marine sediments act as a secondary point source of Pb pollution for the Mediterranean Sea. Multivariate sources of Pb are detected in the agricultural watershed, such as fuel, agrochemicals, waste incineration, industrial effluents (mainly paints and batteries),

Saharan dust and contaminated aerosols, which are accumulated in the lacustrine sediments as revealed by their isotopic compositions. Seasonally dependent human activities such as farming, in addition to weather conditions, affect the Pb source thus inducing seasonal and temporal variations in Pb isotopic signatures. The continuous weathering of carbonate outcrops in the Litani basin results in the dilution of contaminants in the lacustrine sediments. The river inlet brings the most anthropogenically contaminated suspended matter to the reservoir during the wet season. However, the first flush washes out the pollutants from the upper basin, which are transported to the reservoir. Both watersheds are impacted by leaded gasoline, waste incineration, phosphate fertilizer and contaminated aerosols from Europe and North Africa. The magnitude of pollution is higher in the industrial watershed whereas the particularity of the agricultural receiving media amplifies the risk of Pb pollution and its tendency to infiltrate to the groundwater ultimately and to bioaccumulate in the food chain.

The environmental stress exerted by both the phosphate fertilizer factory and the dam since 1950s were discovered for the first time in intact soil cores collected from the corresponding basins. Evidently the phosphate fertilizers factory is contaminating the local soil by dry deposition of fertilizers; moreover, the vehicular activity on the nearby highway and atmospheric deposition contribute greatly to soil pollution. The potential cumulative damage of the fertilizer factory threatens the soil, gorundwater, and sea in Al Jouz basin. While in the agricultural watershed, metals are derived from soil erosion and intensive agricultural activities (mainly for Cu and Cd) in addition to several industrial practices by which metals are associated with organic matter and Fe/Mn oxides. However, Pb has multi-sources in the agricultural watershed, including industrial sources from plastic, paper and paints manufacturing, agrochemicals, vehicle emissions, and atmospheric deposition. Dam establishment induces a geomorphological change in the upper basin thus increases metal contamination and fluxes. Sediments show a better preservation mechanism of historical time line of the watershed ecology compared to soil. Furthermore, the modern core retrieved from reservoir banks, indicates a high sensitivity to watershed changes by which recent environmental management plans were positively reflected on metal fluxes. Reservoir active hydrodynamics shift redox conditions thus altering metals behavior and increase metal lability during fill hydrological mode. The factors controlling the pollutant behavior and its fate were also investigated in packed soil columns, by conducting a leaching column experiment on soil collected from both watersheds. Land use activity showed it capability to affect soil composition by which soil collected from the industrial area contained sulfides and fluorides but insignificant amounts of nitrate. The contrast is true for the soil collected from the agricultural area. Most of the studied elements indicate higher mobility in industrial soil compared to agricultural soil and this could be referred to the soil physiochemical characteristics. The synergetic effect of higher clay and organic matter content, higher cation exchange capacity, and finer grain size of the agricultural soil will induce higher affinity, and thus possess higher retention potentials. As a result, pollutants will accumulate in agricultural

soil and will have higher tendency to bioaccumulate in the food chain, and the fine fraction could be mechanically transport to open water bodies.

Evidently the dam construction alters the geomorphological practices in the upper watershed, thus amplifying the contaminants load arriving to the reservoir in the form of suspended matter, and the sedimentation rate. The influence of the active hydrodynamic dam on pollutants partitioning between the water column and at the water-sediment interface was identified seasonally and spatially. And as a consequence of the reservoir hydrological settings and the water physiochemical characteristics, the hydrological and biogeochemical processes induced a vertical downward transport of chemicals towards the fine grained calcareous sediments during the fill mode. In contrast, during the spill mode the sediments acted as a source for a chemical flux upward through the water column and downward toward groundwater. The sediments behavior and reservoir eutrophication in the spill mode impacted significantly the quality of the water exiting the reservoir in the hypolimnion near the dam zone. However, local hydrodynamics and sediment behavior buffered partially the chemical and thermal stress on the reservoir water quality during the fill mode. The geomorphological features of the reservoir situated in a Mediterranean semi-arid area enhanced the strong hydrological connectivity between surface water and groundwater where the reservoir responded quickly to natural and anthropogenic changes in the upper watershed. The water used for irrigation is enriched in metals and nutrients such as nitrogen in addition to chloride, which threatens to salinize the agricultural soil and increases metal bioavailability and its potential to bioaccumulate in the food chain. Moreover, the nutrient enrichment in the water withdrawn from the reservoir will induce algal growth that may lead to turbine biofouling thus disturbing irrigation canal activity and hydro-project sustainability.

It was found that the reservoir is not acting as one hydrological entity, and it is highly influenced by internal biogeochemical processes, and external hydrometeorological interferences. Diverse topography and semi-arid climatic variations are reflected on dam hydrology. The short residence time minimizes evaporation impact on isotopes where no annual equilibrium is reached during fast climatic and hydrological changes of seasons thus the response is directly reflected on the isotopic composition of the reservoir. The dam lake reacts rapidly to cyclic variations of meterological changes (both continental and orographic rain effects) and land-use activities. The particularity of the reservoir is represented by two modes: the fill mode of high river flow during the rainy season combined with high mineralization and depleted isotopic composition versus the spill mode of high outflow and less mineralization with heavier isotopic composition during the dry season. The varying isotopic composition in time and space allows the identification of different water sectors in the reservoir. The river inlet acts as a closed system without groundwater intrusion where heavy water accumulates, which may act as a sink for contaminants during dry season. The Cz and Dz can be considered as an open water system subjected to dilution by groundwater inflow that causes vertical mixing and reverse stratification. Thus, the

location of planned reservoirs should be established in characterized hydrogeological areas with shallow water table permitting the groundwater inflow to the reservoir. Anthropogenic stress should be compensated by hydrological dilution and the environmental impacts of artificial reservoirs should be assessed to ensure the sustainability of hydro projects in the long term. This study could be extrapolated and applied to similar areas due to its socio-economical importance and the particularity of its geographical location in a semi-arid region bearing diverse topography.

Reservoir water budget was estimated, and the reservoir hydrological regime was reconstructed indicating an active surface gorundwater interaction, using simple hydrological box model applied for the first time on Qaraaoun reservoir. Our mass balance model brings a better understanding of the hydrological regime of Qaraaoun reservoir. In particular, it puts in evidence the significant role of a 2 ways exchange between the lake and ground waters. The reservoir is highly influenced by an underground source and the fluctuations of its intensity are translated by an alternation in the reservoir water budget. The water volume going through this source exceeds at time those delivered by the Litani river or precipitations. Additionally, isotopic data allows identifying the origin of the water coming from the source and shed new light on the overall hydrological dynamics of the entire watershed. These findings have ecological implications for the region because of the use of Qaraaoun Lake water for irrigations purposes. Reservoir bottom water is used for several purposes but mainly for irrigation, and the model output can provide insights about its quality referring to altering hydrometeorogical aspects that control the fill and spill hydrological regimes. This model will found the basis to design new national and regional reservoirs planed in similar geological context in the eastern Mediterranean. Similar modeling approaches can be applied to other lakes and reservoirs subjected to subsurface inflow which is unapproachable for direct measurement and to be hydrologically evaluated and characterized.

This thesis help to improve our knowledge of the case studied and provide a foundation for future hydropower projects, allowing the authorities to establish a road-map for national management plans and to raise the alert for mitigation and management methods to preserve the environment and resource sustainability through list of recommendations. It was found that land use, precipitation, land topography, intrinsic soil properties, pollutant type and magnitude are important factors that control metal fate in the environment. Thus of all these factors should be taken into consideration to achieve effective pollution management plans. Controlled stockpiles and organic ligands could be utilized under various pH conditions to treat fertilizer disposal waste and PG recycling with the objective of reducing their hazardous impact of released contaminants on natural biota. Additionally, sediments risk assessment plans should be firmed up in the agricultural watershed to limit sedimentation rates that decreases the reservoir water capacity and increasing the area of flood plains. Furthermore, the water quality in the spill mode should receive more attention due to its potential hazard for the hydro-project and the

sustainability of the agricultural soil in the long term. Finally, the model outputs can suggest a seasonal water management plan, by which the Litani river authority can control the hydrological parameters, and harnesses the hydrostatic law in the benefit of the hydropower project sustainability. This can be simply achieved by monitoring meteorological conditions and linking it to reservoir water capacity and the water level in the piezometers, in order to regulate the reachable water level in the reservoir. Water collected in the reservoir must be allowed to be diluted by groundwater influx and/or pumped for hydropower project and stored in the irrigating canals to prevent its infiltration to groundwater in accordance with the source flux.

References:

Abi-Ghanem C., Chiffoleau J.F., Bermond A., Nakhlé K., Khalaf G., Borschneck D., Cossa D., (2009). Lead and its isotopes in the sediment of three sites on the Lebanese coast: Identification of contamination sources and mobility, Applied Geochemistry, 24: 1990-1999.
Akin B.S., Atıcı T., Katircioglu H., Keskin F., (2010). Investigation of water quality on Gökcekaya dam lake using multivariate statistical analysis, in Eskisehir, Turkey. Environ Earth Science,63, 1-11.

Alaoui AM., Choura M., Maanan M., Zourarah B., Robin M., Conceicao M-F., Andrade C., Khalid M., Carruesco C., (2010). Metal fluxes to the sediments of the Moulay Bousselham lagoon, Morocco. Environ Earth Sci., 61:275-286.

Al-Charideh A., (2012). Geochemical and isotopic characterization of groundwater from shallow and deep limestone aquifers system of Aleppo basin (north Syria). Environ Earth Sci, 65:1157–1168.

Alemaw B. F., Majauale M., Simalenga T., (2013). Assessment of Sedimentation Impacts on Small Dams—A Case of Small Reservoirs in the Lotsane Catchment. Journal of Water Resource and Protection, 5: 1127-1131.
Al-Masri MS., Amin Y., Ibrahim S., Al-Bich F., (2004). Distribution of some trace metals in Syrian phosphogypsum. Applied Geochemistry, 19: 747-753.

Alva A.K., Sumner M.E., (1988). Effect of phosphogypsum or calcium sulfate on aluminon reactive aluminum in solutions at varying pH. Communications in soil science and plant Analysis, 19: 1715-1730.

Alvarez JM., (2007). Influence of Soil Type on the Mobility and Bioavailability of Chelated Zinc, Journal of Agriculture and Food Chemistry 55: 3568 - 3576.
Ammann A.A., Hoehn E., Koch S., (2003). Ground water pollution by roof runoff infiltration evidenced with multi-tracer experiments Water Research, 37: 1143–1153.
Ammar R., El Samrani AG., Kazpard V., Bassil J., Lartiges B., Saad Z., Chou L., (2013) Applying physicochemical approaches to control phosphogypsum heavy metal releases in aquatic environment, Environmental Science and Pollution Research 20: 9014- 9025.
Aoun M., El Samrani AG., Lartiges BS., Kazpard V., Saad Z., (2010). Releases of phosphate fertilizer industry in the surrounding environment: Investigation on heavy metals and polonium-210 in soil. Journal of Environmental Sciences, 22:1387-1397.

Appleby P.G., Oldfield F., (1983). The assessment of 210Pb data from sites with varying sediment accumulation rates. Hydrobiologia, 103: 29-35.
Aprile F.M., Bouvy M., (2010). Heavy metal levels in surface waters from a tropical river basin, Pernambuco State, northeastern Brazil. Acta Scientiarum. Biological Sciences Maringá, 32: 357-364.

Argese E., Ramieri E., Bettiol C., Pavoni B., Chiozzotto E., Sfriso A., (1997). Pollutant exchange at the water sediment interface in the Venice canals. Water, Air and Soil pollution, 99: 255-263.
Arnon D.A., (1949). Copper Enzymes in Isolated Chloroplasts. Polyphenoloxidase In Beta Vulgaris. Plant Physiology, 24: 1-15.
Asante K.A., Agusa T., Mochizuki H., Ramu K., Inoue S., Kubodera T., Takahashi S., Subramanian A., Tanabe S., (2008). Trace elements and stable isotopes (d13C and d15N) in shallow and deep-water organisms from the East China Sea. Environmental Pollution 156: 862–873.
Assaf H., Saadeh M., (2008). Assessing water quality management options in the Upper Litani Basin, Lebanon, using an integrated GIS-based decision support system, Environmental Modeling & Software 23: 1327–1337.
ASTM (2010) Standard Specification for ASTM Hydrometers, E 100, American Society for Testing and Materials, Philadelphia, PA, USA, 12p

ASTM D 2974 (2007) Standard Test Methods for Moisture, Ash, and Organic Matter of Peat and Other Organic Soils, American Society for Testing and Materials, Philadelphia, PA, USA, 4p

Atkinson CA., Jolley DF., (2007). Simpson SL. Effect of overlying water pH, dissolved oxygen, salinity and sediment disturbances on metal release and sequestration from metal contaminated marine sediments. Chemosphere, 69: 1428–1437.
Attallah M.F., El Afifi E.M., Hilal M.A., El Reefy S.A., (2010), treatment of TENORM waste: phosphogypsum produced in fertilizer industry. Radiochemistry, 52: 441-445.

Audry S., Grosbois C., Bril H., Schafer J., Kierczak J., Blanc G., (2010). Post-depositional redistribution of trace metals in reservoir sediments of a mining/smelting-impacted watershed (the Lot River, SW France). Applied Geochemistry, 25: 778–794.
Awad M.M., Darwich T., (2009). Evaluating Sea Water Quality in the Coastal Zone Of North Lebanon Using TELEMAC-2DTM. Lebanese Science Journal, 10: 35-43.
Awad S., (2011). Isotopic study (^{18}O, ^{2}H) of the ground water in Bekaa' plain (Lebanon). Physics Procedia; 21:13-21.

Awad S., (2013). The role of Isotopes in the determination of the origin of mineralization of the ground water: Plain of Bekaa- Lebanon. International Journal of Environmental Protection; 3: 25-28.

Azoury S., Tronczyński J., Chiffoleau J.-F., Cossa D., Nakhlé K., Schmidt S., Khalaf G., (2013). Historical Records of Mercury, Lead, and Polycyclic Aromatic Hydrocarbons Depositions in a Dated Sediment Core from the Eastern Mediterranean. Environmental Science &Technology, 47: 7101-7109.
Baeza M., Ren J., Krishnamurthy S., Vaughan T.C., (2010). Spatial Distribution of Antimony and Arsenic Levels in Manadas Creek, an Urban Tributary of the Rio Grande in Laredo, Texas. Arch Environ Contam Toxicol., 58: 299-314.
Balkis N., Aksu A., Okus E., Apak R., (2010). Heavy metal concentrations in water, suspended matter, and sediment from Gökova Bay, Turkey, Environ Monit Assess. 167: 359–370.
Balogh SJ., Triplett LD., Engstrom DR., Yabing NH., (2010). Historical trace metal loading to a large river recorded in the sediments of Lake St. Croix, USA. J Paleolimnol., 44: 517-530.

BAMAS review report for Litani Basin Management Advisory Services (BAMAS), bureau for Asia and the near East; U.S. agency for international development (2005). Litani water quality management project.
Banger K., Toor G., Chirenje T., Ma L., (2010). Polycyclic Aromatic Hydrocarbons in Urban Soils of Different Land Uses in Miami, Florida. Soil and Sediment Contamination, 19: 231–243.
Banks JL, Ross DJ, Keough MJ, Eyre BD, Macleod CK., (2012). Measuring hypoxia induced metal release from highly contaminated estuarine sediments during a 40 day laboratory incubation experiment. Science of the Total Environment, 420: 229-237.
Barber L.B., Murphy S.F., Verplanck P.L., sandstorm M.W., Taylor H.E., Furlong E.T., (2006). Chemical Loading into Surface Water along a Hydrological, Biogeochemical, and Land Use Gradient: A Holistic Watershed Approach. Environ. Sci. Technol., 40: 475-486.
Battaglia A., Calace N., Nardi E., Petronio B.M., Pietroletti M., (2007). Reduction of Pb and Zn bioavailable forms in metal polluted soils due to paper mill sludge addition Effects on Pb and Zn transferability to barley, Bioresource Technology, 98: 2993–2999.
Battistoni P., Carniani E., Fratesi V., Balboni P., Tornabuoni P., (2006). Chemical−Physical Pretreatment of Phosphogypsum Leachate. Ind. Eng. Chem. Res, 45: 3237–3242.

Benoit G., Rozan T.F. (2001). ^{210}Pb and ^{137}Cs dating methods in lakes: A retrospective study. Journal of Paleolimnology, 25: 455-465.
Berga, L., 2008. "Dams and Sustainable Development", World Atlas and Industry Guide. The International Journal on Hydropower and Dams, UK.

Bernier X., (2010). Lebanon Viewed Through it Transportation Networks: A "Fluid Network" in a Fragmented Territory? Asia and pacific studies, 7: 33-49.

Béthoux J.-P, Courau P., Nicolas E., Ruiz-Pino D., (1990). Trace metal pollution in the Mediterranean Sea. Oceanologica Acta, 13: 481-488.
Bindler R., Renberg I., Anderson NJ., Appleby PG., Emteryd O., Boyle J., (2001). Pb isotope ratios of lake sediments in West Greenland: inferences on pollution sources, Atmospheric Environment, 35: 4675–4685.
Bindler R., Renberg I., Klaminder J., Emtery O., (2004). Tree rings as Pb pollution archives? A comparison of Pb^{206}/Pb^{207} isotope ratios in pine and other environmental media, The Science of the Total Environment 319: 173–183.
Bird G., Brewer P.A., Macklin M.G., Nikolova M., Kotsev T., Mollov M., Swain C., (2010).Quantifying sediment-associated metal dispersal using Pb isotopes: Application of binary and multivariate mixing models at the catchment-scale, Environmental Pollution 158: 2158-2169.
Blais J.M., Kalff J., (1993). Atmospheric Loading of Zn, Cu, Ni, Cr, and Pb to Lake Sediments: The Role of Catchment, Lake Morphometry, and Physico-Chemical Properties of the Elements. Biogeochemistry, 23: 1-22.
Boehrer B., Schultze M., (2008). Stratification of Lakes. Reviews of Geophysics, RG2005 46:1- 27.

Boisvert J–P., Domenech M., Foissy A., Persello J., Mutin J-C., (2000). Hydration of calcium sulfate hemihydrate (CaSO4·12H2O) into gypsum (CaSO4·2H2O). The influence of the sodium poly(acrylate)/surface interaction and molecular weight. Journal of Crystal Growth, 220: 579-591.

Bollhöfer A. and Rosman K.J.R., (2002).The temporal stability in lead isotopic signatures at selected sites in the Southern and Northern Hemispheres, Geochimica et Cosmochimica Acta, 66: 1375–1386.
Bollhöfer A., Rosman K.J.R.., (2001). Isotopic source signatures for atmospheric lead: The Northern Hemisphere. Geochimica et Cosmochimica Acta, 65:1727–1740.

Bookman R., Driscoll C.T., Effler S.W., Engstrom D. R., (2010). Anthropogenic impacts recorded in recent sediments from Otisco Lake, New York, USA. J Paleolimnol., 43: 449–462.
Bou Kheir R., Cerdan O., Abdallah C., (2006). Regional soil erosion risk mapping in Lebanon. Geomorphology, 82: 347–359.
Bou Kheir R., Greve M. H., Abdallah C., Dalgaard T., (2010). Spatial soil zinc content distribution from terrain parameters: AGIS-based decision-tree model in Lebanon. Environmental Pollution, 158: 520-528.
Bouchaou L., Michelot J-L., (1997). Contribution des isotopes à l'étude de la recharge des aquifères de la region de Beni Mellal (Tadla, Maroc). Hydrochemistry (proceedings of the Rabat Symposium, April 1997) IAHS Publ.244: 37-44.
Brandes JA., Devol AH., (1997). Isotopic fractionation of oxygen and nitrogen in coastal marine sediments. Geochimica et Cosmochimica Acta, 61: 1793-1801.

Bridgen K., Stringer R., Santillo D., (2002). Heavy metals concentration of fertilizer and phosphogypsum waste produced by the Lebanese Chemical Company, Lebanon, Technical Note 13 Greenpease Research Laboratories, University of Exeter.
Broadbent FE., (1953). The soil organic fraction. Advances in Agronmy, 5: 153-183.
Brochet, P., Gerbier, N., 1968. L'évapotranspiration, aspect agrométéorologique, évaluation pratique de l'évapotranspiration potentielle. Monographie n°65 de la Météorologie Nationale, 67 p.
Burnett W.C., Chin P., Deetae S., Panik P., (1988). Release of Radium and Other Decay-Series Isotopes from Florida Phosphate Rock, Final Report, Florida Institute of Phosphate Research; Pub. No. 05-016-059; P181.
Butler II Thomas W., (2007). Application of multiple indicators, including the stable isotopes of water, to differentiate water quality evolution in a region influenced by various agricultural practices and domestic wastewater treatment and disposal. Science of Total Environment, 388: 149-167.

Callender E. Rice K., (2000). The Urban Environmental Gradient: Anthropogenic Influences on the Spatial and Temporal Distributions of Lead and Zinc in Sediments, Environmental Science & Technology, 34: 232-238.

Canete S.J.P., Palad L.J.H, Enriquez E.B, Garcia T.Y, Yulo-Nazarea T., (2008). Leachable ^{226}Ra in Philippine phosphogypsum and its implication in groundwater contamination in Isabel, letye, Philippines. Environ Moint Assess, 142: 337-344.

Carbonell A.A, Porthouse J.D, Mulbah C.K, Deluane R.D, Patrick W.H.J., (1999). Metal soulubility in phosphogypsum-amended sediment under controlled pH and redox conditions. Journal of environmental quality, 28: 232-242.

Cardenas-Escudero C., Morales-Florez V., Perez-Lopez R,. Santos A., Esquivias L., (2011). Procedure to use phosphogypsum industrial waste for mineral CO2 sequestration Short communication, Journal of Hazardous Materials, 196: 431- 435.

Carey R.O., Hochmuth G.J., Martinez C.J., Boyer T.H., Dukes M.D., Toor G.S., Cisar J.L., (2013). Evaluating nutrient impacts in urban watersheds: Challenges and research opportunities (Review). Environmental Pollution, 173: 138-149.

Cartwright I., Weaver T. R., Cendón D.I., Fifield L.K., Tweed S.O., Petrides B., Swane I. (2012). Constraining groundwater flow, residence times, inter-aquifer mixing, and aquifer properties using environmental isotopes in the southeast Murray Basin, Australia. Appl. Geochem; 27:1698-1709.

Casciotti KL., Sigman DM., Hastings MG., Bohlke JK., Hilkert A., (2002). Measurement of the oxygen isotopic composition of nitrate in seawater and freshwater using the denitrifier method. Analytical Chemistry, 74 (19): 4905-4912.

Chaaban FB., Nuwayhid I., Djoundourian S., (2001). A study of social and economic implications of mobile sources on air quality in Lebanon. Transportation Research Part D: Transport and environment 6 347–55.

Chappaz A., Gobeil C., Tessier A., (2008). Geochemical and anthropogenic enrichments of Mo in sediments from perennially oxic and seasonally anoxic lakes in Eastern Canada. Geochimica et Cosmochimica Acta, 72: 170–184.

Chen G., He Z., Stofella P., Yang X., Yu S., Yang J., Calvert D., (2006). Leaching Potential of Heavy Metals (Cd, Ni, Pb, Cu and Zn) from Acidic Sandy Soil Amended with Dolomite Phosphate Rock (DPR) Fertilizers. Journal of Trace Elements in Medicine and Biology, 20: 127-133.

Chillrud S.N., Hemming S., Shuster E.L., Simpson H. J., Bopp R. F., Ross J.M., Pederson D.C., Chaky D.A., Tolley L.-R., Estabrooks F., (2003). Stable lead isotopes, contaminant metals and radionuclides in upper Hudson River sediment cores: implications for improved time stratigraphy and transport processes, Chemical Geology, 199: 53– 70.

Chon H-S, Ohandja D-G, Voulvoulis N., (2012). The role of sediments as a source of metals in river catchments. Chemosphere, 88: 1250-1256.

Choueiri E.M., Choueiri G. M., Choueiri B. M., (2010). Analysis of Accident Patterns in Lebanon, Paper prepared for the 4th International Symposium on Highway Geometric Design June 2 to 5, 2010 Valencia, Spain pp 24.

Chrysochoou M., Dermatas D., Grubb D. G., (2007). Phosphate application to firing range soils for Pb immobilization: The unclear role of phosphate. Journal of Hazardous Materials, 144:1-14.

Clark E.V., Odhiambo B.K., Ricker M.C. (2014). Comparative Analysis of Metal Concentrations and Sediment Accumulation Rates in Two Virginian Reservoirs, USA: Lakes Moomaw and Pelham. Water Air Soil Pollut., 225:1860-1878.

Crocket J.H. and Kabir A., (1981). Geochemical Pathway Studies of Heavy Metals in Lake Sediments from the Sudbury-Temagami Area, Ontario, Journal of Great Lakes Research, 7: 455-466.

Da Conceição F.T., Bonotto D.M., (2006). Radionuclides, Heavy metals and fluorine incidence at Tapira phosphate rocks, Brazil, and their industrial (by) products. Environmental Pollution, 139: 232-243.

Dabous A.A., (2002). Geochemistry of Sediment Cores from Lake Overstreet and Upper Lake Lafayette,Leon County, Florida. Environmental Geosciences, 9: 51–65.

Daou C., Salloum M., Mouneimne AH., Legube B., Ouaini N., (2013). Multidimensionnal Analysis of Two Lebanese Surface Water Quality: Ibrahim and El-Kalb Rivers. Journal of Applied Sciences Research, 9: 2777-2787.

Darwish T., Atallah T., Francis R., Saab C., Jomaa I., Shaaban A., Sakka H., Zdruli P., (2011) Observations on soil and groundwater contamination with nitrate: A case study from Lebanon-East Mediterranean. Agricultural Water Management, 99: 74-84.

Das B., Narwani A., Matthews B., Nordin R., Mazumder A., (2009). Anthropogenic disturbance history influences the temporal coherence of paleoproductivity in two lakes J Paleolimnol, 42:167–181.

Delfino J. J., (1976). Great lakes: chemical monitoring. Environmental Science & Technology, 10: 968-990.

Delsontro T., Mcginnis DF., Sobek S., Ostrovsky I., Wehrli B., (2010). Extreme Methane Emissions from a Swiss Hydropower Resevoir: Contribution from Bubbling Sediments. Environ. Sci. Technol., 44: 2419-2425.

Develle A-L., Herreros J., Vidal L., Sursock A., Gasse F. (2010). Controlling factors on a paleo-lake oxygen isotope record (Yammou'neh, Lebanon) since the Last Glacial Maximum. Quaternary Science Reviews, 29: 865–886.

Diaw M., Faye S., Stichler W., Maloszewski P., (2012). Isotopic and geochemical characteristics of groundwater in the Senegal River delta aquifer: implication of recharge and flow regime. Environ Earth Sci, 66:1011–1020.

Dudas M.J., Arocena J.M., Rutherford P. M., (1995). Heterogeneous distribution of trace elements and fluorine in phosphogypsum by-product. The Science of the total Environment, 162: 149-160.

Duman F., Aksoy A., Demirezen D., (2007). Seasonal Variability of Heavy Metals in Surface Sediment of Lake Sapanca, Turkey, Environ Monit Assess., 133: 277–283.

Durán I., Sánchez-Marín P., Beiras R., (2012). Dependence of Cu, Pb and Zn remobilization on physicochemical properties of marine sediments. Marine Environmental Research, 77: 43-49.

Ebrahimpour M., Mushrifah I., (2008) Heavy metal concentrations in water and sediments in TasikChini, a freshwater lake, Malaysia. Environ Monit Assess., 141: 297–307.

Edelshtein, K.K., Grechushnikova, M.G., Datsenko, Y.S., Puklakov, V.V., 2012. Diagnostic Modelling of Within_Water Processes in Reservoirs. Water Resources. 39, 432–445.

Edgell H. S., (1997). Karst and hydrogeology of Lebanon. Carbonates and Evaporites;12: pp 220-235.

Ekpo BO, and Ibok UJ., (1998). Seasonal variation and partition of trace metals (Fe, Zn, Cu, Mn, Cr, Cd and Pb) in surface sediments: relationship with physico-chemical variables of water from the Calabar River, South Eastern Nigeria. Environmental Geochemistry and Health, 20: 113-121.

El Samad O., Baydoun R., Nsouli B., Darwish T., (2013). Determination of natural and artificial radioactivity in soil at North Lebanon province. Journal of Environmental Radioactivity, 125: 36-39.

El Samad O., Zahraman K., Baydoun R., Nasreddine M., (2007). Analysis of radiocaesium in the Lebanese soil one decade after the Chernobyl accident. Journal of Environmental Radioactivity 92: 72-79.

El-Fadel M., Zeinati M., Jamali D., (2000). EIA procedure Framework for environmental impact assessment in Lebanon. Environmental Impact Assessment Review, 20: 579–604.

El-Fadel M., Zeinati M., Jamali D., (2001). Water resources management in Lebanon: institutionalcapacity and policy options. Water Policy, 3: 425–448.

El-Fadel, M., Maroun R., Bsat R., Makki M., Reiss P., and Rothberg D., (2003). Water quality assessment of the Upper Litani river basin and Lake Qaraoun – Lebanon. Integrated Water and Coastal Resources Management - Indefinite Quantity Contract. Bureau for Asia and the Near East. U.S. Agency for International Development. 77p

El-Fadel, M., Maroun, R., Bsat, R., Makki, M., Reiss, P., Rothberg, D., 2003. Water quality assessment of the Upper Litani river basin and Lake Qaraoun – Lebanon. Integrated Water and Coastal Resources Management – Indefinite

Ellis A.S., Johnson T.M., Bullen T.D., (2004). Using Chromium Stable Isotope Ratios to Quantify Cr (VI) Reduction: Lack of Sorption Effects. Environmental Science & Technology, 38: NO. 13.

Elmotfy SE., Shokir E M., (2003). Effect of surface active agents on electrokinetic and wettability changes of reservoir rocks. Emirates Journal for Engineering Research, 8: 35-40.

Erel Y., Kalderon– Asael B., Dayan U., Sandler A., (2007) European Atmospheric Pollution Imported by Cooler Air Masses to the Eastern Mediterranean during the summer, Environ. Sci. Technol., 41: 5198-5203.

Erel Y., Torrent J., (2010). Contribution of Saharan dust to Mediterranean soils assessed by sequential extraction and Pb and Sr isotopes, Chemical Geology, 275: 19–25.

Ersen A., Smith A., Chotard T., (2006). Effect of mailc and citric acid on the crystallization of gypsum investigated by coupled acoustic emission and electric counductivity techniques. Journal Mater Science, 41: 7210-7217.

Escalante-Garcia R.X., Magallanes-Rivera J.I., Gorokhovsky A., (2009). Hydration reactions and microstructural characteristics of hemihydrate with citric and malic acid Construction and Building Materials, 23: 1298-1305.

Escobar J., WhitmoreT.J., Kamenov, G.D. Riedinger-Whitmore M.A., (2013). Isotope record of anthropogenic lead pollution in lake sediments of Florida, USA, Journal of Paleolimnology, 49: 237-252.

Fagel N., Bertrand S., Mattielli N., Gilson D., Chirinos L., Gille L., Urrutia R., (2010). Geochemical evidence (C, N and Pb isotopes) of recent anthropogenic impact in south-central Chile from two environmentally distinct lake sediment records, Journal of quaternary science, 25: 1100–1112.

Fakhri M., Abboud - Abi Saab M., Romano J-C., (2008). The use of sediments to assess the impact of selaata phosphate plant on batroun coastal area (Lebanon, levantine basin). Lebanese Science Journal, 9.

Fakhri M., Abboud - Abi Saab M., Romano J-C., Mouawad R., (2009). Impact of phosphate factory on the biological characteristics of North Lebanon surface sediments (Levantine Basin) hal-00357034, version 1 - 29 Jan 2009.

FAO (2009). Irrigation in the Middle East region in Figures-AQUASTAT Survey-Lebanon: 16 pages.

Farmer J.G., MacKenzie A.B., Eades L.J., Kirika A., Bailey-Watts A.E., (1997). Influences on the extent and record of heavy metal pollution in sediment cores from Loch Tay in a mineralised area of Scotland, Journal of Geochemical Exploration, 58: 195-202.

Fenicia, F., Savenije, H.H.G., Matgen, P., Pfister, L., 2006. Is the groundwater reservoir linear? Learning from data in hydrological modelling. Hydrol. Earth Syst. Sci.10, 139-150.

Figueiredo RO., Ovalle ARC., Eduardo de Rezende C., Martinelli A.L., (2011). Carbon and Nitrogen in the Lower Basin of the Paraíba do Sul River,Southeastern Brazil: Element fluxes and biogeochemical processes, Ambi-Agua, 6: 7-37.

Filella M., Belzile N., Chen Y-W., (2002). Antimony in the environment: a review focused on natural waters: I. Occurrence. Earth-Science Reviews, 57:125-176.

Firsova L.P. (2010), Film-Forming synthetic polyelectrolytes for phosphogypsum modification. Russian journal of applied chemistry, 83: 18-22.

Fitzpatrick M.L., Long D.T., Pijanowski B.C., (2007). Exploring the effects of urban and agricultural land use on surface water chemistry, across a regional watershed, using multivariate statistics. Applied Geochemistry, 22: 1825–1840.

Friedl, G., Wüest, A., 2002. Disrupting biogeochemical cycles-Consequences of damming. Aquat.Sci. 64, 55-65.

Froehlich K.F.O., Gonfiantini R., Rozanski K., (2005). Isotopes in Lake Studies: A Historical Perspective. Isotopes in the Water Cycle, Chapter 11: 139-150.

Frostick A., Bollhöfer A., Parry D., (2011). A study of radionuclides, metals and stable lead isotope ratios in sediments and soils in the vicinity of natural U-mineralisation areas in the Northern Territory, Journal of Environmental Radioactivity, 102: 911-918.

Fu J., Mai B., Sheng G., Zhang G.,Wang X., Peng P., Xiao Xianming., Ran R.,Cheng F., Peng X., Wang Z Tang U. W., (2003). Persistent organic pollutants in environment of the Pearl River Delta, China: an overview. Chemosphere, 52: 1411–1422.

Gadd GM., Griffiths AJ., (1978). Microorganisms and Heavy Metal Toxicity. Microbial Ecology, 4: 303-317.

Geara D., Moilleron R., El Samarani A., Lorgeoux C., Chebbo G., (2010). State of Art about Water Uses and wastewater Management in Lebanon. Lebanese Science Journal, 11: 139-152.

Gibson J.J., Reid R., (2010). Stable isotope fingerprint of open-water evaporation losses and effective drainage area fluctuations in a subarctic shield watershed. Journal of Hydrology; 381: 142–150.

Gibson, J.J., Sadek, M.A., Stone D.J.M., Hughes, C.E., Hankin, S., Cendon, D.I., Hollins, S.E., (2008). Evaporative isotope enrichment as a constraint on reach water balance along a dryland river. Isotopes in Environmental and Health Studies. 44, 83-98.

Golueke G., McGathey P.H., (1971). "Comprehensive studies of solid waste management, 3rd Annual report SERL," Berkeley, 1971.

Gomes L., Arrúe J. L., López M. V., Sterk G., Richard D., (2009). "Soil Aerosol Production in a Semi-arid Agricultural Area of Spain: The WELSONS project, 1-42.

Gomes L., Arrue J.L., Lopez M.V., Sterk G., Richard D., Gracia R., Sabre M., Gaudichet A., Frangi J.P., (2003). Wind erosion in a semiarid agricultural area of Spain: the WELSONS project. CATENA, 52: 235–256.

Gondal M.A., Hussain T., (2006). Determination of poisonous metals in wastewater collected from paint manufacturing plant using laser-induced breakdown spectroscopy, Talanta, 71: 73-80.

Gonfiantini, R., (1986). Environmental isotopes in lake studies. In Handbook of Environmental Isotope Geochemistry, P. Fritz, J.Ch. Fontes (Eds), Elsevier, NewYork. 3, 113–168.

GREENPEACE Mediterranean-Background Information Industrial Pollution in Lebanon, January 1998: 9 pages.

Greenwood, R., Kendall, K., (1999). "Selection of Suitable Dispersants for Aqueous Suspensions of Zirconia and Titania Powders using Acoustophoresis," Journal of the European Ceramic Society, 19: 479-488.

Grezzi G., Ayuso R.A., De Vivo B., Lima A., Albanese S., (2011). Lead isotopes in soils and groundwaters as tracers of the impact of human activities on the surface environment: The Domizio-Flegreo Littoral (Italy) case study, Journal of Geochemical Exploration, 109:51-58.

Grünberger O., Montoroi J.-P., Nasri S., (2004). Quantification of water exchange between a hill reservoir and groundwater using hydrological and isotopic modeling (El Gouazine, Tunisia). Geoscience, 336: 1453–1462.

Guan B., Ye Q., Lou W., Yang L., Kong B., (2011). Effect of particle size distribution on the hydration and compressive strength development of α-calcium sulfate hemihydrate paste. Powder Technology, 207: 208-214.

Gupta S., Nayek S., Saha R.N., (2011). Temporal changes and depth wise variations in pit pond hydrochemistry contaminated with industrial effluents with special emphasis on metal distribution in water-sediment system. Journal of Hazardous Material, 183: 125-131.

Gupta, S.K., Deshpande, R.D., (2004). An insight into the dynamics of Lake Nainital (Kumaun Himalaya, India) using stable isotope data. Hydrological Sciences. 49, 1099-1113.

Halder J., Decrouy L., Vennemann T.W., (2013). Mixing of Rhône River water in Lake Geneva (Switzerland-France) inferred from stable hydrogen and oxygen isotope profiles. Journal of hydrology, 477: 152-164.

Hansmann W., Köppel V., (2000). Lead-isotopes as tracers of pollutants in soils, Chemical Geology 171: 123–144.

Harlavan Y., Almogi-Labin A., Herut B., (2010). Tracing Natural and Anthropogenic Pb in Sediments along the Mediterranean Coast of Israel Using Pb Isotopes, Environ., Sci. Technol., 44: 6576–6582.

Hart BT., Van Dok W., Djuangsih N., (2002). Nutrient budget for Saguling Reservoir, West Java, Indonesia. Water Research, 36: 2152–2160.

Hartley W., Dickinson N.M., (2010). Exposure of an anoxic and contaminated canal sediment: Mobility of metal (loid)s. Environmental Pollution, 158: 649–657.

Haynes W.M., (2011). Handbook of Chemistry and Physics edition 2011-2012 page 4-56.

He T., Feng X., Guo Y., Qiu G., Li Z., Liang L., Lu J., (2008). The impact of eutrophication on the biogeochemical cycling of mercury species in a reservoir: A case study from Hongfeng Reservoir, Guizhou, China. Environmental Pollution, 154: 56-67.

Herndon E.M., Jin L., Brantley S.L., (2011). Soils Reveal Widespread Manganese Enrichment from Industrial Inputs, Environmental Science & Technology, 45: 241–247.

Hiller E., Jurkovic L., Sutriepka M., (2010). Metals in the Surface Sediments of Selected Water Reservoirs, Slovakia. Bull Environ. Contam Toxicol, 84: 635-640.

Hodges SC., (2010). Soil Fertility Basics. Soil Science Extension, North Carolina State University.

Hoefs J., (2009). Stable Isotope Geochemistry, Isotope Fractionation Processes of Selected Elements, chapter 2: 35-92.ISBN:978-3-540-70703-5.

Hohmann R., Kipfer R., Peeters F., Piepke G.,Imboden D. M., Shimaraev M. N., (1997). Processes of deep-water renewal in Lake Baikal. American Society of Limnology and Oceanography, 42: 841-855.

Hong S., Lee K., Hu SD., Hou S., Burn-Nunes LJ., Barbante C., Boutron C.F., Rosman K.J.R., (2011). Isotopic signatures for natural versus anthropogenic Pb in high-altitude Mt. Everest ice cores during the past 800 years, Science of The Total Environment 412: 194-202.

Houri A., and El Jeblawi S.W., (2007). Water quality assessment of Lebanese coastal rivers during dry season and pollution load into the Mediterranean Sea. Journal of Water and Health, 05.4: 615-623.

Hren MT., Sheldon ND., (2012).Temporal variations in lake water temperature: Paleoenvironmental implications of lake carbonate d18O and temperature records, Earth and Planetary Science Letters 337–338: 77–84.

Hu X., Wang C., Zou L., (2011) Characteristics of heavy metals and Pb isotopic signatures in sediment cores collected from typical urban shallow lakes in Nanjing, China, Journal of Environmental Management, 92: 742-748.

Huang T., Pang Z., (2012). The role of deuterium excess in determining the water salinisation mechanism: A case study of the arid Tarim River Basin, NW China. Applied Geochemistry; 27: 2382–2388.

Ignatius, A.R., Jones J.W., (2014). Small Reservoir Distribution, Rate of Construction, and Uses in the Upper and Middle Chattahoochee Basins of the Georgia Piedmont, USA, 1950–2010. International Journal of Geo-Information. 3, 460-480.

Izquierdo M., Tye A.M., Chenery S.R., (2012). Sources, lability and solubility of Pb in alluvial soils of the River Trent catchment, U.K., Science of The Total Environment 433 110–122.

Jaakola E., Tattari S., Ekholm P., Pietola L., Posch M., Barlund I., (2012). Simulated effect of gypsum amendment on phosphorus losses from agricultural soils. Agricultural and food science, 21: 292-306.

Jacksont A., Kipphutr G., Hessleina N.D., Schindler B. W., (1980). Experimental study of trace metal chemistry in soft-water lakes at different pH levels. Can. I. Fish. Aquat. Sci.volume, 37: 387-402.

Jeelani G., Bhat NA., Shivanna K., Bhat MY., (2011). Geochemical characterization of surface water and spring water in SE Kashmir Valley, western Himalaya: Implications to water–rock interaction J. Earth Syst. Sci., 120: 921-932.

Jiann K-T., Wen L-S., Santschi P. H., (2005). Trace metal (Cd, Cu, Ni and Pb) partitioning, affinities and removal in the Danshuei River estuary, a macro-tidal, temporally anoxic estuary in Taiwan. Marine Chemistry, 96: 293– 313.

Jonsson C.E., Leng M.J., Rosqvist G.C., Seibert J., Arrowsmith C., (2009). Stable oxygen and hydrogen isotopes in sub-Arctic lake waters from northern Sweden. Journal of Hydrology, 376: 143-151.

Jurado A., Vàzquez-Suñé E., Carrera J., López de Alda M., Pujades E., Barceló D., (2012). Emerging organic contaminants in groundwater in Spain: A review of sources, recent occurrence and fate in a European context. Science of the Total Environment, 440: 82–94.

Jurdi M., Korfali S.I., Karahagopian Y., Davies B.E., (2002). Evaluation of water Quality of The Qaraaoun Reservoir, Lebanon: Suitability For Multipurpose Usage. Environmental Monitoring and Assessment, 77: 11–30.

Juteau M., Michard A., Albarede F., (1986). The Pb - Sr- Nd isotope geochemistry of some recent circum-Mediterranean granites, Contributions to Mineral Petrol, 92: 331-340.

Kamennaya NA., Ajo-Franklin CM., Northen T., Jansson C., (2012). Cyanobacteria as Biocatalysts for Carbonate Mineralization Minerals, 2: 338-364.

Kannan N., Kim M., HeeHong S., Jin Y., Yim U., Ha Y., Son Y., Choi D-L., Shim W., (2012). Chemical tracers, sterol biomarkers and satellite imagery in the study of a river plume ecosystem in the Yellow Sea. Continental Shelf Research, 33: 29–36.

Kaown D., Koh D-C., Lee K-K., (2009). Effects of groundwater residence time and recharge rate on nitrate contamination deduced from d18O, dD, 3H/3He and CFCs in a small agricultural area in Chuncheon, Korea. Journal of Hydrology, 366: 101–111.

Kassir L. N., Darwish T., Shaban A., Lartiges B., Ouaini N., (2012 b). Mobility of selected trace elements in Mediterranean red soil amended with phosphogypsum: experimental study. Environ Monit Assess, 184: 4397–4412.

Kassir L. N., Darwish T., Shaban A., Olivier G., Ouaini N., (2012 c). Mobility and bioavailability of selected trace elements in Mediterranean red soil amended with phosphate fertilizers: Experimental study. Geoderma, 189–190: 357–368.

Kassir L. N., Lartiges B., Ouaini N., (2012 a). Effects of fertilizer industry emissions on local soil contamination: a case study of a phosphate plant on the east Mediterranean coast. Environmental Technology, 33: 873-885.

Kavvadias V., Doula M.K., Komnitsas K., Liakopoulou N., (2010). Disposal of olive oil mill wastes in evaporation ponds: Effects on soil properties. Journal of Hazardous Materials, 182: 144–155.

Kaysi I., Mahmassani H., Arnaout S., Katta L., (2000). Phasing out lead in automotive fuels: conversion considerations, policy formulation, and application to Lebanon, Transportation Research Part D 5, 403-418.

Khair K., Aker N., Haddad E., Jurdi M., Hachach A., (1994). The Environmental Impacts of Humans on Groundwater in Lebanon. Water, Air and Soil Pollution, 78: 37-49.

Khayat S., Ghanem M., Tamimi A., Haddad M., Geyer S., Hötzl H., Ali W., Mölle P. (2009). Hydrochemistry and isotope hydrogeology in the Jericho area/Palestine. The Water of the Jordan Valley Chapter 3; 3.3.4: 325-348.

Kober B., Wessels M., Bollhöfer A., Mangini A., (1999). Pb isotopes in sediments of Lake Constance, Central Europe constrain the heavy metal pathways and the pollution history of the catchment, the lake and the regional atmosphere, Geochimica et Cosmochimica Acta, 63: 1293–1303.

Kögel-Knabner I., Guggenberger G., Kleber M., Kandeler E., Kalbitz K., Scheu S., Eusterhues K., Leinweber P., (2008). Organo-mineral associations in temperate soils: Integrating biology, mineralogy, and organic matter chemistry (review article). J. Plant Nutr. Soil Sci., 171: 61–82.

Komárek M., Ettler V., Chrastný V., Mihaljevič M., (2007). Lead isotopes in environmental sciences: A review, Environment International 34 562–577.

Korfali S. I., and Davies B. E., (2000). Total and Extractable Trace Elements in Lebanese River Sediments: Dry Season Data. Environmental Geochemistry and Health, 22: 265–273.

Korfali S. I., and Davies B. E., (2004). Speciation of metals in sediment and water in a river underlain by limestone: role of carbonate species for purification capacity of rivers. Advances in Environmental Research 8, 599–612.

Korfali S. I., and Jurdi M., (2011a). Speciation of metals in bed sediments and water of Qaraaoun Reservoir, Lebanon. Environ Monit Assess., 178: 563–579.

Korfali S. I., and Jurdi M., (2011b). Suitability of surface water for domestic water use: Awali River caase study. European Water. 35, 3-12.

Korfali S. I., Jurdi M., Davies B. E., (2006). Variation of Metals in Bed Sediments of Qaraaoun Reservoir, Lebanon. Environmental Monitoring and Assessment, 115: 307–319.

Kouzayha A., Al Ashi A., Al Akoum R., Al Iskandarani M., Budzinski H., Jaber F., (2013). Occurrence of Pesticide Residues in Lebanon's Water Resources. Bull Environ Contam Toxicol, 91:503–509.

Kralik, M., Humer, F., Fank, J., Harum, T., Klammler, G., Gooddy, D., Sültenfuß, J.,Gerber, C., Purtschert, R.,(2014). Using 18O/2H, 3H/3He, 85Kr and CFCs to determine mean residence times and water origin in

the Grazer and Leibnitzer Feld groundwater bodies (Austria), Applied Geochemistry, doi:http://dx.doi.org/10.1016/j.apgeochem.2014.04.001.
Kraus TEC., Bergamaschi BA., Hernes PJ., Doctor D., Kendall C., Downing BD., Losee RF., (2011). How reservoirs alter drinking water quality: Organic matter sources, sinks, and transformations. Lake and Reservoir Management, 27: 205-219.
Kremer B., Kazmierczak J., Stall LJ., (2008). Calcium carbonate precipitation in cyanobacterial mats from sandy tidal flats of the North Sea. Geobiology, 6: 46-56.
Krivtsov V., Sigee DC., (2005). Importance of biological and abiotic factors for geochemical cycling in a freshwater eutrophic lake. Biogeochemistry, 74: 205–230.
Kroschwitz J.I., Howe-Grant M., Kirk-Othmer (1995). Encyclopedia of Chemical Technolog (4th ed.). Wiley, USA 1995, 10: 453–475.
Kumar U., Saravana, Sharma S., Navada S.V., (2008). Recent studies on surface water–groundwater relationships at hydro-projects in India using environmental isotopes. Hydrol. Proces, 22: 4543–4553.
Kutiel H.H., Furman H., (2003). Dust Storms in the Middle East: Sources of Origin and their Temporal Characteristics Indoor Built Environ.12: 419–426.
Kylander M.E, Weiss D.J., Martínez C.A., Spiro B., Garcia-Sanchez R., Coles B.J., (2005). Refining the pre-industrial atmospheric Pb isotope evolution curve in Europe using an 8000 year old peat core from NW Spain., Earth and Planetary Science Letters, 240: 467– 485.
Lafuente A.L., González C., Quintana J. R., Vázques A., Romero A., (2008). Mobility of Heavy Metals in Poorly Developed Carbonate Soils in the Mediterranean Region. Geoderma, 145: 238-244.
Lanzón M., García-Ruiz P.A., (2011). Effect of citric acid on setting inhibition and mechanical properties of gypsum building plasters Construction and Building Materials, 28: 506-511.

Lapworth D.J., Baran N., Stuart M.E., Ward R.S., (2012). Emerging organic contaminants in groundwater: A review of sources, fate and Occurrence (Review). Environmental Pollution, 163: 287-303.
Lavilla I., Filgueiras A.V., Valverde F., Millos J., Palanca A., Bendicho C., (2006). Depth Profile of Trace elements in a sediment core of a high-altitude lake deposit at the Pyrenees, Spain. Water, Air, and Soil Pollution, 172: 273–293.
Lee K.K., Lee J.Y., Kim Y.C., Yi M.J., (2004), Hydrogeological investigation and discharge control of a nutrient-rich acidic solution from a costal phosphogypsum stack at Yeocheon, Korea. Water, air and soil pollution, 151:143-164.
Legret M., Odie L., Demare D., Jullien A., (2005). Leaching of heavy metals and polycyclic aromatic hydrocarbons from reclaimed asphalt pavement, Water Research 39: 3675-3685.
Lenzi M., Gennaro P., Mercatali I., Persia E., Solari D., Porrello S., (2013). Physico-chemical and nutrient variable stratifications in the water column and in macroalgal thalli as a result of high biomass mats in a non-tidal shallow-water lagoon. Marine Pollution Bulletin, 75: 98–104.
Lesven L., Lourino-Cabana B., Billon G., Recourt P., Ouddane B., Mikkelsen O., Boughriet A., (2010). On metal diagenesis in contaminated sediments of the Deûle river (northern France). Applied Geochemistry, 25: 1361–1373.

Li C., Zhao L., Hana J., Wanga R., Xiong C., Xie X., (2011). Synthesis of citrate-stabilized hydrocolloids of hydroxyapatite through a novel two-stage method: A possible aggregates–breakdown mechanism of colloid formation. Journal of Colloid and Interface Science, 360: 341-349.
Li H-C., Stott L.D., Hammond D.E., (1997). Temperature and salinity effect on 18O fractionation for rapidly precipitated carbonates: Laboratory experiments with alkaline lake water. Episodes; 20: 193-198.
Li J., Li F., Liu Q., Zhang Y., (2014). Tracemetal in surfacewater and groundwater and its transfer in a Yellow River alluvial fan: Evidence from isotopes and hydrochemistry. Science of the Total Environment, 472: 979–988.
Li X-D., Liua C-Q., Harueb M., Lia S-L., Liua X-L., (2010). The use of environmental isotopic (C, Sr, S) and hydrochemical tracers to characterize anthropogenic effects on karst groundwater quality: A case study of the Shuicheng Basin, SW China. Applied Geochemistry, 25: 1924-1936.

Liang K., Hu X., Li S., Huang C., Tang Y. (2014). Anthropogenic Effect on Deposition Dynamics of Lake Sediments Based on 137Cs and 210Pbex Techniques in Jiuzhaigou National Nature Reserve, China, Chin. Geogra. Sci., 24: 180–190.

Liang X.Q, Nie ZY, He M M, Guo R, Zhu CY, Chen YX, Stephan K., (2013). Application of 15N–18O double stable isotope tracer technique in an agricultural nonpoint polluted river of the Yangtze Delta Region. Environ Sci Pollut Res, 20: 6972–6979.

Lopez P., Navarro E., Marce R., Ordoñez J., Caputo L., Armengol J., (2006). Elemental ratios in sediments as indicators of ecological processes in Spanish reservoirs. Limnetica, 25 (1-2): 499-512.

Louri˜no-Cabana B., Lesven L., Charriau A., Billon G., Ouddane B., Boughriet A., (2011). Potential risks of metal toxicity in contaminated sediments of Deûle River in Northern France. Journal of Hazardous Materials, 186: 2129–2137.

Luck J.M., Othman D.B., (1998). Geochemistry and water dynamics. II. Trace metals and Pb-Sr isotopes as tracers of water movements and erosion processes, Chem. Geol., 150: 263-282.

Luo, L., Lin, H., Schmidt, J., (2010). Quantitative Relationships between Soil Macropore Characteristics and Preferential Flow and Transport. Soil Science Society of America Journal, 74: 1929–1937

Luther S.M., Poulsen L., Dudas M.J., Rutherford P. M., (1996). Fluoride sorption and mineral stability in an Alberta soil interacting with phosphogypsum leachate. Can. J. Soil Sci, 76: 83-91.

Lyons T. W., Werne J. P., Hollander D. J., Murray R.W., (2003). Contrasting sulfur geochemistry and Fe/Al and Mo/Al ratios across the last oxic-to-anoxic transition in the Cariaco Basin, Venezuela. Chemical Geology, 195: 131– 157.

Lysandrou M., and Pashalidis I., (2008). Uranium chemistry in stack solutions and leachates phophogypsum disposed at a coastal area in Cyprus. Journal of Environmental Radioactivity, 99: 359–366.

Majoube, M., (1971). Fractionnement en oxygene-18 et en deuterium entre l'eau et sa vapeur. Journal of Chemistry and Physics 197, 1423-1436.

Makishima A., Nagender B., Nakamura N., Eizo, (2007). Precise determination of Pb isotope ratios by simple double spike MC-ICP-MS technique without Tl addition, Journal of Analytical Atomic Spectrometry, 22: 407–410.

Mangion P., (2011). Biogeochemical Consequences of Sewage Discharge on Mangrove Environments in East Africa. Vrije Universiteit Brussel, Faculty of Science Earth System Sciences Analytical and Environmental Chemistry, Annex 4: 179- 208.

Manzoor S., Shah MH., Shaheen N., Khalique A., (2006). Jaffa M. Multivariate analysis of trace metals in textile effluents in relation to soil and groundwater, Journal of Hazardous Materials 137: 31-37.

Marshall W.L., and Slusher R. (1966). Thermodynamics of calcium sulfate dihydrate in aqueous Sodium solutions, 0-110°. The journal of physical chemistry, 70: 4015-4027.

Martin JM., Whitfield M., (1983).The significance of the river input of chemical elements to the ocean. In Trace metals in sea water. Wong, CS., Boyle, E., Bruland, KW. Burton, JD. Goldb erg, ED. (eds). New York: Plenum, pp: 265-296.

Martín-Puertas C., Valero-Garcés BL., Mata MP., Moreno A., Giralt S., Martínez-Ruiz F., Jime´nez-Espejo F., (2009). Geochemical processes in a Mediterranean Lake: a high-resolution study of the last 4,000 years in Zonăr Lake, southern Spain, J Paleolimnol, 46: 405-421.

Masciopinto C., (2013). Management of aquifer recharge in Lebanon by removing seawater intrusion from coastal aquifers. Journal of Environmental Management, 130: 306-312.

Masson E., Meilliez F., (2008). Ground and water levels change in the Scheldt Basin, Integrated Water Management: Practical Experiences and Case Studies, 207–217.

Massoud M.A., (2012). Assessment of water quality along a recreational section of the Damour River in Lebanon using the water quality index. Environ Monit Assess., 184: 4151–4160.

Massoud M.A., El-Fadel M., Scrimshaw M.D., Lester J.N., (2006). Factors influencing development of management strategies for the Abou Ali River in Lebanon I: Spatial variation and land use. Science of the Total Environment, 362: 15– 30.

Maszkowska J., Kołodziejska M., Białk-Bielinska A., Mrozik W., Kumirska J., Stepnowski P., Palavinskas R., Kruger O., Kalbe U, (2013). Column and batch tests of sulfonamide leaching from differenttypes of soil. Journal of Hazardous Materials, 260:468– 474.

Matisoff G., Bonniwell E. C., Whiting P. J., (2002). Soil Erosion and Sediment Sources in an Ohio Watershed using Beryllium-7, Cesium-137, and Lead-210. J. Environ. Qual., 31: 54–61.
Mayr C., Lücke A., Stichler W., Trimborn P., Ercolano B., Oliva G., Ohlendorf C., Julio S., Fey M., Haberzettl T., Janssen S., Schäbtiz F, Schleser G.H., Wille M., Zolitschka B., (2007). Precipitation origin and evaporation of lakes in semi-arid Patagonia (Argentina) inferred from stable isotopes (δ18O, δ2H). Journal of Hydrology, 334: 52-63.

Mclean, J.E. and Bledsoe, B.E., (1992). Ground Water Issue, Behavior of Metals in Soils. USEPA, EPA/540/S-92/018. Pp.1–25.

Meffe R., De Bustamante I., (2014). Emerging organic contaminants in surface water and groundwater: A first overview of the situation in Italy (review). Science of the Total Environment, 481: 280–295.
Meredith K.T., Hollins S.E., Hughes C.E., Cendón D.I., Hankin S., Stone D.J.M. (2009). Concentrations within the Darling River between Bourke and Wilcannia due to variable flows, saline groundwater influx and evaporation. Journal of Hydrology; 378: 313-324.
Merz M., (1992). The Biology of Carbonate Precipitation by Cyanobacteria. Facies, 26: 81-102.
Miao S., DeLaune RD., Jugsujinda A., (2006). Influence of sediment redox conditions on release/solubility of metals and nutrients in a Louisiana Mississippi River deltaic plain freshwater lake. Science of The Total Environment, 371: 334-343.
Mikac I., Fiket Ž., Terzić S., Barešić N., Mikac J., Ahel M., (2011). Chemical indicators of anthropogenic impacts in sediments of the pristine karst lakes. Chemosphere, 84: 1140-1149.
Miller JR., Kolenbrander L., Lord M., Yurkovich S., Mackin G., (2003). Assessment of changing land-use practices on basin sediment yields and provenance in western north Carolina using multivariate finger printing techniques. Report No. 345 Water Resources Research Institute of The University of North Carolina, WRRI Project No. 70 18 1, USGS Project No. 1434-HQ-96-GR-02689, June, 2003.
Ministry of Agriculture (2003), National action program to combat destination Lebanon. United Nations Convention to Combat Desertification, pp. 265.
Miralles J., Véron A.J., Radakovitch O., Deschamps P., Tremblay T., Hamelin B., (2006). Atmospheric lead fallout over the last century recorded in Gulf of Lions sediments (Mediterranean Sea), Marine Pollution Bulletin, 52:1364–1371.
Mishra C.S.K., Nayak S., Guru B.C., Rath M., (2011). Effect of phosphogypsum on the soil physico-chemical properties, microbial load and enzyme activities. Journal of environmental biology, 32: 613-617.
Monna F., Lancelot J., Croudace I., Cundace AB., Lewis JT., (1997). Pb Isotopic Composition of Airborne Particulate Material from France and the Southern United Kingdom: Implications for Pb Pollution Sources in Urban Areas Environ. Sci. Technol. 31: 2277-2286.
Morford J.L., Russel A.D., Emerson S., (2001). Trace metal evidence for changes in the redox environment associated with transition from terrigenous clay to diatomaceous sediment, Saanich Inlet, BC. Marine Geology, 174: 335-369.
Mortimer R. J. G. and Raeà J. E., (2000). Metal Speciation (Cu, Zn, Pb, Cd) and Organic Matter in Oxic to Suboxic Salt Marsh Sediments, Severn Estuary, Southwest Britain. Marine Pollution Bulletin, 40: 377-386.
Mouri G., Takizawa S., Oki T., (2011). Spatial and temporal variation in nutrient parameters in stream water in a rural-urban catchment, Shikoku, Japan: Effects of land cover and human impact. Journal of Environmental Management, 92: 1837-1848.
Moussa S., El-Fadel M., Saliba N.A., (2006) Seasonal, diurnal and nocturnal behaviors of lower carbonyl compounds in the urban environment of Beirut, Lebanon. Atmospheric Environment, 40: 2459–2468
Mullaney, J.R., Lorenz, D.L., Arntson, A.D., (2009). Chloride in groundwater and surface water in areas underlain by the glacial aquifer system, northern United States: U.S. Geological Survey Scientific Investigations Report 2009–5086, 41 p.
Nehme N., Haydar C., Koubaissy B., Fakih M., Awad S., Toufaily J., Villieras F., Hamieh T. (2014). Metal concentrations in river water and bed sediments of the Lower Litani River Bassin, Lebanon. Journal of Advances in Chemistry, 8: 1590-1601.

Newman D.J., Perault D.R., Shahady T.D. (2006). Watershed Development and Sediment Accumulation in a Small Urban Lake. Lake and Reservoir Management, 22: 303-307.
NF ISO 10390 (2005) Qualité du sol - Détermination of pH, AFNOR, 11p OECD (2004) Guidelines for the Testing of Chemicals 312, Leaching in Soil Columns, 15p

NF ISO 10693 (1995) Qualité du sol - Détermination de la teneur en carbonate - Méthode volumétrique, AFNOR, 11p

NF ISO 11265 (1995) Qualité du sol - Détermination de la conductivité électrique spécifique, AFNOR, 7p

NF X31-106 (2002) Qualité des sols - Détermination du calcaire actif, AFNOR, 6p

NF X31-107 (2003) Qualité du sol - Détermination de la distribution granulométrique des particules du sol - Méthode à la pipette, AFNOR, 20p.

Nuttle, W.K., 2002. Review and Evaluation of Hydrologic Modeling Tools for the Coastal Mangroves and Florida Bay. Salinity-Based Performance Measures Project: prepared for Everglades National Park April 2002, 1-37.
Ocampo C.J., Sivapalan M., Oldham C.E., (2006). Field exploration of coupled hydrological and biogeochemical catchment responses and a unifying perceptual model. Advances in Water Resources, 29: 161-180.
Organization for Economic Co-operation and Development, "OECD Guidelines for the Testing of Chemicals 105, Water Solubility," OECD, 1995.
Östlund P., Sternbeck J., (2001). Total Lead and Stable Lead Isotopes in Stockholm Sediments, Water, Air and Soil Pollution: Focus 1:229-239.
Othman I., Al Oudat M., Al Masri MS., (1997) Lead levels in roadside soils and vegetation of Damascus city, Sci Total Environ., 207: 43-48.
Othman I., Al-Masri MS., (2007). Impact of phosphate industry on the environment: a case study, Appl Radiat Isot., 65:131–141.
Pathak P., Wani S.P., Singh P., Sudi R., (2004). Sediment flow behaviour from small agricultural watersheds. Agricultural Water Management, 67: 105–117.
Peretyazhko T., Van Cappellen P., Meile M., Musso M., Regnier P., Charlet L., (2005). Biogeochemistry of Major Redox Elements and Mercury in a Tropical Reservoir Lake (Petit Saut, French Guiana). Aquatic Geochemistry, 11: 33-55.
Petelet-Giraud E., Negrel Ph., Gourcy L., Schmidt C., Schirmer M. (2007). Geochemical and isotopic constraints on groundwater-surface water interactions in a highly anthropized site. The Wolfen/Bitterfeld megasite (Mulde subcatchment, Germany). Environmental Polution;148: 707-717.
Petit J.C.J., Bouezmarni M., Roevros N., Chou L., (2009). The use of acidimetric titration as a novel approach to study particulate trace metal speciation and mobility: Application to sediments of the Scheldt estuary. Applied Geochemistry, 24: 1875-1888.

Pham M. K., Povinec P. P., Nies H., Betti M., (2013). Dry and wet deposition of ^{7}Be, ^{210}Pb and ^{137}Cs in Monaco air during 1998-2010: Seasonal variations of deposition fluxes. Journal of Environmental Radioactivity, 120: 45-57.
Pleysier, J. L., Jou, A., (1980). "A Single-extraction Method Using Silver-thiourea for Measuring Exchangeable Cations and Effective CEC in Soils with Variable Charges," Soil Science, 129: 205-211.

Poulton D.J., (1992). Heavy Metals and Toxic Organic Contaminants in Effluents, Water, and Sediments of the Bay of Quinte, Lake Ontario. Journal of Great Lakes Research, 18: 390-404.
Qin D., Qian Y., Han L., Wang Z., Li C., Zhao Z., (2011). Assessing impact of irrigation water on groundwater recharge and quality in arid environment using CFCs, tritium and stable isotopes, in the Zhangye Basin, Northwest China. Journal of Hydrology 405: 194–208.
Qu J., peng J., Baizhan L., (2011). Effect of citric acid on the crystal morphology of gypsum and its action mechanism. Advanced materials research, 250-253: 321-326.

Ramadan H.H., Beighley R.E., Ramamurthy A.S., (2013). Temperature and Precipitation Trends in Lebanon's Largest River: The Litani Basin. Journal of Water Resources Planning and Management; 139: 86-95.

Rauch J.N., (2010). Global Spatial Indexing of the Human Impact on Al, Cu, Fe, and Zn Mobilization, Environmental Science & Technology, 44: 5728–5734.

Renberg I., Brännvall M-L., Bindler R., Emteryd O., (2002). Stable lead isotopes and lake sediments a useful combination for the study of atmospheric lead pollution history, The Science of the Total Environment, 292: 45–54.

Rentería-Villalobos M., Vioque I., Mantero J., Manjón G., (2010). Radiological, chemical and morphological characterizations of phosphate rock and phosphogypsum from phosphoric acid factories in SW Spain. Journal of Hazardous Materials, 181: 193-203.

Rez-Loépez R., A´lvarez-Valero A M., Nieto J M., (2007). Changes in mobility of toxic elements during the production of phosphoric acid in the fertilizer industry of Huelva (SW Spain) and environmental impact of phosphogypsum wastes. Journal of Hazardous Materials, 148: 745-750.

Rhodes A., Newton R.M., Pufal A., (2001). Influences of Land Use on Water Quality of a Diverse New England Watershed. Environmental Science & Technology, 35: 3640-3645.

Rigaud S., Radakovitch O., Couture R-M., Deflandre B., Cossa D., Garnier C., Garnier J-M., (2013). Mobility and fluxes of trace elements and nutrients at the sediment–water interface of a lagoon under contrasting water column oxygenation conditions. Applied Geochemistry, 31: 35–51.

Roussiez V., Ludwig W., Monaco A., Probst J-L., Bouloubassi I., Buscail R., Saragoni G., (2006). Sources and sinks of sediment-bound contaminants in the Gulf of Lions (NW Mediterranean Sea): A multi-tracer approach. Continental Shelf Research, 26: 1843–1857.

Roussiez V., Ludwig W., Probst J-L., Monaco A., (2005). Background levels of heavy metals in surficial sediments of the Gulf of Lions (NW Mediterranean): An approach based on 133Cs normalization and lead isotope measurments. Environmental pollution, 138: 167-177.

Ruiz-Fernández A. C., Hillaire-Marcel C., Páez-Osuna F., Ghaleb B., Caballero M. (2007). 210Pb chronology and trace metal geochemistry at Los Tuxtlas, Mexico, as evidenced by a sedimentary record from the Lago Verde Crater Lake. Quaternary Research, 67:181–192.

Ruiz-Fernández A.C., Hillaire-Marcel C., Páez-Osuna F., Ghaleb B., Caballero M. (2007). 210Pb chronology and trace metal geochemistry at Los Tuxtlas, Mexico, as evidenced by a sedimentary record from the Lago Verde Crater Lake. Quaternary Research, 67: 181–192.

Rutherford P. M., Dudas M. J., Samek R. A. (1994). Environmental impacts of phosphogypsum Review Article. Science of the Total Environment, 149: 1-38.

Saad Z. and Kazpard V. (2007). Seasonal effect on the isotopic pattern of rainwater in Lebanon. Journal of Environmental Hydrology; 15: 9.

Saad Z., Kazpard V., El Samrani A, Slim K., (2005). Chemical and Isotopic Composition of Rainwater In Coastal And Highland Regions In Lebanon. Journal of Environmental Hydrology; 13: 1-11.

Saad Z., Kazpard V., El Samrani A., Aoun M., Amacha N., Saadeh M., (2009). Chemical and environmental isotope investigation on hydrodynamics of Monomictick Lake: A case study on Qaraoun, Lebanon. Journal of Environmental Hydrology; 17, 35: 1-10.

Saad Z., Kazpard V., El Samrani AG., Slim K., Ouaini N., (2006). Use of Hydrochemistry and Environmental Isotopes to Evaluate Water Quality, Litani River, Lebanon, Journal of Environmental Hydrology, 2: 14pp.

Saadeh M., Semerjian L., Amacha N., (2012). Physicochemical Evaluation of the Upper Litani River Watershed, Lebanon, Scientific World Journal pp 8 doi: 10.1100/2012/462467.

Sacks, L.A., Lee, T.M., Swancar, A., 2013. The suitability of a simplified isotope-balance approach to quantify transient groundwater-lake interactions over a decade with climatic extremes. Journal of hydrology 2013; http://dx.doi.org/10.1016/j.jhydrol.2013.12.012

Sankararamakrishnan N., and Guo Q., (2005). Chemical tracers as indicator of human fecal coliforms at storm water outfalls. Environment International, 31:1133 – 1140.

Saulnier I., Mucci A., (2000). Trace metal remobilization following the resuspension of estuarine sediments: Saguenay Fjord, Canada. Applied Geochemistry, 15: 191-210.

Schemmel F., Mikes T., Rojay B., Mulch A. (2013). The Impact of Topography on Isotopes in Precipitation Across The Central Anatolian Plateau (Turkey). American Journal of Science, 313: 61-80.

Schmidt S., Howa H., Mouret A., Lombard F., Anschutz P, Labeyrie L. (2009) Particle fluxes and recent sediment accumulation on the Aquitanian margin of Bay of Biscay. Continental Shelf Research, 29: 1044–1052.

Schucknecht A., Matschullat J., Reimann C., (2011). Lead and stable Pb-isotope characteristics of tropical soils in north-eastern Brazil, Applied Geochemistry, 26: 2191-2200.

Seibert, J., McDonnell, J.J., 2002. On the dialog between experimentalist and modeler in catchment hydrology: Use of soft data for multicriteria model calibration. Water Resources Research. 38, 1-14 doi:10.1029/2001WR000978.

Shaban A., (2014). Physical and Anthropogenic Challenges of Water Resources in Lebanon. Journal of Scientific Research & Reports. Article no. JSRR.2014.008: 479-498.

Shaban A., Nassif N., (2007). Pollution in Qaraaoun Lake, Central Lebanon. Journal of Environmental Hydrology, 15: 1-14.

Shaban A., Robinson C., El-Baz F., (2009). Using MODIS Images and TRMM Data to Correlate Rainfall Peaks and Water Discharges from the Lebanese Coastal Rivers. J. Water Resource and Protection, 4: 227-236.

Shaban A., Telesca L., Darwich T., Amacha N., (2014). Analysis of Long-Term Fluctuations in Stream Flow Time Series: An Application to Litani River, Lebanon. Acta Geophysica, 62: 164-179.

Shakeri A., Moore F., (2010). The impact of an industrial complex on freshly deposited sediments, Chener Rahdar river case study, Shiraz, Iran, Environ Monit Assess. 169, 321–334.

Sherr EB., Caron DA., Sherr BF., (1993). Staining of Heterotrophic Protists for Visualization via Epifluorescence Microscopy, Chapter 26 213- 229. Kemp P.F., Cole J. J., Sherr B.F., Sherr E.B. 1993 Handbook of Methods in Aquatic Microbial Ecology. Lewi Pupl., Boca Raton 2013; FL 33431 777p.

Siebert C., Geyer S., Möller P., Rosenthal E., Berger D., Guttman J., (2009). Lake Tiberias and its dynamic hydrochemical environment The Water of the Jordan Valley Chapter 3; 2.3.4: 219-246.

Sigg L., Kuhn A., Xue H., Kiefer E., Kistler D., (1995). Cycles of trace elements (Copper and Zinc) in eutrophic lake. Advances in Chemistry, 8: 177-194. Huang C. O'Melia C., Morgan J., (1995). Aquatic Chemistry, 244 DOI: 10.102/ BA-1995-0244.

Sigman DM., Casciotti KL., Andreani M., Barford C., Galanter M., Böhlke JK., (2001). A bacterial method for the nitrogen isotopic analysis of nitrate in seawater and freshwater. Analytical Chemistry, 73: 4145-4153.

Singh AP., Srivastava CP., Srivastava P., (2008) Relationships of Heavy Metals in Natural Lake Waters with Physico-chemical Characteristics of Waters and Different Chemical Fractions of Metals in Sediments. Water Air Soil Pollut., 188: 181–193.

Singh M., Davis D., Somashekar R.K., Prakash K.L., Shivanna K., (2010). Environmental isotopes investigation in groundwater of Challaghatta valley, Bangalore: A case study. African Journal of Environmental Science and Technology; 4: 226-233.

Singh N.B., Middendorf B., (2007). Calcium sulphate hemihydrate hydration leading to gypsum crystallization Review Article. Progress in Crystal Growth and Characterization of Materials, 53: 57-77.

Skoulikidis N., Kaberi H., Sakellariou D., (2008). Patterns, origin and possible effects of sediment pollution in a Mediterranean lake. Ecological Effects of water – level Fluctuations in Lake. Hydrobiologia, 613: 71–83.

Smith B.R., and Sweett F., (1971). The crystallization of calcium sulfate dihydrate. Journal of Colloid and Interface Science, 37: 612-618.

Standley L.J., Kaplan L.A., Smith D., (2000). Molecular Tracers of organic matter sources to surface water resources. Environ. Sci. Technol., 34: 3124-3130.

Steele M.K., Aitkenhead-Peterson J.A., (2011). Long-term sodium and chloride surface water exports from the Dallas/Fort Worth region. Science of the Total Environment, 409: 3021–3032.

Stein E.D., Tiefenthaler L.L., (2005). Dry-Weather Metals And Bacteria Loading In An Arid, Urbanwatershed: Ballona Creek, California. Water, Air, and Soil Pollution 164: 367–382.

Stille P., Pourcelot L., Granet M., Pierret M.-C., Guéguen F., Perrone T., Morvan G., Chabaux F., (2011). Deposition and migration of atmospheric Pb in soils from a forested silicate catchment today and in the past (Strengbach case): Evidence from 210Pb activities and Pb isotope ratios, Chemical Geology, 289: 140-153.

Stone M., and Droppo I. G., (1996). Distribution of lead, copper and zinc in size-fractionated river bed sediment in two agricultural catchments of southern Ontario, Canada, Environmental Pollution, 93: 353-362.

Strydom C. A., Groenewald E.M., Potgieter J.H. (1997) Thermogravimetric studies of the synthesis of CaS from gypsum, CaSO4.2H2O and phosphogypsum. Journal of Thermal Analysis, 49: 1501-1507.

Sultan M., Sturchio N.C., Gheith H., Abdel Hady Y., El Anbeawy M., (2000). Chemical and Isotopic Constraints on the Origin of Wadi El- Taraf Ground Water, Eastern Desert, Egypt. Ground water; 38: 743-751.

Syrovetnik K., Malmstrom M.E., Neretnieks I., (2007). Accumulation of heavy metals in the Oostriku peat bog, Estonia: Determination of binding processes by means of sequential leaching. Environmental Pollution, 147: 291-300.

Taher AG., Soliman AA., (1999) Heavy metal concentrations in surficial sediments from Wadi El Natrun saline lakes, Egypt. International Journal of Salt Lake Research, 8: 75–92.

Taillefert M., Lienemann C-P., Gaillard J-F., Perret D., (2000) Speciation, reactivity, and cycling of Fe and Pb in a meromictic lake. Geochimica et Cosmochimica Acta, 64:169-183.

Taillefert M., Neuhuber S., Bristow G., (2007). The effect of tidal forcing on biogeochemical processes in intertidal salt marsh sediments, Geochemical transaction 8: pp 15 doi:10.1186/1467-4866-8.

Tayibi H., Choura M., López F.A., Alguacil F.J., López DA. (2009). Environmental impact and management of phosphogypsum. Journal of Environmental Management, 90: 2377-2386.

Teranes J.L., McKenzie J. A., Bernascon S.M., Lotter A.F., Sturm M., (1999). A study of oxygen isotopic fractionation during bio-induced calcite precipitation in eutrophic Baldeggersee, Switzerland. Geochimica et Cosmochimica Acta, 63: 1981-1989.

Thapalia A., Borrok D. M., Vanmetre P.C., Musgrove M.N., Landa E. R., (2010). Zn and Cu Isotopes as Tracers of Anthropogenic Contamination in a Sediment Core from an Urban Lake, Environmental Science & Technology, 44: 1544–1550.

Thevenon F., Felippe de Alencastro L., Loizeau J-L., Adatte T.,Grandjean D., Wildi W., Poté J., (2013). A high-resolution historical sediment record of nutrients, trace elements and organochlorines (DDT and PCB) deposition in a drinking water reservoir (Lake Brêt, Switzerland) points at local and regional pollutant sources. Chemosphere, 90: 2444–2452.

Thien, S. J., Graveel, J.G., (2003). Laboratory Manual for Soil Science, Agricultural and Environmental Principles, Preliminary ed., Iowa: Kendall/Hunt publishing company, p. 207.

Thornthwaite, C.W., Mather, J.R., (1955). The Water Balance. Publications in Climatology, Drexel Institute of Climatology. 8, 1-104.

Tranchida G., Oliveri E., Angelone M., Bellanca A., Censi P., D'Elia M., Neri R., Placenti F., Sprovieri M., Mazzola S., (2010). Distribution of rare earth elements in marine sediments from the Strait of Sicily (western Mediterranean Sea): Evidence of phosphogypsum waste contamination. Marine Pollution Bulletin, 62: 182-191.

Tuna A.L., Yilmaz F., Demirak A., Ozdemir N., (2007). Sources and distribution of trace metals in the saricay stream basin of southwestern turkey. Environ Monit Assess., 125: 47–57.

Turner, K.W., Wolfe, B.B., Edwards, T.W.D., 2010. Characterizing the role of hydrological processes on lake water balances in the Old Crow Flats, Yukon Territory, Canada, using water isotope tracers. Journal of Hydrology. 386, 103-117.

UNDP/MoE, 2010. United Nations Development Program/Ministry of Environment Provision of Services to conduct Desk Studies and Field Assessments to Complete the Vulnerability and Adaptation (V&A) and the Mitigation Chapters of Lebanon's Second National Communication 2010, Final report chapter 4, pp94.

UNEP, Lebanon Post –Conflict Environmental Assessment, (2007). Can be found on this site www.unep.org/pdf/Lebanon_PCOB_Report.pdf.

Van Griethuysen C., Luitwieler M., Joziasse J., Koelmans A. A. (2005). Temporal variation of trace metal geochemistry in floodplain lake sediment subject to dynamic hydrological conditions. Environmental Pollution, 137: 281-294

Venäläinen S.H., (2011). Apatite ore mine tailings as an amendment for remediation of a lead-contaminated shooting range soil Original. Science of The Total Environment, 409: 4628-4634.

Vitoria L., Otero N., Soler A., Canals A. (2004). Fertilizer Characterization: Isotopic Data (N, S, O, C, and Sr). Environmental Science & Technology, 38: 3254- 3262.

Waked A. and Afif C., (2012). Emissions of air pollutants from road transport in Lebanon and other countries in the Middle East region. Atmospheric Environment, 61: 446-452.

Wall LG., Tank JL., Royer TV., Bernot MJ., (2005). Spatial and temporal variability in sediment denitrification within an agriculturally influenced reservoir. Biogeochemistry, 76: 85–111.

Walley C.D., (1997). The lithostratigraphy of Lebanon: a review, Lebanese Sci. Bull. 10 81–108.

Wang C., Wang J., Yang Z., Mao C., Ji J., (2013). Characteristics of lead geochemistry and the mobility of Pb isotopes in the system of pedogenic rock–pedosphere–irrigated riverwater–cereal–atmosphere from the Yangtze River delta region China, Chemosphere article in press p: 9.

Wang J., Bi Y., Pfister G., Henkelmann B., Zhu K., SchrammK-W., (2009). Determination of PAH, PCB, and OCP in water from the Three Gorges Reservoir accumulated by semipermeable membrane devices (SPMD). Chemosphere, 75: 1119–1127.

Wassenaar L.I., Athanasopoulos P., Hendry M.J., (2011) Isotope hydrology of precipitation, surface and ground waters in the Okanagan Valley, British Columbia, Canada. Journal of Hydrology, 411: 37–48.

Wei G., Yang Z., Cui B., Li B., Chen H., Bai J.H., Dong S.K., (2009). Impact of Dam Construction on Water Quality and Water Self-Purification Capacity of the Lancang River, China. Water Resour Manage, 23: 1763–1780.

Wijaya A. R., Ouchi A.K., Tanaka K., Shinjo R., Ohde S., (2012). Metal contents and Pb isotopes in road-side dust and sediment of Japan, Journal of Geochemical Exploration, 118: 68–76.

Wildi W., (2010). Environmental hazards of dams and reservoirs. NEAR Curriculum in Natural Environmental Science, Terre et Environnement, 88: 187-197.

Wong C.S.C., Li X.D., (2004). Pb contamination and isotopic composition of urban soils in Hong Kong, Sci Total Environ. 319: 185–195.

Wu W., Xu S., Lu H., Yang J., Yin H., Liu W., (2011). Mineralogy, major and trace element geochemistry of riverbed sediments in the headwaters of the Yangtze, Tongtian River and Jinsha River. Journal of Asian Earth Sciences, 40: 611–621.

Xia P., Meng X., Feng A., Yin P., Wang X., Zhang J. (2012). 210Pb Chronology and Trace Metal Geochemistry in the Intertidal Sediment of Qinjiang River Estuary, China. J. Ocean Univ. China (Oceanic and Coastal Sea Research), 11: 165-173.

Xu, C.Y., Singh, V.P., 1998. A Review on Monthly Water Balance Models for Water Resources Investigations. Water Resources Management. 12, 31–50.

Xue HB., Gächter R., Sigg L., (1997). Comparison of Cu and Zn cycling in eutrophic lakes with oxic and anoxic Hypolimnion. Aquat.sci, 59: 176–189.

Yammine P., Kfoury A., El-Khoury B., Nouali H., El-Nakat H., Ledoux F., Cazier F., Courcot D., Aboukaïs A., (2010). A preliminary evaluation of the inorganic chemical composition of atmospheric tsp in the Selaata Region, North Lebanon, Lebanese Sci J. 1: 13–29.

Yang L., Song X., Zhang Y., Han D., Zhang B., Long D., (2012). Characterizing interactions between surface water and groundwater in the Jialu River basin using major ion chemistry and stable isotopes. Hydrol. Earth Syst Sci, 16: 4265–4277.

Yang Z., Wang Y., Shen Z., Niu J., Tang Z., (2009). Distribution and speciation of heavy metals in sediments from the mainstream, tributaries, and lakes of the Yangtze River catchment of Wuhan, China. Journal of Hazardous Materials, 166: 1186-1194.

Yaun T., Wang J., Li Z., (2010). Measurement and modeling of Solubility for calcium sulfate dihydrate and calcium hydroxide in NaOH/KOH solutions. Fluid Phase Equilibria, 297: 129-137.

Yi, Y., Brock, B.E., Falcone, M.D., Wolfe, B.B., Edwards, T.W.D., 2008. A coupled isotope tracer method to characterize input water to lakes. Journal of Hydrology. 350, 1– 13.

Yin L., Hou G., Dou Y., Tao Z., Li Y., (2011). Hydrogeochemical and isotopic study of groundwater in the Habor Lake Basin of the Ordos Plateau, NW China. Environ Earth Sci 64: 1575–1584.
Yin R., Feng X., Shi W., (2010). Application of the stable-isotope system to the study of sources and fate of Hg in the environment: A review. Applied Geochemistry, 25: 1467–1477.
Yuan H-Z., Shen J., Liu E-F., Wang J-J., Meng X-H., (2011). Assessment of nutrients and heavy metals enrichment in surface sediments from Taihu Lake, a eutrophic shallow lake in China. Environ Geochem Health, 33: 67–81.
Yuan X, Deng X, Shen Z, Gao Y., (2007). Speciation and potential remobilization of heavy metals in sediments of the Taihu Lake, China. Chinese Journal of Geochemistry, 26: 384- 393.
Zhang G-L., Yang F-G., Zhao W-J., Zhao Y-G., Yang J-L, Gong Z-T., (2007). Historical change of soil Pb content and Pb isotope signatures of the cultural layers in urban Nanjing, CATENA, 69: 51-56.
Zhang, Y-K., Bai, E-W., Libra, R., Rowden, R., Liu, H., 1996. Simulation of spring discharge from a limestone aquifer in Iowa, USA. Journal of hydrogeology. 4, 41-54.
Zhao L. Y.L., Schulin R., Nowack B., (2009). Cu and Zn mobilization in soil columns percolated by different irrigation solutions. Environmental Pollution, 157: 823–833.

Zhao S., Feng C., Wang D., Liu Y., Shen Z., (2013). Salinity increases the mobility of Cd, Cu, Mn, and Pb in the sediments of Yangtze Estuary: relative role of sediments' properties and metal speciation, Chemosphere 91: 977-984.
Zhao S., Shi X., Li C., Zhang H., Wu Y., (2014). Seasonal variation of heavy metals in sediment of Lake Ulansuhai, China. Chemistry and Ecology, 30:1: 1-14.
Zhizhaev A. M., Merkulova E. N., Bragin I. V., (2007). Copper Precipitation from Sulfate Solutions with Calcium Carbonates. Russian Journal of Applied Chemistry, 80: 1632-1635.
Zhu L., Guo L., Gao Z., Yin G., Lee B., Wang F., Xu J., (2010). Source and distribution of lead in the surface sediments from the South China Sea as derived from Pb isotopes, Marine Pollution Bulletin, 60: 2144-2153.
Zhumanova M.O., Usanboev N.Kh., Namazov S.S., Beglov B.M., (2012). Organo-Mineral Sulfur Containing Fertilizers on the basis of Oxidized Brown coal and Phosphogypsum. Russian Journal of applied chemistry, 85: 485-488.
Zingg A., Winnefeld F., Holzer L., Pakusch J., Beckerb S., Gauckler L., (2008). Adsorption of polyelectrolytes and its influence on the rheology, zeta potential, and microstructure of various cement and hydrate phases. Journal of Colloid and Interface Science, 323: 301–312.

Annex 1

Al Jouz basin

Table A1.1: Dissolved metal concentration in the industrial area river and sea coast September 2012.

sample	Cu (µg/l)	Fe (µg/l)	Zn (µg/l)	Cr (µg/l)	Cd (µg /l)	Mn (µg/l)	Pb (µg/l)
Sea North	179	542	100	887	0.250	248	0.898
Sea 1 South	188	618	79	1351	0.262	249	0.895
Sea 2 South	192	608	93	968	0.268	252	0.903
Sea 3 South	192	617	69	1059	0.256	250	0.912
River	35	97	56	225	0.007	104	0.281

Table A1.2: Dissolved metal concentration in the industrial area river and sea coast March 2012.

sample	Fe (µg/l)	Zn (µg/l)	Cr (µg/l)	Ca (mg/l)
Sea North	91o	59	1420	270.205
Sea South	981	59	1392	277.89
River	95	5	21	62.98
River estuary	74	7	41	60.195

Annex 2

Sediments

Table A2.1: Trace metal variation seasonally and spatially in lacustrine sediments.

Sample	Pb (mg/Kg)	Cd (mg/Kg)
Ri Sep 2011	24.08	0.63
Cz1 Sep 2011	21.83	0.65
Cz2 Sep 2011	15.69	0.51
Dz Sep 2011	24.15	0.61
Ri Nov 2011	20.19	0.38
Cz1 Nov 2011	17.62	0.34
Cz2 Nov 2011	15.53	0.49
Cz3 Nov 2011	19.96	0.47
Dz Nov 2011	17.51	0.81
Ri March 2012	21.34	0.46
Cz March 2012	14.11	0.42
Dz March 2012	18.90	0.59

Table A2.2: Metal fractionation resulted from chemical titration where buffering detected in the experimental pH behavior is due to Ca release compared to theoretical one in reservoir sediments at Cz.

Sediment Cz	Al	Ca	Fe	K	Mg	Si	Zn
Bulk %	3.62	24.76	0.13	0.35	0.88	6.22	0.01
% of HCl reactivity	3	80	19	6	47	0.6	27
Residual	97	20	81	94	53	99.4	73

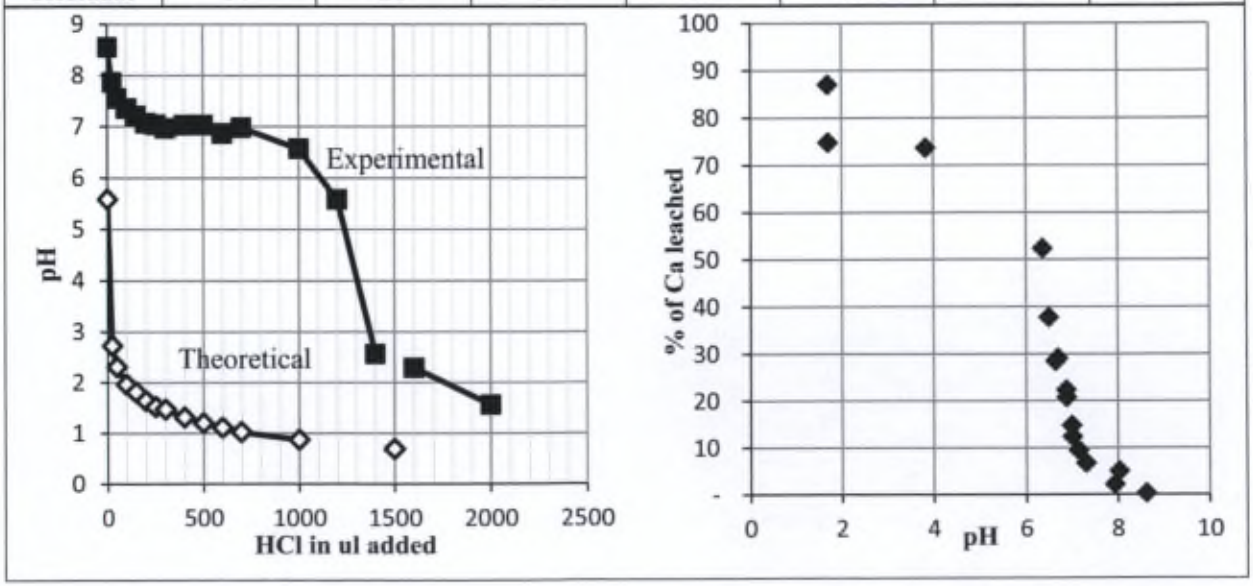

Annex 3

Soil cores

Table A3.1: Metal content in industrial soil core profile (Ic) retrieved next to the factory.

Ic Depth (cm)	Al %	Ca %	K ppm	Mg ppm	Si %	Zn ppm	Fe %	Mn ppm	Cu ppm	Pb ppm	Cd ppm
3	7.1	2.9	6805	5178	15.7	124	3.2	2045	35.30	53.64	0.45
6	7.3	2.2	6861	5238	16.1	115	3.3	1811	38.14	101.14	0.53
9	7.4	1.0	6540	4624	14.2	101	3.4	1889	40.67	43.45	0.5
12	7.2	0.9	6547	4427	14.5	116	3.4	1997	44.22	47.97	0.42
15	7.1	0.7	6299	4150	17.6	95	3.5	1875	49.2	34.33	-
20	7.9	0.6	6815	4727	16.6	97	3.4	1862	47.32	25.40	0.47
25	8.5	0.6	7135	5112	21.0	103	3.7	1883	42.91	29.25	0.46
30	8.4	0.6	3925	5246	2.31	120	3.6	1739	35.01	28.64	0.39
35	7.8	0.6	6505	4472	16.3	105	3.6	1707	29.11	46.78	0.45
40	8.5	0.6	7030	5162	15.1	114	3.5	1785	34.63	25.43	0.45
50	8.8	0.5	6859	5182	18.2	95	3.7	1974	33.78	23.23	0.39
60	8.9	0.5	6693	5247	18.5	88	3.8	1469	34.54	27.27	0.38

Table A3.2: Metal content in Agricultural soil core profile (Ac) retrieved next to the dam eastern side.

Ac Depth (cm)	Al %	Ca %	K ppm	Mg ppm	Si %	Zn ppm	Fe %	Mn ppm	Cu ppm	Pb ppm	Cd ppm
3	3.2	21.2	3819	6348	7.8	172	1.5	347	41.58	40.49	0.68
6	2.9	22.6	4160	6397	7.9	179	1.4	342	38.47	26.97	0.81
9	2.6	21.7	3417	5956	7.4	184	1.3	309	38.15	22.28	1.07
12	2.5	23.1	3964	6419	7.6	184	1.2	306	36.76	21.64	1.09
15	2.3	24.4	3546	6243	8.0	177	1.1	292	38.26	20.76	0.89
20	2.3	24.0	3606	6137	8.1	165	1.1	274	39.35	20.52	0.81
25	2.2	27.2	3254	5581	7.0	143	1.1	235	40.27	18.09	0.71
30	1.2	30.6	2406	4327	4.6	115	0.7	175	41.1	14.55	0.56
35	2.4	24.9	3964	7848	8.1	137	1.2	324	42.27	9.12	0.74
40	2.5	23.8	4051	8380	8.8	127	1.3	345	37.05	10.29	0.68
50	2.6	23.6	3984	8145	8.8	134	1.3	338	38.64	9.44	0.72
60	2.8	22.	4617	9357	9.7	141	1.4	359	38.89	11.43	0.7
70	2.8	20.5	4320	10548	10.2	132	1.4	343	35.22	9.63	0.72

Annex 3

Soil cores

Table A3.3: Metal content in Agricultural soil core profile (Bc) retrieved from reservoir banks.

Bc Depth (cm)	Al %	Ca %	K ppm	Mg ppm	Si %	Zn ppm	Fe %	Mn ppm	Cu ppm	Pb ppm	Cd ppm
3	2.9	26.7	3307	5515	5.9	131	2.1	158	24.68	9.12	0.59
6	2.3	27.7	2510	2440	4.9	126	1.6	114	19.28	7.3	0.62
12	3.0	26.3	3406	5425	6.2	124	2.0	140	21.37	8.9	0.67
15	3.8	23.1	3967	6186	7.6	165	2.7	185	29.86	10.5	0.95
20	4.2	21.9	4167	6325	8.2	171	2.9	205	35.39	10.82	1.05
25	3.9	23.2	3999	6201	7.7	163	2.7	209	33.17	10.49	0.97
30	5.1	18.3	4766	6516	10.6	219	3.7	295	44.61	11.83	1.22
35	4.9	17.9	4729	6505	10.4	209	3.4	289	43.27	11.59	1.24
40	6.2	12.4	5764	7172	11.5	258	4.6	449	50.11	12.91	1.48
45	6.9	11.6	6430	7891	12.0	274	4.9	440	54.41	13.46	1.54
50	6.7	11.4	6322	7283	12.9	278	4.8	412	55.79	13.68	1.53
60	7.8	7.6	7336	7623	14.4	334	5.6	428	66.23	31.41	2.16
70	8.2	7.5	6998	8195	14.6	329	5.8	492	103.92	16.11	1.94
85	8.5	6.9	7746	8025	14.7	335	5.9	987	65.89	15.6	-

Annex 4

Litani basin- Mid of the rainy season

Table A4.1: Qaraoun reservoir water chemistry during the rainy season (March 2012).

sample	pH	T°C	Ec (µS/cm)	Do (mg/L)	CaCO3 (mg/l)	Na+ (mg/l)	K+ (mg/l)	Cl- (mg/l)	PO4 (mg/l)	NO3 (mg/l)	SO4 (mg/l)	NO2 (mg/l)	Cu (µg/l)	Cd (µg/l)
Ri 0m	8.2	17.4	548	17		24.4	7.5	4.18	29.79	26.75	44.62	0.33	10.43	1.06
Ri 1m	8.13	16.9	560	27	327	26.2	7.4	0	nd	nd	150.4	54.32	1.99	0.54
Ri 3m	8.12	15.7	560	22	378	25.1	7	0	nd	nd	163.4	54.31	0.81	1.21
Ri 5m	8.18	16.9	564	21	338	25.2	8.4	0	nd	nd	256.5	54.03	1.62	1.04
Ri 10m	8.08	16.1	555	21	365	28.7	5.8	2.61	28.75	26.28	89.15	0.32	5.28	1.17
Ri 15m	8.12	16.2	564	23	353	26.8	5.6	0.24	30.15	26.95	205.39	0.32	0.9	1.5
Ri 20m	8.12	16.7	564	15	364	28.9	5.9	2.91	30.05	26.75	86.66	0.34	3.04	2.41
Ri 25m	8.11	16.9	564	19	366	28.8	5.8	0.62	28.71	25.94	112.31	0.33	1.45	0.52
Ri 30m	8.1	17.2	565	21	385	29.9	6	1.16	29	26.11	103.67	0.33	2.7	0.61
Cz 0m	8.19	16.2	563	23	339	27.7	5.8	2.174	28.26	25.66	43.49	0.31	27.7	5.8
Cz 1m	8.26	9.8	562	3	377	28.6	6	nd	nd	nd	nd	nd	28.6	6
Cz 3m	8.24	15.9	562	4	339	29.3	5.7	4.32	29.73	26.57	47.65	0.33	29.3	5.7
Cz 5m	8.18	17.9	555	5	323	28.8	5.9	4.00	29.64	26.672	49.43	0.34	28.8	-5.9
Cz 10m	8.11	16.9	560	25	388	27.9	5.8	0.89	29.86	26.87	159.89	0.33	27.9	-5.8
Cz 15m	8.24	14.0	560	26	397	28.3	5.8	0.79	30.01846	26.81	140.5108	0.3494	28.3	5.8
Cz 20m	8.12	17.2	565	27	352	29.2	5.9	2.00	29.97	26.89	115.1932	0.34651	29.2	5.9
Cz 25m	8.13	19.3	565	24	306	28.7	5.9	0.89	28.64	25.84	112.4	0.33	28.7	5.9
Cz 30m	8	18.6	565	27	-	29.9	6	0.16	28.93	25.58	127.93	0.34	29.9	6
Dz om	8.17	13.9	560	4	374	28.4	5.7	2.6	28.32	25.69	42.61	0.33	7.79	nd
Dz 1m	8.18	13.1	561	4	363	26.9	5.7	3.873	29.37	35.54	43.046	0.325	7.71	nd
Dz 3m	8.16	9.7	558	5	368	28.5	5.8	3.5	29.86	26.62	68.48	0.34	8.30	0.21
Dz 5m	8.21	12.6	565	5	305	29.1	5.9	3.85	28.183	25.54	43.46	0.34	2.28	0.05
Dz 10m	8.23	11.4	565	6	321	29.7	5.8	4.15	29.88	26.71	49.45	0.34	4.126	0.002
Dz 15m	8.25	11.8	565	5	362	-27.6	5.7	3.05	28.87	26.97	47.11	0.29	2.586	0.7
Dz 20m	8.22	12.2	565	8	369	29.2	5.9	3.7	28.38	25.71	51.39	0.35	2.57	0.92
Dz 25m	8.19	11.2	565	4	352	-29.6	5.8	2.23	28.63	25.83	47	0.36	2.29	0.19
Dz 30m	8.22	12.9	568	3	359	30	5.9	2.34	28.91	26.03	47.91	0.34	4.79	0.15
Dz 35m	8.16	11.9	568	7	364	26.9	5.6	2.13	28.82	25.97	77.25	0.34	7.18	1.06

Annex 4

Litani basin- Mid of the rainy season

Table A4.2: Qaraoun reservoir water chemistry during mid of rainy season (April 2013).

sample	pH	T℃	Ec (µS/cm)	TDS (mg/l)	Do (mg/L)	CaCO3 (mg/l)	NH4 (mg/l)	Cl⁻ (mg/l)	NO2 (mg/l)	NO3 (mg/l)	SO4 (mg/l)	Ca (mg/l)	Mg (mg/l)
Ri 0m	8.14	15.7	5.1	349	513	193	1.86	22.08	1.27	16.13	25.02	58.02	15.18
Ri 1m	8.05	15.1	6	348	512	166	1.81	19.72	1.25	11.4	21.85	62.36	15.26
Ri 3m	8.08	15.1	5.2	348	512	172	1.57	23.75	1.24	19.82	24.03	58.63	15.19
Ri 5m	8.23	15.1	4.2	345	508	174	0.87	21.14	1.25	15.71	28.73	61.15	15.5
Cz 0m	8.58	14.5	3.2	347	510	171	0.67	-	-	-	-	62.58	15.16
Cz 1m	8.66	13.8	4.1	345	506	148	0.52	23.21	1.27	20.39	31.09	60.46	15.19
Cz 3m	8.6	13.7	3.8	345	508	142	0.45	25.5	-	19.21	33.37	60.94	15.26
Cz 5m	8.66	13.8	3.7	344	507	166	0.45	26.07	-	19.21	33.79	61.38	15.4
Cz 10m	8.6	13.7	5.1	345	507	165	0.43	23.34	1.25	17.95	30.73	59.49	15.39
Cz 15m	8.48	13.9	5.2	346	508	147	0.56	22.79	1.26	18.62	31.23	61.95	15.25
Cz 20m	8.16	12.7	5.2	352	517	195	0.39	25.04	1.036	20.6	35.06	62.92	15.21
Cz 25m	7.93	12.6	5.9	353	517	172	0.81	30.59	-	19.29	31.04	58.96	15.48
Es 0m	8.53	15.7	2.7	345	508	149	1.01	23.29	1.21	17.69	30.47	58.31	15.04
Es 1m	8.6	14.3	3.1	345	507	161	0.53	22.54	1.23	18.52	30.95	61.48	15.27
Es 2m	8.59	14.1	2.6	343	505	146	0.48	22.46	1.24	19.29	31.04	58.96	15.48
Ws 0m	8.7	16.1	1.7	335	492	4195	4.26	35.93	na	71.57	34.04	51.55	15.37
Ws 1m	8.68	14.6	1.7	345	507	166	0.47	21.59	1.22	17.75	30.68	61	15.4
Ws 2m	8.58	14.2	3.2	344	507	177	0.67	21.59	1.21	17.86	30.4	56.6	15.29
Dz om	8.79	14.7	1.6	340	501	157	0.27	28.45	1.5	31.77	58.59	15.45	33.71
Dz 1m	8.69	14.2	3.1	343	504	152	0.47	22.05	1.29	31.1	59.52	15.47	18.32
Dz 3m	8.73	14	4.8	344	501	167	0.37	23.92	1.26	31.34	59.51	15.49	21.59
Dz 5m	8.52	13.8	3.1	346	509	144	0.43	26.38	1.57	31.42	57.43	15.57	31.65
Dz 10m	8.62	13.6	4.7	346	508	143	0.32	22.22	1.51	30.98	65.07	15.72	18.47
Dz 15m	8.28	13.1	5.1	352	517	159	0.37	22.22	1.19	31.69	60.61	15.78	19.36
Dz 20m	8.21	12.6	7.2	352	517	155	0.31	22.28	1.03	32.64	61.76	15.32	8.45
Dz 25m	8.17	12.2	6.6	353	520	157	0.18	22.1	1.01	32.8	61.71	15.37	7.53

Annex 4

Litani basin- Mid of the rainy season

Table A4.3 Qaraoun reservoir water chemistry during mid of rainy season (April 2013).

sample	Al (µg/l)	Cr (µg/l)	Mn (µg/l)	Co (µg/l)	Ni (µg/l)	Cu (µg/l)	Zn (µg/l)	As (µg/l)	Cd (µg/l)	Pb (µg/l)
Ri 0m	28.89	1.24	1.51	3.95	1.05	0.34	3.29	0.02	0.005	0.12
Ri 1m	24.8	0.18	1.79	3.95	1.28	0.69	2.10	0.32	0.003	0.11
Ri 3m	23.78	0.47	2.0	3.95	1.24	0.40	4.05	0.25	0.009	0.17
Ri 5m	27.15	0.37	2.10	3.93	1.09	0.71	2.39	0.21	0.008	0.37
Cz 0m	44.06	0.63	0.71	3.95	1.22	0.45	5.06	0.21	0.014	0.38
Cz 1m	24.15	0.52	0.27	3.92	1.00	0.21	1.39	0.14	0.039	0.92
Cz 3m	10.25	0.85	0.32	3.92	1.00	0.25	0.72	0.23	0	0.21
Cz 5m	9.288	0.01	0.22	3.91	1.09	0.25	0.59	0.31	0.001	0.19
Cz 10m	1.57	0.11	0.18	3.91	0.99	0.22	0.57	0.32	0.005	0.12
Cz 15m	1.71	0.10	0.18	3.91	1.06	0.24	4.49	0.33	0	0.15
Cz 20m	37.51	0.12	0.35	3.91	1.23	0.47	4.16	0.23	0.009	0.45
Cz 25m	27.94	0.43	0.29	3.89	1.15	0.29	1.59	0.19	0.006	0.16
Es 0m	75.25	0.39	2.12	3.99	1.25	0.56	6.72	0.32	0.013	0.03
Es 1m	29.42	0.94	0.60	3.93	1.03	0.29	3.12	0.08	0.004	0.23
Es 2m	0.87	0.03	0.56	3.92	1.10	0.23	0.38	0.32	0	0.35
Ws 0m	29.87	0.31	0.83	3.94	1.18	0.46	4.66	0.17	0.011	0.21
Ws 1m	34.07	0.31	0.41	3.91	1.06	0.37	4.98	0.21	0.003	0.33
Ws 2m	31.59	0.57	0.29	3.92	1.02	0.25	0.75	0.18	0.001	0.14
Dz om	24.63	0.44	0.54	4.01	1.84	0.63	3.15	0.29	0.027	0.71
Dz 1m	24.43	0.15	0.36	3.95	1.54	0.43	0.99	0.27	0.007	0.22
Dz 3m	32.22	1.14	0.52	3.96	1.49	0.55	3.66	0.03	0.009	0.27
Dz 5m	29.98	0.51	0.22	3.93	1.39	0.33	1.65	0.18	0.002	0.19
Dz 10m	22.20	0.06	0.24	3.92	1.26	0.32	1.36	0.27	0.002	0.19
Dz 15m	25.41	0.28	0.26	3.91	1.78	0.52	1.91	0.23	0.005	0.28
Dz 20m	39.37	1.02	0.62	3.94	1.60	0.62	2.57	0.08	0.012	0.37
Dz 25m	23.46	0.41	0.31	3.92	5.71	0.79	3.76	0.18	0.03	0.29

Annex 5

Litani basin- transition season

Table A5.1: Qaraaoun reservoir water physicochemistry during the transition season (July 2013).

sample	pH	T C°	Ec (µS/cm)	TDS (mg/l)	Chlorophyll (µg/l)	Cl^- (mg/l)	NO_2^- (mg/l)	NO_3^- (mg/l)	SO_4^{-2} (mg/l)
Dz0	8.91	23.6	328	223	35.39	28.75	na	8.37	29.41
Dz1	8.85	23.3	331	225	8.48	23.41	na	7.69	27.66
Dz3	8.72	23.1	333	226	24.44	22.85	1	7.81	27.03
Dz5	8.54	23	335	228	4.06	23.06	na	7.78	27.36
Dz10	8.15	22.3	351	239	1.48	22.87	0.99	8.46	27.12
Dz15	7.69	20.6	418	284	0	na	na	na	na
Dz20	7.73	18.9	447	304	0	22.63	1.27	9.69	27.79
Dz25	7.79	16.9	494	336	0	21.63	1.94	10.83	27.63
Dz30	7.8	17.4	503	344	0	21.85	1.86	11.39	28.16

Table A5.2: Qaraaoun metal content during transition season (July 2013).

sample	Al (µg/l)	Cr (µg/l)	Mn (µg/l)	Co (µg/l)	Ni (µg/l)	Cu (µg/l)	Zn (µg/l)	As (µg/l)	Cd (µg/l)	Pb (µg/l)
Dz om	0.98	0.06	0.84	3.90	0.59	0.41	1.09	0.34	0.01	0.19
Dz 1m	0.55	0.02	0.42	3.89	0.59	0.19	1.49	0.33	0.001	0.18
Dz 3m	1.69	0.02	0.07	3.88	0.51	0.20	0.61	0.32	0.005	0.05
Dz 5m	0.83	0.003	0.59	3.89	0.50	0.12	1.87	0.32	0.003	0.07
Dz 10m	1.77	0.03	0.064	3.89	0.58	0.15	3.03	0.32	0.004	0.06
Dz 20m	1.39	0.02	3.72	3.93	1.86	0.35	11.67	0.37	0.005	0.13
Dz 25m	0.17	0.04	8.36	3.93	0.99	0.18	1.75	0.34	0.004	0.05
Dz 30m	1.96	0.12	1.03	3.92	2.59	0.35	4.85	0.36	0.004	0.01

Annex 6

Litani basin- End of the dry season

Table A6.1: Qaraoun reservoir water chemistry during end of the dry season (September 2011).

sample name	Ec (µS/cm)	Na^+ (mg/l)	K^+ (mg/l)	PO4 (mg/l)	Cl (mg/l)	NO3 (mg/l)	SO4 (mg/l)	Cr (mg/)l	Zn (µg/l)	Cu (µg/l)	Cd (µg/l)	Mn (µg/l)	Pb (µg/l)	Fe (µg/l)
Ri 1	362	34.6	4	0.70	23.88	2.75	28.79	0.53	31.6	45.3	0.68	1.21	0.13	92.5
Ri 2	376	33.6	4.1	0.44	23.93	3.7	35.34	0.16	31.2	51.3	0.05	1.72	0.15	87.9
Cz1 0m	368	33.4	3.9	0.67	27.95	3.19	33.42	0.31	22.7	57.4	0.14	2.92	0.14	53.5
Cz1 5m	371	32.3	4	0.76	28.75	4.51	34.20	0.24	93.8	49.8	0.47	11.73	0.06	56.9
Cz1 10m	380	31	3.9	0.92	27.77	3.95	33.26	0.20	42.3	46.6	3.2	24.24	0.05	78.3
Cz1 15m	387	29.3	4.1	0.69	28.41	4.04	33.60	0.35	22.25	49.1	1.3	111	0.10	101
Cz2 0m	376	31.7	4.1	0.73	28.94	4.36	34.03	0.15	10.9	51.9	nd	2.07	0.23	70.1
Cz2 5m	370	47.5	4.5	0.57	29.79	3.73	35.49	0.18	13.7	53.5	nd	9.68	0.21	18.7
Cz2 10m	376	32.3	4.2	0.91	28.95	3.48	34.42	0.26	92.3	42.5	0.14	30.31	0.12	194
Cz3	376	32.9	4.2	1.23	29.60	3.389	35.333	0.8592	89.4	48.2	0.18	5.297	0.19	122
Cz4	374	34.7	4.3	0.76	28.77	3.32	34.24	0.25	12.8	46.4	0.42	1.93	0.1991	35.1
Cz5	376	35.2	4.2	0.85	28.40	3.24	33.85	0.5497	16.3	56.3	0.06	0.26	0.19	65.2
Cz5 5m	371	35.7	4.2	0.68	29.91	4.33	39.576	0.12	81.3	57.8	0.005	9.91	0.08	39.3
Cz5 10m	373	34.7	3.9	0.73	28.81	3.22	33.22	0.09	57	59.9	3.5	9.58	0.10	46.3
Cz5 15m	370	33.7	4.1	0.79	28.33	4.79	33.67	0.18	153	200	nd	14.08	0.15	60
Cz5 20m		17.2	4.2	1.06	35.52	2.91	35.12	0.28	179	150	3.7	115	0.11	95.96
Dz 0m	371	35.7	4.1	1.04	29.48	3.31	35.05	0.12	13.5	49.9	0.33	5.45	0.12	67.2
Dz 5m	368	35.6	4	0.30	18.23	2.85	30.43	0.29	20.8	45.6	0.05	10.27	0.07	29.5
Dz 10m	375	36.1	4.1	0.81	30.87	3.37	35.37	0.50	165	44.9	0.41	11.94	0.05	50.1
Dz 15m	374	34.2	4	0.99	28.73	3.23	33.99	0.29	66.1	45	6.2	14.69	0.11	33.8

Annex 6

Litani basin- End of the dry season

Table A6.2: Qaraoun reservoir water chemistry during end of the dry season (September 2012).

sample	pH	Ec (µS/cm)	TDS (mg/l)	Do (mg/L)	CaCO3 (mg/l)	Na+ (mg/l)	K+ (mg/l)	F- (mg/l)	Cl- (mg/l)	NO2 (mg/l)	NO3 (mg/l)	SO4 (mg/l)	Ca (mg/l)	Mg (mg/l)
Ri 0m	8.47	337	228	6.6	215	13.5	3.1	0.301	23.74	1.05	5.54	29.35	62.79	16.07
Ri 1m	8.3	340	231	6.5	215	13	3	0.30	23.76	1.08	5.48	29.45	64.79	16.09
Ri 3m	7.93	343	232	6.3	217	13.8	2.9	0.31	23.89	1.07	5.90	29.30	58.48	14.37
Ri 5m	6.99	356	242	5.8	188	13.2	2.8	0.301	23.75	1.07	5.5	29.19	63.95	14.27
Ri 10m	7.87	349	237	5.9	229	14	2.95	0.301	23.65	1.07	5.64	29.18	65.2	14.31
Cz 0m	8.3	340	231	6.6	197	14.8	2.7	0.309	23.81	1.09	5.55	29.38	56.71	16.28
Cz 1m	8.25	338	229	6.5	202	13.5	3	0.307	23.79	1.09	5.59	29.30	59.32	16.02
Cz 3m	8.32	337	228	7.6	109	13.2	3.1	0.311	23.72	1.06	5.62	29.36	62.18	15.89
Cz 5m	8.11	337	229	6.3	205	13	3.1	0.308	23.86	1.08	5.56	29.29	62.78	16.14
Cz 10m	7.93	341	231	6.6	205	13.2	3.2	0.306	23.80	1.07	6.37	29.38	50.48	16.29
Cz 15m	8.01	338	229	6.2	211	12.6	2.7	0.307	23.81	1.07	5.89	29.36	56.83	16.01
Cz 20m	7.76	337	229	6.2	205	12.1	3.2	0.311	23.65	1.07	5.62	29.56	60.16	15.71
Cz 25m	7.98	343	232	6.5	221	12.6	3.2	0.307	23.57	1.08	5.83	29.10	57.49	15.79
Es 0m	8.2	339	229	6.3	208	10	3.4	0.301	23.71	1.06	5.58	29.43	67.19	14.34
Ws 0m	8.37	339	230	6.8	208	10	3.3	0.302	24.02	1.05	7.05	29.38	50.26	14.47
Dz om	7.92	335	232	6.7	208	11.2	3.3	0.32	23.71	1.09	5.83	29.34	52.73	15.97
Dz 1m	7.57	336	232	6.1	201	9.7	3.2	0.31	23.77	1.09	5.73	29.13	57.63	16
Dz 3m	7.7	336	232	6.3	200	9.6	3.2	0.32	23.74	1.09	5.8	29.09	54.14	16.1
Dz 5m	6.8	347	239	6.1	172	9	3.2	0.32		1.09	5.85	29.12	54.22	15.79
Dz 10m	7.75	338	232	6	200	9.5	3.2	0.33	23.7	1.09	5.79	29.15	59.86	15.66
Dz 15m	7.25	341	235	6.1	199	9	3.1	0.32	23.68	1.09	5.8	29.09	55.44	15.84
Dz 20m	7.74	337	233	6.1	205	8.6	3.3	0.32	23.71	1.11	6.16	29.21	63.37	15.91
Dz 25m	7.78	338	233	6.7	217	8.5	3.1	0.31	23.57	1.08	5.63	29.15	57.49	16.05

Table A6.3: Dissolved metal concentration during end of the dry season in Qaraaoun reservoir (September 2012).

sample	Al (µg/l)	Cr (µg/l)	Mn (µg/l)	Co (µg/l)	Ni (µg/l)	Cu (µg/l)	Zn (µg/l)	As (µg/l)	Cd (µg/l)	Pb (µg/l)
Ri 0m	3.43	0.06	0.61	3.95	0.67	0.85	3.48	0.43	0.004	0.07
Ri 1m	3.61	0.07	0.555	3.96	0.82	0.92	2.29	0.47	0.004	0.25
Ri 3m	7.02	0.08	0.511	3.94	1.07	1.09	4.12	0.48	0.026	0.55
Ri 5m	2.89	0.13	0.409	3.93	0.80	0.69	12.50	0.46	0.005	0.85
Ri 10m	3.75	0.1	0.990	3.95	0.67	0.85	3.48	0.43	0.004	0.07
Cz 0m	2.91	0.11	0.605	3.95	0.84	1.34	2.73	0.52	0.003	0.12
Cz 1m	4.31	0.03	0.345	3.95	0.99	1.58	4.12	0.50	0.002	0.38
Cz 3m	5.01	0.05	0.289	3.95	1.30	0.75	6.81	0.47	0.002	0.54
Cz 5m	2.97	0.07	0.189	3.93	0.75	1.57	5.21	0.47	0.004	0.09
Cz 10m	6.78	0.06	0.348	3.95	1.17	0.74	18.94	0.49	0.004	0.94
Cz 15m	3.06	0.02	0.251	3.94	0.92	0.99	1.78	0.49	0.003	0.13
Cz 20m	1.47	0.08	5.441	4.06	0.94	1.17	6.68	0.52	0.005	0.12
Cz 25m	2.83	0.03	0.605	3.93	1.58	1.41	7.07	0.49	0.003	0.19
Es 0m	0.26	0.15	0.074	3.79	0.01	0.04	0.10	0.15	0.005	0.002
Ws 0m	4.19	0.03	0.261	3.95	0.79	1.08	4.36	0.45	0	0.10
Dz om	2.29	0.01	0.41	3.93	0.88	1.19	1.69	0.47	0.002	0.07
Dz 1m	2.84	0.001	0.39	3.93	1.09	1.39	4.79	0.46	0.002	0.37
Dz 3m	3.24	0.04	0.21	3.93	1.25	0.55	5.32	0.48	0.002	0.16
Dz 5m	2.08	0.03	0.18	3.94	1.12	0.93	5.12	0.49	0.003	0.39
Dz 10m	1.89	0.01	0.17	3.94	0.98	1.81	3.54	0.45	0.003	0.16
Dz 15m	1.95	0.02	0.45	3.95	1.26	1.64	3.9.49	0.52	0	1.27
Dz 20m	2.61	0.06	0.62	3.94	0.94	0.97	3.04	0.48	0.002	0.11
Dz 25m	4.45	0.02	1.97	3.96	1.43	1.37	8.96	0.49	0.003	0.96

Annex 7

Litani basin- First Flush

Table A7.1: Qaraoun reservoir water chemistry during the first flush (November 2012).

sample name	Na^+ (mg/l)	K^+ (mg/l)	PO4 (mg/l)	Cl (mg/l)	NO3 (mg/l)	SO4 (mg/l)	NO2 (mg/l)	Zn (mg/l)	Cr (mg/)l	Cu (µg/l)	Cd (µg/l)	Mn (µg/l)	Pb (µg/l)
Ri 0m	31.4	12.2	0.099	18.61	4.001	31.69	0.13	0.012	0.02	0.78	0.24	16.31	7.04
Ri 5m	31.6	12.1	0.15	18.72		31.78		0.011	0.04	0.86	0.21	2.89	8.39
Ri 10m	31.7	12.1	0.12	18.56	6.24	31.77	0.14	0.017	0.06	0.29	0.096	0.09	nd
Cz1 0m	28	12.2	nd	nd	nd	nd	nd	0.015	0.065	1.44	0.32		nd
Cz1 5m	28.2	13	nd	nd	nd	nd	nd	0.012	0.07	4.49	0.10	1.49	nd
Cz1 10m	28.7	11.8	nd	nd	nd	nd	nd	0.012	0.09	0.77	0.13	1.26	17.77
Cz1 15m	31.4	12.2	0.1	18.612	4.00	31.69	0.13	0.012	0.03	0.78	0.24	16.31	nd
Cz2 0m	29.7	12	0.09	18.574	4.28	31.076	0.158	0.012	0.09	4.59	0.09	0.66	nd
Cz2 5m	30.9	11.8	0.14	18.319	4.28	30.96	0.153	0.013	0.06	2.72	0.13	0.45	16.28
Cz2 10m	31.1	9.4	0.15	18.319	4.43	31.29	0.155	0.015	0.07	5.10	0.15	6.87	nd
Cz2 15m	28	12	nd	18.718	4.2	30.57	0.144	0.014	0.07	2.03	0.18	4.49	18.83
Cz2 20m	29.5	11.8	nd	nd	nd	nd	nd	0.014	0.04	2.36	0.27	1.35	nd
Cz2 25m	29.4	11.8	nd	nd	nd	nd	nd	nd	nd	nd	nd	nd	nd
Dz 0m			nd	nd	nd	nd	nd	0.01	0.10	4.13	0.25	3.21	2.473
Dz 5m	30.7	11.7	nd	nd	nd	nd	nd	0.015	0.06	1.98	0.13	2.58	19.4
Dz 10m	23.9	9.2	nd	nd	nd	nd	nd	0.012	0.05	2.74	0.13	1.36	3.36
Dz 15m	nd	nd	nd	nd	nd	nd	nd	0.014	0.06	3.01	0.04	2.87	10.71

Annex 7

Litani basin- First Flush

Table A7.2: Qaraoun reservoir surface water chemistry during the first flush (November 2012).

sample	Coi N	Coi E	Na^+ (mg/l)	K^+ (mg/l)	PO4 (mg/l)	Cl (mg/l)	NO3 (mg/l)	SO4 (mg/l)	Cu (µg/l)	Cd (µg/l)	Mn (µg/l)	Zn (mg/l)	Cr (mg/l)	Pb (µg/l)
A	33.54881	35.69161	29.8	12.1	1.3	28.78	4.66	34.93	3.54	0.32	0.67	0.09	0.06	2.43
B	33.54932	35.69134	30.6	12.2	1.38	28.76	4.53	34.95	3.72	0.27	2.86	0.01	0.06	2.67
C	33.55032	35.69115	30.4	12.1	1.245	28.84	4.48	34.98	1.19	0.21	1.24	0.01	0.06	2.39
D	33.55071	35.69123	30.3	12.1	1.133	28.88	5.47	35.03	1.09	0.17	0.66	0.01	0.06	7.87
E	33.55126	35.69095	30.8	12	1.23	28.88	4.42	34.97	0.88	0.22	0.61	0.01	0.08	14.1
F	33.55199	35.69118	31.2	12	1.107	28.90	6.33	35.09	0.41	0.32	0.61	0.01	0.04	4.26
G	33.55392	35.69112	30.6	12	1.238	28.83	5.45	34.97	1.89	0.35	0.77	0.01	0.05	10.02
H	33.55467	35.69098	31	11.9	1.18	28.77	4.74	34.88	3.13	0.2	0.97	0.01	0.07	10.06
J	33.55927	35.69103	31.1	12.2	1.04	28.8	5.92	34.91	0.67	0.15	0.69	0.01	0.04	2.36
K	33.55735	35.69135	31.4	12	0.68	17.98	4.77	32.07	5.58	0.07	3.85	0.01	0.05	9.59
L	33.55982	35.6914	28.9	12	-	-	-	-	3.27	0.22	4.61	0.01	0.06	13.62
M	33.56196	35.69168	28.6	11.8	0.55	18.12	5.61	31.98	4.82	0.67	1.01	0.01	0.09	3.22
N	33.56363	35.69184	29.4	11.9	0.51	17.96	3.85	31.98	4.09	0.71	1.1	0.01	0.09	9.45
O	33.5686	35.69238	31.6	12	0.65	18.18	3.96	32.02	2.33	0.23	1.24	0.01	0.09	4.78
R	33.56903	35.6925	31.7	12	-	-	-	-	4.07	0.38	0.64	0.01	0.04	4.01
S	33.57808	35.69481	32	12.1	-	28.98	3.87	35.19	1.89	0.3	1.26	0.01	0.05	2.89

Annex 7

Litani basin- First Flush

Table A7.3: Qaraoun reservoir water chemistry during the first flush (October 2012).

sample	pH	T℃	Ec (µS/cm)	TDS (mg/l)	Do (mg/L)	CaCO3 (mg/l)	NH4 (mg/l)	Cl- (mg/l)	NO2 (mg/l)	NO3 (mg/l)	SO4 (mg/l)	Ca (mg/l)	Mg (mg/l)
Ri 0m	20.5	8.08	346	236	6.6	215	0.42	22.04	4.54	5.05	25.21	39.97	11.98
Ri 1m	19.9	8.55	343	235	6.2	204	0.29	21.19	4.45	5.09	25.08	39.71	12.13
Ri 3m	20	7.89	345	236	4.6	197	0.39	21.21	4.61	5.05	24.94	37.83	13.15
Ri 5m	19.6	7.81	348	238	4.4	198	0.52	22.03	4.75	6.77	24.89	39.9	13.37
Cz 0m	21.2	8.22	345	237	6.1	197	0.35	21	4.78	5.25	24.61	36.87	13.31
Cz 1m	20.4	8.36	344	234	5	204	0.29	20.95	4.9	5.33	24.46	36.17	13.15
Cz 3m	20	7.93	347	237	5.4	215	0.38	22.8	5.39	5.33	24.52	38	13.19
Cz 5m	19.7	7.77	348	238	3.7	217	0.44	-	-	-	-	40.36	13.19
Cz 10m	19.8	7.8	348	239	4.3	226	0.39	22.1	5.84	5.24	53.55	40.83	12.87
Cz 15m	19.6	7.83	346	237	5.2	208	0.53	20.52	5.75	5.09	54.8	36.78	12.89
Es 0m	20.7	7.69	342	240	6.8	213	0.34	21.38	4.23	5.32	25.45	43.85	12.59
Es 1m	20.1	8.24	343	235	6	206	0.39	21.26	4.32	5.17	25.16	38.94	12.64
Es 2m	20.3	8.12	343	235	20.3	8.12	0.38	21.35	4.24	5.57	25.23	39.21	12.73
Ws 0m	21.2	8.39	342	234	7.2	221	0.39	21.34	4.32	5.16	25.29	43.91	12.73
Ws 1m	20.9	8.5	342	234	7.1	208	0.35	21.38	4.62	5.14	24.98	40.91	12.61
Ws 2m	20.3	8.23	343	235	6.7	225	0.39	21.43	4.46	5.15	25.1	40.99	12.38
Dz om	20.4	8.65	342	234	7.8	210	0.42	20.307	5.928	5.098	54.398	37.84	13.23
Dz 1m	20.1	8.75	341	232	7.1	212	0.38	20.223	6.328	5.068	55.069	36.57	13.04
Dz 3m	20	8.58	343	234	6	210	0.40	21.41	2.56	5.43	26.78	39.27	13.25
Dz 5m	19.7	8.23	346	236	4.3	212	0.36	21.47	2.59	5.52	26.8	32.83	13.36
Dz 10m	19.5	8.03	349	240	5.2	223	0.42	21.83	3.39	5.58	26.71	35.71	13.19
Dz 15m	19.5	7.76	352	241	4.4	192	0.51	21.89	3.42	5.66	26.61	38.28	13.25
Dz 20m	19.3	7.66	374	255	4.3	241	0.84	21.78	3.29	8.66	25.9	36.41	13.17
Dz 25m	18.6	7.47	450	308	2.4	328	1.88	21.534	3.501	11.348	22.847	57.25	13.75

Table A7.4: Qaraoun reservoir water metal content during the first flush (October 2012).

sample	Al (µg/l)	Cr (µg/l)	Mn (µg/l)	Co (µg/l)	Ni (µg/l)	Cu (µg/l)	Zn (µg/l)	As (µg/l)	Cd (µg/l)	Pb (µg/l)
Cz 0m	5.78	0.14	0.29	3.9	0.74	0.66	1.67	0.34	0.004	0.04
Cz 3m	7.11	0.20	0.33	3.91	0.93	0.62	3.84	0.42	0.033	0.75
Cz 5m	5.94	0.26	0.38	3.91	0.88	0.43	1.52	0.38	0.001	0.14
Cz 10m	4.59	0.53	0.52	3.91	0.85	0.54	1.66	0.34	0.003	0.08
Cz 15m	5.58	0.05	1.52	3.94	0.97	0.46	2.08	0.39	0.002	0.05
Dz om	7.54	0.53	0.37	3.91	0.86	1.42	0.84	0.33	0.004	0.07
Dz 1m	8.22	0.19	0.14	3.90	0.95	0.69	1.47	0.33	0.001	0.17
Dz 3m	11.19	1.81	1.06	3.91	0.91	1.48	0.98	0.32	0.003	0.12
Dz 5m	9.13	0.21	0.18	3.90	0.91	0.51	1.14	0.32	0.003	0.07
Dz 10m	7.64	0.36	0.24	3.90	0.92	0.46	0.73	0.39	0.004	0.08
Dz 15m	4.67	0.57	0.16	3.90	1.24	0.75	1.97	0.39	0.014	0.45
Dz 20m	4.59	0.004	0.52	3.90	0.98	0.39	1.37	0.37	0.004	0.32
Dz 25m	3.09	0.16	0.59	3.93	0.98	0.44	3.47	0.35	0.004	0.17

Annex 8

Litani basin- Piezometers

Table A8.1: Nutrients and metal content in piezometers during September 2011.

sample name	Ec (µS/cm)	Na^+ (mg/l)	K^+ (mg/l)	PO4 (mg/l)	Cl (mg/l)	NO3 (mg/l)	Mn (µg/l)	Zn (µg/l)	Cr (µg/l)	Pb (µg/l)
S1	249	10	0.3	1.4	11.8	3.4	93.4	310	45.8	0.17
S4	168.3	13.1	0.7	nd	21.4	4.9	14.1	11700	110.7	0.24
S5	103.8	14.9	1.4	nd	nd	nd	14.9	10100	119.8	0.11

Table A8.2: Nutrients and metal content in piezometers during April 2012.

sample	pH	T℃	Ec (µS/cm)	DCO (mg/L)	CaCO3 (mg/l)	Na+ (mg/l)	K+ (mg/l)	Cl- (mg/l)	PO4 (mg/l)	NO3 (mg/l)	SO4 (mg/l)	NO2 (mg/l)	Cu (µg/l)	Cd (µg/l)
S5	8.7	10.1	115.6	28	120	15	3.7	0	10.92	0.56	23.36	-	7.7	1.6
S6	8.3	8.2	460	25	256	18.9	3.3	5.98	15.49	-	37.89	-	5.99	0.8
RM Bis 17	7.29	9.0	549	16	330	11.2	3.4	3.58	6.73	16.95	197	-	6.44	1.76
KCO 309	8.17	7.9	79.8	24	212	8.6	3.1	1.17	16.08	-	10.18	-	4.81	0.32
KCO 209	9.3	7.9	79.8	13	128	15.3	2.8	-	7.71	-	34.35	-	0.49	0.18

TableA8.3: Nutrients and metal content in piezometers during October 2012.

sample	pH	T℃	Ec (µS/cm)	TDS (mg/l)	Do (mg/L)	CaCO3 (mg/l)	NH4 (mg/l)	Cl- (mg/l)	NO2 (mg/l)	NO3 (mg/l)	SO4 (mg/l)	Ca (mg/l)	Mg (mg/l)
S1	24.4	7.91	200	136	4	157	0.221	12.98	2.63	na	3.86	29.52	6.28
S4	23.9	7.59	220	150	4.3	193	0.585	17.74	2.83	na	na	29.48	10.05
S5	23.9	8.29	119.6	81	3.8	101	0.143	na	na	na	na	14.32	3.09
S6	23.8	7.24	463	315	4.6	361	0.156	na	na	na	na	62.21	6.57
RM Bis 17	23.6	6.91	416	283	3.4	330	2.34	13.4	2.2	na	2.64	52.93	17.02
Canal 900	23.5	6.99	482	328	6.8	324	1.573	18.72	3.65	12.28	19.41	57.81	12.88

Table A8.4: Nutrients and metal content in piezometers during October 2012

sample	Al (µg/l)	Cr (µg/l)	Mn (µg/l)	Co (µg/l)	Ni (µg/l)	Cu (µg/l)	Zn (µg/l)	As (µg/l)	Cd (µg/l)	Pb (µg/l)
S1	M6.64	0.397	12.35	3.826	0.57	0.75	3.90	0.24	0.002	0.092
RM Bis 17	M5.87	-0.089	33.43	3.912	0.69	0.50	0.92	0.41	0.005	0.012
S4	7.809	0.527	23.020	3.949	0.88	0.89	2.95	0.48	0.004	0.046
S5	M7.18	0.646	4.38	3.81	0.48	2.78	2.42	0.13	0.002	0.117
Canal 900	6.62	0.337	76.13	4.24	1.09	1.92	2.93	0.25	0.002	0.121

Annex 9

Litani basin- Environnemental isotopes ($\delta^{18}O$; $\delta^{2}H$)

September -2011	$\delta^{2}H/^{1}H$ (‰)	$\sigma\ \delta^{2}H/^{1}H$	$\delta^{18}O/^{16}O$ (‰)	$\sigma\delta^{18}O/^{16}O$
Ri 1	-26.70	0.141	-4.46	0.035
Ri 2	-26.23	0.423	-4.42	0.153
Cz1 0m	-26.23	0.113	-4.27	0.044
Cz1 5m	-26.72	0.371	-4.40	0.106
Cz1 10m	-27.02	0.187	-4.44	0.082
Cz1 15m	-26.73	0.081	-4.38	0.131
Cz2 0m	-26.51	0.463	-4.14	0.118
Cz2 5m	-26.02	0.597	-4.47	0.165
Cz2 10m	-25.85	0.441	-4.55	0.150
Cz3	-27.36	0.107	-4.06	0.035
Cz4	-27.50	0.148	-4.10	0.044
Cz5	-27.29	0.248	-4.09	0.043
Cz5 5m	-27.31	0.092	-4.13	0.036
Cz5 10m	-27.47	0.214	-4.16	0.023
Cz5 15m	-27.43	0.212	-4.12	0.077
Cz5 20m	-28.35	0.334	-4.36	0.023
Dz 0m	-27.68	0.333	-3.92	0.066
Dz 5m	-26.74	0.220	-4.15	0.032
Dz 10m	-27.25	0.088	-3.98	0.023
Dz 15m	-26.67	0.297	-4.02	0.056
GW S1	-29.17	0.528	-5.08	0.032
GW S4	-31.97	0.139	-5.36	0.031
GW S5	-34.25	0.216	-5.50	0.048

Novembre -2011	$\delta^{2}H/^{1}H$ (‰)	$\sigma\ \delta^{2}H/^{1}H$	$\delta^{18}O/^{16}O$ (‰)	$\sigma\delta^{18}O/^{16}O$
A	-26.14	0.394	-4.36	0.060
B	-26.45	0.421	-4.34	0.071
C	-26.36	0.329	-4.28	0.018
D	-26.28	0.398	-4.04	0.115
E	-26.78	0.363	-4.05	0.083
F	-26.16	0.342	-4.02	0.013
G	-25.04	0.129	-4.07	0.039
I	-26.04	0.231	-3.98	0.040
J	-26.23	0.398	-4.12	0.025
K	-25.93	0.196	-4.17	0.062
L	-25.57	0.148	-4.29	0.054
M	-25.09	0.434	-4.38	0.061
N	-25.69	0.119	-4.37	0.058
Q	-24.95	0.332	-4.37	0.095
R	-25.43	0.332	-3.36	0.045
S	-24.02	0.063	-4.44	0.045

Annex 9

Litani basin- Environnemental isotopes ($\delta^{18}O$; $\delta^{2}H$)

Novembre -2011	$\delta^{2}H/^{1}H$ (‰)	$\sigma\ \delta^{2}H/^{1}H$	$\delta^{18}O/^{16}O$ (‰)	$\sigma\delta^{18}O/^{16}O$
Ri 0m	-26.18	0.356	-4.49	0.066
Ri 5m	-25.65	0.250	-4.41	0.064
Ri 10m	-26.05	0.270	-4.39	0.067
Cz1 0m	-27.09	0.417	-4.02	0.042
Cz1 5m	-26.31	0.167	-3.96	0.039
Cz1 10m	-25.27	0.143	-4.06	0.020
Cz1 15m	-24.93	0.171	-4.15	0.057
Cz2 0m	-26.67	0.267	-4.00	0.047
Cz2 5m	-26.51	0.315	-3.92	0.045
Cz2 10m	-26.78	0.115	-3.94	0.018
Cz2 15m	-26.75	0.161	-3.99	0.030
Cz2 20m	-26.35	0.282	-3.92	0.057
Cz2 25m	-26.15	0.207	-4.07	0.012
Dz 0m	-25.89	0.389	-3.96	0.055
Dz 5m	-25.42	0.182	-3.90	0.043
Dz 10m	-25.62	0.239	-3.85	0.016
Anjar water spring	-40.91	0.271	-6.62	0.013
Litani River (Jeb Jannine)	-38.95	0.321	-6.39	0.030
Tributary Ain delb	-36.40	0.508	-6.47	0.052
Tributary Khreizet	-34.14	0.191	-6.26	0.050

March-2012	$\delta^{2}H/^{1}H$ (‰)	$\sigma\ \delta^{2}H/^{1}H$	$\delta^{18}O/^{16}O$ (‰)	$\sigma\delta^{18}O/^{16}O$
Ri 0m	-32.74	0.077	-5.62	0.041
Ri 1m	-32.94	0.162	-5.76	0.079
Ri 3m	-32.17	0.285	-5.98	0.050
Ri 5m	-32.17	0.307	-5.91	0.032
Ri 10m	-32.09	0.127	-5.94	0.048
Ri 15m	-32.18	0.341	-5.95	0.042
Ri 20m	-32.07	0.203	-5.94	0.040
Ri 25m	-32.41	0.128	-5.86	0.059
Ri 30m	-32.77	0.320	-5.70	0.103
Cz 0m	-32.81	0.154	-5.72	0.051
Cz 1m	-32.92	0.058	-5.73	0.022
Cz 3m	-32.32	0.165	-6.05	0.061
Cz 5m	-32.56	0.009	-5.97	0.058
Cz 10m	-31.85	0.209	-5.98	0.036
Cz 15m	-31.96	0.058	-6.02	0.016
Cz 20m	-32.40	0.308	-5.87	0.017
Cz 25m	-32.43	0.085	-5.77	0.038
Cz 30m	-32.58	0.403	-5.68	0.072
Dz om	-33.66	0.122	-5.57	0.043
Dz 1m	-32.81	0.284	-5.73	0.071
Dz 3m	-32.52	0.301	-6.00	0.081
Dz 5m	-32.35	0.206	-5.99	0.050
Dz 10m	-31.92	0.063	-6.00	0.073
Dz 15m	-31.99	0.178	-5.98	0.026
Dz 20m	-32	0.217	-5.92	0.054
Dz 25m	-32.11	0.175	-5.82	0.024
Dz 30m	-32.58	0.369	-5.82	0.036
Dz 35m	-32.85	0.138	-5.78	0.028
S5	-33.81	0.456	-5.83	0.065
S6	-31.62	0.056	-5.65	0.027
Rm bis 17	-29.93	0.237	-5.01	0.065
KCO209	-30.63	0.054	-5.58	0.034
KCO3 309	-33.00	0.196	-6.17	0.093

Annex 9

Litani basin- Environnemental isotopes ($\delta^{18}O$; $\delta^{2}H$)

June-2012	$\delta^{2}H/^{1}H$ (‰)	$\delta^{18}O/^{16}O$ (‰)
Ri 0 m	-31.46	-7.31
Ri 5m	-31.19	-7.39
Ri 10m	-31.29	-7.33
Ri 15m	-36.36	-7.92
Ri 20m	-35.07	-7.8
Cz 0m	-32.15	-7.59
Cz 5m	-31.33	-7.75
Cz 10	-31.65	-7.74
Cz 15m	-35.14	-7.88
Cz 20m	-30.08	-7.69
Dz zero meter	-32.48	-7.7
Dz 5m	-32.42	-7.64
Dz 10m	-32.82	-7.63
Dz 15m	-36.39	-8.24
Dz 20m	-30.4	-8.15
Kco309	-33.08	-7.83
kco209	-26.62	-7.65
rm17bis	-30	-7.31
S6	-31.25	-7.73
S5	-35.49	-7.83

September-2012	$\delta^{2}H/^{1}H$ (‰)	$\sigma\,\delta^{2}H/^{1}H$	$\delta^{18}O/^{16}O$ (‰)	$\sigma\delta^{18}O/^{16}O$
Ri 0m	-28.22	0.236	-4.71	0.034
Ri 1m	-28.9	0.081	-4.70	0.020
Ri 3m	-28.62	0.204	-4.62	0.053
Ri 5m	-28.3	0.081	-4.63	0.025
Ri 10m	-29.27	0.095	-4.61	0.025
Cz 0m	-29.42	0.204	-5.21	0.058
Cz 1m	-29.95	0.129	-5.17	0.030
Cz 3m	-29.10	0	-5.34	0.023
Cz 5m	-29.40	0.082	-5.27	0.051
Cz 10m	-29.32	0.050	-5.31	0.012
Cz 15m	-29.45	0.129	-5.33	0.013
Cz 20m	-29.17	0.150	-5.51	0.045
Cz 25m	-29.30	0.141	-5.01	0.047
Es 0m	-28.62	0.377	-5.31	0.078
Ws 0m	-28.08	0.109	-4.66	0.040
Dz om	-31.28	0.278	-5.30	0.037
Dz 1m	-31.20	0.081	-5.31	0.033
Dz 3m	-30.27	0.359	-5.33	0.017
Dz 5m	-29.85	0.173	-5.36	0.021
Dz 10m	-29.72	0.126	-5.32	0.040
Dz 15m	-29.70	0.070	-5.30	0.043
Dz 20m	-29.22	0.125	-5.24	0

Annex 9

Litani basin- Environnemental isotopes ($\delta^{18}O$; $\delta^{2}H$)

October-2012	$\delta^{2}H/^{1}H$ (‰)	$\sigma\ \delta^{2}H/^{1}H$	$\delta^{18}O/^{16}O$ (‰)	$\sigma\delta^{18}O/^{16}O$
Ri 0m	-26.99	0.073	-5.17	0.049
Ri 1m	-27.45	0.022	-5.16	0.021
Ri 3m	-27.97	0.549	-5.15	0.046
Ri 5m	-26.55	0.035	-5.04	0.026
Cz 0m	-26.05	0.040	-5.01	0.0126
Cz 1m	-26.25	0.148	-5.01	0.021
Cz 3m	-27.47	0.150	-4.86	0.017
Cz 5m	-28.27	0.442	-4.90	0.062
Cz 10m	-27.22	0.049	-4.72	0.033
Cz 15m	-26.42	0.032	-4.84	0.017
Es 0m	-26.76	0.242	-5.47	0.022
Es 1m	-27.36	0.155	-5.42	0.059
Es 2m	-27.47	0.076	-5.45	0.021
Ws 0m	-27.87	0.556	-5.41	0.017
Ws 1m	-26.57	0.096	-5.40	0.037
Ws 2m	-26.48	0.036	-5.38	0.009
Dz om	-27.00	0.174	-4.68	0.025
Dz 1m	-26.99	0.286	-4.75	0.028
Dz 3m	-27.34	0.527	-4.81	0.016
Dz 5m	-26.09	0.044	-4.63	0.031
Dz 10m	-26.47	0.157	-4.69	0.065
Dz 15m	-26.52	0.089	-4.79	0.023
Dz 20m	-27.34	0.202	-4.95	0.033
Dz 25m	-30.87	0.502	-5.60	0.133
S1	-29.25	0.420	-6.15	0.037
rim bis 17	-30.81	0.197	-6.46	0.033
S4	-30.81	0.197	-6.46	0.033
s5	-32.75	0.127	-6.63	0.043
s6	-30.69	0.221	-6.34	0.041
canall 900	-31.22	0.191	-6.35	0.008

Annex 9

Litani basin- Environnemental isotopes ($\delta^{18}O$; $\delta^{2}H$)

April-2013	$\delta^{2}H/^{1}H$ (‰)	$\sigma\ \delta^{2}H/^{1}H$	$\delta^{18}O/^{16}O$ (‰)	$\sigma\delta^{18}O/^{16}O$
Ri 0m	-34.75	0.250	-6.12	0.017
Ri 1m	-33.57	0.181	-6.27	0.020
Ri 3m	-33.41	0.140	-6.26	0.017
Ri 5m	-32.84	0.045	-6.16	0.026
Cz 0m	-34.07	0.498	-6.83	0.085
Cz 1m	-33.64	0.388	-6.74	0.091
Cz 3m	-33.12	0.277	-6.40	0.033
Cz 5m	-33.22	0.247	-6.17	0.042
Cz 10m	-33.03	0.340	-6.11	0.136
Cz 15m	-32.86	0.199	-6.08	0.111
Cz 20m	-32.78	0.078	-6.21	0.038
Cz 25m	-31.29	1.076	-5.96	0.153
Es 0m	-34.71	0.175	-5.86	0.005
Es 1m	-32.27	0.341	-6.02	0.011
Es 2m	-32.92	0.290	-5.96	0.066
Ws 0m	-30.09	0.793	-5.75	0.175
Ws 1m	-35.34	0.214	-5.79	0.140
Ws 2m	-33.62	0.484	-6.11	0.027
Dz om	-35.58	0.065	-7.45	0.097
Dz 1m	-36.25	0.303	-7.04	0.042
Dz 3m	-35.59	0.548	-7.34	0.080
Dz 5m	-33.72	0.654	-7.24	0.045
Dz 10m	-33.49	0.008	-6.96	0.046
Dz 15m	-32.97	0.020	-6.96	0.017
Dz 20m	-33.04	0.314	-6.91	0.051

July-2013	$\delta^{2}H/^{1}H$ (‰)	$\sigma\ \delta^{2}H/^{1}H$	$\delta^{18}O/^{16}O$ (‰)	$\sigma\delta^{18}O/^{16}O$
Dz0	-34.78	0.444	-9.13	0.037
Dz1	-33.55	0.206	-9.12	0.033
Dz3	-33.83	0.033	-9.08	0.042
Dz5	-34.32	0.058	-9.11	0.019
Dz10	-34.52	0.283	-8.97	0.026
Dz15	-35.95	0.076	-9.42	0.059
Dz20	-36.23	0.367	-9.47	0.043
Dz25	-37.43	0.232	-9.54	0.012

Annex 10

Publications

Published

1- Ammar R., El Samrani AG., Kazpard V., Bassil J., Lartiges B., Saad Z., Chou L. Applying physicochemical approaches to control phosphogypsum heavy metal releases in aquatic environment, *Environmental Science and Pollution Research,* 20 (2013) 9014-9025.(DOI 10.1007/s11356-013-1875-7)

Submitted

2- Ammar R., Kazpard V., El Samrani AG., Benoit M., Lartiges B., Amacha N., Saad Z., Chou L. Geochemical Investigation of Two contrasted Mediterranean Watersheds: Tracing the Origin and Pathways of Contaminants Using Pb Isotopes. Submitted to *Journal of hazardous material*; HAZMAT-D-14-01124, under review.

3 -Ammar R., Kazpard V., El Samrani AG., Amacha N., Saad Z., Chou L. Hydrodynamics influence on reservoir sustainability in semiarid climate: physicochemical analysis coupled to environmental isotopic study. Submitted to *Journal of Hydrology*; HYDROL16716, under review.

4- Ammar R., Kazpard V., Wazne M., El Samrani AG., Amacha N., Saad Z., Chou L. Reservoir sediments: A sink or source of chemicals at the surface water-groundwater interface. Submitted to *Journal of Environmental Monitoring and Assessment*; EMAS-S-14-01467.

To be submitted

5- Ammar R., Kanbar H., Kazpard V., Wazne M., El Samrani AG., Amacha N., Schmidt S., Roveros N., Saad Z., Chou L. Metal behavior in intact cores and packed columns: Comparison between industrial and agricultural watersheds in eastern Mediterranean. To be submitted to *Journal of Environmental Pollution.*

6- Ammar R., Laruelle GG., Kazpard V., El Samrani AG., Amacha N., Regnier P., Saad Z., Chou L. Quantification of groundwater fluxes using hydrological box model: Balancing water budget in semi-arid reservoir. To be submitted to *Journal of Hydrology.*